

**Synergistic Approach to Exploration of the Microstructure of Novel, Tunable
Solvents for Reactions, Separations and Catalyst Recycle**

A Dissertation
Presented to
The Academic Faculty

By

Malina Elizabeth Janakat

In Partial Fulfillment
Of the Requirements for the Degree
Doctor of Philosophy in Chemical and Biomolecular Engineering

Georgia Institute of Technology

May, 2006

**Synergistic Approach to Exploration of the Microstructure of Novel, Tunable
Solvents For Reactions, Separations and Catalyst Recycle**

Approved By:

Dr. Charles A. Eckert
School of Chemical and Biomolecular
Engineering
Georgia Institute of Technology

Dr. Charles L. Liotta
School of Chemistry and Biochemistry
Georgia Institute of Technology

Dr. William J. Koros
School of Chemical and Biomolecular
Engineering
Georgia Institute of Technology

Dr. Rigoberto Hernandez
School of Chemistry and Biochemistry
Georgia Institute of Technology

Dr. Aryn S. Teja
School of Chemical and Biomolecular
Engineering
Georgia Institute of Technology

Date Approved: February 8, 2006

The most exciting phrase to hear in science, the one that heralds new discoveries, is not
'Eureka!', but 'That's funny....'
-Isaac Asimov

For Mike

ACKNOWLEDGMENTS

Albert Szent-Györgi said, “Research is to see what everybody else has seen, and to think what nobody else has thought.” While a seemingly obvious statement, it is certainly a feat which is easier said than done. I thank my advisors, Professors Chuck Eckert and Charlie Liotta, for always thinking what nobody else has thought challenging me to do the same. I hope that lesson stays with me.

Dr. Eckert always seemed to know when I needed a critic and when I needed a cheerleader – and was adept at being both. He helped me figure out what questions were important to ask and when I drowned in details he helped me see the big picture. In addition to guiding the course of my research, he also made efforts to help me develop as a communicator and public speaker. I hope I have learned from him.

Dr Liotta’s enthusiasm was in endless supply and a breath of fresh air. Anytime something unexpected happened he could explain why, draw out the mechanism, energy diagram, molecular orbitals etc. to support his claim and give a reference to the journal or book where he read about it – usually including the researchers, year, and even the month in which is appeared. He would then come up with a reason why it’s a good thing. I hope that optimism stays with me.

I thank the other members of my committee: Professors Rig Hernandez, Aryn Teja and William Koros. From giving advice to offering explanations to loaning out equipment, their efforts really helped me along the way.

I thank Deborah Babykin for taking care of the administrative details that would have otherwise slowed everything down. She had a knack for knowing everything, and when she didn't she knew who did. Her effort and assistance have been invaluable and have made life as a graduate student significantly easier.

I thank all of the current and former graduate students in this research group for their friendship, support and assistance. I couldn't have done any of this without them. In particular I would like to thank Dr. Jason Hallett, who was my 'go-to-guy' for just about every problem I had in the lab and my primary caffeine supplier; Dr. Jie Lu, whose patience was priceless when I asked her the same questions over and over, Dr. Josh Brown, our resident "MacGyver", who could fix anything, always gave way more information than I asked for and was always really nice about it; Dr. David Bush, whose expertise and insight are unmatched, and who is an "Excel ninja"; Dr. Chris Kitchens, whose equipment-repair skills rival those of Josh; and Natalie Maxey and Laura Draucker, who did a lot of work to help me get some of my projects moving. I also thank the many undergraduate assistants: Jovy Roach, Kyle Ross, Oxana Selivanova, Stuart Terrett, Laura Nunez, Stan Hill and Kristen Kitagawa for doing my more tedious laboratory tasks.

I also thank the friends who I have made along the way; particularly Heather DiBiaso, James Broering, Ross Weikel and Beckie Jones. They were always up for a good time and available to provide laughs, support and a shoulder to cry on.

I thank my family: my older brother, JJ, for actually wanting to talk to me about my research; my younger brother, Omar, for providing endless laughs and insanity; my late father, Sozar, for always encouraging my curiosity and making me do my homework

when I got home from school; and my mother, Jean, for her infinite emotional support, her pride in me and for making sure I never starved or froze by providing me with an emergency credit card.

Finally, I thank Michael Karle, my best friend and the love of my life. His love, support, patience, good humor and proofreading made this work possible. He was always ready with a hug, a pep-talk, a silly dance or a chocolate truffle – whatever I needed that particular day – to help maintain my sanity and keep a smile on my face. I also thank my cats, Dakota and Pumpkin, for being goofy, cuddly and really bad.

TABLE OF CONTENTS

| | | |
|------------------|--|-------|
| ACKNOWLEDGEMENTS | | v |
| LIST OF TABLES | | xi |
| LIST OF FIGURES | | xiii |
| NOMENCLATURE | | xviii |
| SUMMARY | | xxi |
| CHAPTER I | INTRODUCTION | 1 |
| CHAPTER II | BACKGROUND | 6 |
| | Introduction | 6 |
| | Applications of Gas-Expanded Liquids | 7 |
| | Studying the Cybotactic Region of Supercritical Fluids | 9 |
| | References | 17 |
| CHAPTER III | EXPERIMENTAL DETERMINATION AND MODEL PREDICTION OF SOLID SOLUBILITY OF MULTI-FUNCTIONAL COMPOUNDS IN PURE AND MIXED NON-ELECTROLYTE SOLVENTS | 21 |
| | Introduction | 21 |
| | Background on the MOSCED Model | 24 |
| | Experimental | 26 |
| | Materials | 26 |
| | Apparatus and Methods | 27 |
| | Experimental Results and Discussion | 29 |
| | Pure Solvents | 29 |
| | Mixed Solvents | 33 |
| | Thermodynamic Modeling Results and Discussion | 45 |
| | Pure Solvents | 45 |
| | Mixed Solvents | 51 |
| | Paradigm for Solvent Selection | 55 |
| | Summary | 55 |

| | | |
|------------|---|-----|
| | References | 57 |
| CHAPTER IV | MENSCHUTKIN REACTION KINETICS, PI STAR AND Z-VALUES AS PROBES OF LOCAL POLARITY OF CO ₂ -EXPANDED ACETONITRILE | 59 |
| | Introduction | 59 |
| | Background on Menschutkin Reaction | 59 |
| | Background on pi star measurements | 61 |
| | Background on Z-Value Measurements | 62 |
| | Experimental | 63 |
| | Materials | 63 |
| | Apparatus | 64 |
| | Procedure | 64 |
| | Results and Discussion | 67 |
| | Reaction Kinetics | 67 |
| | Pi Star Shifts | 73 |
| | Z-values | 76 |
| | Dipole Moment of the Transition State | 80 |
| | Temperature Dependence: Determination of the Activation Energy | 83 |
| | Summary | 84 |
| | References | 86 |
| CHAPTER V | DIFFUSION COEFFICIENTS IN CO ₂ - EXPANDED METHANOL BY THE TAYLOR- ARIS DISPERSION TECHNIQUE | 88 |
| | Introduction | 88 |
| | Experimental | 90 |
| | Materials | 90 |
| | Apparatus | 90 |
| | Procedure | 91 |
| | Results and Discussion | 93 |
| | Summary | 98 |
| | References | 99 |
| CHAPTER VI | CONCLUSIONS AND RECOMMENDATIONS | 100 |
| | Solid Solubility in Pure and Mixed Solvents | 101 |
| | Conclusions | 101 |
| | Recommendations | 102 |
| | Local Polarity of Gas-Expanded Liquids | 103 |
| | Conclusions | 103 |
| | Recommendations | 105 |
| | Diffusion Coefficients in Gas-Expanded Liquids | 108 |
| | Conclusions | 108 |
| | Recommendations | 108 |
| | Microviscosity of Gas-Expanded Liquids | 110 |

| | | |
|------------|---|-----|
| | Conclusions | 110 |
| | Recommendations | 110 |
| | Final Summary | 112 |
| | References | 113 |
| APPENDIX A | SUMMARIZED DATA FROM CHAPTER III | 114 |
| APPENDIX B | VALIDATION OF TAYLOR-ARIS DISPERSION MEASUREMENTS | 127 |
| | Introduction | 127 |
| | Diagnostics | 127 |
| | Influence of Detection Wavelength | 127 |
| | Influence of Amount of Solute Injected | 128 |
| | Influence of Flow Rate | 132 |
| | Influence of Pressure | 133 |
| | Influence of System Temperature | 133 |
| | Influence of Chiller Temperature | 134 |
| | Summary of System Requirements | 136 |
| | Determination of System Requirements | 137 |
| | References | 138 |
| APPENDIX C | MICROVISCOSITY: FLUORESCENT EXCITATION OF A MOLECULAR ROTOR AS A PROBE OF THE CYBOTACTIC REGION OF GAS-EXPANDED LIQUIDS | 139 |
| | Introduction | 139 |
| | Experimental | 141 |
| | Materials | 141 |
| | Apparatus | 142 |
| | Procedure | 143 |
| | Analysis | 144 |
| | Results and Discussion | 148 |
| | Summary | 157 |
| | References | 158 |
| VITA | | 160 |

LIST OF TABLES

| | | |
|-----------|---|-----|
| Table 3-1 | Experimental solubility vs. literature values using the dilution method for anthracene at 298 K. | 29 |
| Table 3-2 | Experimental solubility vs. literature values using the direct sampling method for anthracene at 298 K. | 29 |
| Table 3-3 | Heats of fusion and melting temperatures of solids. | 46 |
| Table 3-4 | Regressed MOSCED parameters for all solids using Wilson and UNIQUAC g^E models. | 46 |
| Table 4-1 | Partial molal volumes of the transition states of typical Menshutkin reactions. | 72 |
| Table 4-2 | Activation volumes of typical Menshutkin reactions. | 72 |
| Table 5-1 | Our data compared with literature data for several solutes in methanol. | 96 |
| Table 6-1 | Potential Menshutkin reaction solvents. | 109 |
| Table A-1 | Solubility of 3-nitrophthalimide in pure solvents – Experimental values and predictions. | 117 |
| Table A-2 | Solubility of 3-nitrophthalimide in mixtures of ethanol and ethyl acetate – Experimental values and predictions. | 118 |
| Table A-3 | Solubility of 3-nitrophthalimide in mixtures of isopropanol and nitromethane – Experimental values and predictions. | 119 |
| Table A-4 | Solubility of 3-nitrophthalimide in mixtures of dioxane and 2-butanone – Experimental values and predictions. | 119 |
| Table A-5 | Solubility of 3-nitrophthalimide in mixtures of DMF and chloroform – Experimental values and predictions. | 120 |
| Table A-6 | Solubility of 5-fluoroisatin in pure solvents – Experimental values and predictions. | 120 |

| | | |
|------------|--|-----|
| Table A-7 | Solubility of 5-fluoroisatin in mixtures of ethanol and ethyl acetate – Experimental values and predictions. | 121 |
| Table A-8 | Solubility of 5-fluoroisatin in mixtures of isopropanol and nitromethane – Experimental values and predictions. | 122 |
| Table A-9 | Solubility of 5-fluoroisatin in mixtures of dioxane and 2-butanone – Experimental values and predictions. | 122 |
| Table A-10 | Solubility of 5-fluoroisatin in mixtures of DMF and chloroform – Experimental values and predictions. | 123 |
| Table A-11 | Solubility of benzimidazole in pure solvents – Experimental values and predictions. | 123 |
| Table A-12 | Solubility of benzimidazole in mixtures of ethanol and ethyl acetate – Experimental values and predictions. | 125 |
| Table A-13 | Solubility of benzimidazole in mixtures of isopropanol and nitromethane – Experimental values and predictions. | 125 |
| Table A-14 | Solubility of benzimidazole in mixtures of dioxane and 2-butanone – Experimental values and predictions. | 126 |
| Table A-15 | Solubility of benzimidazole in mixtures of DMF and chloroform – Experimental values and predictions. | 126 |
| Table A-16 | Solubility of 2-amino-5-nitrobenzophenone in pure solvents – Experimental values and predictions. | 127 |
| Table A-17 | Solubility of 2-amino-5-nitrobenzophenone in mixtures of ethanol and ethyl acetate – Experimental values and predictions. | 128 |
| Table A-18 | Solubility of 2-amino-5-nitrobenzophenone in mixtures of Isopropanol and nitromethane – Experimental values and predictions. | 128 |
| Table A-19 | Solubility of 2-amino-5-nitrobenzophenone in mixtures of dioxane and 2-butanone – Experimental values and predictions. | 129 |
| Table A-20 | Solubility of 2-amino-5-nitrobenzophenone in mixtures of DMF and chloroform – Experimental values and predictions. | 129 |
| Table B-1 | Detector wavelength and concentration requirements for all solutes studied. | 140 |

LIST OF FIGURES

| | | |
|------------|---|----|
| Figure 2-1 | Bubble point curves for CO ₂ with acetone, ethanol, methanol at 25 °C. | 7 |
| Figure 2-2 | Diffusion coefficient of benzene in supercritical CO ₂ as a function of pressure and temperature. | 10 |
| Figure 2-3 | Diffusion coefficient of benzene in supercritical CO ₂ as a function of fluid viscosity. | 11 |
| Figure 2-4 | Local mole fractions of methanol in the cybotactic region of 4-nitroanisole vs. pressure for two different bulk mole fractions. | 15 |
| Figure 3-1 | Structures of solid compounds studied. | 23 |
| Figure 3-2 | Flow chart for procedure to determine MOSCED parameters. | 27 |
| Figure 3-3 | Solubility of 3-nitrophthalimide in various organic solvents at 283, 298 and 313 K. | 30 |
| Figure 3-4 | Solubility of 5-fluoroisatin in various organic solvents at 283, 298 and 313 K. | 32 |
| Figure 3-5 | Solubility of benzimidazole in various organic solvents at 283, 298 and 313 K. | 33 |
| Figure 3-6 | Solubility of 2-amino-5-nitrobenzophenone in various organic solvents at 283, 298 and 313 K. | 34 |
| Figure 3-7 | 3-Nitrophthalimide in mixtures of ethanol and ethyl acetate, measured data and predictions (solid lines UNIQUAC, dashed lines Wilson) at 283, 298 and 313 K. | 36 |
| Figure 3-8 | 3-Nitrophthalimide in mixtures of isopropanol and nitromethane, measured data and predictions (solid lines UNIQUAC, dashed lines Wilson) at 283, 298 and 313 K. | 36 |
| Figure 3-9 | 3-Nitrophthalimide in mixtures of dioxane and 2-butanone, measured | 37 |

| | | |
|-------------|--|----|
| | data and predictions (solid lines UNIQUAC, dashed lines Wilson) at 283, 298 and 313 K. | |
| Figure 3-10 | 3-Nitrophthalimide in mixtures of chloroform and DMF, measured data and predictions (solid lines UNIQUAC, dashed lines Wilson) at 283, 298 and 313 K. | 37 |
| Figure 3-11 | 5-Fluoroisatin in mixtures of ethanol and ethyl acetate, measured data and predictions (solid lines UNIQUAC, dashed lines Wilson) at 283, 298 and 313 K. | 38 |
| Figure 3-12 | 5-Fluoroisatin in mixtures of isopropanol and nitromethane, measured data and predictions (solid lines UNIQUAC, dashed lines Wilson) at 283, 298 and 313 K. | 39 |
| Figure 3-13 | 5-Fluoroisatin in mixtures of dioxane and 2-butanone, measured data and predictions (solid lines UNIQUAC, dashed lines Wilson) at 283, 298 and 313 K. | 39 |
| Figure 3-14 | 5-Fluoroisatin in mixtures of chloroform and DMF, measured data and predictions (solid lines UNIQUAC, dashed lines Wilson) at 283, 298 and 313 K. | 40 |
| Figure 3-15 | Benzimidazole in mixtures of ethanol and ethyl acetate, measured data and predictions (solid lines UNIQUAC, dashed lines Wilson) at 283, 298 and 313 K. | 41 |
| Figure 3-16 | Benzimidazole in mixtures of isopropanol and nitromethane, measured data and predictions (solid lines UNIQUAC, dashed lines Wilson) at 283, 298 and 313 K. | 41 |
| Figure 3-17 | Benzimidazole in mixtures of dioxane and 2-butanone, measured data and predictions (solid lines UNIQUAC, dashed lines Wilson) at 283, 298 and 313 K. | 42 |
| Figure 3-18 | Benzimidazole in mixtures of chloroform and DMF, measured data and predictions (solid lines UNIQUAC, dashed lines Wilson) at 283, 298 and 313 K. | 43 |
| Figure 3-19 | 2-Amino-5-nitrobenzophenone in mixtures of ethanol and ethyl acetate, measured data and predictions (solid lines UNIQUAC, dashed lines Wilson) at 283, 298 and 313 K. | 44 |
| Figure 3-20 | 2-Amino-5-nitrobenzophenone in mixtures of isopropanol and nitromethane, measured data and predictions (solid lines UNIQUAC, dashed lines Wilson) at 283, 298 and 313 K. | 44 |

| | | |
|-------------|--|----|
| Figure 3-21 | 2-Amino-5-nitrobenzophenone in mixtures of dioxane and 2-butanone, measured data and predictions (solid lines UNIQUAC, dashed lines Wilson) at 283, 298 and 313 K. | 45 |
| Figure 3-22 | 2-Amino-5-nitrobenzophenone in mixtures of chloroform and DMF, measured data and predictions (solid lines UNIQUAC, dashed lines Wilson) at 283, 298 and 313 K. | 45 |
| Figure 3-23 | Mole fraction solubility of 3-nitrophthalimide in various solvents from 283 to 313 K versus MOSCED predictions. | 47 |
| Figure 3-24 | Mole fraction solubility of 5-fluoroisatin in various solvents from 283 to 313 K versus MOSCED predictions. | 48 |
| Figure 3-25 | Mole fraction solubility of benzimidazole in various solvents from 283 to 313 K versus MOSCED predictions. | 49 |
| Figure 3-26 | Mole fraction solubility of 2-amino-5-nitrobenzophenone in various solvents from 283 to 313 K versus MOSCED predictions. | 50 |
| Figure 3-27 | Intramolecular hydrogen bonding in 2-amino-5-nitrobenzophenone. | 51 |
| Figure 4-1 | Reaction of tri-butylamine with methyl <i>p</i> -nitrobenzenesulfonate. | 61 |
| Figure 4-2 | Polar transition state of the reaction of tri-butylamine with methyl <i>p</i> -nitrobenzenesulfonate. | 61 |
| Figure 4-3 | Typical UV spectrum of the reaction of tri-butylamine with methyl <i>p</i> -nitrobenzenesulfonate. | 62 |
| Figure 4-4 | <i>N,N</i> -dimethyl-4-nitroaniline. | 63 |
| Figure 4-5 | 1-Ethyl-4-carbomethoxypyridinium iodide. | 64 |
| Figure 4-6 | Typical absorbance vs. time plot of the reaction of tri-butylamine with methyl <i>p</i> -nitrobenzenesulfonate. | 66 |
| Figure 4-7 | Second order rate constants for Menshutkin reaction in CO ₂ -expanded acetonitrile as a function of composition. | 69 |
| Figure 4-8 | First order rate constants for Menshutkin reaction in CO ₂ -expanded acetonitrile as a function of composition. | 70 |
| Figure 4-9 | Density of Acetonitrile + CO ₂ . | 71 |

| | | |
|-------------|--|----|
| Figure 4-10 | <i>Cis-trans</i> isomerization of azo-benzenes in CO ₂ -expanded dioxane as a function of CO ₂ pressure. | 73 |
| Figure 4-11 | Dielectric constants of CO ₂ -expanded methanol as a function of CO ₂ pressure. | 74 |
| Figure 4-12 | π^* of CO ₂ -expanded acetonitrile, 40 °C, compared with other solvents. | 75 |
| Figure 4-13 | Correlation of π^* with second order rate constants. | 76 |
| Figure 4-14 | Correlation of π^* with second order rate constants for GXL and pure solvents. | 77 |
| Figure 4-15 | Z-values of CO ₂ -expanded acetonitrile as a function of CO ₂ composition, T=40 °C, and Z-values of conventional solvents. | 78 |
| Figure 4-16 | Correlation of Z-value with second order rate constants. | 79 |
| Figure 4-17 | Z-values of CO ₂ -expanded acetonitrile as a function of CO ₂ composition, T=40 °C, and Z-values of conventional solvents. | 79 |
| Figure 4-18 | Correlation of Z-values with π^* of CO ₂ -expanded acetonitrile. | 80 |
| Figure 4-19 | Correlation of Z-values with π^* of CO ₂ -expanded acetonitrile and conventional solvents. | 81 |
| Figure 4-20 | Kirkwood plot of data – Fit with and without the end points. | 82 |
| Figure 4-21 | Polarity probe data and dielectric constants of CO ₂ / acetonitrile mixtures, normalized to pure acetonitrile, 40 °C. | 84 |
| Figure 4-22 | Determination of the activation energy of the Menshutkin reaction. | 85 |
| Figure 5-1 | Taylor-Aris dispersion. | 91 |
| Figure 5-2 | Flow profiles for the original pulse, slow diffusion and fast diffusion. | 91 |
| Figure 5-3 | Solutes studied. | 92 |
| Figure 5-4 | Supercritical fluid chromatograph. | 93 |
| Figure 5-5 | Diffusion coefficients of benzene in CO ₂ -expanded methanol as a function of weight fraction of CO ₂ , 313 K, 150 bar. | 96 |
| Figure 5-6 | Diffusion coefficients of benzene, pyridine, pyrimidine, pyrazine | 97 |

and 1,3,5-triazine in CO₂-expanded methanol as a function of volume fraction of methanol, 313 K, 150 bar.

| | | |
|-------------|---|-----|
| Figure 5-7 | Diffusion coefficients of benzene, pyridine, pyrimidine, pyrazine and 1,3,5-triazine in CO ₂ -expanded methanol as a function of mass fraction of methanol, 313 K, 150 bar. | 98 |
| Figure 5-8 | Diffusion coefficients of various pseudoplanar molecules in ethanol, 298.2K, ambient pressure. | 99 |
| Figure 5-9 | Viscosity of CO ₂ -expanded methanol as a function of mass fraction of methanol calculated from diffusion coefficients of benzene measured at 313 K, 150 bar via the Stokes-Einstein equation. | 99 |
| Figure 6-1 | Structure of hexamethyltetraamine. | 106 |
| Figure B-1 | Influence of detector wavelength and injected amount of solute on the diffusion coefficient of benzene in methanol, 313 K, 100 bar, $v_{\text{Methanol}}=0.2$ ml/min. | 131 |
| Figure B-2 | Influence injected amount of solute on the diffusion coefficient of toluene in methanol, 313 K, 100 bar, $v_{\text{Methanol}}=0.2$ ml/min, 260 nm. | 132 |
| Figure B-3 | Influence injected amount of solute on the diffusion coefficient of 2-naphthol in methanol, 313 K, 100 bar, $v_{\text{Methanol}}=0.2$ ml/min, 274 nm. | 133 |
| Figure B-4 | Influence injected amount of solute on the diffusion coefficient of phenol in methanol, 313K, 100 bar, $v_{\text{Methanol}}=0.2$ ml/min, 272 nm. | 134 |
| Figure B-5 | Influence injected amount of phenol on the peak area 313 K, 100 bar, $v_{\text{Methanol}}=0.2$ ml/min, 272 nm. | 134 |
| Figure B-6 | Influence of methanol flow rate on the diffusion coefficient of benzene, 313 K, 100 bar, 0.01 mg injection. | 135 |
| Figure B-7 | Influence of hydrostatic pressure of methanol on the diffusion coefficient of benzene, 313 K, 0.01 mg injection, $v_{\text{Methanol}}=0.2$ ml/min. | 136 |
| Figure B-8 | Influence of temperature of methanol on the diffusion coefficient of benzene, 100 bar, 0.01 mg injection, $v_{\text{Methanol}}=0.2$ ml/min. | 137 |
| Figure B-9 | Influence of temperature of methanol on the diffusion coefficient of toluene, 14 bar, 0.01 mg injection, $v_{\text{Methanol}}=0.2$ ml/min. | 138 |
| Figure B-10 | Influence of chiller temperature on the diffusion coefficient of toluene, 313 K, 100 bar, 0.01 mg injection, $v_{\text{Methanol}}=0.2$ ml/min. | 138 |

| | | |
|--------------|---|-----|
| Figure C-1 | Structure of DCVJ in both the ground state and excited state. | 143 |
| Figure C-2 | Simplified fluorescence emission mechanism. | 144 |
| Figure C-3 | Fluorescence emission potential diagram for DCVJ excitation. | 145 |
| Figure C-4 | Fluorescence emission spectra of DCVJ in conventional liquid solvents at 25 °C ($C_{\text{DCVJ}} = 4.5 \times 10^{-6}$ mol/L). | 147 |
| Figure C-5 | Viscosity dependence of fluorescence intensity of DCVJ for the liquid solvents in Figure C-4. | 148 |
| Figure C-6 | Confirmation of calibration technique by comparison with mixtures of 2-propanol and ethylene glycol at 25 °C. | 149 |
| Figure C-7 | Confirmation of measurement technique by comparison with literature data for 2-propanol and ethylene glycol mixtures at 25 °C. | 150 |
| Figure C-8 | Concentration behavior of fluorescent intensity of DCVJ measured at the intensity maximum and at 450 nm. | 152 |
| Figure C-9 | Comparison between bulk and microviscosity of mixtures of methanol and cyclohexane at 50°C. | 153 |
| Figure C-10 | Microviscosity of mixtures of methanol and carbon dioxide compared with bulk viscosity values at 40°C. | 154 |
| Figure C-11 | Effect of hydrostatic pressure on the microviscosity of methanol as compared to the bulk viscosity at 40°C. | 156 |
| Figure C-12 | Effect of hydrostatic pressure on the microviscosity of a mixture of 0.55 methanol and 0.45 CO ₂ as compared to the bulk viscosity of methanol at 40 °C. | 157 |
| Figure C-13 | Microviscosity of ethane-expanded methanol at 40 °C. | 158 |
| Figure C-14 | Microviscosity of mixtures of methanol and CO ₂ compared with bulk viscosity values at 40 °C. | 159 |
| Figure C-15: | Extrapolation of calibration curve to the viscosity of CO ₂ . | 159 |

NOMENCLATURE

Abbreviations

| | |
|-----------------|--|
| CO ₂ | Carbon dioxide |
| COSMO | Conductor-like screening model |
| DCVJ | 9-(dicyanovinyl) julolidine |
| DIPPR | A particular physical property database |
| DMF | <i>N,N</i> -Dimethyl formamide |
| DMSO | Dimethylsulfoxide |
| GAS | Gas-antisolvent separation |
| GC-FID | Gas chromatography with flame ionization detection |
| HMTA | Hexamethylaminetetraamine |
| GXL | Gas-expanded liquid |
| HPLC | High performance liquid chromatography |
| MOSCED | Modified separation of cohesive energy density |
| SC | Supercritical |
| SCF | Supercritical fluid |
| SLE | Solid-liquid equilibria |
| UNIFAC | Universal functional activity coefficient |
| UNIQUAC | Universal quasi-chemical theory |
| UV-vis | Ultraviolet-visible spectroscopy |
| VLE | Vapor-liquid equilibria |

Common Constants and Dimensionless Groups

| | |
|----------|---|
| h | Planck's constant, 6.626×10^{-34} J-sec |
| κ | Boltzmann's constant, 1.381×10^{-23} J/K |
| Re | Reynolds Number |
| De | Dean Number |
| Sc | Schmidt Number |

Notation

| | |
|------------------|---|
| A | Absorbance |
| A,B | Reactants and Products in general |
| C | Constant |
| D _{1,2} | Diffusion coefficient of species 1 into species 2 |
| ΔC_p | Difference in heat capacity of two equilibrium species |
| E _T | Solvatochromic polarity scale, Electronic transition energy |
| F | Fluorescence emission |
| g ^E | Molar excess Gibb's energy |

| | |
|-------------------------|---|
| H | Height of a theoretical plate |
| ΔH_{fus} | Enthalpy of fusion |
| k | Reaction rate constant, Activation / deactivation rate |
| k_{nr} | Nonradiative activation / deactivation rate |
| k_{r} | Radiative activation / deactivation rate |
| L | Length |
| P | Pressure |
| P_s | Spectral polarity index |
| R | Universal gas constant |
| r | Radius |
| S | Electronic State |
| T | Temperature |
| t | Time |
| T_m | Melting temperature |
| \bar{u}_0 | Average velocity of fluid flow |
| v | Volumetric flow rate |
| $W_{1/2}$ | Width of a peak at half of its height |
| x | Mole fraction |
| x^{ideal} | Ideal solubility |
| π^* | Kamlet-Taft polarity / polarizability parameter |
| ϵ | Dielectric constant |
| Φ_{f} | Fluorescence quantum yield |
| γ | Activity coefficient of a solid in solution |
| γ^{∞} | Infinite dilution activity coefficient |
| η | Viscosity |
| λ | Wavelength of light |
| λ_{max} | Wavelength corresponding to a maximum in absorbance frequency |
| ν | Frequency of light |
| σ | Variance of a Gaussian curve, Collision diameter |

Subscripts

| | |
|----------|--|
| s | Of a particular solid in solution |
| c | Calculated |
| e | Experimental |
| max | Maximum value for said parameter |
| obs | Observed parameter |
| 0 | At time = 0, At lowest energy (ground) state |
| ∞ | As time approaches infinity |
| r | Retention, Radiative |
| i | For an individual molecule |
| 1 | At first excited state |
| nr | Non-radiative |

Superscripts

| | |
|----------|------------------------|
| ∞ | At infinite dilution |
| Ideal | Under ideal conditions |

SUMMARY

Gas-expanded liquids (GXLs) are a new and benign class of pressure-tunable liquid solvents which show tremendous promise as the next sustainable processing medium. In order to realize the potential of GXLs fully, it is necessary to elucidate their cybotactic region and gain an understanding of where properties are different in the bulk- and micro-scales and how local structure and order affect both reactions and separations. This work explores the cybotactic region of GXLs and probes the existence and implications of those differences.

This study is started by exploring the cybotactic region of ambient liquid mixtures. Thermodynamic models based on intermolecular forces are used to predict the solubility of multi-functional solids in a variety of solvent mixtures. While this part does not lend any insight into GXLs directly, it acts as a stepping stone in both understanding the intermolecular forces that govern the cybotactic region and by opening the gateway to studying solid solubility in GXLs.

The rest of the study focuses on the differences between bulk and local properties of GXLs. Different probes of polarity in the cybotactic region are compared and the solute dependence of the local structure is explored. Bulk transport properties are measured with different probes in an effort to see if molecular interactions play a role in governing diffusion processes in GXLs.

CHAPTER I

INTRODUCTION

The endorsement and employment of environmentally benign solvents in a multitude of traditional chemical processes has received increased attention in recent years. The prevalence of environmental and public health issues in society and politics have driven all facets of the chemical industry towards more sustainable processes.¹ With the rising cost of waste remediation, it is imperative to look at the entire life cycle of a chemical process, not just the cost of starting materials or the ‘ease’ of reaction steps. Efforts made to make processes ‘greener’ include a myriad of improvements such as minimizing energy consumption, waste generation and the need for downstream processing.² Perhaps the most promising means for such improvements is through the use of environmentally benign solvents.

Both liquid and supercritical carbon dioxide are among the leading ‘green’ alternatives to conventional organic solvents. However, liquid CO₂ is a poor solvent and, due to the requisite high pressures, supercritical fluids are not often practical for use in industrial processes. In order to bridge the gap between the utility of conventional solvents and the benign nature of CO₂, the chemical community has begun to explore gas-expanded liquids (GXLs) as the next ‘green’ alternative.

This project focuses on studying the cybotactic region, the region where the solvent structure is influenced by the solute-solute and solute-solvent interactions^{3, 4} of gas-expanded liquids. It is part of a larger initiative to understand GXs fully – both on a macroscopic and microscopic scale – by incorporating experimentation and simulations synergistically. The experimental and theoretical aspects of this study work together in the following way: experimentation provides information to ensure the correctness of the interaction parameters in the theoretical models. Once the parameters are determined, they can be used to design GXs for applications that are difficult to develop by purely empirical means. This study primarily explores the experimental aspect of this endeavor.

Chapter II of this study provides an extensive review of measurements on the cybotactic region of supercritical fluids. A variety of probes for studying myriad local properties of supercritical CO₂, other supercritical fluids and supercritical mixtures are explored. A solid foundation for the work covered in the thesis is developed and presented.

Before one can fully explore the cybotactic region of a gas-expanded liquid it is important to gain an understanding of solute-solvent interactions on the molecular level of liquids. In Chapter III, a paradigm for solvent selection for crystallization is presented based on solid solubility measurements and predictions. The predictive models take into account different intermolecular interactions. The molecular interactions in the cybotactic region of ambient pure liquids and liquid mixtures help elucidate interactions that may exist in the cybotactic region of GXs. Appendix A serves as a companion to Chapter III.

For GXs to be useful as reaction solvents it is necessary to understand a variety of solvent properties in both the bulk phase and in the cybotactic region. The polarity in the cybotactic region is probed using a model S_N2 reaction of a tosylate compound with an amine in Chapter IV. The measurements are made in terms of reaction kinetics which, due to the presence of a very polar transition state, are extremely sensitive to changes in local polarity. These reactions are used extensively in determining the polarity of a variety of solvents such as traditional organic solvents and ionic liquids but have never been used to study gas-expanded liquid systems. These results are complemented by measurement of the Kamlet-Taft parameter π^* and Kosower's Z-value as additional measures of polarity. The three measures are compared and contrasted against one another and the calculated dielectric constant of the mixed solvent. CO_2 -expanded acetonitrile is studied in this chapter.

Chapter V explores bulk transport properties of CO_2 -expanded methanol. An extensive background of the peak-broadening technique of Taylor and Aris to measure binary diffusion coefficients is given. Five nitrogen-containing aromatic compounds are studied using the Taylor-Aris method in various mixtures of methanol and CO_2 . The diffusion coefficients are compared as a function of CO_2 composition and as a function of molecular structure. These data are used in conjunction with the Stokes-Einstein equation to estimate the viscosity of gas-expanded liquids. Information on the validation of the methods is presented in Appendix B.

A comprehensive discussion of the application of microviscosity measurements to gas-expanded liquid systems appears in Appendix C. This work complements that done in Chapter V and can also be related to it via a Stokes-Einstein relationship in order to

deduce information on local diffusivity. Microviscosity is measured by following the internal rotation of a fluorophore as a result of excitation via fluorescence. This technique has been used to study rates of polymerization, protein formation and the variation of viscosity of room-temperature ionic liquids as a function of CO₂ composition, but has not been used to study traditional solvents expanded with CO₂. The challenges of studying microviscosity via this technique are explored and data in CO₂-expanded methanol and acetone are presented.

Chapter VI provides a summary and overview of the implications of the included research as well as proposed future work. Applications of gas-expanded liquids are reiterated and the need for understanding the microstructure in developing such applications is discussed.

REFERENCES

1. Dartt, C. B.; Davis, M. E., Catalysis for environmentally benign processing. *Ind. Eng. Chem. Res.* **1994**, 33, 2887-2899.
2. Anastas, P. T.; Warner, J. C., Green Chemistry: Theory and Practice. **1998**.
3. Zagrobelny, J.; Betts, T. A.; Bright, F. V., Steady-state and time resolved fluorescence investigations of pyrene excimer formation in supercritical carbon dioxide. *J. Am. Chem. Soc.* **1992**, 114, 5249-5257.
4. Zagrobelny, J.; Bright, F. V., Influence of solute-fluid clustering on the photophysics of pyrene emission in supercritical ethane and trifluoromethane. *J. Am. Chem. Soc.* **1992**, 114, (20), 7821-7826.

CHAPTER II

BACKGROUND

Introduction

Gas-expanded liquids are created by dissolving large quantities of gas, typically CO₂, into organic liquids. Since liquid and supercritical CO₂ are poor solvents, especially concerning charged or polar solutes, combining CO₂ with organics that are good solvents can yield a wide range of solvation properties. GXLs are roughly intermediate in terms of solvent power and transportability when compared to gases and liquids, expressing more liquid-like characteristics than supercritical fluids. CO₂ has a substantial solubility in a variety of organic solvents such as alcohols and ketones at relatively moderate pressures (Figure 2-1).¹ This affords the ability to tune solvent properties such as polarity, dielectric constant and the solubility of a third component, for instance a non-condensable gas such as hydrogen or oxygen.²⁻⁵ Furthermore, due to its easy removal and recycle as well as its environmentally benign nature, CO₂ is an ideal anti-solvent.^{2,5}

Thorough exploitation of a GXL requires detailed knowledge of its cybotactic region, the region where the solvent structure is influenced by solute-solute and solute-solvent interactions.^{6,7} Fluids ranging from incompressible to supercritical exhibit local composition effects that may differ greatly from their bulk compositions. While many

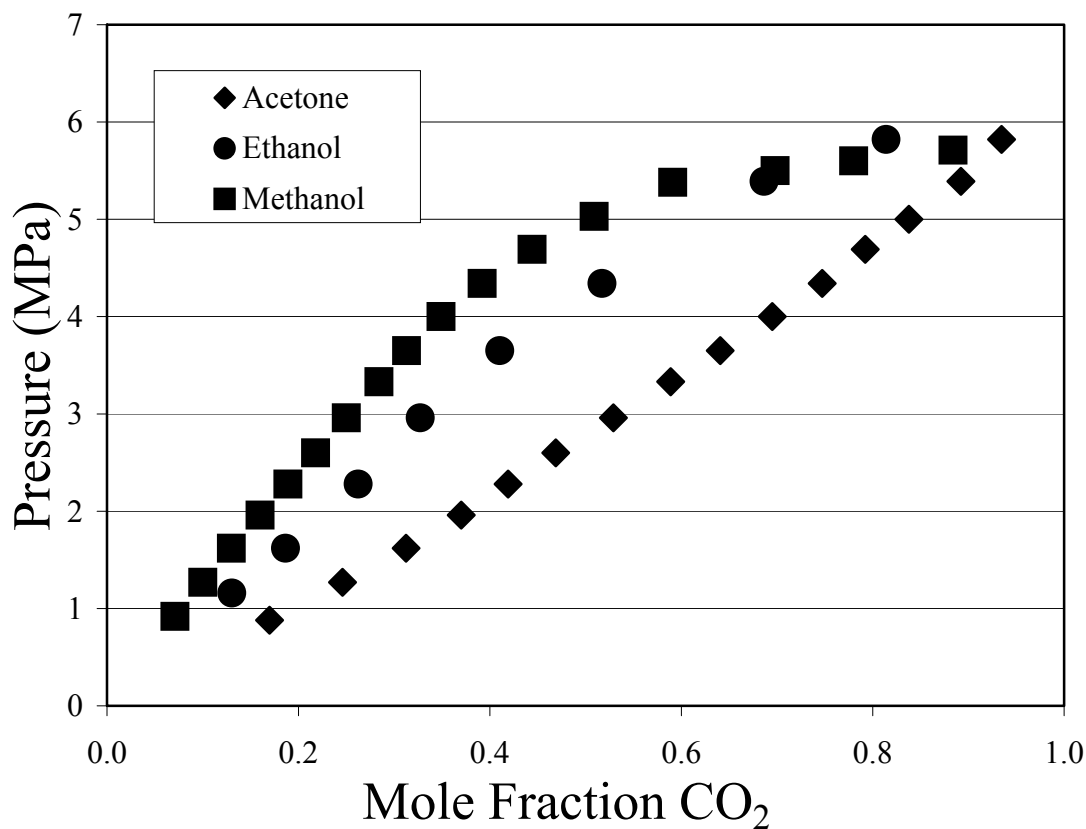


Figure 2-1: Bubble point curves for CO₂ with Acetone, Ethanol, Methanol at 25 °C.¹

experiments measure bulk or average properties, determination of heterogeneities in the cybotactic region requires the use of experiments that probe specifically the local environment and simulations that permit exploration of said environments. An understanding of the non-uniformity of the local solvent structure in GXs can lead to insight about how the aforementioned structure affects the chemistry of the solutes.

Applications of Gas-Expanded Liquids

While the focus of this work is fundamental properties of gas-expanded liquids, it is important to mention some applications of these systems in order to demonstrate the importance of elucidating the cybotactic region. One common application of GXs is currently in gas-antisolvent (GAS) separations.² Applications of GAS in particle

formation span a variety of industries from drug delivery⁸ to deactivation of explosives⁹ to production of antibacterial nanoparticles.¹⁰ Furthermore, GAS techniques have been used to purify many species, for example organic acids¹¹ and β -carotene,¹² by crystallization from solution. Along the same lines, GXLs have been used as HPLC mobile phases to perform separations in reversed-phase HPLC,¹³ size-exclusion chromatography,¹⁴ and chiral separations.¹⁵

Because the addition of CO₂ to traditional organic solvents changes a number of properties, including solvation properties, GXL systems have been used to some extent as solubility switches. In many cases, solutes that are soluble in CO₂-expanded solvents will fall out of solution when the CO₂ is removed and vice versa. For example, the addition of CO₂ to a biphasic system of a fluoruous solvent and an organic solvent causes the phases to become miscible.^{16, 17} The opposite effect is seen in cases of water-soluble organics and an aqueous phase, where the addition of CO₂ forces the phases to split.¹⁸ Both systems have applications in catalyst recycle and product recovery.

While much work has been done in the area of GAS and phase behavior, many more applications of GXLs are on the horizon. The advantages that GXLs as reaction media present over typical organic solvents are twofold: the gas-solubility enhancement^{3, 4} and the *in situ* formation of alkylcarbonic acid.¹⁹ The use of GXLs as reaction solvents has been explored to some degree.^{3, 19} The acid-catalyzed hydrolysis of β -pinene has proven successful in CO₂-expanded alcohols due to the formation of alkylcarbonic acid.²⁰

Before any of the above processes can be fully understood or optimally modeled, detailed knowledge of the cybotactic region of the CO₂-expanded liquids must be

ascertained. Since there is little data about the microstructure of GXLs it is instructive to see how data on the cybotactic region of supercritical fluids were measured and use that as a springboard for this task.

Studying the Cybotactic Region of Supercritical Fluids

A considerable amount of work has already been done studying the cybotactic region of supercritical fluids. Many of the same techniques will be used to probe the cybotactic region of GXLs. Some of the techniques that follow will be used in this particular study while others are discussed as a means for exploring potential areas of inhomogeneity in the cybotactic region.

Before one can fully appreciate nuances within the cybotactic region of a fluid, it is imperative to study bulk properties of that fluid in such a way that data about the cybotactic region can be deduced; for example by mathematical modeling and simulation. One way to do this is by using binary diffusion coefficients of a variety of solutes in that solvent and then using structure/property relationships to deconvolute effects in the cybotactic region. Molecular dynamics simulations can be used to “measure” the sensitivity of the diffusion coefficient to properties such as van der Waals forces, thus providing insight into the cybotactic region of the fluid.²¹

Binary diffusion coefficients have been measured for many solutes²² including substituted benzenes,²³⁻²⁸ ketones,^{29, 30} contaminants,³¹ flavor compounds,³² food dyes³³ and vitamins^{27, 30, 34} in supercritical CO₂.²² Regardless of what the solute is, the general trends are the same. Increased pressure – and therefore increased fluid density – results in decreased binary diffusion coefficients (Figure 2-2).²² Increased temperature leads to increased diffusivity (Figure 2-2).²² For homologous series, increased chain length or

other steric effects also result in slower diffusion.^{23, 29} Diffusion coefficients decrease as a function of fluid viscosity (Figure 2-3).²²

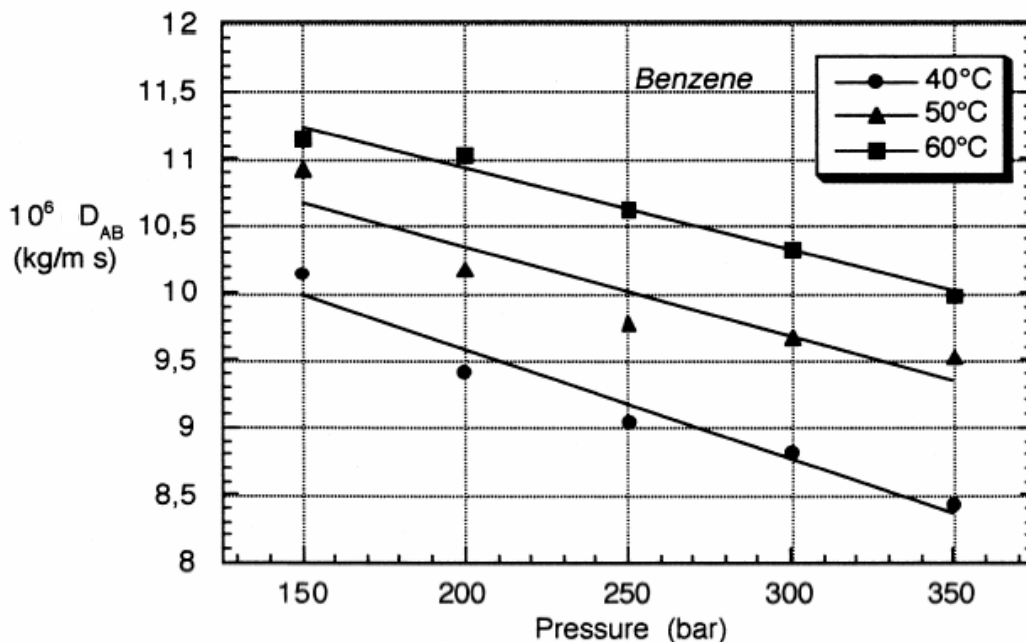


Figure 2-2: Diffusion coefficient of benzene in supercritical CO₂ as a function of pressure and temperature.²²

There are a variety of model reactions that probe solvent effects in the cybotactic region of supercritical fluids and gas-expanded liquids. The *cis-trans* isomerization of a substituted azobenzene is an excellent probe for solvent polarity as it equilibrates faster in more polar media.³⁵⁻³⁷ When studied in supercritical CO₂, the reaction rate increases with increased pressure, and therefore density, indicating an increase in solvation, and therefore probably polarity, in the cybotactic region of this probe molecule.³⁸

Several researchers use Diels-Alder reactions to study local polarity, solvent strength and other solvent effects. In most cases, the transition state of the reaction tends to be slightly more polar than the substrate and therefore it interacts more strongly with the polar solvents.³⁹⁻⁴² In other words, the more polar the surrounding medium, the more

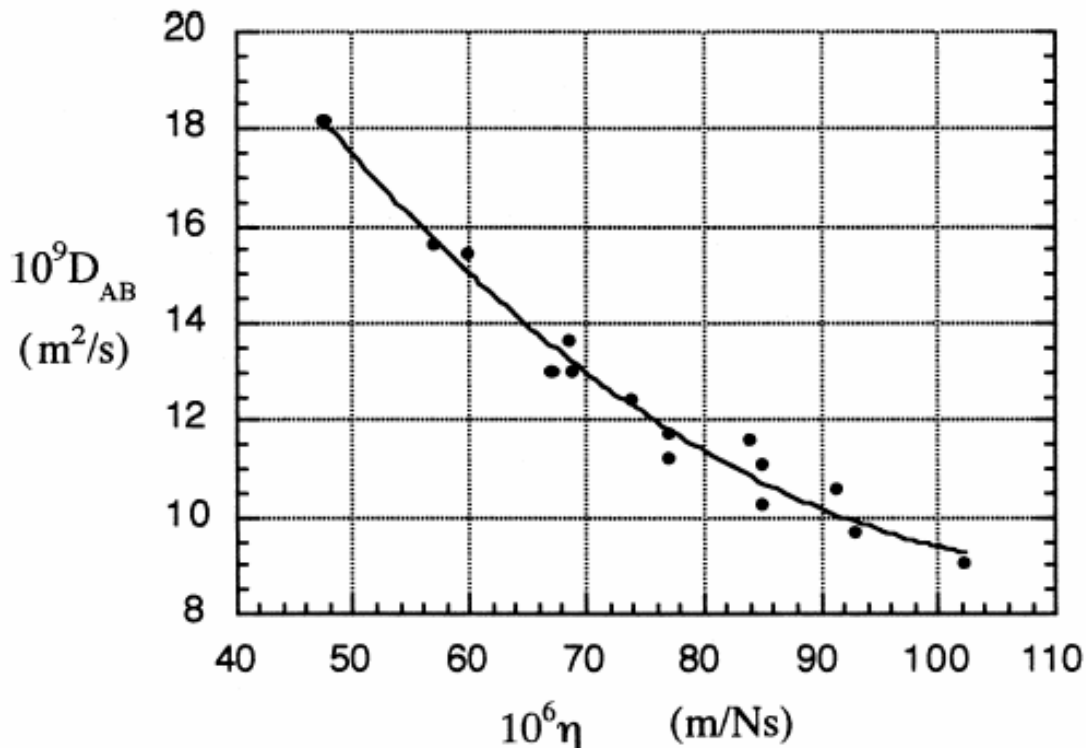


Figure 2-3: Diffusion coefficient of benzene in supercritical CO₂ as a function of fluid viscosity.²²

stable the transition state and therefore the faster the reaction. Thus, with few exceptions,⁴² the rates of Diels-Alder reactions in supercritical and liquid CO₂ are generally somewhat slower than those observed in traditional solvents due to their non-polar nature.^{43, 44} Also, most studies indicate that increasing the fluid density / pressure increases the observed reaction rate,⁴⁰ with exceptions having been observed in the vicinity of the mixture critical point.⁴² Selectivities of Diels-Alder reactions in scCO₂ are comparable to those observed in hydrocarbon solvents and tend to be slower than those in polar solvents.⁴¹

In the case of the cycloaddition between 9-hydroxymethylantracene and *N*-ethylmaleimide, reaction in non-polar solvents increases the rate of reaction.³⁹ This is a result of solvophobic effects,⁴¹ transition state destabilization as a result of the

surrounding solvent, and clustering, where the diene and dienophile tend to hydrogen bond with each-other, thus forming clusters from preferential solvation.³⁹ Such clusters are enhanced by a decrease in solvent polarity. Consistent with other local polarity probes, the rate of this particular Diels-Alder reaction is increased in supercritical CO₂ as compared to polar solvents, indicating that the cybotactic region exhibits decreased polarity. Furthermore, the rate decreases with CO₂ pressure, indicating that the local polarity must increase with an increase in pressure, which is also consistent with the aforementioned studies.^{38, 40, 42}

Reaction kinetics is not the only probe for local polarity and other solvent effects. Solvatochromism is a widely used technique for understanding solvent polarity in the cybotactic region because shifts are very sensitive to changes in the local environment of the dilute solute. The Kamlet-Taft parameter, π^* ,⁴⁴ and E_T ⁴⁰ values of a variety of solvatochromic indicators have been used to study changes in local polarity as a function of pressure, and therefore density, in the cybotactic region of supercritical CO₂. Whether the probe is 4-nitroanisole, 4-nitroaniline, phenol blue, pyridinium *N*-phenoxide betaine dye, or any of the many other probes, the value of π^* or E_T increases with increasing pressure and density of the supercritical fluid, indicating an increase in polarity in the cybotactic region of the probe molecule with an increase in CO₂ density. Such findings are consistent with the Diels-Alder studies mentioned above.^{39, 41, 42}

Polarity is not the only effect that has been studied in the cybotactic region of supercritical CO₂. A variety of sources report clustering or aggregation of solvent molecules about solutes in the cybotactic region around the critical point of CO₂.⁴⁵ Local densities in supercritical fluids have been reported as larger than the bulk densities.

Furthermore, density measurements as a function of solute composition indicate that molal volumes of nonvolatile organic solutes, namely naphthalene, camphor and tetrabromomethane, near the critical point of CO₂ get very large and negative in magnitude relative to the bulk partial molal volume of the solvent, also consistent with the aforementioned clustering.⁴⁵

Product distributions of the Diels-Alder reaction between isoprene and maleic anhydride or methyl acrylate in supercritical CO₂ have been studied as a function of pressure, with particular attention given to the critical region.⁴⁰ In both cases, the product distribution is very sensitive to pressure especially near the critical point. In the case of isoprene reacting with methyl acrylate, around the critical point the product distribution is approximately 50% of each isomer. As pressure is increased, the product distribution approaches that of conventional solvents. This result is attributed to steric effects – the clustering of the CO₂ around the diene holds it in place, allowing a product that would normally be sterically hindered from formation.⁴⁰

Cybotactic region probing has not been limited to supercritical CO₂. Local densities in several other supercritical fluids have been reported as larger than the bulk densities. As in the cases mentioned above, the cybotactic region within these solvents can be elucidated by studying solvatochromic shifts of dilute solutes.^{46, 47} Supercritical ethylene, fluoroform and chlorotrifluoromethane have all been studied by analyzing shifts of phenol blue.⁴⁶ Solvatochromic shift data of 9-(α -perfluoroheptyl- β,β -dicyanovinyl) julolidine have been used to characterize the solvent strength of sub- and supercritical ethane, propane and dimethyl ether.⁴⁷ Much like in the case of supercritical CO₂, there

appears to be clustering of these solvent molecules, or local density enhancements, around the solute near the critical density.

One way in which the clustering manifests itself is in terms of the solvent's spectral polarity index values (P_s),⁴⁸ the normalized transition energy scale that has been referenced to that of perfluorohexane, which show a maximum at the solvent's critical density. The larger the P_s value, the greater solvent strength. Deviations towards higher values of P_s translate to enhanced cohesive energy density, indicating that the transition energy for the dye is lower than expected. Thus the excited state is more stabilized than expected. This behavior is attributed to an enhancement of the local density in the cybotactic region of the solute molecule compared to the bulk density of the solvent near the solvent's critical point.^{46, 47, 49}

Polarities and aggregation in the cybotactic region of supercritical mixtures of CO₂ with methanol⁵⁰ and propanol⁵¹ have been measured by studying solvatochromic shifts, namely π^* , of 4-nitroanisole⁵⁰ and 2-nitroanisole.⁵¹ In both cases a drastic increase in the solvent polarity for the supercritical mixtures with an increase in system pressure is observed. Furthermore, the local composition of methanol in the cybotactic region of the probe molecule was much higher than the bulk composition and decreased in pressure (Figure 2-4). The maximum is indicative of competing effects: likely the preferable solvation of 4-nitroanisole by more polar but less compact methanol molecules at low pressure and the creation of a more compact solvation shell by CO₂ molecules at higher pressures. These differences between the bulk and cybotactic region are attributed to van der Waals forces.

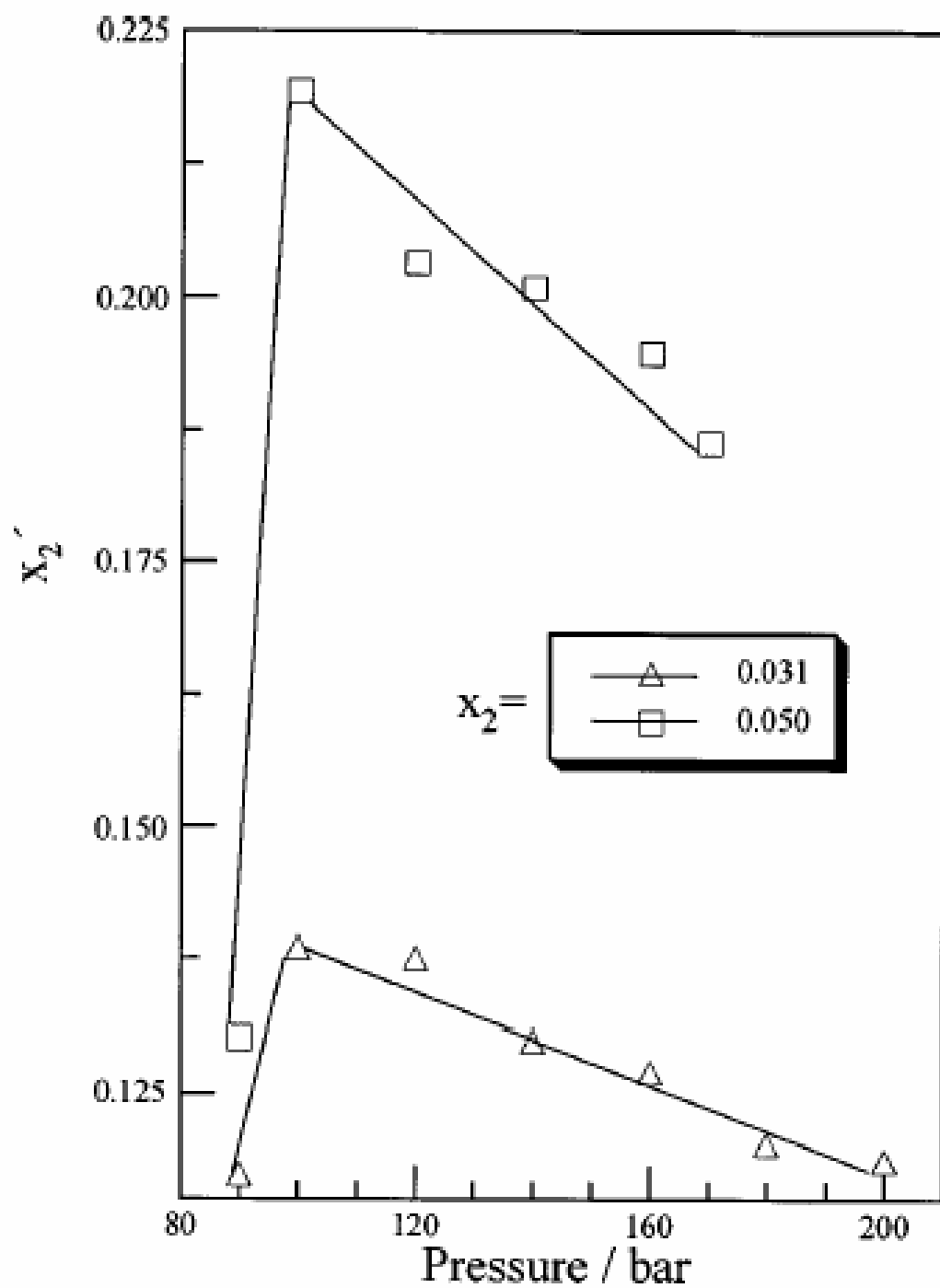


Figure 2-4: Local mole fractions of methanol in the cybotactic region of 4-nitroanisole vs. pressure for two different bulk mole fractions.⁵⁰

Langmuir adsorption equilibria calculations were applied to determine the number of solvent molecules in the first solvation shell as a function of fluid density. Comparing the results with known density data, it was determined that for densities between 0.3-0.9 g/cm³, 4-nitroanisole could accommodate eight molecules in its cybotactic region, with anywhere from three to five CO₂ molecules depending on the fluid density.

In this study, some of the same techniques are used to explore the cybotactic region of gas-expanded liquids. Solid solubility measurements and models are used to understand solvent-solute interactions of non-expanded solvents as a jumping-off point for studying gas-expanded liquids. Diffusion coefficients are measured for a variety of nitrogen-containing conjugated ring compounds in an effort to study differences in the response of the cybotactic region to the different compounds. Reactions and solvatochromic measurements in CO₂-expanded solvents provide insight on polarity effects as a function of CO₂ composition and potential clustering effects. Fluorescence of a chromophore in an effort to understand clustering as a function of CO₂ composition is employed in several GXL systems. Knowledge of the cybotactic region of gas-expanded liquids obtained in this work will open new avenues of pursuit for using these environmentally benign solvent systems in chemical processing.

REFERENCES

1. Chang, C. J.; Chiu, K.-L.; Day, C.-Y., A new apparatus for the determination of P-x-y diagrams and Henry's constants in high pressure alcohols with critical carbon dioxide. *J. Supercrit. Fluids* **1998**, 12, 223-237.
2. de la Fuente Badilla, J. C.; Peters, C. J.; de Swann Arons, J., Volume expansion in relation to the gas-antisolvent process. *J. Supercrit. Fluids* **2000**, 19, 13-23.
3. Wei, M.; Ghezai, T. M.; Busch, D. H.; Subramaniam, B., Carbon dioxide-expanded solvents: Unique and versatile media for performing homogeneous catalytic oxidations. *J. Am. Chem. Soc.* **2002**, 124, (11), 2513-2517.
4. Musie, G.; Wei, M.; Subramaniam, B.; Busch, D. H., Catalytic oxidations in carbon dioxide-based reaction media, including novel carbon dioxide-expanded phases. *Coord. Chem. Rev.* **2001**, 219-2211, 789-820.
5. Kordikowski, A.; Schenk, A. P.; Van Nielen, R. M.; Peters, C. J., Volume expansions and vapor-liquid equilibria of binary mixtures of a variety of polar solvents and certain near-critical solvents. *J. Supercrit. Fluids* **1995**, 8, 205-216.
6. Zagrobelny, J.; Betts, T. A.; Bright, F. V., Steady-state and time resolved fluorescence investigations of pyrene excimer formation in supercritical carbon dioxide. *J. Am. Chem. Soc.* **1992**, 114, 5249-5257.
7. Zagrobelny, J.; Bright, F. V., Influence of solute-fluid clustering on the photophysics of pyrene emission in supercritical ethane and trifluoromethane. *J. Am. Chem. Soc.* **1992**, 114, (20), 7821-7826.
8. Winters, M. A.; Knutson, B. L.; Debenedetti, P. G.; Sparks, H. G.; Przybycien, T. M.; Stevenson, C. L.; Prestrelski, S. J., Precipitation of proteins in supercritical carbon dioxide. *J. Pharmaceutical Sciences* **1996**, 85, (6), 586-594.
9. Gallagher, P. M.; Coffey, M. P.; Krukoni, V. J.; Hillstrom, W. W., Gas antisolvent recrystallization of RDX: Formation of ultra-fine particles of a difficult-to-comminute explosive. *J. Supercrit. Fluids* **1992**, 5, (2), 130-142.
10. Reverchon, E.; Della, G., Production of anti-biotic micro- and nano-particles by supercritical antisolvent precipitation. *Powder Technology* **1999**, 106, (1), 23-29.

11. Shishikura, A.; Kanamori, K.; Takahashi, H.; Kinbara, H., Separation and purification of organic acids by gas antisolvent crystallization. *J. Agric. Food Chem.* **1994**, 42, 1993-1997.
12. Chang, C. J.; Randolph, A. D., Separation of beta-carotene mixtures precipitated from liquid solvents with high-pressures of carbon dioxide. *Biotechnol. Prog.* **1991**, 7, 275-276.
13. Lee, S. T.; Olesik, S. V.; Fields, S. M., Applications of reversed-phase high performance liquid chromatography using enhanced fluidity liquid mobile phases. *J. Microcolumn Sep.* **1995**, 7, (5), 477-483.
14. Yun, H.; Olesik, S. V.; Marti, E. H., Improvements in polymer characterization by size-exclusion chromatography and liquid chromatography at the critical condition by using enhanced-fluidity liquid mobile phases with packed capillary columns. *Anal. Chem.* **1998**, 70, (3298-3303).
15. Sun, Q.; Olesik, S. V., Chiral separations performed by enhanced-fluidity liquid chromatography on a macrocyclic antibiotic chiral stationary phase. *Anal. Chem.* **1999**, 71, 2139-2145.
16. Ablan, C. D.; Hallett, J. P.; West, K. N.; Jones, R. S.; Eckert, C. A.; Liotta, C. L.; Jessop, P. G., Use and recovery of a homogenous catalyst with carbon dioxide as a solubility switch. *Chem. Comm.* **2003**, 24, 2972-2973.
17. West, K. N.; Hallett, J. P.; Jones, R. S.; Bush, D.; Liotta, C. L.; Eckert, C. A., Carbon dioxide-induced miscibility of fluoruous and organic solvents for recycling homogeneous catalysts. *Ind. Eng. Chem. Res.* **2004**, 43, (16), 4827-4832.
18. Lu, J.; Lazzaroni, M. J.; Hallett, J. P.; Bommarius, A. S.; Liotta, C. L.; Eckert, C. A., Tunable solvents for homogenous catalyst recycle. *Ind. Eng. Chem. Res.* **2004**, 43, (7), 1586-1590.
19. West, K. N.; Wheeler, C.; McCarney, J. P.; Griffith, K. N.; Bush, D.; Liotta, C. L.; Eckert, C. A., In situ formation of alkylcarbonic acids carbon dioxide. *J. Phys. Chem.* **2001**, 105, (3947-3948).
20. Chamblee, T. S.; Weikel, R. R.; Nolen, S. A.; Liotta, C. L.; Eckert, C. A., Reversible in situ acid formation for beta-pinene hydrolysis using carbon dioxide expanded liquid and hot water. *Green Chemistry* **2004**, 6, 382-386.
21. Coelo, L. A. F.; de Oliveira, J. V.; Tavares, F. W.; Matthews, M. A., Role of attractive forces in self-diffusion and mutual diffusion in dense simple fluids and real substances. *Fluid Phase Equilibria* **2002**, 194-197, 1131-1140.

22. Suarez, J. J.; Medina, I.; Bueno, J. L., Diffusion coefficients in supercritical fluids: Available data and graphical correlations. *Fluid Phase Equilibria* **1998**, 153, 167-212.
23. Bueno, J. L.; Saurez, J. J.; Dizy, J.; Medina, I., Infinite dilution diffusion coefficients: benzene derivatives as solutes in supercritical carbon dioxide. *J. Chem. Eng. Data* **1993**, 38, 344-349.
24. Sassiati, P. R.; Mourier, P.; Caude, M. H.; Rosset, R. H., Measurement of diffusion coefficients in supercritical carbon dioxide and correlation with the equation of Wilke and Chang. *Anal. Chem.* **1987**, 59, 1164-1170.
25. Gonzalez, L. M.; Bueno, J. L.; Medina, I., Measurement of diffusion coefficients for 2-nitroanisole, 1,2-dichlorobenzene and tert-butylbenzene in carbon dioxide containing modifiers. *J. Supercrit. Fluids* **2002**, 24, 219-229.
26. Gonzalez, L. M.; Bueno, J. L.; Medina, I., Determination of binary diffusion coefficients of anisole, 2,4-dimethyl phenol and nitrobenzene in supercritical carbon dioxide. *Ind. Eng. Chem. Res.* **2001**, 40, 3711-3716.
27. Funazukuri, T.; Kong, C. Y.; Kagei, S., Measurements of binary diffusion coefficients for some low volatile compounds in supercritical carbon dioxide by input-output response technique with two diffusion columns connected in series. *Fluid Phase Equilibria* **2002**, 194-197, 1169-1178.
28. Funazukuri, T.; Kong, C. Y.; Kagei, S., Infinite dilution binary diffusion coefficients of benzene in carbon dioxide by the Taylor dispersion technique at temperatures from 308.15 to 328.15 K and pressures from 6 to 30 MPa. *Int. J. Thermophys.* **2001**, 22, (6), 1643-1660.
29. Funazukuri, T.; Kong, C. Y.; Kagei, S., Infinite-dilution binary diffusion coefficients of 2-propanone, 2-butanone, 2-pentanone, and 3-pentanone in carbon dioxide by the Taylor dispersion technique from 308.15 K in the pressure range from 8-35 MPa. *Int. J. Thermophys.* **2000**, 21, (6), 1279-1290.
30. Funazukuri, T.; Kong, C. Y.; Murooka, N.; Kagei, S., Measurements of binary diffusion coefficients and partition ratios for acetone, phenol, alpha-tocopherol and beta-carotene in supercritical carbon dioxide with a poly(ethylene glycol)-coated capillary column. *Ind. Eng. Chem. Res.* **2000**, 39, 4462-4469.
31. Fu, H.; Coelo, L. A. F.; Matthews, M. A., Diffusion coefficients of model contaminants in dense CO₂. *J. Supercrit. Fluids* **2000**, 18, 141-155.
32. Filho, C. A.; Silva, C. M.; Quadri, M. B.; Macedo, E. A., Tracer diffusion coefficients of citral and D-limonene in supercritical carbon dioxide. *Fluid Phase Equilibria* **2003**, 204, 65-73.

33. Mantell, C.; Rodriguez, M.; Martinez de la Ossa, E., Measurement of the diffusion coefficient of a model food dye (malvidin 3,5-diglucoside) in a high pressure carbon dioxide-methanol system by the chromatographic peak-broadening technique. *J. Supercrit. Fluids* **2003**, *25*, 57-68.
34. Funazukuri, T.; Ishiwata, Y., Diffusion coefficients of linoleic acid methyl ester, vitamin K3 and indole in mixtures of carbon dioxide and n-hexane at 313.2 K, and 16.0 MPa and 25.0 MPa. *Fluid Phase Equilibria* **1999**, *164*, 117-129.
35. Schanze, K. S.; Mattox, T. F.; Whitten, D. G., Solvent effects on the thermal cis-trans isomerization and charge-transfer absorption of 4-(diethylamino)-4'-nitroazobenzene. *J. Org. Chem.* **1983**, *48*, (17), 2808-2813.
36. Asano, T.; Okada, T., Thermal Z-E isomerization of azobenzenes. The pressure, solvent and substituent effects. *J. Org. Chem.* **1984**, *49*, (23), 4387-4391.
37. Asano, T.; Yano, T.; Okada, T., Mechanistic study of thermal - Z-E isomerization of azobenzenes by high-pressure kinetics. *J. Am. Chem. Soc.* **1982**, *104*, (18), 4900-4904.
38. Dillow, A. K.; Brown, J. S.; Liotta, C. L.; Eckert, C. A., Supercritical fluid tuning of reaction rates: The cis-trans isomerization of 4-4'disubstituted azobenzenes. *J. Phys. Chem. A* **1998**, *102*, (39), 7609-7617.
39. Garcia, J. I.; Mayoral, J. A.; Salvatella, L., Solvent effects on the 9-hydroxymethylanthracene + N-ethylmaleimide Diels-Alder reaction. A theoretical Study. *J. Org. Chem.* **2005**, *70*, (4), 1456-1458.
40. Ikushima, Y.; Saito, N.; Arai, M., Supercritical carbon dioxide as reaction medium: examination of its solvent effects in the near-critical region. *J. Phys. Chem.* **1992**, *96*, 2293-2297.
41. Qian, J.; Timko, M. T.; Allen, A. J.; Russell, C. J.; Winnik, B.; Buckley, B.; Steinfeld, J. I.; Tester, J. W., Solvophobic acceleration of Diels-Alder reactions in supercritical carbon dioxide. *J. Am. Chem. Soc.* **2004**, *126*, (17), 5465-5474.
42. Thompson, R. L.; Glaser, R.; Bush, D.; Liotta, C. L.; Eckert, C. A., Rate variations of a hetero-Diels-Alder reaction in supercritical fluid carbon dioxide. *Ind. Eng. Chem. Res.* **1999**, *38*, 4220-4225.
43. Hyatt, J. A., Liquid and supercritical carbon dioxide as organic solvents. *J. Org. Chem.* **1984**, *49*, 5097-5101.
44. Sigman, M. E.; Lindley, S.; Leffler, J. E., Supercritical carbon dioxide - Behavior and solvatochromic indicators in media of different densities. *J. Am. Chem. Soc.* **1985**, *49*, (107), 1471-1472.

45. Eckert, C. A.; Ziger, D. H.; Johnston, K. P.; Ellison, T. K., The use of partial molal volume data to evaluate equations of state for supercritical fluid mixtures. *Fluid Phase Equilibria* **1983**, 14, 167-175.
46. Kim, S.; Johnston, K. P., Molecular interactions in dilute supercritical fluid solutions. **1987**, 26, 1206-1213.
47. Lemert, R. M.; DeSimone, J. M., Solvatochromic characterization of near- and supercritical ethane, propane and dimethyl ether using 9-(α -perfluoroheptyl- β,β -dicyanovinyl)julolidine. *J. Supercrit. Fluids* **1991**, 4, 186-193.
48. Freed, B. K.; Biesecker, J.; Middleton, W. J., Spectral polarity index: A new method for determining the relative polarity of solvents. *J. Fluor. Chem.* **1990**, 48, 63-75.
49. Yonker, C. R.; Frye, S. L.; Kalkwarf, D. R.; Smith, R. D., Characterization of supercritical solvents using solvatochromic shifts. *J. Phys. Chem.* **1986**, 90, 3022-3026.
50. Bulgarevich, D. S.; Sako, T.; Sugeta, T.; Otake, K.; Sato, M.; Uesugi, M.; Kato, M., Microscopic Solvent Structure of Supercritical Carbon Dioxide and its Mixtures with Methanol in the Cybotactic Region of the Solute Molecule. *J. Chem. Phys.* **1998**, 108, (10), 3915-3921.
51. Yonker, C. R.; Smith, R. D., Solvatochromic behavior of binary supercritical fluids: the carbon dioxide/2-propanol system. *J. Phys. Chem.* **1988**, 92, 2374-2378.

CHAPTER III

EXPERIMENTAL DETERMINATION AND MODEL PREDICTION OF SOLID SOLUBILITY OF MULTI-FUNCTIONAL COMPOUNDS IN PURE AND MIXED NON-ELECTROLYTE SOLVENTS

Introduction

The knowledge of solid-liquid equilibria is of clear importance for the design of crystallization processes such as cooling-, evaporative-, and salting-out or anti-solvent crystallization. The MOSCED model has been applied successfully to the prediction of solid solubility in various pure and mixed organic solvents, including aqueous solvent mixtures.^{1,2} In this study the model is further applied to the correlation and prediction of newly-measured solubility values of some interesting, mostly unstudied multi-functional solids.

The application of this work leads to a new paradigm for solvent selection via thermodynamic models with a minimum of experimental data. Many complex compounds, especially pharmaceuticals and pharmaceutical pre-cursors, are thermally unstable. Thus there exists a need to develop purification techniques that can be performed using little to no heat. Crystallization is an obvious solution, but without a means to predict the solubility of the compounds it is difficult to know where to begin the solvent selection process. Furthermore, there are many cases where having mixtures of multiple solvents leads to better separation potential than pure solvents due to synergistic

effects, but predicting such mixtures is an even greater challenge.³⁻⁸ Currently, solvent selection for crystallization is costly and wasteful in time, energy and materials. The goal of this study is to develop a good predictive technique for solvent selection that would make developing a separation more cost efficient and environmentally benign.

The four compounds studied, 3-nitrophthalimide, 5-fluoroisatin, 2-amino-5-nitrobenzophenone, and benzimidazole (Figure 3-1) were chosen for their complexity. The interactions in solution resulting from the structures and functionalities of the compounds should test the MOSCED model adequately.

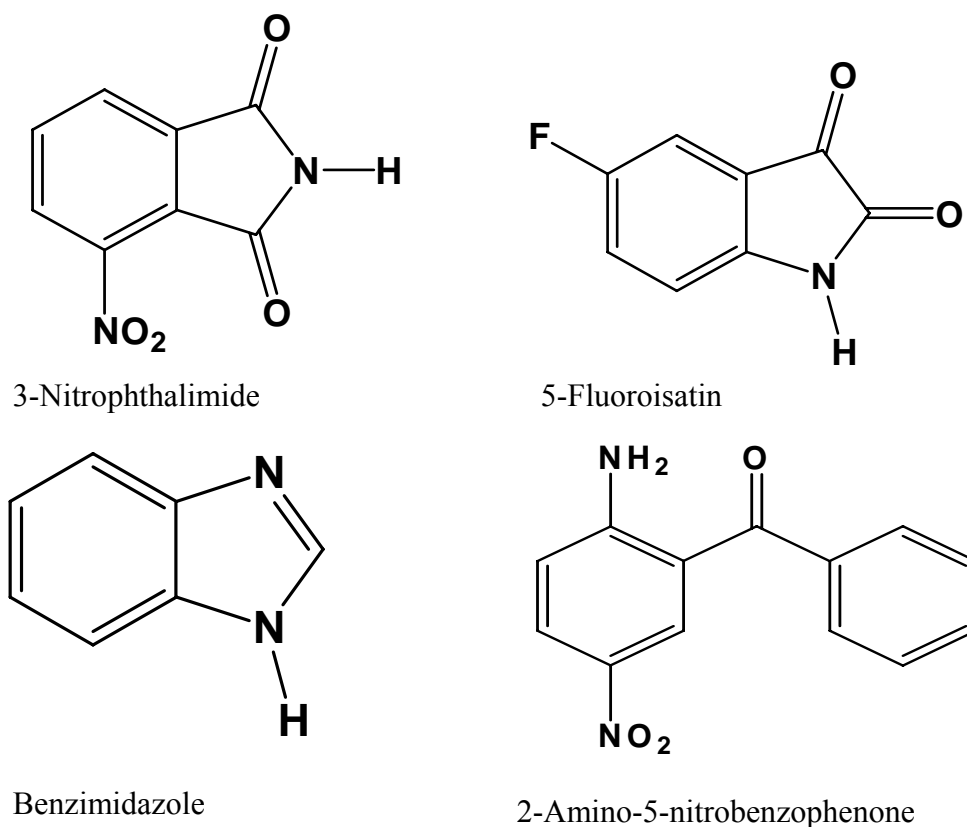


Figure 3-1: Structures of the solid compounds studied.

The organic solvents were chosen to represent a variety of types including polar aprotic, aromatic, and associated compounds and should give a good indication of the

possible solute-solvent interactions. The solubility is measured in several pure and mixed solvents that may potentially produce a synergistic effect on the solubility.

The two most prevalent methods for measuring solid-liquid equilibria are the dynamic (synthetic) method⁵ and the static (analytical) method.⁹ In the dynamic method the solubility is most often determined by adding a known amount of solid to a known amount of solvent and changing the temperature until the solution goes from a two phase solid-liquid equilibrium to a single liquid phase. This is similar to the cloud-point determinations often done for liquid-liquid equilibria, where a phase change is observed visually¹⁰.

In the static method a saturated liquid sample is equilibrated for a given amount of time after which a sample is carefully withdrawn and analyzed by physical or chemical analysis. In a variety of this technique known as the dry residue method¹¹ a sample of known mass and volume is drawn from the equilibrium liquid phase and put into an open container; the volatile solvent is then evaporated leaving only the solid solute. The mass of the remaining solid compared to the mass of the solvent evaporated, which is calculated by difference, can be used to determine the solubility. While this method is relatively easy to perform and requires only a good balance and a vacuum oven, it is limited to cases where the solubility of the solute is high, the solute has a negligible vapor pressure and the solvent is volatile.

Acree and coworkers have used another static technique in their measurement of the solubility of polyaromatic solids in organic solvents using an ultra-violet detector to measure the solubility. This method is superior to the above in that it can be used in cases where the solubility is low, but it is limited to solvents that do not have UV

signatures. In this study the solid-liquid equilibria data were measured with a static method using a gas chromatograph with flame ionization detector for composition analysis because it provides the capability to prepare the equilibrium mixtures of the solutes in all the solvents and analyze them with an automatic sampler simultaneously.

Background on MOSCED Model

The MOSCED model¹² is used to predict infinite dilution activity coefficients of the solids in the liquid solvents; parameters for the UNIQUAC or Wilson g^E model are fit to the limiting activity coefficients and the solid-liquid equilibria at finite concentrations are predicted for the pure and binary mixed solvents. The possible interactions in solution are discussed given the optimum pure component solute descriptors. The MOSCED model does not require extensive solubility data; rather data for a small but chemically diverse solvent set is sufficient to describe the possible interactions for a given solute.

The extension of the MOSCED model to predict activity coefficients for a saturated solution requires the calculation of the ideal solubility of the solid solute in the solvent. If one takes the standard state as the hypothetical sub-cooled liquid of the pure solid solute at the same temperature of the solution then the solubility can be found from equation 3-1 where ΔH_{fus} is the enthalpy of fusion at the melting point temperature T_m , R is the universal gas constant, ΔC_p is the difference in heat capacity of the sub-cooled liquid and crystalline solute, γ_s is the activity coefficient of the solid in the solution, x_s is the equilibrium concentration in the solution, and x^{ideal} is the ideal solubility and is independent of the solvent. Equation 3-1 makes the following assumptions: the difference between the molar volume of the liquid solute and solid is negligible, the

$$x^{ideal} = x_S \gamma_S = \exp \left[\frac{-\Delta H_{fus}}{RT_m} \left(\frac{T_m}{T} - 1 \right) - \frac{\Delta C_p}{R} \left(\ln \frac{T_m}{T} - \frac{T_m}{T} + 1 \right) \right] \quad \text{Eq. 3-1}$$

difference between the heat capacity is insensitive to temperature changes and the triple point temperature is the same as the melting point temperature.

The infinite dilution activity coefficients of the solute in the liquid phase are calculated using MOSCED and used to fit interaction parameters for the g^E model. The activity coefficient (γ_S) and mole fraction concentration of the solute in the liquid phase (x_S) are found that satisfy the relationship in equation 3-1. The solute MOSCED parameters are found by minimizing the sum of squared error between experimental and calculated solubility values. A Visual Basic program is used to perform this calculation, a flow chart of the procedure exists in Figure 3-2. The prediction made by the MOSCED model yields an activity coefficient value for both the dilute hypothetical sub-cooled liquid solute in the liquid solvent phase and the activity coefficient of the dilute liquid in the hypothetical sub-cooled liquid. Both activity coefficients are used to find the interaction parameters in the two-parameter activity coefficient model. The solid phase in equilibrium with the saturated liquid solution is assumed to be pure solute and contain no liquid solvent; therefore the activity of the dilute liquid solvent in the sub-cooled liquid solute is only an artifact of the calculation technique.

It is important to note that MOSCED is used instead of UNIFAC because the molecules are too complex for UNIFAC to handle. While there are parameters for many groups, it is not comprehensive enough to be able to reconcile the interactions of multifunctional ring-compounds.¹³

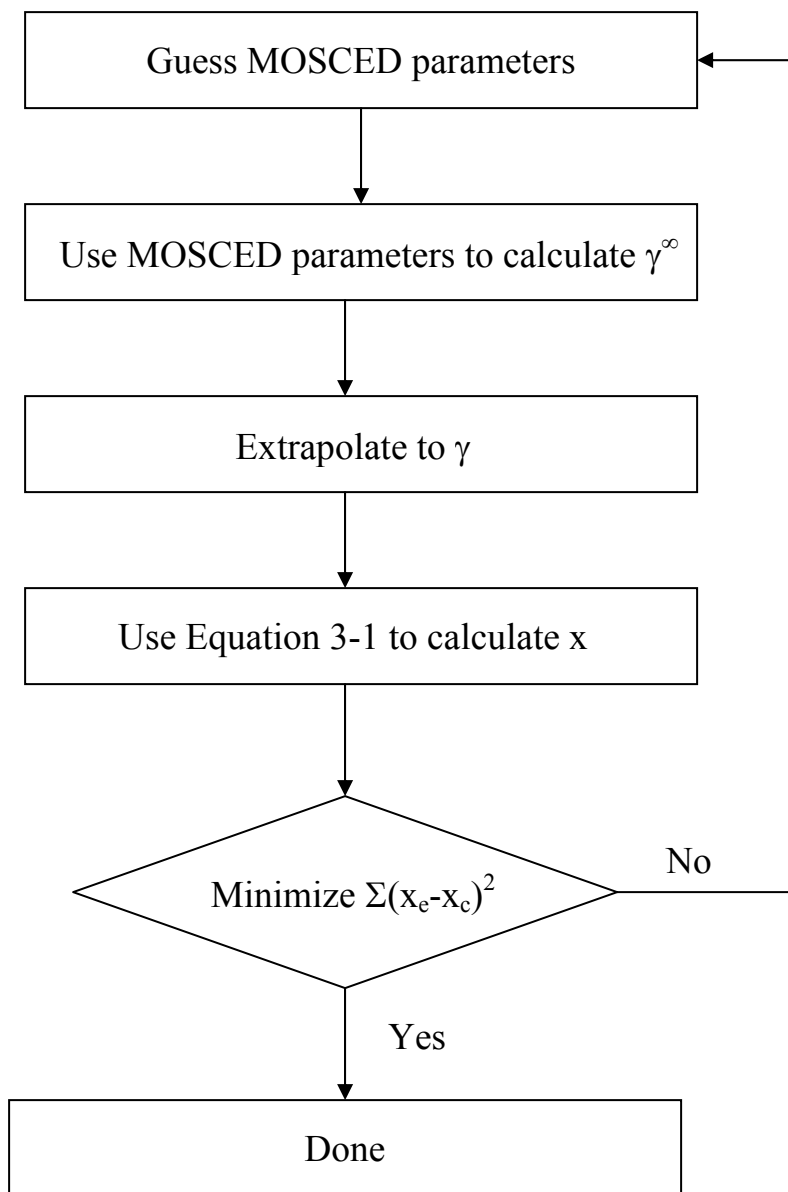


Figure 3-2: Flow chart for procedure to determine MOSCED parameters.

Experimental

Materials

The liquid organic solvents were used as received and include: methanol (Aldrich, HPLC, 99.93%), ethanol (Aldrich, anhydrous, 99.5%), 2-propanol (Aldrich, anhydrous, 99.5%), 2-butanone (Aldrich, 99.8+%), ethyl acetate (Fisher, ACS, 99.9%), chloroform

(Aldrich, 99.8%), dichloromethane (Riedel-deHaën, 99.8%), acetonitrile (Aldrich, HPLC, 99.93%), nitromethane (Aldrich, HPLC, 98.7%), dioxane (Aldrich, 99+%), N,N-dimethylformamide (Aldrich, anhydrous, 99.8%), toluene (Aldrich, anhydrous, 99.8%), cyclohexane (Aldrich, anhydrous, 99.5%), heptane (Aldrich, HPLC, 99+%) benzyl alcohol (Aldrich, 98%) and chlorobenzene (Aldrich, 99%).

All solids were used as received: Benzil (Aldrich, 98%), phenanthrene (Aldrich, 98%), 2-amino-5-nitrobenzophenone (Acros, 98+%), 5-fluoroisatin (Acros, 98%), 3-nitrophthalimide (Acros, 97%) and benzimidazole (Acros, 98%).

Apparatus and Methods

Two methods were used to determine equilibrium solubility of the solids in the organic solvents. The two methods are essentially identical except for how the saturated solution is sampled and whether the sample is diluted prior to analysis. For the first method, equilibrium solutions were prepared in glass vials containing both a solid and liquid phase, sealed with a plastic lined cap (Fisher, 02-912-058) and placed in a temperature-controlled water bath. The saturated solutions were agitated for three to five days to ensure equilibrium. A sample of known volume of the saturated liquid phase was removed from the vial using a volumetric pipette accurate to ± 0.005 ml and the sample mass recorded. The sample was diluted with acetone, up to a 25:1 ratio. The concentration of the sample was determined using a GC-FID with a calibration curve for the response prepared over a concentration range. To determine the accuracy of this method it was compared to the experimental data for the solubility of benzil¹⁴ and phenanthrene¹⁵ in several different solvents. The results are compared to the literature values in Table 3-1.

Table 3-1: Experimental solubility vs. literature values using the dilution method for anthracene at 298 K.

| Solute | Solvent | x^{exp} | x^{lit} | %AAD |
|--------------|---------------|------------------|------------------|--------|
| Benzil | Methanol | 0.00738 | 0.00783 | -5.7% |
| Benzil | 2-Propanol | 0.00837 | 0.00831 | 0.7% |
| Benzil | Ethyl Acetate | 0.13768 | 0.14550 | -5.4% |
| Benzil | Toluene | 0.13474 | 0.15040 | -10.4% |
| Benzil | Cyclohexane | 0.01107 | 0.01068 | 3.7% |
| Phenanthrene | Methanol | 0.00543 | 0.00589 | -7.8% |
| Phenanthrene | Ethanol | 0.01282 | 0.01114 | 15.1% |
| Phenanthrene | Cyclohexane | 0.03943 | 0.03648 | 8.1% |
| Phenanthrene | 1-Octanol | 0.05672 | 0.05418 | 4.7% |
| Phenanthrene | Ethyl Acetate | 0.13443 | 0.14990 | -10.3% |
| Phenanthrene | 1,4-Dioxane | 0.21352 | 0.21650 | -1.4% |

For sparingly soluble solids a second method was used that varied slightly from the above method. Equilibrium vials were prepared in the same way and placed in vials with pierceable septa. The sample vials were placed in a temperature-controlled sample tray and agitated periodically for three days. The sample tray was attached directly to an automatic sampler on the gas chromatograph and samples were taken directly from the equilibrium vials and injected directly on the GC column and analyzed by FID. To determine the accuracy of this method, the solubility of anthracene was compared to the literature values¹⁶ and the results are shown in Table 3-2. This method was used interchangeably with the above to determine the solubility of all four solids.

Table 3-2: Experimental solubility vs. literature values using the direct sampling method for anthracene at 298 K.

| Solute | Solvent | x^{exp} | x^{lit} | %AAD |
|------------|-----------------|------------------|------------------|------|
| Anthracene | Heptane | 0.00122 | 0.00157 | -22% |
| Anthracene | Cyclohexane | 0.00150 | 0.00157 | -5% |
| Anthracene | Toluene | 0.00713 | 0.00736 | -3% |
| Anthracene | Dioxane | 0.00698 | 0.00838 | -17% |
| Anthracene | Methanol | 0.00034 | 0.00025 | 35% |
| Anthracene | Acetone | 0.00376 | 0.00432 | -13% |
| Anthracene | Tetrahydrofuran | 0.01384 | 0.01204 | 15% |

The melting point was determined using a Mettler-Toledo melting point apparatus. The enthalpy of fusion at the melting point for all the solids was determined using differential scanning calorimetry at a heating rate of 5 °C/min under nitrogen flow.

Experimental Results and Discussion

In general, all solutes are very soluble in DMF and rather insoluble in alkanes, alcohols and chlorinated compounds. Solubility in DMF is always higher than ideal while alkanes are always lower. Mixtures including alcohols tend to show synergistic effects while mixtures of DMF and chloroform never exhibit them.

Pure Solvents

The solubility of 3-nitrophthalimide as a function of temperature in fifteen pure solvents is shown in Figure 3-3. The solubility increases with increasing temperature for

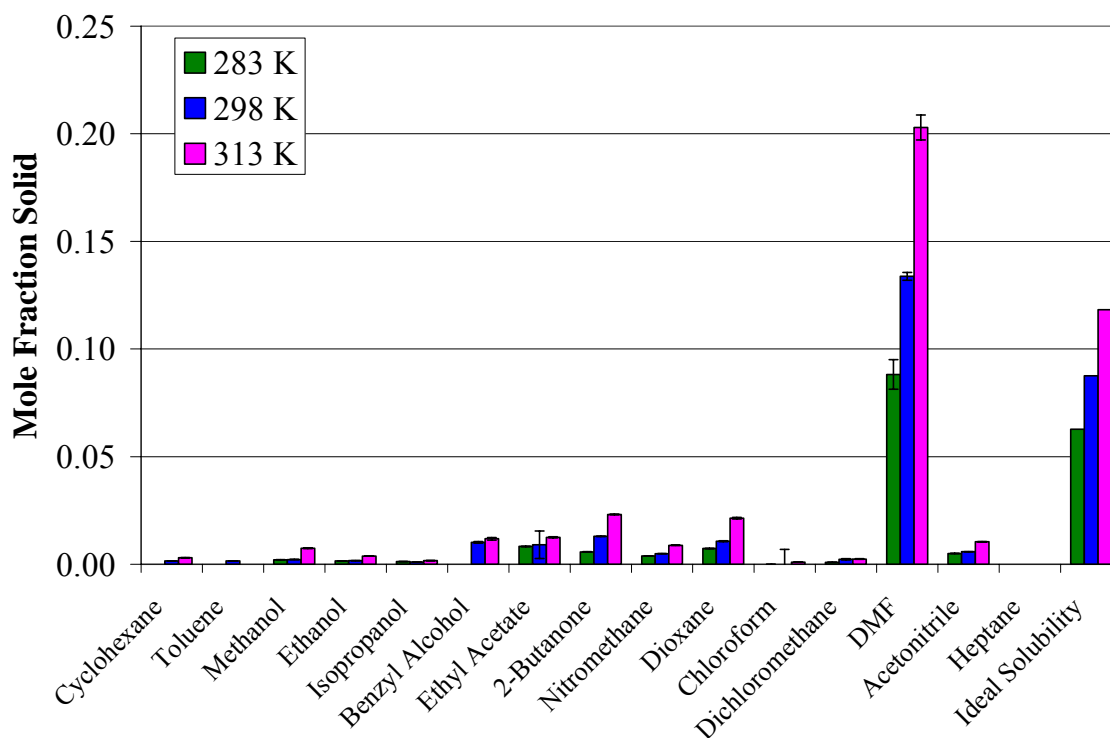


Figure 3-3: Solubility of 3-nitrophthalimide in various organic solvents at 283, 298 and 313 K.

all compounds. 3-Nitrophthalimide is most soluble in the very polar and strongly hydrogen bond-accepting compound N,N-dimethylformamide. For this solvent the solubility is greater than the ideal solubility, demonstrating strong specific interactions that most likely result from the acidic proton of the 3-nitrophthalimide hydrogen bonding with the basic moieties – namely the carbonyl group and the nitrogen atom – of the solvent. The solubility is lower in the relatively less basic solvents of 2-butanone, dioxane, ethyl acetate, acetonitrile and nitromethane. The solubility is lower still in the associated solvents of ethanol and 2-propanol. This indicates that the hydrogen bond association interactions of these solvents are stronger than solute-solvent interactions. In the acidic and essentially non-basic chlorinated solvents, the solubility is also small, indicating a weak hydrogen bond-accepting ability of the solute. The solubility is lowest in the non-polar, non-hydrogen bonding solvents of toluene and cyclohexane, most likely due to 3-nitrophthalimide's polarity and ability to hydrogen bond with itself.

The solubility of 5-fluoroisatin in the same fifteen solvents studied as a function of temperature is shown in Figure 3-4. The solubility trend is very similarly to that of the previously discussed 3-nitrophthalimide. The only exception is that for nitromethane the solubility does not appear to increase with increasing temperature. Nitromethane was difficult to sample due to its high density; sometimes particles would stay suspended and centrifugation did not always settle out all particles. This is not surprising considering the similarity in structure of the two molecules. The solubility is highest in the strongly basic and polar N,N-dimethylformamide, less so in the associated alcohol solvents, and least in the non-polar aromatic and alkane solvents. The characteristics of both 5-fluoroisatin and 3-nitrophthalimide in solution can thus be summarized as polar

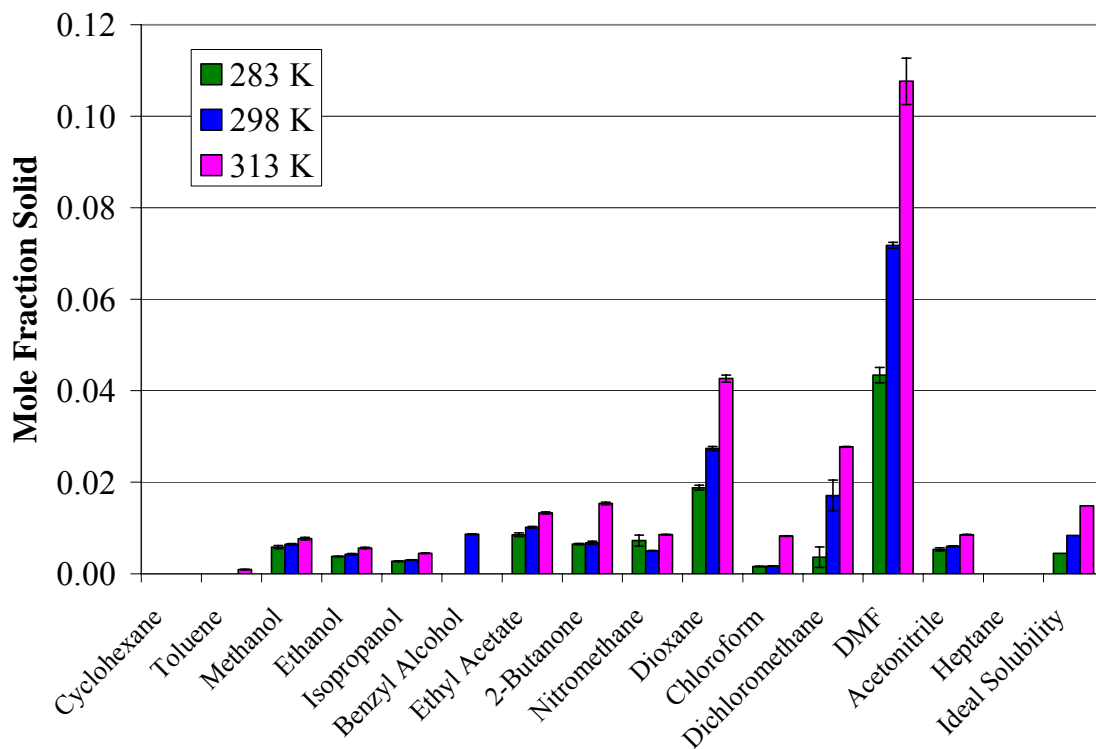


Figure 3-4: Solubility of 5-fluoroisatin in various organic solvents at 283, 298 and 313 K.

compounds with a strong hydrogen bond-donating ability and a weaker hydrogen bond accepting ability.

The solubility of benzimidazole in fifteen organic solvents at the same three temperatures is shown in Figure 3-5. The highest solubility by far is in the polar and basic solvent *N,N*-dimethylformamide. This is probably due to a strong dipolarity of the solute and a strong acidity as a result of the single hydrogen attached to a nitrogen. It is next most soluble in the hydrogen bonding alcohols, indicating the ability of the solute to donate a proton. While the previous two solids also have the ability to hydrogen bond, the proton in benzimidazole is even more acidic due to the electron-withdrawing and conjugated nature of the nitrogen-containing ring. The solubility is lower in non-basic chloroform, which hydrogen bonds more weakly than alcohols. In the relatively weaker

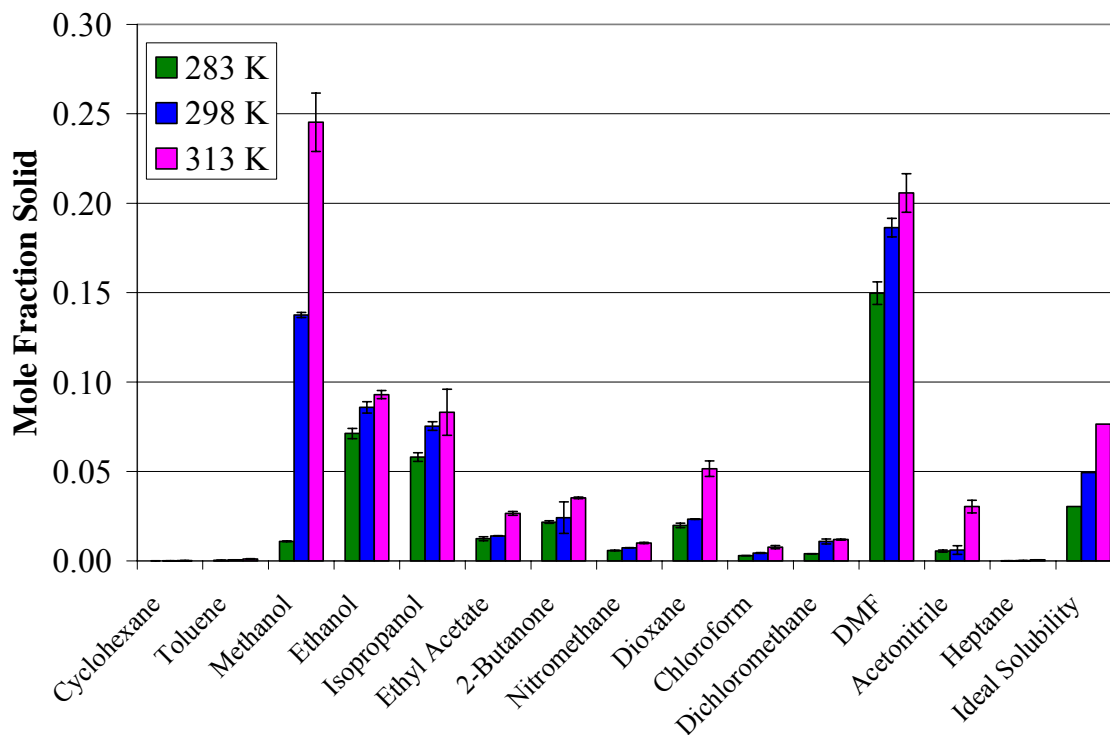


Figure 3-5: Solubility of benzimidazole in various organic solvents at 283, 298 and 313 K.

basic and aprotic solvents (when compared to DMF) of dioxane, 2-butanone, and nitromethane, the solubility is slightly less than the hydrogen bond-donating solvents. We can conclude the characteristics of benzimidazole in solution are a dipolar molecule with significant hydrogen bond acidity and therefore proton-donating ability.

The solubility of 2-amino-5-nitrobenzophenone in seventeen organic solvents as a function of temperature is shown in Figure 3-6. The solute is most soluble in the polar and basic solvents of benzonitrile, 2-butanone, and dioxane and slightly less but similarly soluble in the acidic and non-basic chlorinated solvents dichloromethane and chloroform. This is expected since the solute molecule contains both a strong hydrogen donating group (primary amine) that can associate with the basic solvents and a strong hydrogen bond donating group (nitro group) that can associate with the acidic solvents. This also

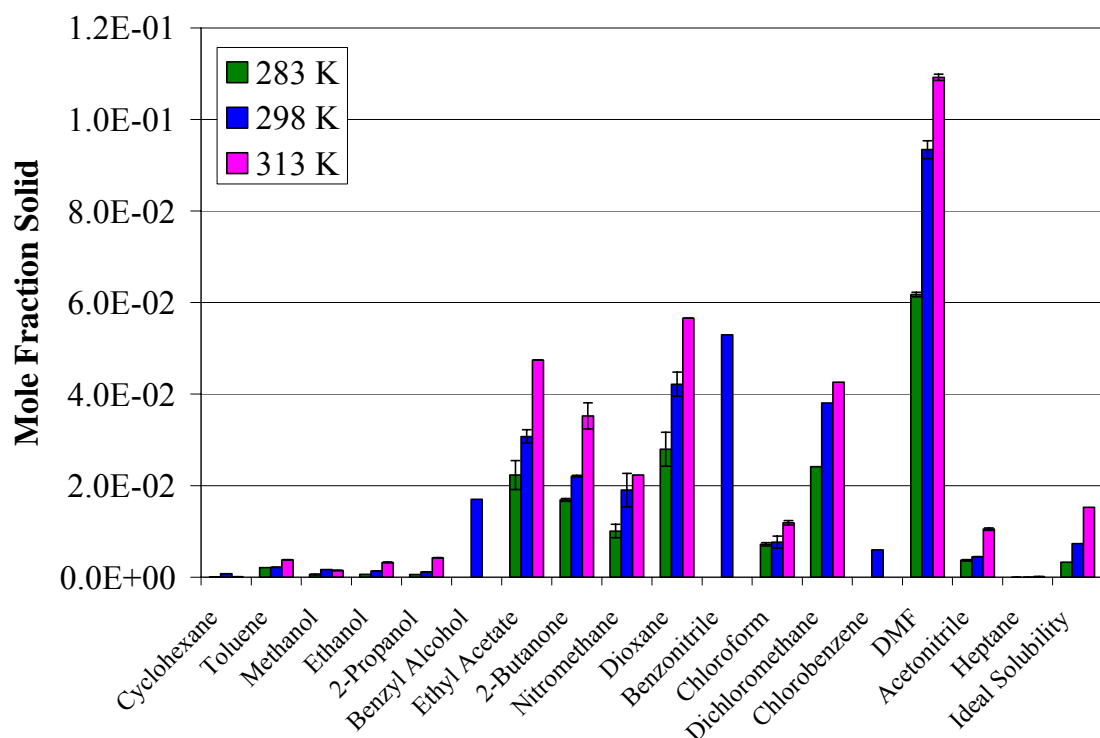


Figure 3-6: Solubility of 2-amino-5-nitrobenzophenone in various organic solvents at 283, 298 and 313 K.

indicates that the self association of the solute through hydrogen bonds is not strong enough to prevent solvation by these acidic and basic solvents. The solubility is lowest in the associated alcohol solvents indicating the strength of the hydrogen bond-donating and -accepting ability of the solute is less than that of the solvent.

All experimental data are summarized in Appendix A. In the thermodynamic modeling section the intuitive characterization of the solute molecules will be compared to the characteristic descriptors correlated from the MOSCED model.

Mixed Solvents

The solubilities of all four solids were measured at 283, 298 and 313 K in the mixed solvent pairs of ethanol + ethyl acetate, nitromethane + isopropanol, dioxane + 2-butanone and DMF + chloroform. Data are compared to model predictions and are

shown in this section but the prediction results will be discussed in the thermodynamic modeling section.

For 3-nitrophthalimide there is a maximum in solubility at 0.25 mole fraction of alcohol for both solvent pairs that contain an alcohol, with the maximum being the largest for the nitromethane + isopropanol pair at approximately twice the solubility in pure nitromethane at 40 °C. At sufficiently low alcohol concentrations in the mixed solvent, the alcohol will be less self-associated in solution without forming large hydrogen bond complexes and thus will be available to solvate the basic nitro- and carbonyl-groups of the 3-nitrophthalimide compound and result in an increase in solubility over that of the pure ethyl acetate or nitromethane solvent. The solubilities as a function of solvent composition for both solvent pairs are shown in Figures 3-7 and 3-8.

A similar effect seems to occur in the 2-butanone + dioxane system where a maximum occurs at 25% dioxane. Both the carbonyl groups of the 2-butanone and the oxygens in the dioxane have the ability to interact with the carbonyl- and nitro-groups of the solute, thus complimenting one another at an optimum solvent mixture. The effect appears to be most pronounced at 25 °C. Data are shown in Figure 3-9. For mixtures of chloroform and N,N-dimethyl formamide there does not seem to be any synergistic effect of the solvents. Solubility increases linearly as a function of increased DMF (Figure 3-10).

In the case of 5-fluoroisatin both alcohol-containing solvent pairs demonstrate similar behavior, with a maximum in solubility for both solvent pairs at 0.50 mole fraction of the solvent and at nearly twice the solubility of the more soluble pure component in the case of isopropanol + nitromethane. The solubilities as a function of

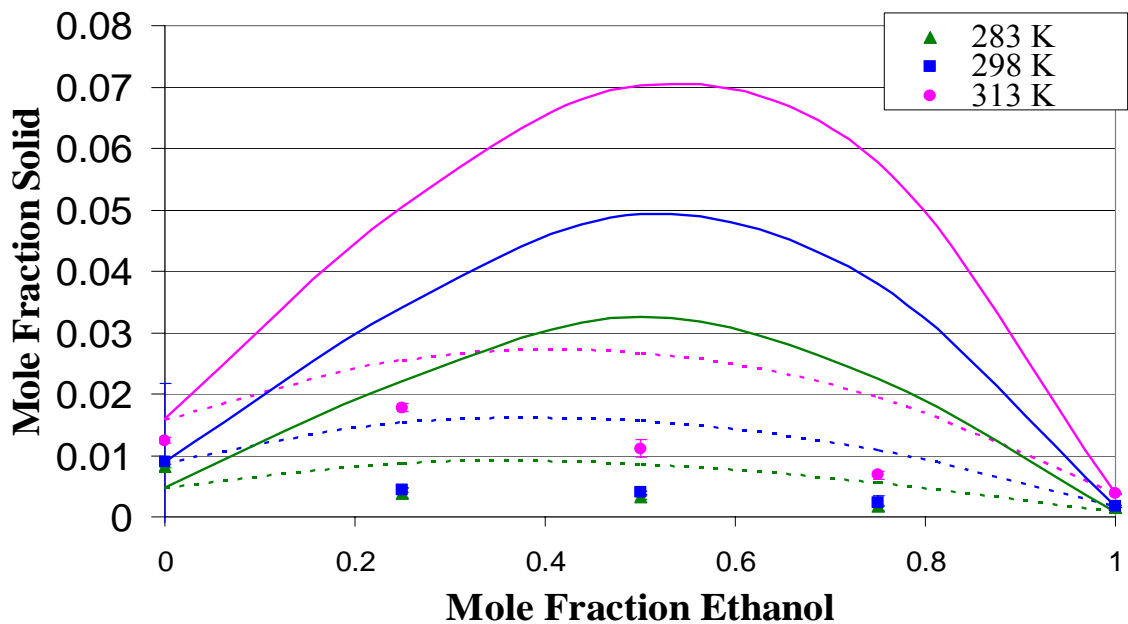


Figure 3-7: 3-Nitrophthalimide in mixtures of ethanol and ethyl acetate, measured data and predictions (solid lines UNIQUAC, dashed lines Wilson) at 283, 298 and 313 K.

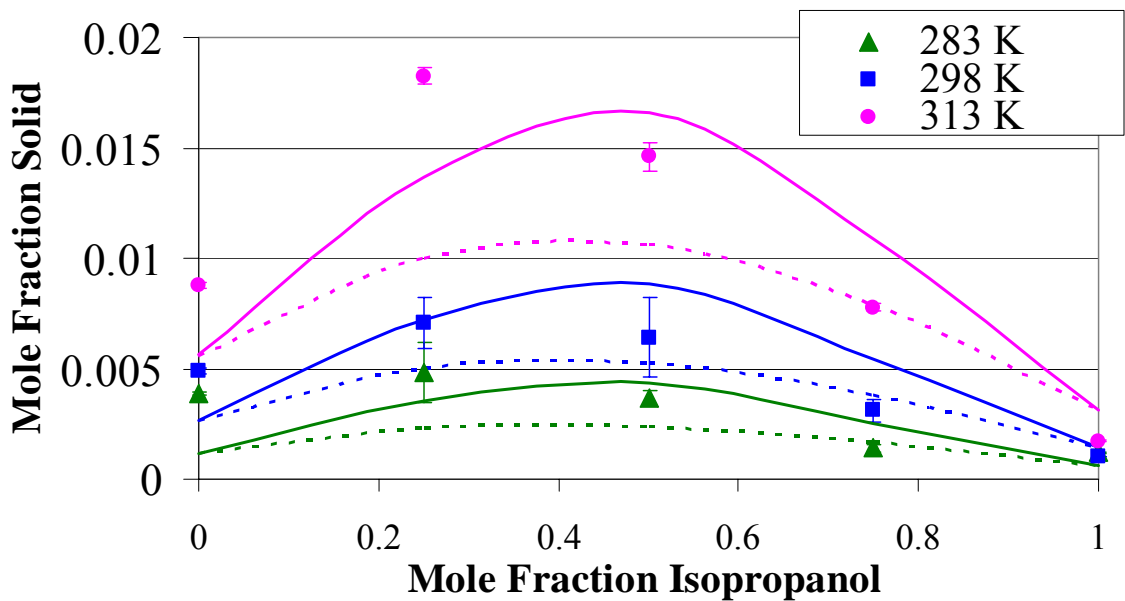


Figure 3-8: 3-Nitrophthalimide in mixtures of isopropanol and nitromethane, measured data and predictions (solid lines UNIQUAC, dashed lines Wilson) at 283, 298 and 313 K.

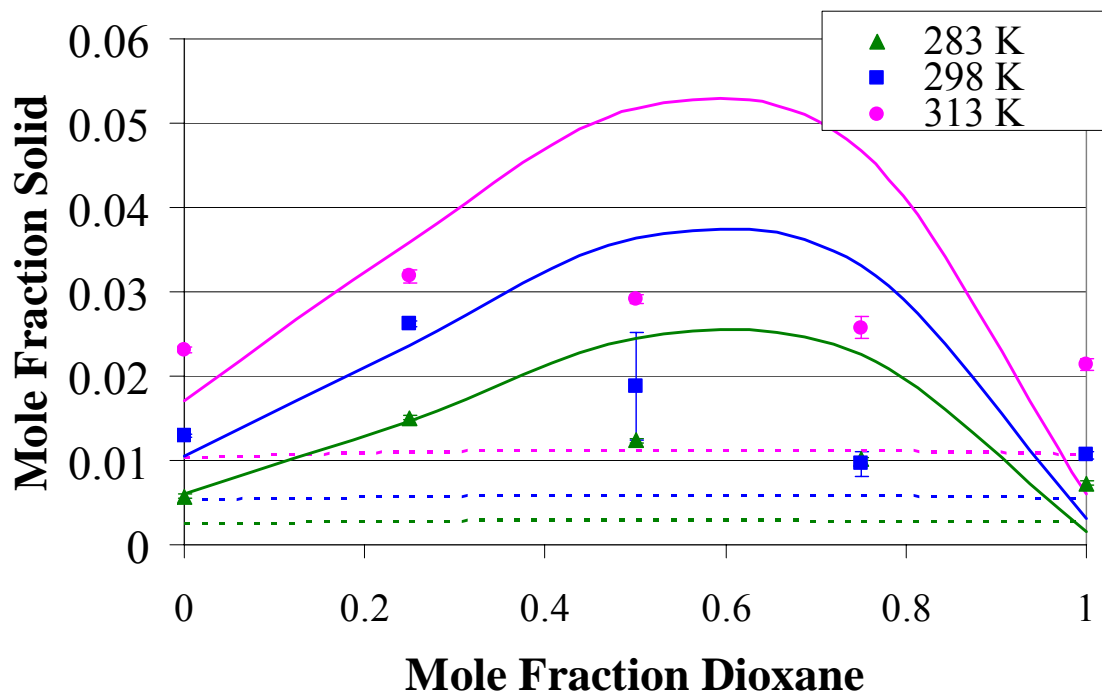


Figure 3-9: 3-Nitrophthalimide in mixtures of dioxane and 2-butanone, measured data and predictions (solid lines UNIQUAC, dashed lines Wilson) at 283, 298 and 313 K.

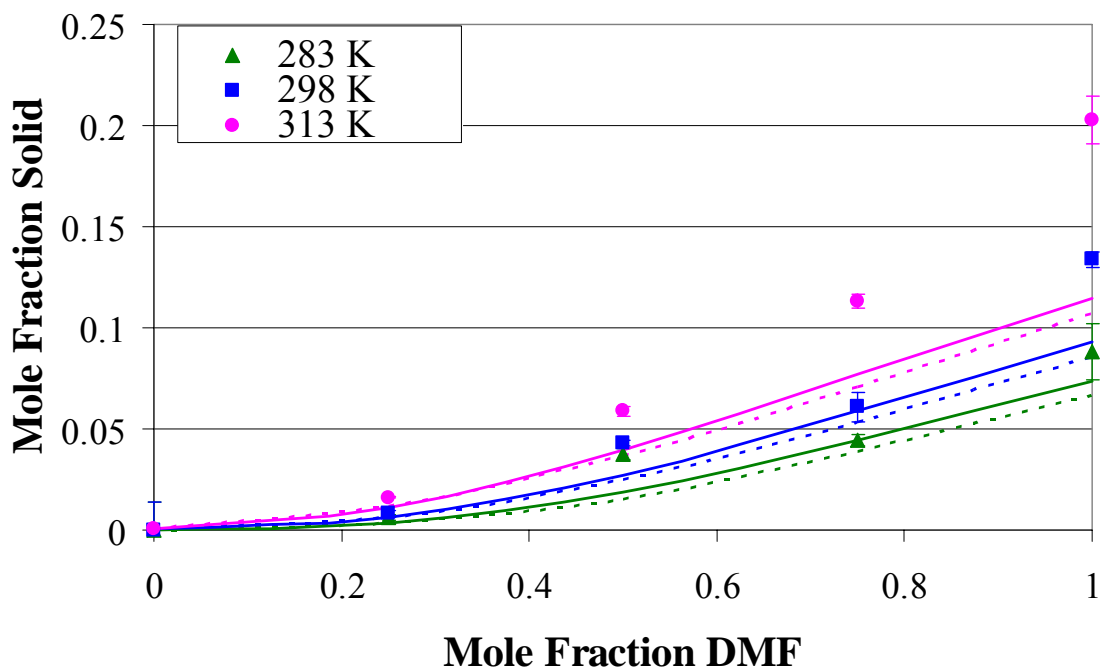


Figure 3-10: 3-Nitrophthalimide in mixtures of chloroform and DMF, measured data and predictions (solid lines UNIQUAC, dashed lines Wilson) at 283, 298 and 313 K.

solvent composition for both solvent pairs are shown in Figures 3-11 and 3-12. The hydrogen bond-donating ability of ethanol and 2-propanol and hydrogen bond-accepting ability of the basic solvent also can explain the synergistic effects of the solvent pair. No synergistic effects appear in the other two solvent pairs. (Figures 3-13 and 3-14).

It is not surprising that both above compounds, being of similar structure, demonstrate a maximum in solubility for the same alcohol-containing solvent pairs. However, the position and magnitude of the maximum as a function of solvent concentration is different. This difference may be due to the degree of self-association possible for the two solutes. While both compounds have similar hydrogen bond-donating groups with both possessing secondary amines, 3-nitrophthalimide has a greater number of hydrogen bond accepting moieties with the presence of the nitro group. In the

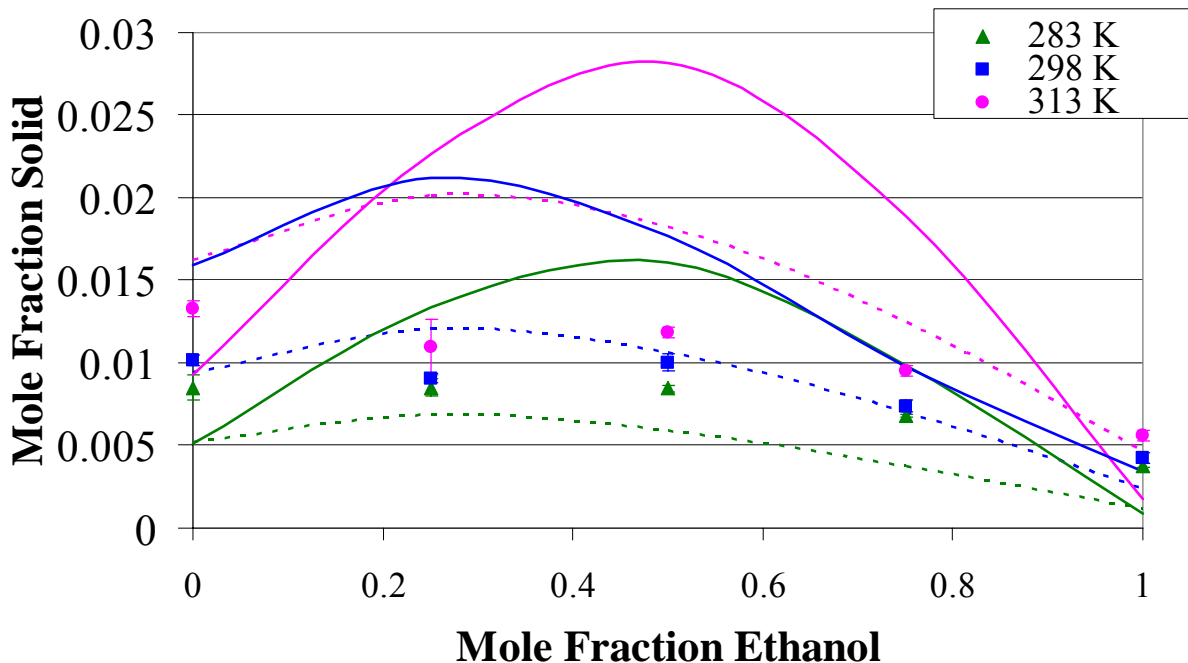


Figure 3-11: 5-Fluoroisatin in mixtures of ethanol and ethyl acetate, measured data and predictions (solid lines UNIQUAC, dashed lines Wilson) at 283, 298 and 313 K.

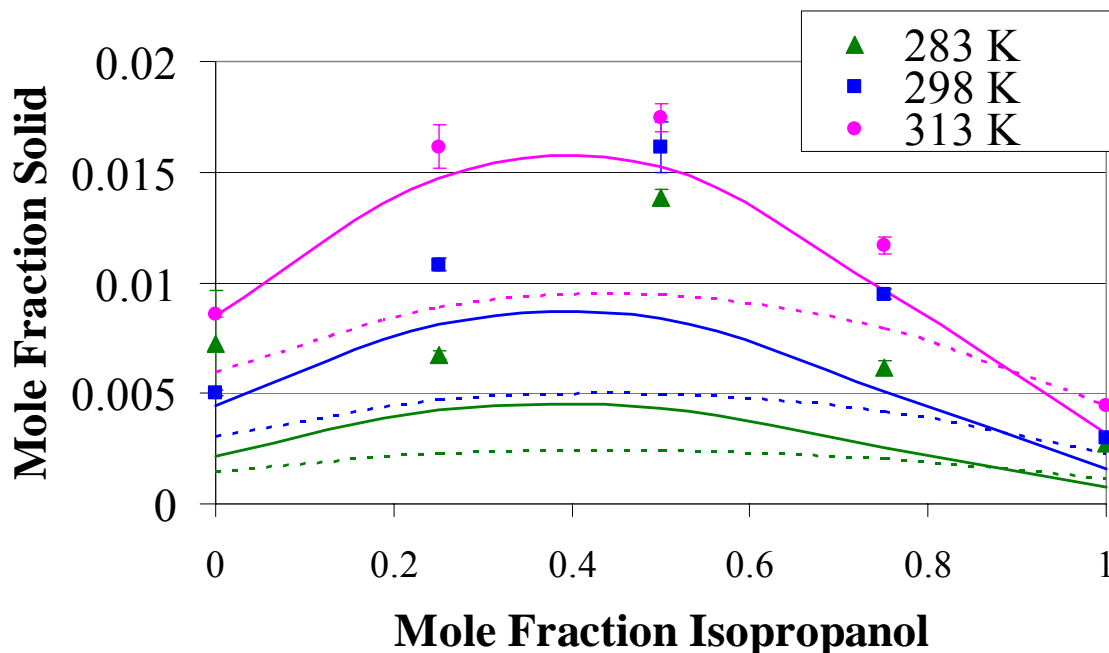


Figure 3-12: 5-Fluoroisatin in mixtures of isopropanol and nitromethane, measured data and predictions (solid lines UNIQUAC, dashed lines Wilson) at 283, 298 and 313 K.

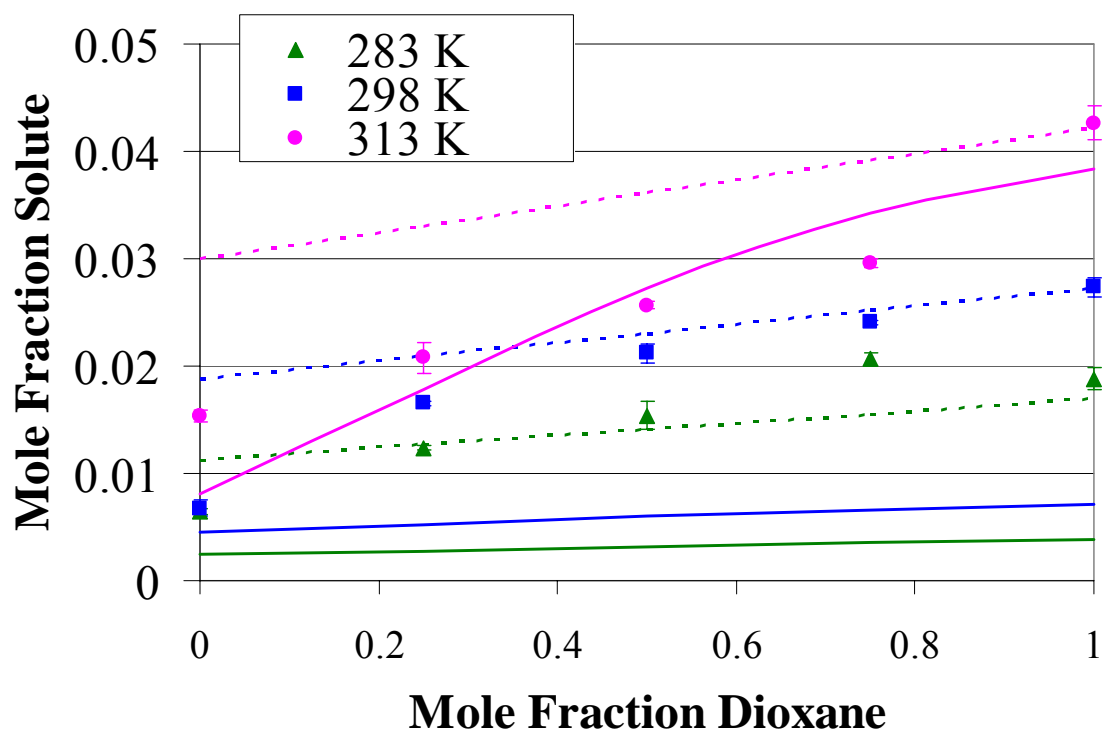


Figure 3-13: 5-Fluoroisatin in mixtures of dioxane and 2-butanone, measured data and predictions (solid lines UNIQUAC, dashed lines Wilson) at 283, 298 and 313 K.

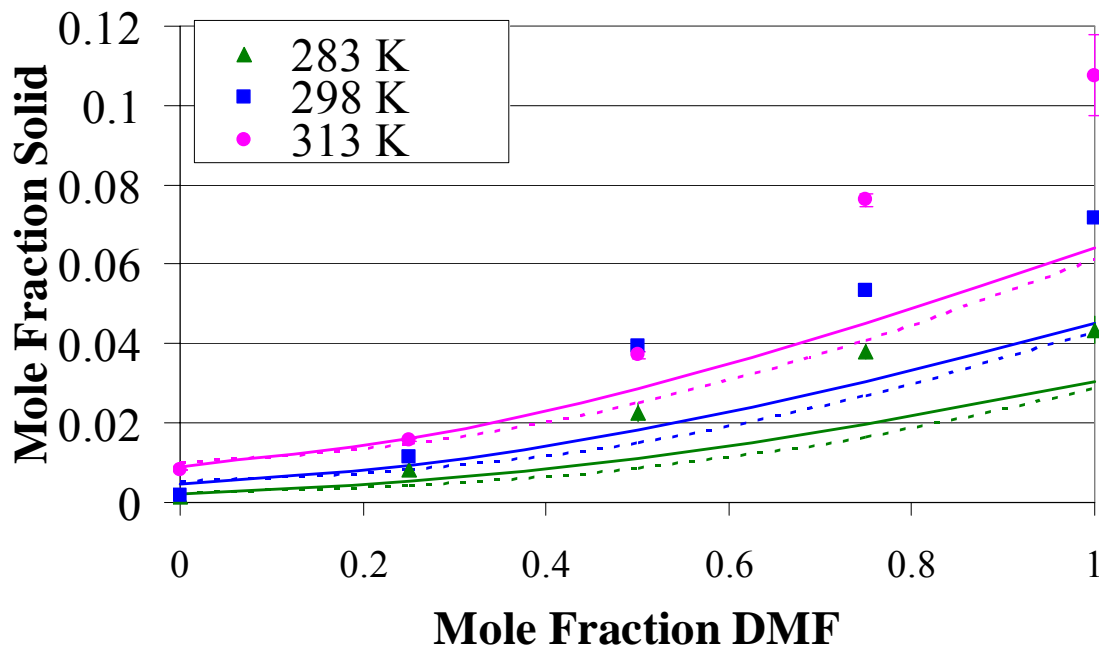


Figure 3-14: 5-Fluoroisatin in mixtures of chloroform and DMF, measured data and predictions (solid lines UNIQUAC, dashed lines Wilson) at 283, 298 and 313 K.

case of the 3-nitrophthalimide, there is greater competition for forming hydrogen bonds in solution because of the stronger self-association possible with the solute, whereas with 5-fluoroisatin more free solute is available and both basic and acidic solvents can effectively associate with the molecule.

Benzimidazole also exhibits a maximum in solubility for the alcohol-containing solvent pairs, but at different concentrations. In the ethanol + ethyl acetate system, there is a maximum in solubility at 0.75 mole fraction ethanol while in the isopropanol + nitromethane system the maximum occurs at approximately 0.5 mole fraction (Figures 3-15 and 3-16). The hydrogen on the secondary nitrogen of the solute is very acidic, solvating strongly with the hydroxyl groups on the alcohols. Thus it makes sense that they would be more soluble as more alcohol is added to the system. The difference in location of the maximum can be explained by comparing the other solvents in each

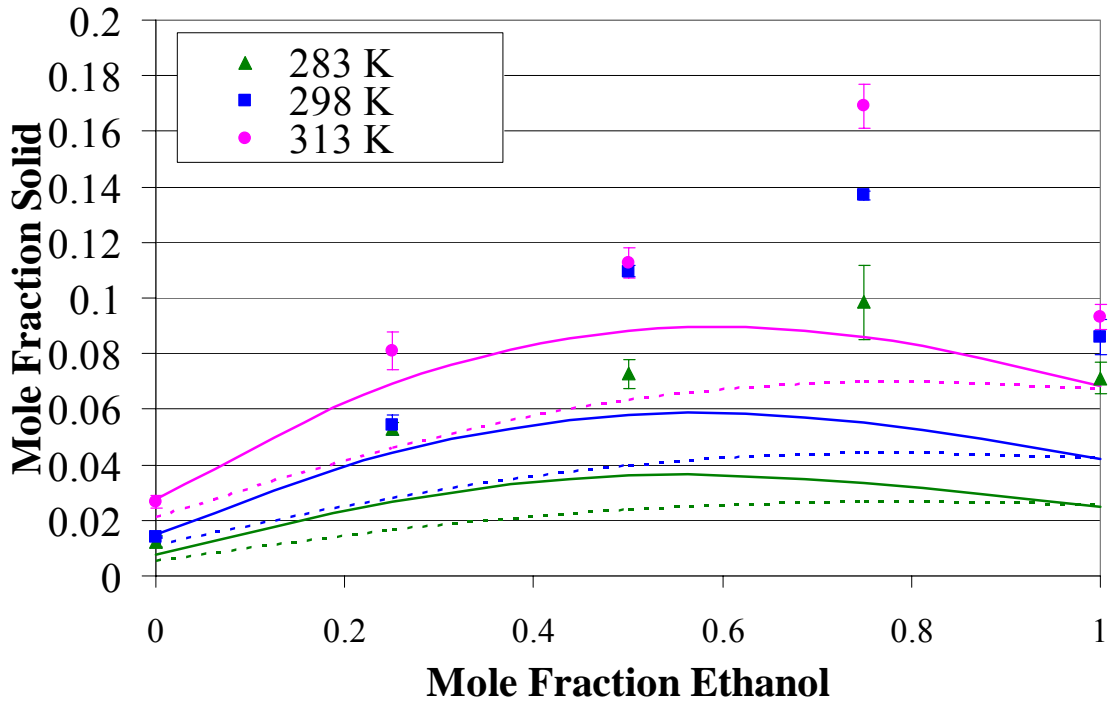


Figure 3-15: Benzimidazole in mixtures of ethanol and ethyl acetate, measured data and predictions (solid lines UNIQUAC, dashed lines Wilson) at 283, 298 and 313 K.

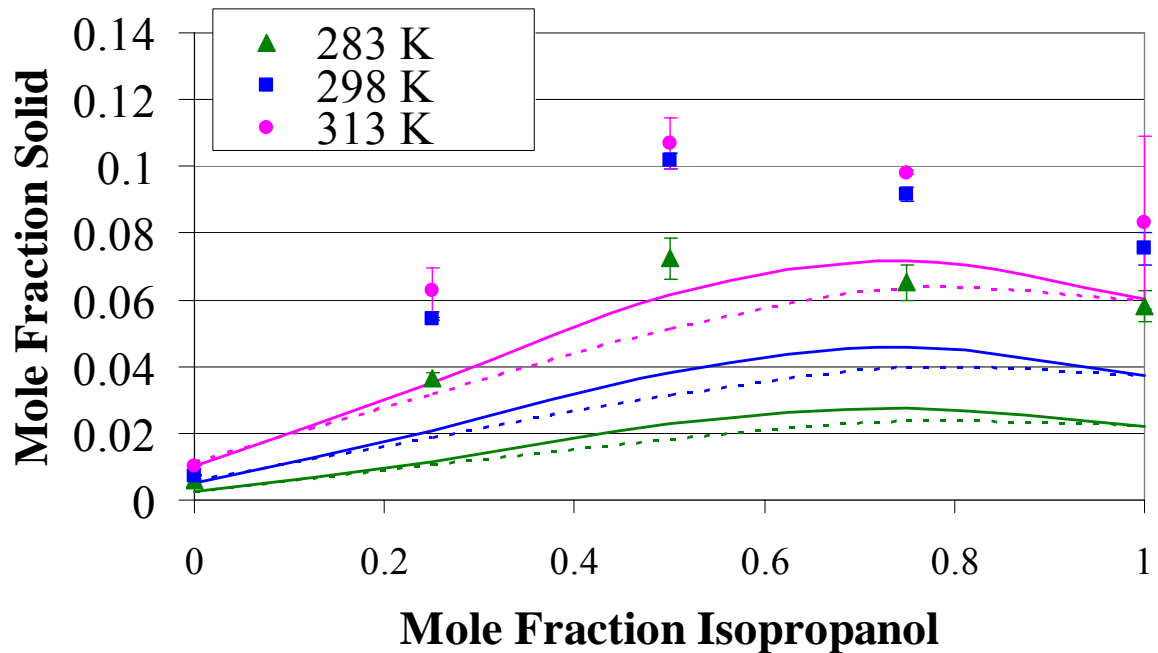


Figure 3-16: Benzimidazole in mixtures of isopropanol and nitromethane, measured data and predictions (solid lines UNIQUAC, dashed lines Wilson) at 283, 298 and 313 K.

system. Nitromethane is more polar than ethyl acetate, therefore having a stronger effect on solvating the fairly polar and highly hydrogen-bonding solute. Thus the synergy between nitromethane and isopropanol is more pronounced, producing a maximum at an equimolar mixture. The solute tends to interact preferentially with ethyl acetate over ethanol; while there is a synergistic effect, it occurs when ethanol is the more abundant solvent. Much like in the case of 5-fluoroisatin, no synergistic effects appear in the other two solvent pairs (Figures 3-17 and 3-18).

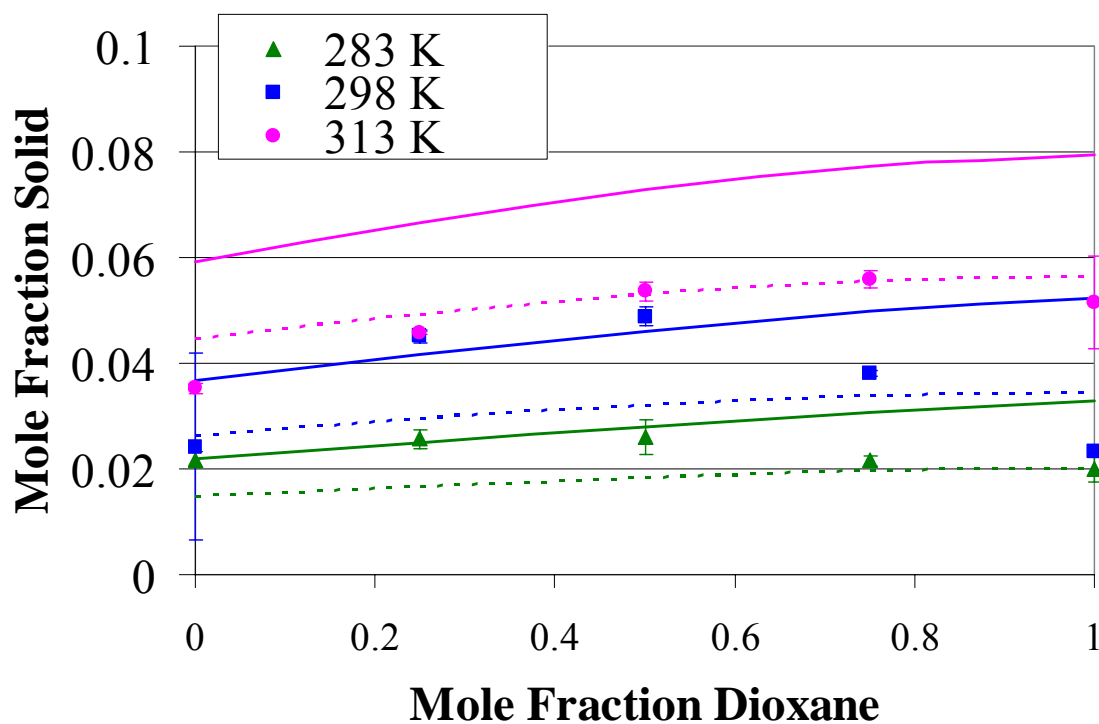


Figure 3-17: Benzimidazole in mixtures of dioxane and 2-butanone, measured data and predictions (solid lines UNIQUAC, dashed lines Wilson) at 283, 298 and 313 K.

Contrary to the behavior of the other solutes studied, 2-amino-5-nitrobenzophenone does not demonstrate a maximum in solubility in any of the solvent pairs tested. In fact, for both alcohol-containing solvent pairs, the alcohol appears to

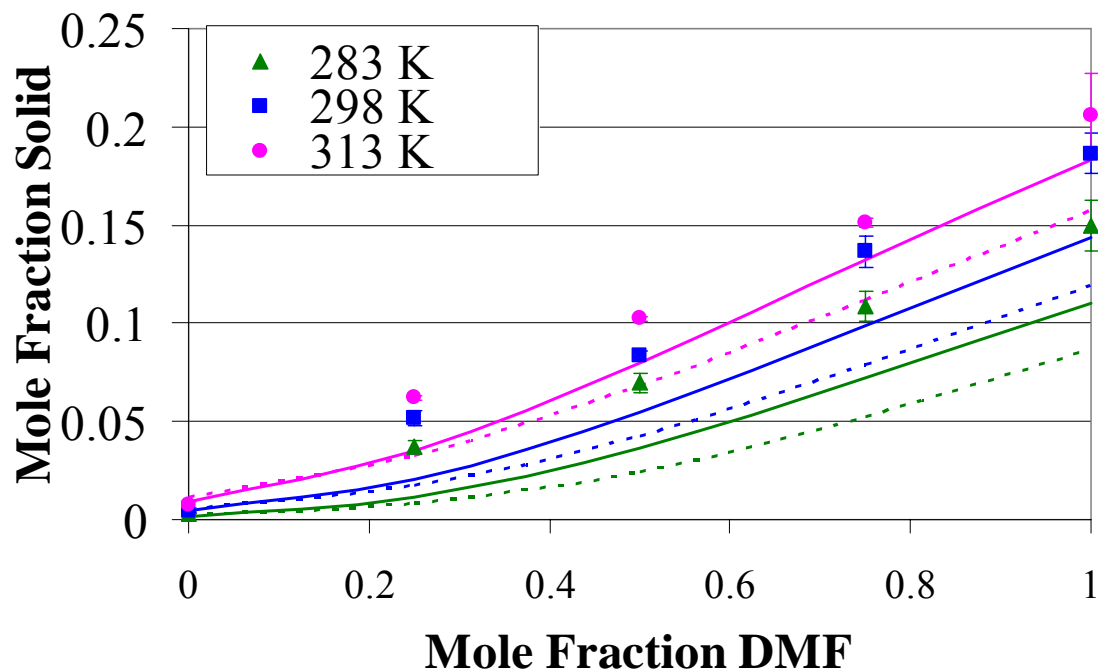


Figure 3-18: Benzimidazole in mixtures of chloroform and DMF, measured data and predictions (solid lines UNIQUAC, dashed lines Wilson) at 283, 298 and 313 K.

behave as an anti-solvent, where an addition of a small fraction of ethanol or isopropanol decreases the solubility dramatically. This again can be explained considering the potential hydrogen bonds that can form. The solid will be self-associated in solution, given the hydrogen bonds possible between the primary amine and the nitro or carbonyl group. In a pure, basic, aprotic solvent, namely ethyl acetate or nitromethane, the solvent is able to effectively associate some of the solid compound. With the addition of small amounts of ethanol or isopropanol, the basic solvent can now also associate with the protic alcohol, thus leaving more solid to self-associate and decreasing the solubility. The solubilities as a function of solvent composition for both solvent pairs are shown in Figures 3-19 and 3-20. In the other two solvent pairs, shown in Figures 3-21 and 3-22, the solubility behavior is almost linear with respect to the solvent mixture composition, indicating that there are no synergistic effects between the two solvents.

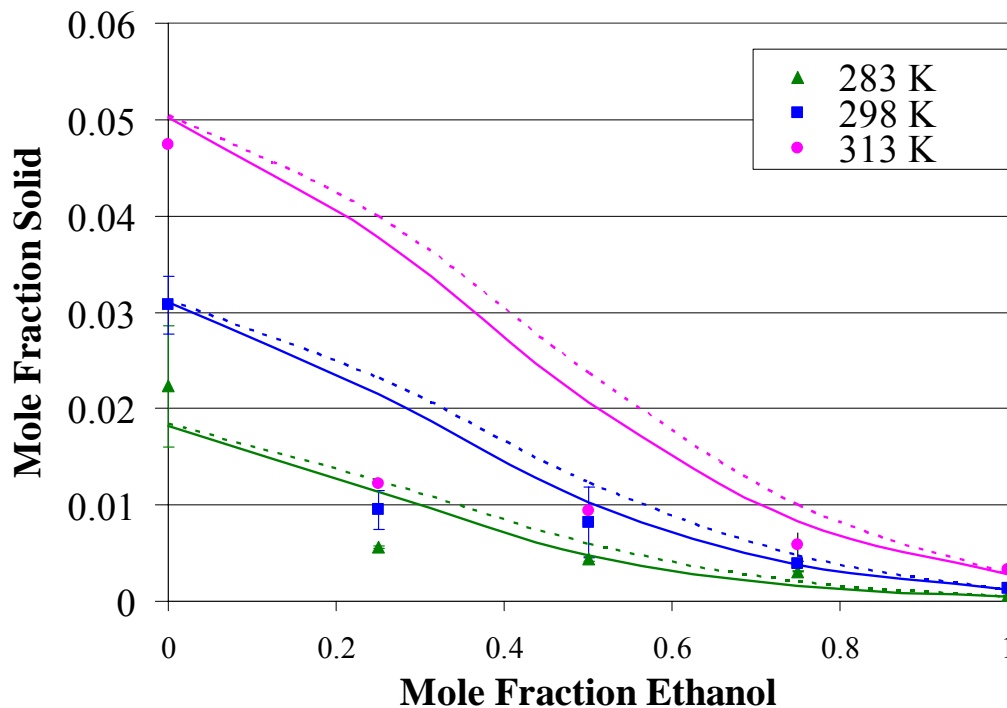


Figure 3-19: 2-Amino-5-nitrobenzophenone in mixtures of ethanol and ethyl acetate, measured data and predictions (solid lines UNIQUAC, dashed lines Wilson) at 283, 298 and 313 K.

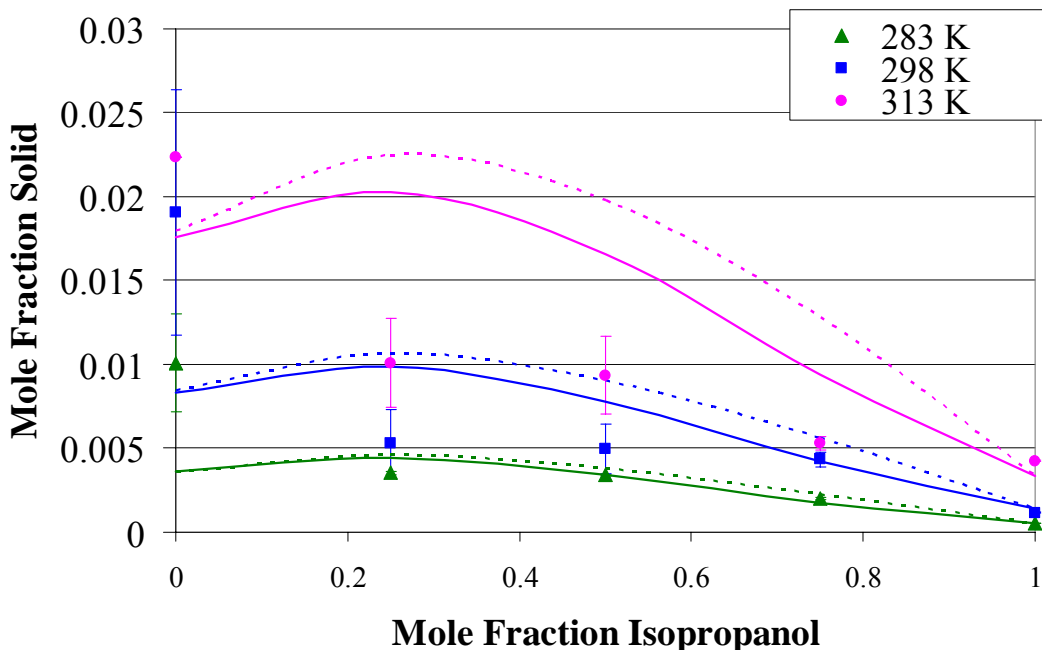


Figure 3-20: 2-Amino-5-nitrobenzophenone in mixtures of isopropanol and nitromethane, measured data and predictions (solid lines UNIQUAC, dashed lines Wilson) at 283, 298 and 313 K.

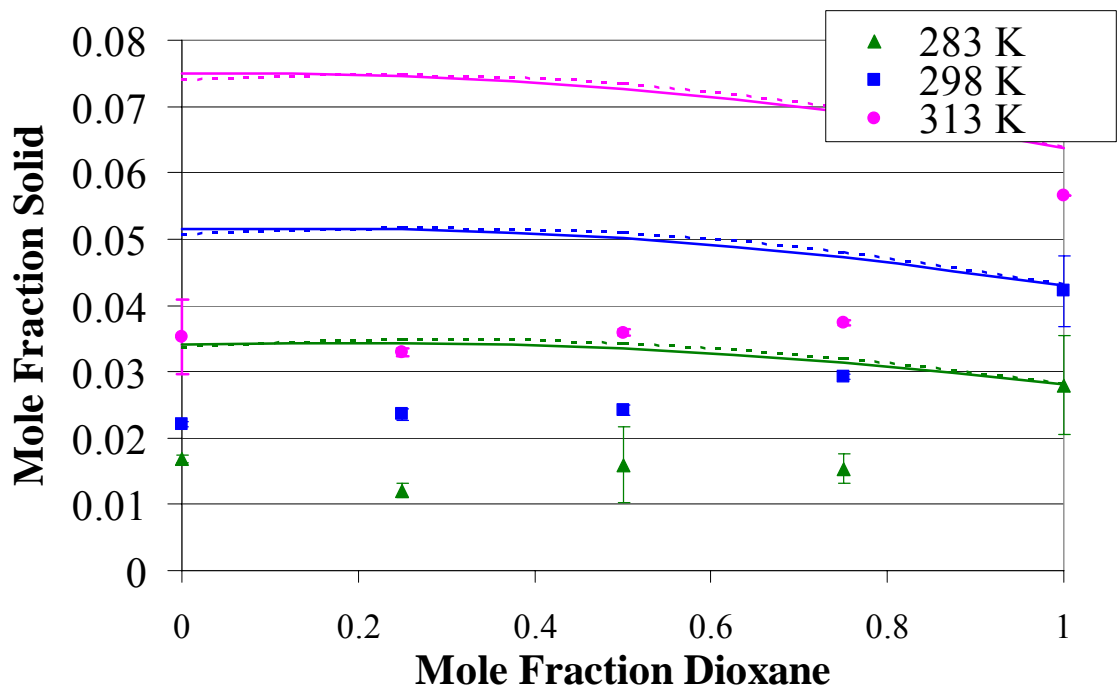


Figure 3-21: 2-Amino-5-nitrobenzophenone in mixtures of dioxane and 2-butanone, measured data and predictions (solid lines UNIQUAC, dashed lines Wilson) at 283, 298 and 313 K.

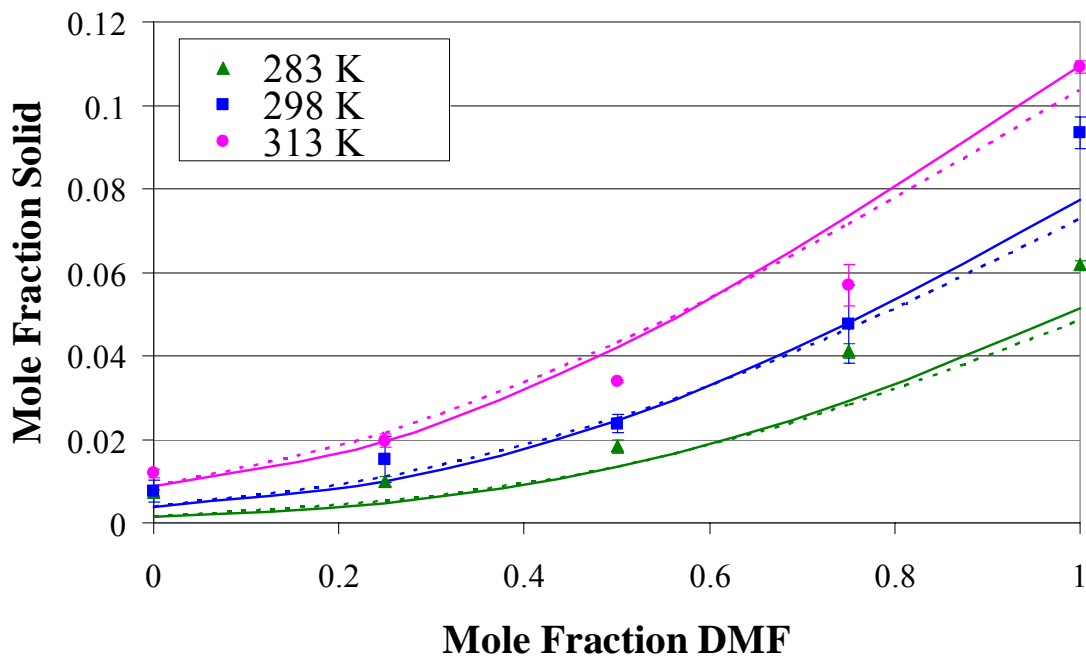


Figure 3-22: 2-Amino-5-nitrobenzophenone in mixtures of chloroform and DMF, measured data and predictions (solid lines UNIQUAC, dashed lines Wilson) at 283, 298 and 313 K.

Thermodynamic Modeling Results and Discussion

The MOSCED model correlates the solubility of some multifunctional solid compounds in a variety of solvents well.^{1, 2} In this section, the model is applied to the solutes investigated in this study. The melting points, heats of fusion and the regressed MOSCED parameters of all solids are shown in Tables 3-3 and 3-4.

Table 3-3: Heats of fusion and melting temperatures of solids.

| Solute | $\Delta H_{\text{fus}} (\pm 10\%)$ kJ/mol | T_m K |
|-----------------------------|--|------------|
| 3-Nitrophthalimide | 34.0 | 487 |
| 5-Fluoroisatin | 29.6 | 498 |
| Benzimidazole | 22.7 | 444 |
| 2-Amino-5-Nitrobenzophenone | 37.9 | 440 |

Table 3-4: Regressed MOSCED parameters for all solids using Wilson and UNIQUAC g^E models.

| | 3-Nitrophthalimide | | 5-Fluoroisatin | |
|-----------|--------------------|---------|----------------|---------|
| | Wilson | UNIQUAC | Wilson | UNIQUAC |
| λ | 15.21 | 15.20 | 16.71 | 16.25 |
| τ | 8.81 | 8.80 | 6.76 | 8.04 |
| α | 13.10 | 13.04 | 6.93 | 6.68 |
| β | 5.63 | 5.62 | 5.80 | 5.70 |
| q | 0.9 | 0.9 | 0.9 | 0.9 |

| | Benzimidazole | | 2-Amino-5-Nitrobenzophenone | |
|-----------|---------------|---------|-----------------------------|---------|
| | Wilson | UNIQUAC | Wilson | UNIQUAC |
| λ | 16.21 | 16.73 | 14.06 | 14.04 |
| τ | 4.22 | 4.16 | 8.12 | 8.11 |
| α | 12.15 | 13.35 | 7.29 | 7.22 |
| β | 11.12 | 9.80 | 1.83 | 1.84 |
| q | 0.9 | 0.9 | 0.9 | 0.9 |

Pure Solvents

A comparison of the experimental versus predicted solubility and of the Wilson versus the UNIQUAC g^E model is shown in Figure 3-23 for 3-nitrophthalimide. Wilson

and UNIQUAC appear to do equally well in terms of determining appropriate parameters for solvents where the solubility is high and equally poorly for solvents where the solubility is low. MOSCED is able to predict accurately the solubility over nearly three orders of magnitude, predicting the greater than ideal solubility ($x_l > 0.0873$ at 298 K) exhibited in the very polar and basic solvent DMF and the moderately low solubility in alcohols. MOSCED tends to overpredict the solubility in chloroform at low temperatures regardless of which g^E model is used. It also seems to underpredict the solubility in cyclohexane when Wilson is used.

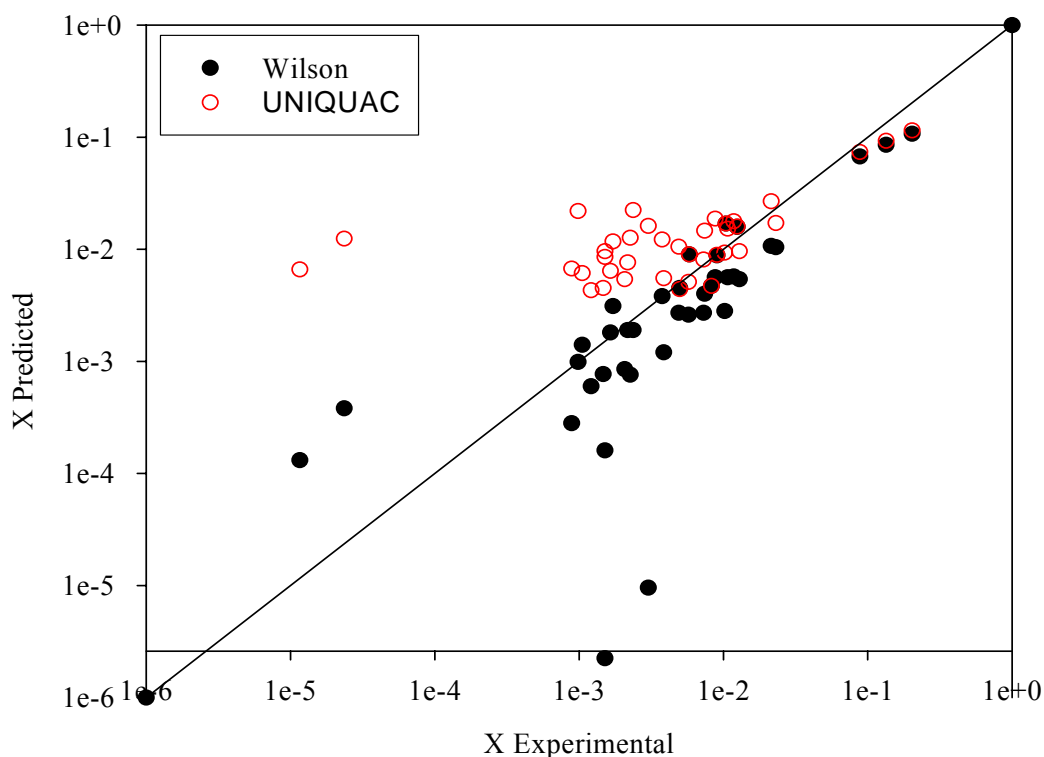


Figure 3-23: Mole fraction solubility of 3-nitrophthalimide in various solvents from 283 to 313 K versus MOSCED predictions.

The MOSCED model is also able to correlate the solubilities of 5-fluoroisatin (Figure 3-24). It tends to underpredict the solubility values for this compound somewhat more often than it did the previous compound, but not by as much. The model does

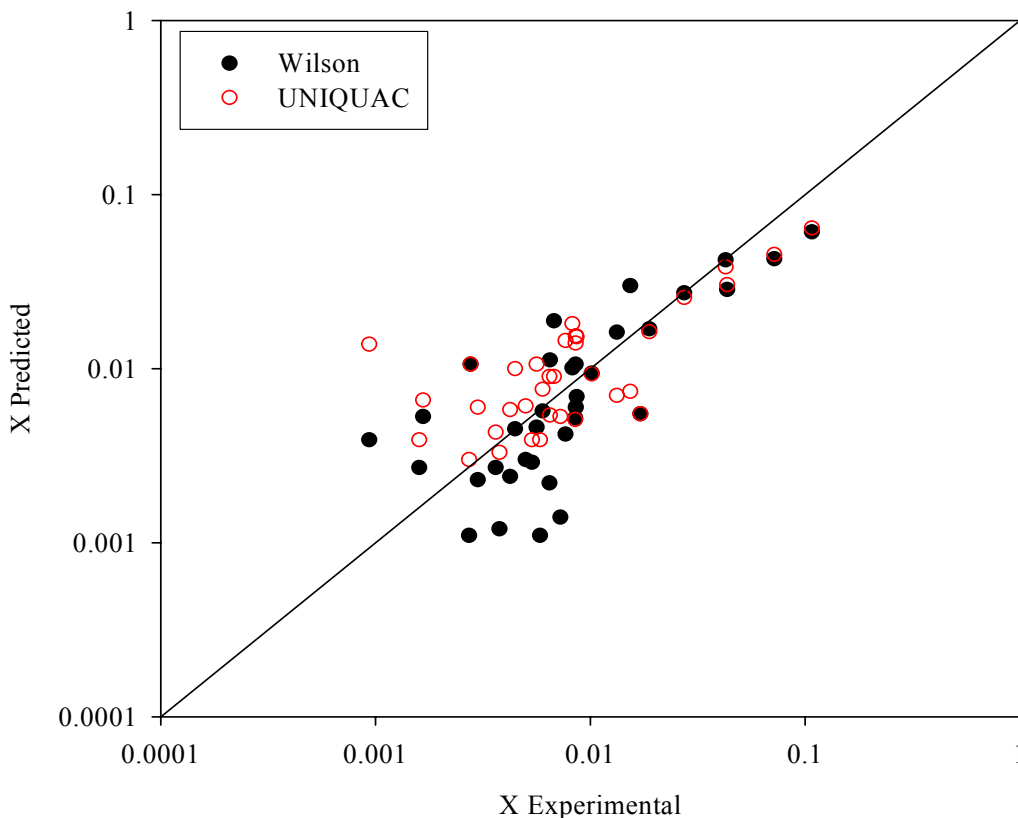


Figure 3-24: Mole fraction solubility of 5-fluoroisatin in various solvents from 283 to 313 K versus MOSCED predictions.

equally well, as in the case of 3-nitrophthalimide, whether UNIQUAC or Wilson is used in conjunction with the activity coefficients. There are no obvious outliers to mention. The regressed solute parameters for 3-nitrophthalimide and 5-fluoroisatin characterize the two compounds very similarly. Both have a large dispersion term and a modest dipolarity term similar in magnitude to that of pyrrolidone solvents, with which it shares some similar structural elements. The 3-nitrophthalimide in fact has a slightly larger dipolarity term, which may be due to the position of the nitrous group, whereas the 5-fluoroisatin compound possesses a fluorine side group. The hydrogen bond basicity terms are also similar in magnitude for both compounds, but 5-fluoroisatin has an acidity term about twice as large as 3-nitrophthalimide. We speculate that this may be because the

secondary amine in 5-fluoroisatin is positioned between two carbonyls, where the electronegative carbonyls would be balanced by a more positive proton. In 3-nitrophthalimide, the secondary amine only neighbors one carbonyl group and would be less protic.

When applied to benzimidazole, the MOSCED model works quite well across four orders of magnitude, as shown in Figure 3-25. The only strong outliers to mention are the low-solubility toluene and cyclohexane, which are overpredicted when the

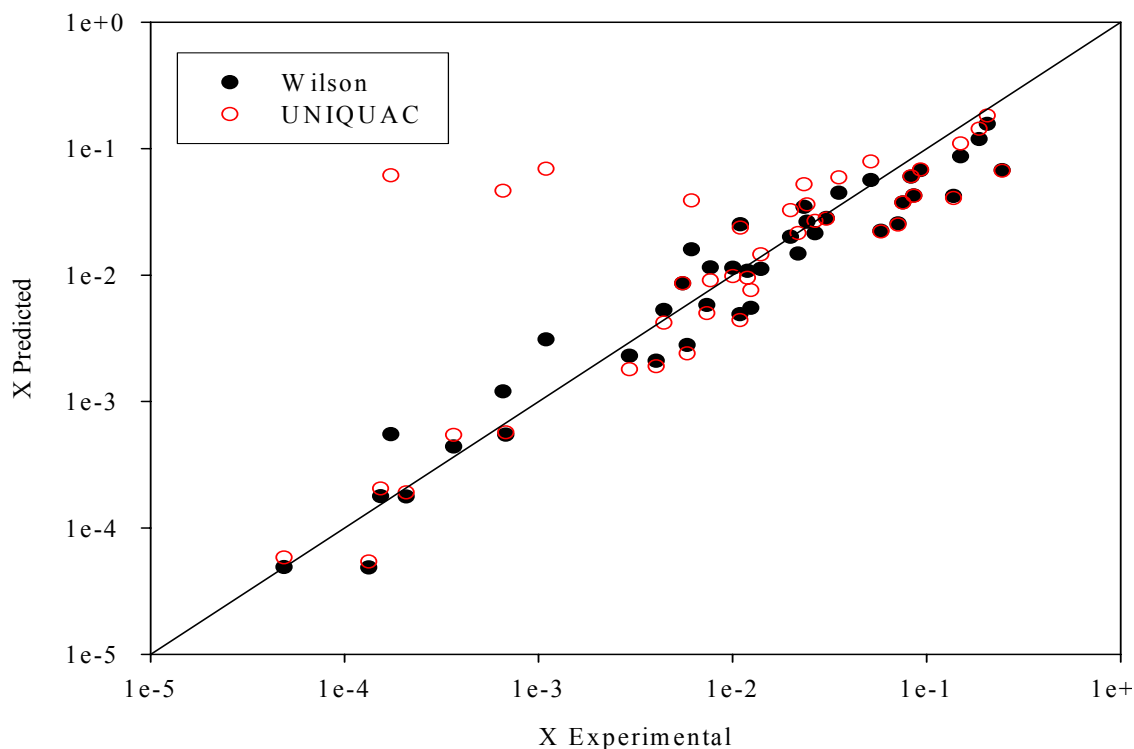


Figure 3-25: Mole fraction solubility of benzimidazole in various solvents from 283 to 313 K versus MOSCED predictions.

UNIQUAC g^E model is used. However it generally tends to underpredict the solubility when it does not exactly reproduce the experimental data. Examination of the compound descriptors indicates a relatively low dipolarity compared to the others solutes but high acidity and basicity. The high hydrogen bond acidity comes as no surprise because the

proton on the secondary amine is quite acidic. The high basicity can be attributed to the other nitrogen in the ring. An analogy as to why this compound is so much more basic than the other compounds studied can be drawn by comparing the very basic pyridine to the much less basic aniline. Like benzimidazole, pyridine contains a nitrogen atom in the conjugated ring which results in hydrogen-bonding basicity. Aniline – like the other compounds – does not have any conjugation with its nitrogen atom, resulting in a less basic nitrogen.

The MOSCED model is able to correlate the solubilities of 2-amino-5-nitrobenzophenone across nearly 4 orders of magnitude accurately, as shown in Figure 3-26. As in the previous case, there are no strong outliers and it tends to underpredict the

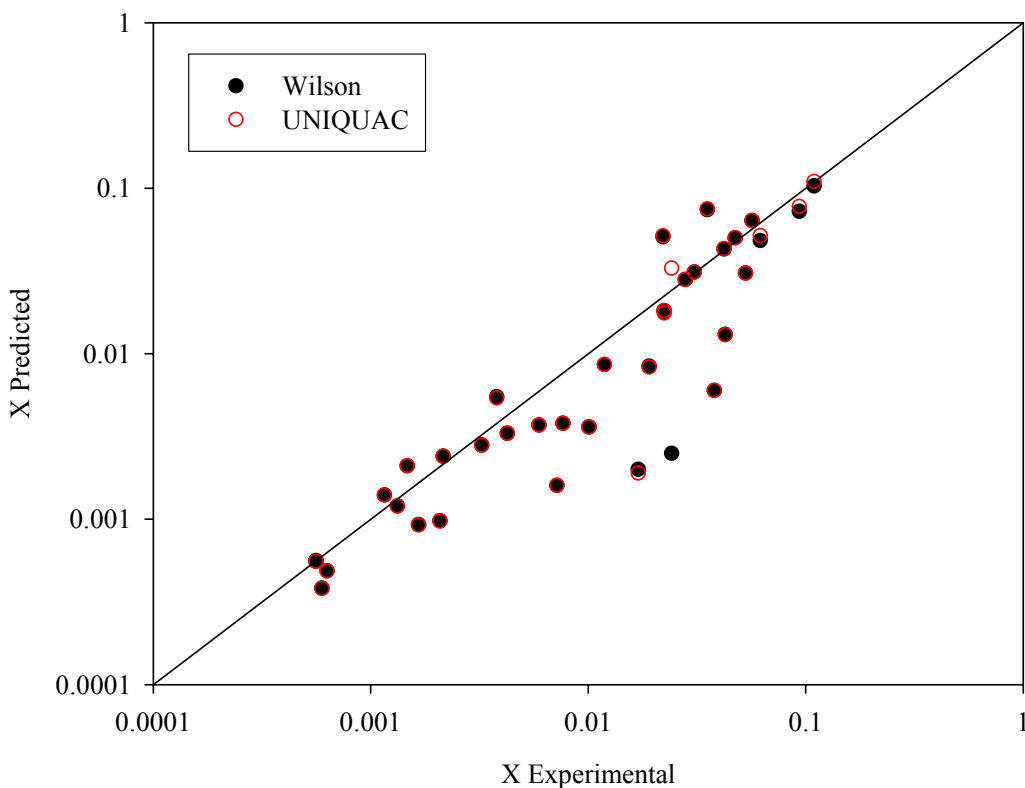


Figure 3-26: Mole fraction solubility of 2-amino-5-nitrobenzophenone in various solvents from 283 to 313 K versus MOSCED predictions.

solubility in the cases when it does not exactly reproduce the experimental data. The compound descriptors, especially the hydrogen bonding parameters, are smaller than might be expected. Comparing the 2-amino-5-nitrobenzophenone descriptors to those of the similarly-structured but smaller *p*-nitroaniline, the dispersion and dipolarity terms are similar; however the acidity term is 1.8, nearly 20% of the value for *p*-nitroaniline. One possible explanation is the existence of an intramolecular hydrogen bond between the carbonyl group and the hydrogen molecule of the secondary amine. The carbonyl is not sterically hindered from rotation and it can easily be in a position to form a hydrogen bond with the neighboring amine, leaving only one acidic proton available for hydrogen bond-donating with the solvent. One possible configuration of the molecule is shown in Figure 3-27. The carbonyl-amine hydrogen bond results in the formation of a six-member ring, thus stabilizing the structure. It may also be possible for both hydrogens to interact with the free electrons on the carbonyl in a 3-dimensional manner, where the protons are orthogonal to the benzene ring plane.

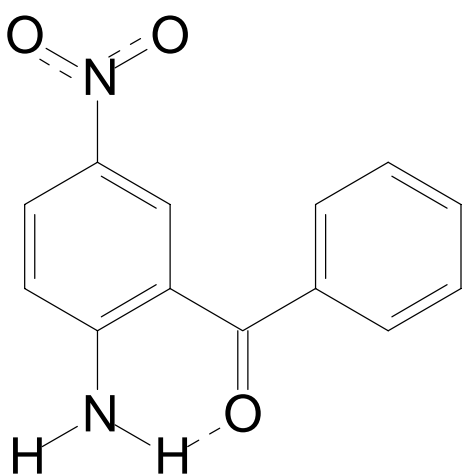


Figure 3-27: Intramolecular hydrogen bonding in 2-amino-5-nitrobenzophenone.

Mixed Solvents

In order to predict the solubility of solid compounds in mixed solvents, the MOSCED model must predict the mutual activity coefficients of the solvent pair in addition to the prediction of the activity coefficient of the solid in the pure solvent. This makes the predictions more dependent upon the ability of the activity coefficient model to describe accurately the effect of concentration on the activity coefficient away from the infinite dilution region. The results of the predictions for all solids in all solvent pairs appear on the same graphs as the experimental data in Figures 3-7 through 3-22.

For mixtures of ethanol and ethyl acetate, MOSCED was able to predict the correct qualitative behavior. In the case of 3-nitrophthalimide (Figure 3-7), Wilson tends to work better than UNIQUAC in predicting the composition of and solubility at the maximum, but neither works particularly well. For 5-fluoroisatin, MOSCED works almost equally poorly using either Wilson or UNIQUAC to obtain the solubility from the activity coefficients. When UNIQUAC is used it predicts a higher solubility for 298 K than it does for 313 K, which is peculiar. It can be speculated that this is just an artifact of the UNIQUAC g^E model, which can give anomalous results when both predicted γ^∞ values are less than unity.

Out of the four solids in this solvent system, MOSCED appears to predict the behavior of benzimidazole the best. In the ethyl acetate rich portion of the graph (Figure 3-15) the solubility is predicted rather well. However, once the solution is mostly ethanol, MOSCED appears to fail regardless of the activity coefficient model used. This is probably because MOSCED underpredicts the solubility of benzimidazole in pure ethanol. It appears that if MOSCED was forced to work at both end points then it would

predict the correct phase behavior. As shown in Figure 3-19, MOSCED predicts the general trend of the solubility of 2-amino-5-nitrobenzophenone in ethanol + ethyl acetate mixtures quite successfully. However, it does not capture the anti-solvent effect of the alcohol. This can likely be attributed to MOSCED's limitations in properly predicting the interactions between solvents and therefore the resulting self-association of the solid.

In the case of mixtures of isopropanol and nitromethane, MOSCED tends to predict a maximum in solubility for all four solids studied, even in the case where there is no experimental maximum. When UNIQUAC is used MOSCED does very well in predicting the magnitude of the maximum for 3-nitrophthalimide (Figure 3-8). Wilson tends to underpredict the solubility at all temperatures. Both activity coefficient models cause MOSCED to predict the maximum at an equimolar mixture of solvents, though the actual maximum is at approximately 0.75 nitromethane by mole. Figure 3-12 shows the predictions for 5-fluoroisatin in this solvent system. In this case, MOSCED correctly predicts a maximum at an equimolar solvent mixture but underpredicts the solubility at all points except for the pure solvents. MOSCED performs better in conjunction with UNIQUAC than with Wilson.

As is consistent with the case of the ethanol + ethyl acetate system, MOSCED appears to predict the general solubility behavior of benzimidazole in the isopropanol + nitromethane solvent system well in the region of more nitromethane, but falls short in the region where there is more isopropanol (Figure 3-16). Again, this is a result of MOSCED underpredicting the solubility of benzimidazole in isopropanol. It once again appears that if MOSCED could predict both end points well then it would predict the behavior well. MOSCED's ability to predict the solubility of 2-amino-5-

nitrobenzophenone is also similar to that of the previous solvent system in that it fails to predict the anti-solvent behavior of the alcohol (Figure 3-20). This can also be attributed to MOSCED's limitations in properly predicting the interactions between the solvents.

MOSCED performs consistently worse in the system of dioxane + 2-butanone than any other solvent system for all solids. Data and predictions for 3-nitrophthalimide are compared in Figure 3-8. While the data indicate a slight maximum in solubility for the system that is 25% dioxane by mole, MOSCED does not predict that maximum regardless of which activity coefficient model is used. UNIQUAC shows a maximum at 60% dioxane while Wilson indicates no maximum at all. In the case of 5-fluoroisatin, MOSCED correctly predicts that there is no maximum in solubility in this particular solvent mixture (Figure 3-13). However, it predicts only the general trend of the solubility behavior and not the quantity. When Wilson is used the solubility in pure dioxane is predicted well but the solubility in 2-butanone is overpredicted. However, it appears that if MOSCED was able to predict the solubility of 2-butanone well when using Wilson as a g^E model then it would have predicted the overall phase behavior well. UNIQUAC did not work well.

When the solubility of benzimidazole is predicted with activity coefficients generated by Wilson, MOSCED works well at 283 and 313 K and captures the solubility values at many of the solvent compositions (Figure 3-17). When used in conjunction with UNIQUAC, MOSCED works only at 283K and gets worse as temperature increases. Data and predictions for 2-amino-5-nitrobenzophenone are compared in Figure 3-21. In this case whether Wilson or UNIQUAC is used in conjunction with MOSCED does not

seem to matter as the behavior is predicted similarly; in both cases the predictions are bad.

MOSCED performs the best overall in the solvent system of Chloroform + DMF for all solids. There do not appear to be any solvent-solvent interactions that impact the solubility of any of the four compounds, and MOSCED does a good job of predicting that regardless of the activity coefficient model used. In the cases of 3-nitrophthalimide and 5-fluoroisatin (Figures 3-10 and 3-14, respectively), MOSCED fails to predict the solubilities in DMF which causes it to not predict the overall equilibrium behavior well. However, it appears that if the solubility in DMF was predicted well then the mixture behavior would have been predicted well. MOSCED predicts the solubility values of both benzimidazole and 2-amino-5-nitrophenone well in this solvent mixture (Figures 3-18 and 3-22, respectively).

For the example systems considered here, the accuracy of the predictions of the mixed solvent systems seems dependent upon both the correct prediction of the pure solvent solubilities and the proper selection of an activity coefficient model. The accuracy of the predictions appears to be less dependent upon the accuracy of the binary solvent pair, though a dependence is still there. In other words, when the pure solvent solubilities are predicted correctly then the mixed solvent solubilities are more likely to be predicted correctly. This may be because the MOSCED model has less average error for binary solvent predictions, and this error is less significant when compared to the larger error in the solid solubility predictions.

Paradigm for Solvent Selection

One of the goals of this project was to develop a technique to use MOSCED to select solvents for crystallization processes. The results of this study demonstrate that appropriate solvents can be selected successfully by taking a few specific data. In order to select an appropriate solvent system for a new compound, the solubility of the compound must be measured in approximately 10-20 solvents with different functionalities, such as the solvent list used in this study, at several temperatures. MOSCED parameters for the solid are then fit to the measured solubility data. The MOSCED parameters can then be used to determine the solubility behavior of the solid in any solvent pair of any composition or temperature. From these model-generated data, it is possible to choose the solvent pair that shows the appropriate temperature behavior for the desired separation.

Summary

The solubilities of four multi-functional solid compounds were measured in a variety of organic solvents at several temperatures and in four binary mixed solvent systems. The MOSCED model was relatively successful at correlating the solubilities with few exceptions. The pure component descriptors were found to match the intuitive chemical/physical sense of the pure compounds. The model was also able to correctly predict the existence of maxima in solubility and at least qualitatively matched the experimental solubility in most cases. The application of the MOSCED model to mixed solvent pairs was limited by the quality of the pure solvent predictions.

The results of this study show promise in the area of solvent selection. Using the technique outlined in this paper, crystallization solvents for multi-functional compounds can be selected after only taking a relatively small number of data.

REFERENCES

1. Lazzaroni, M. J. Optimizing solvent selection for separation and reaction. 2005.
2. Lazzaroni, M. J.; Bush, D.; Eckert, C. A.; Frank, T. C.; Gupta, S.; Olson, J. D., Revision of MOSCED parameters and extension to solid solubility calculations. *Ind. Eng. Chem. Res.* **2005**, 44, (11), 4075-4083.
3. Domanska, U., Solubility of 2,5-dimethylphenol and 3,4-dimethylphenol in binary solvent mixtures containing alcohols. *Fluid Phase Equilibria* **1988**, 40, 259-277.
4. Domanska, U., Solubility of n-alkanols in binary solvent mixtures. *Fluid Phase Equilibria* **1989**, 46, 223-248.
5. Domanska, U., Vapor-liquid-solid equilibrium of eicosanoic acid in one- and two-component solvents. **1986**, 26, 201-220.
6. Domanska, U.; Bogel-Lukasik, E., Solubility of benzimidazoles in alcohols. *J. Chem. Eng. Data* **2003**, 48, (4), 951-956.
7. Domanska, U.; Kozłowska, M. K., Solubilities, partition coefficients, density and surface tension for imidazoles + octan-1-ol or + water or + n-decane. *J. Chem. Eng. Data* **2002**, 47, (3), 456-466.
8. Letcher, T. M.; Redhi, G. G.; Radloff, S. E., Liquid-liquid equilibria of the ternary mixtures with sulfolane at 303.15 K. *J. Chem. Eng. Data* **1996**, 41, (3), 634-638.
9. deFina, K. M.; Sharp, T. L.; Chuca, I.; Spurgin, M. A.; Acree, W. E. J.; Green, C. E.; Abraham, M. H., Solubility of the pesticide monuron in organic nonelectrolyte solvents. Comparison of observed versus predicted values based upon mobile order theory. *Phys. Chem. Liq.* **2002**, 40, (3), 255-268.
10. Chen, S.-J.; Radosz, M., Density-tuned polyolefin phase equilibria. 1. Binary solutions of alternating poly(ethylene-propylene) in subcritical and supercritical propylene, 1-butene, and 1-hexene. Experiment and Flory-Patterson model. *Macromolecules* **1992**, 25, (12), 3089-3096.

11. Granberg, R. A.; Rasmuson, A. C., Solubility of paracetamol in pure solvents. *J. Chem. Eng. Data* **1999**, 44, (6), 1391-1395.
12. Thomas, E. R.; Eckert, C. A., Prediction of limiting activity coefficients by a modified separation of cohesive energy density model and UNIFAC. *Ind. Eng. Chem. Process Des. Dev.* **1984**, 23, 194-209.
13. Gmehling, J.; Li, J.; Schiller, M., A modified UNIFAC model: 2. Present parameter matrix and results for different thermodynamic properties. *Ind. Eng. Chem. Res.* **1993**, 32, (1), 178-193.
14. Fletcher, K. A.; Pandey, S.; McHale, M. E. R.; Acree, W. E., Jr., Solubility of benzil in organic nonelectrolyte solvents. Comparison of observed versus predicted values based upon mobile theory. *Phys. Chem. Liq.* **1996**, 33, (3), 181-190.
15. Hernandez, C. E.; De Fina, K. M.; Roy, L. E.; Sharp, T. L.; Acree, W. E., Jr., Solubility of phenanthrene in organic nonelectrolyte solvents. Comparison of observed versus predicted values based upon Mobile Order theory. *Can. J. Chem.* **1999**, 77, (9), 1465-1470.
16. Roy, L. E.; Hernandez, C. E.; Acree, W. E., Jr., Solubility of anthracene in organic nonelectrolyte solvents. Comparison of observed versus predicted values based upon mobile order theory. *Polycyclic Aromatic Compounds* **1999**, 31, (1), 105-116.

CHAPTER IV

MENSCHUTKIN REACTION KINETICS, PI STAR AND Z-VALUES AS PROBES OF LOCAL POLARITY OF CO₂-EXPANDED ACETONITRILE

Introduction

Gas-antisolvent separation was described in some detail in Chapter II and briefly mentioned in Chapter III as an application of gas-expanded liquids.¹⁻⁴ This particular separation technique works on the principle that solvent properties such as polarity, density, etc. undergo dramatic changes upon the addition of carbon dioxide to the bulk liquid, thus forcing a change in phase behavior. Knowledge of how these properties change for various solvents as a function of CO₂ composition can lead to opportunities in design of reactions and separation process development. In this chapter, we explore the effect of CO₂ on the local polarity of acetonitrile by using a Menshutkin reaction as a molecular probe. This work is complemented by measuring the solvatochromic property π^* and the Kosower Z-value of CO₂-expanded acetonitrile.

Background on Menshutkin Reaction

The Menshutkin reaction is a nucleophilic substitution reaction with an S_N2 mechanism between a nitrogen base, typically a tertiary amine, and a sulfonate or an alkyl halide to form a quaternary ammonium salt in which the formal hybridization of the nitrogen atom is sp^2 or sp^3 .^{5,6} This class of reactions is a good probe of polarity because

its transition state is much more polar than the reactants, thus it has a strong kinetic dependence on the polarity of the surrounding medium. It has been studied in a variety of media from organic solvents⁷ to ionic liquids^{7, 8} to the gas phase.⁹

In this study we have chosen the reaction of tri-butylamine with methyl *p*-nitrobenzenesulfonate, as illustrated in Figure 4-1. This reaction is well-characterized and has been used to study the polarity and nucleophilicity of ionic liquids.^{7, 8} The

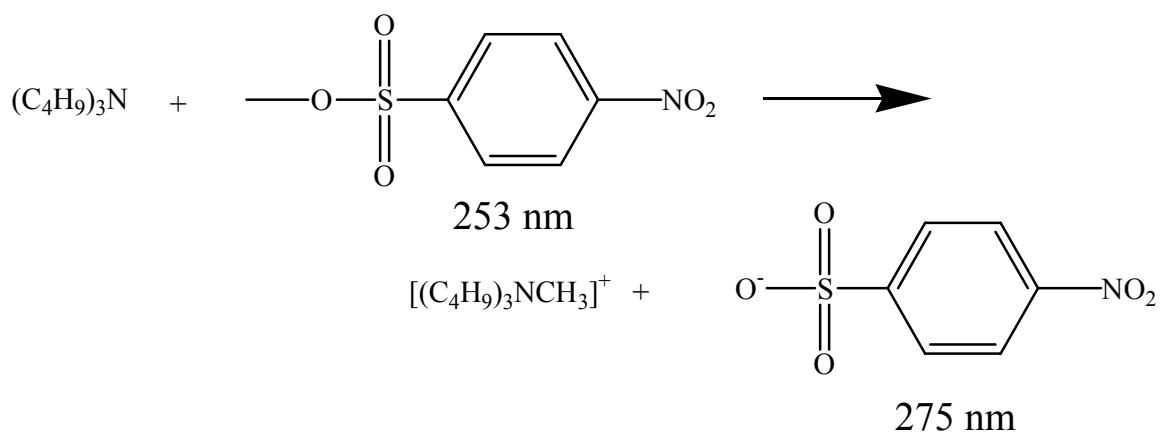


Figure 4-1: Reaction of tri-butylamine with methyl *p*-nitrobenzenesulfonate.

substrate has a λ_{max} at 253 nm while the product, the *p*-nitrobenzenesulfonate ion, has a λ_{max} at 275 nm. Because the two peaks are sufficiently separated, the reaction can be monitored *in situ* via UV-vis spectroscopy. The corresponding polar transition state, which plays a key role in probing the polarity in the cybotactic region, is shown in Figure 4-2. For each reaction it was possible to record absorbance values at 253 nm and 275 nm at known time intervals and use them to determine the rate of the reaction. An isosbestic point is always observed. Figure 4-3 shows a typical absorbance spectrum of the reaction over time.

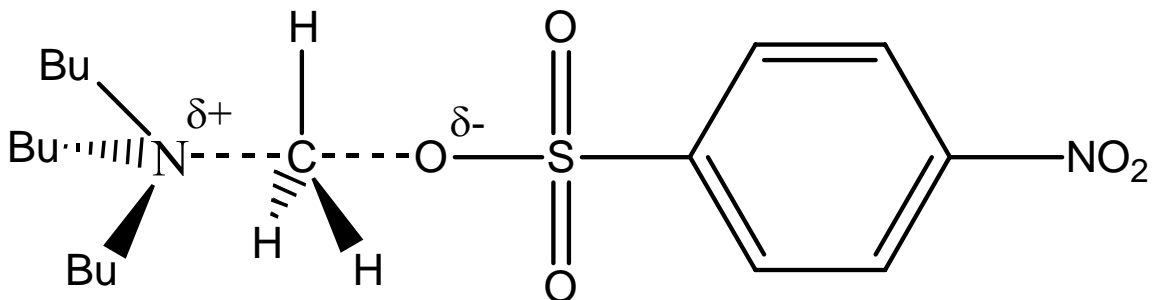


Figure 4-2: Polar transition state of the reaction of tri-butylamine with methyl *p*-nitrobenzenesulfonate.

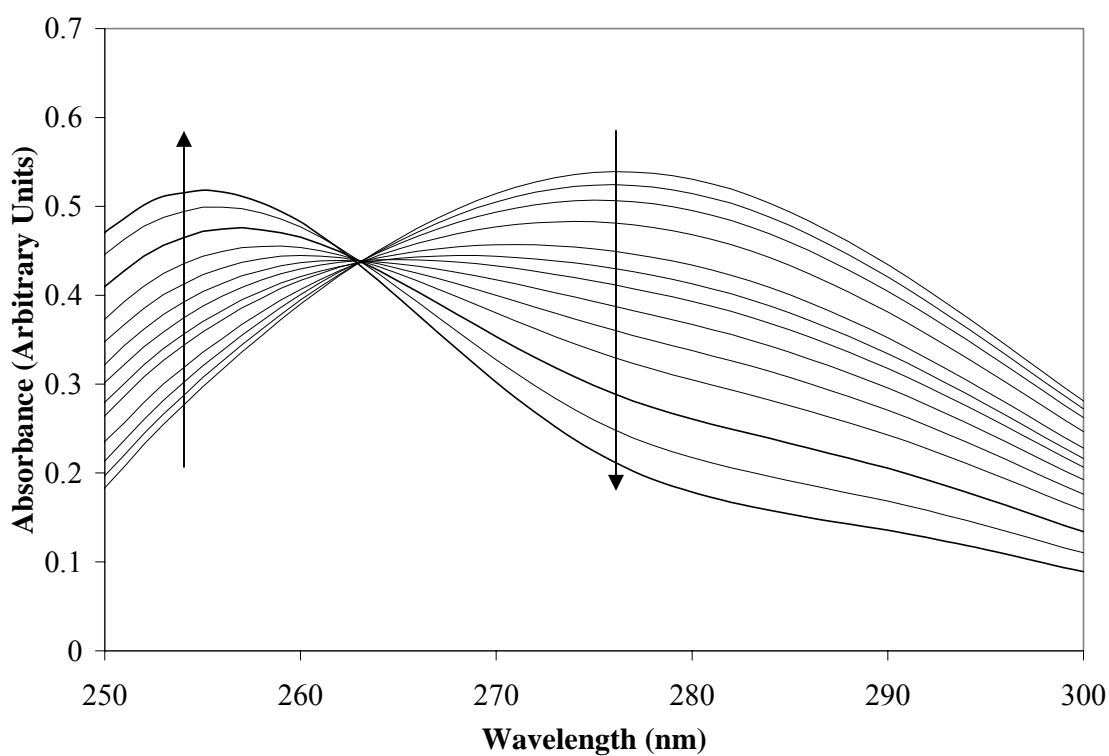


Figure 4-3: Typical UV spectra of the reaction of tri-butylamine with methyl *p*-nitrobenzenesulfonate. Arrows indicate increasing time.

Background on π^ Measurements*

The Kamlet-Taft dipolarity / polarizability parameter, π^* , provides a comprehensive measure of a solvent's ability to stabilize a solute molecule based on dielectric effects.¹⁰⁻¹² Because it is a measure of a probe molecule's response to its

surroundings upon excitation, π^* is a quantitative index of the solvent's dipolarity / polarizability in the cybotactic region of the ground state of the probe molecule.¹² The technique has been used extensively for measuring the polarity of pure solvents, ambient liquid mixtures^{13, 14} and CO₂-expanded solvents.^{10, 15} The experimental determination of individual π^* values are typically obtained from the shifts of the electronic absorption maxima of seven designated spectroscopic indicators.^{10, 11}

In this study *N,N*-dimethyl-4-nitroaniline (Figure 4-4) was the only probe chosen because this measurement serves as a complement to other measurements. The solvatochromic absorbance of *N,N*-dimethyl-4-nitroaniline corresponding to the spectral band at the longest wavelength is attributed to the $\pi \rightarrow \pi^*$ electronic transition due to an intramolecular charge transfer from N-(CH₃)₂ to NO₂ (electron donor to electron acceptor) through the aromatic system. A more polar solvent results in a greater electronic transition and therefore absorbance wavelength.

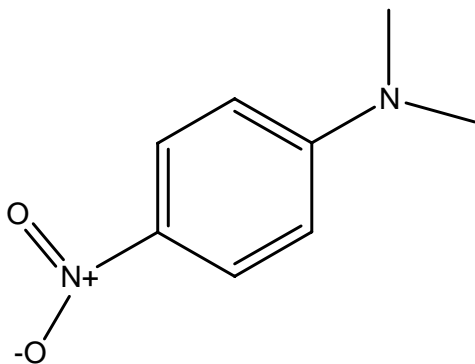


Figure 4-4: *N,N*-dimethyl-4-nitroaniline.

Background on Z-Value Measurements

Kosower developed a polarity parameter called the Z-value based on his findings that the charge-transfer light absorption band of 1-alkylpyridinium iodides is very

sensitive to solvent.^{16, 17} The Z-value is defined as the transition energy (E_T) for the longest wavelength absorption band observed for 1-ethyl-4-carbomethoxypyridinium iodide (Figure 4-5) in that solvent.¹⁷ This is not unlike scales such as E_T30 , Nile Red, Crystal Violet, etc.¹⁸ Governing equations are found in the experimental procedure section. A higher Z-value indicates a higher polarity.^{16, 17}

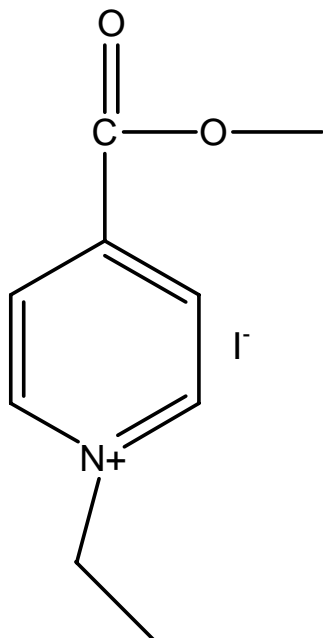


Figure 4-5: 1-Ethyl-4-carbomethoxypyridinium Iodide.

Experimental

Materials

Carbon dioxide was purchased from Airgas and filtered before use. Tri-n-butylamine (ReagentPlus, $\geq 98.5\%$), 1-Ethyl-4-carbomethoxypyridinium iodide (97%) and Acetonitrile (HPLC, $\geq 99.9\%$) were purchased from Sigma-Aldrich. Methyl *p*-nitrobenzenesulfonate and *N,N*-dimethyl-4-nitroaniline were purchased from Acros Organics. All solvents were used as received. No assays for water content were performed.

Apparatus

A stainless steel vessel with two sapphire windows (6.4 mm thick) was constructed for high pressure UV-vis spectroscopy. The windows were sealed with Teflon gaskets capable of withstanding pressures over 250 bar. The cell has a path length of 2.2 cm and an internal volume of 13 ml. Temperature was controlled with a refrigerated constant temperature flow bath (VWR 1150) with a mixture of ethylene glycol and water as the heat transfer fluid and monitored with a thermocouple and readout (Omega). The temperature variation was maintained within $\pm 0.1^\circ\text{C}$ of the set point. Pressure was monitored by a pressure transducer and readout (Druck) with an uncertainty of 0.01% in the range of 0-207 bar. A Teflon-coated, magnetic spin bar constantly agitated the contents of the cell to facilitate equilibrium. All measurements were performed on a Hewlett-Packard 8453 diode array UV-vis spectrophotometer (1 nm resolution and ± 0.2 nm wavelength accuracy). All measurements were performed in the same apparatus.

Procedure

The total liquid volume for each Menschutkin reaction was 11 ml. Stock solutions of tri-butylamine (2.8×10^{-2} M) and methyl *p*-nitrobenzenesulfonate (3.13×10^{-2}) in acetonitrile were made. Enough acetonitrile was added to the cell such that the total liquid volume in the reactor would be 11 ml upon addition of the reactants and the CO_2 . The cell was sealed to prevent evaporation as the liquid in the cell was allowed to reach an equilibrium temperature. An appropriate amount of each stock solution was added such that the final concentrations of reactants were 2.6×10^{-3} in tri-butylamine and 2.6×10^{-5} in methyl *p*-benzenesulfonate. A 100-fold excess of amine is used to achieve *pseudo*-

first-order kinetics. The cell was quickly sealed and an appropriate amount of CO₂ was added. Phase behavior data of CO₂ and acetonitrile at 25 °C and 40 °C were obtained from the literature.² The reaction progressed until the intensity of the product peak became comparable to that of the original reactant peak; ranging from 6 hours to 4 days depending on the temperature and composition.

Peak intensities at 253 nm and 275 nm were recorded and plotted as a function of time. A typical curve is shown in Figure 4-6. Data were treated by a least-squares fitting procedure¹⁹ using a user-defined function in OriginLab Software Package (version

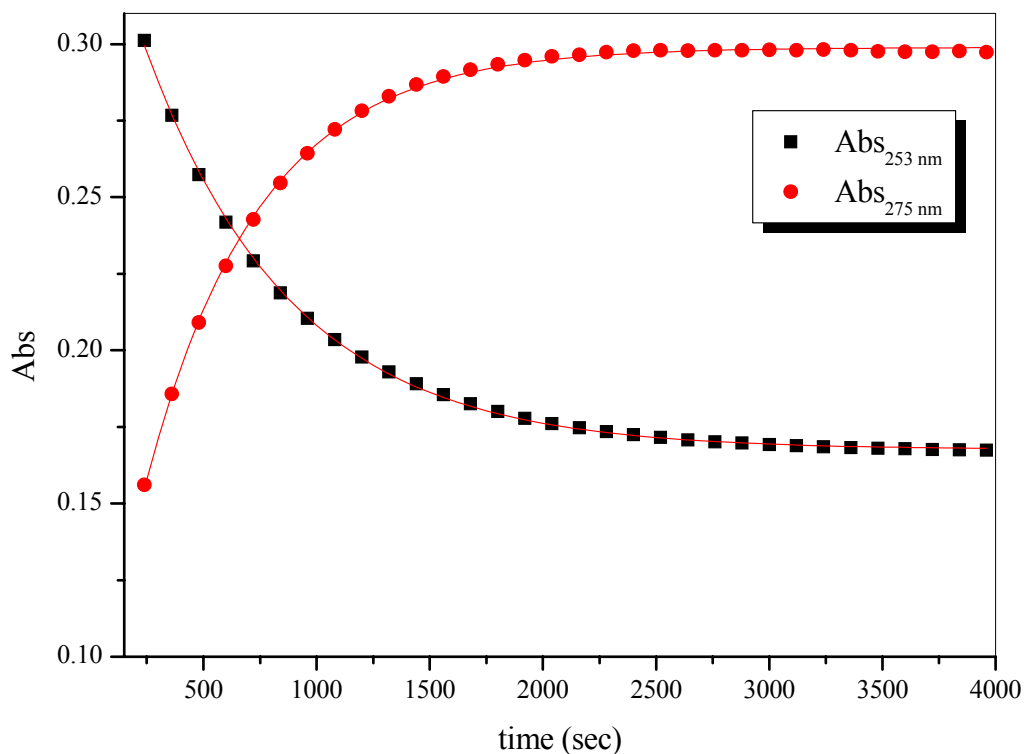
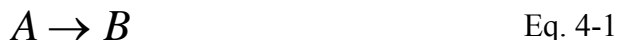


Figure 4-6: Typical absorbance vs. time plot of the reaction of tri-butylamine with methyl *p*-nitrobenzenesulfonate.

7.5, Student Version). Equations 4-1, 4-2 and 4-3 are fit to the data in order to determine the *pseudo*-first-order rate constant, k_{obs} . The model is based on a typical “A to B”

reaction where A_0 is the initial amount of substrate and B_∞ is the final amount of product. A and B are the amounts of substrate and product, respectively, at a given time, t . The constants C_1 and C_2 are required to correct for the fact that the UV absorbance is not zero when the concentration of A or B is equal to zero. The resulting k_{obs} value was divided by the initial concentration of the amine to convert it to a second-order rate constant.



$$A = A_0 e^{-k_{obs}t} + C_1 \quad \text{Eq. 4-2}$$

$$B = B_\infty (1 - e^{-k_{obs}t}) + C_2 \quad \text{Eq. 4-3}$$

For the solvatochromic measurements, a stock solution of *N,N*-dimethyl-4-nitroaniline (2×10^{-2} M) was prepared in ethanol. An appropriate amount of the stock solution was put into each of three flasks in order to make solutions (2×10^{-4} M) with acetonitrile (solvent of interest), DMSO and cyclohexane (reference solvents). Spectra of the DMSO and cyclohexane solutions were taken for reference. A known amount of acetonitrile solution was added to the cell which was already at the appropriate temperature. The cell was sealed and CO_2 was added incrementally with a spectrum taken at each loading after equilibrium was reached. The data were confirmed by releasing CO_2 incrementally and taking spectra upon reaching equilibrium.

As mentioned above, cyclohexane ($\pi^*=0.00$) and DMSO ($\pi^*=1.00$) were measured as reference solvents for normalization of the π^* scale. Quantification of π^* for different acetonitrile / CO_2 mixtures is given by Equation 4-4, where ν is the frequency (cm^{-1}) of the solvatochromic peak maximum in the corresponding solvent.

$$\pi^* = \frac{V_{Mixture} - V_{Cyclohexane}}{V_{DMSO} - V_{Cyclohexane}} \quad \text{Eq. 4-4}$$

For the Z-value measurements, a solution of the probe molecule of the appropriate concentration (2.23×10^{-2} M) was made in acetonitrile, methanol and benzene (reference solvents). A known amount of acetonitrile solution was added to the thermostated cell in the same manner described above. The cell was sealed and CO₂ was added incrementally with a spectrum taken at each loading after equilibrium was reached. The data were confirmed by releasing CO₂ incrementally and taking spectra upon reaching equilibrium.

Quantification of the Z-value for different acetonitrile / CO₂ mixtures is given by Equation 4-5, where λ is the wavelength of the position of the maximum in angstroms. This equation is derived from the definition of the Z-value, which is described above as the transition energy (E_T) for the longest wavelength absorption band observed for 1-ethyl-4-carbomethoxypyridinium iodide. This definition is given in mathematical terms in Equation 4-6, where E_T is the transition energy, h is Planck's constant (6.624×10^{27} erg-second), and ν is the frequency (λ^{-1}) of the photon which produces the transition.

$$Z = \frac{2.859 * 10^5}{\lambda} \quad \text{Eq. 4-5}$$

$$Z = E_T = h\nu \quad \text{Eq. 4-6}$$

Results and Discussion

Reaction Kinetics

Second-order reaction rates measured in CO₂ / acetonitrile mixtures at 25 and 40 °C at compositions up to 0.776 CO₂ are presented in Figure 4-7. As expected, there is

generally a decrease in reaction rate as CO₂ composition is increased. The behavior is approximately “S-shaped”. At 25 °C there appears to be a slight increase in reaction rate at low compositions of CO₂ which is followed by a sharp decrease as more CO₂ is added. At 40 °C this peak disappears.

There are several explanations for the presence of the peak. First of all it may be attributed to experimental uncertainty. The change in rate is smaller than the accuracy of

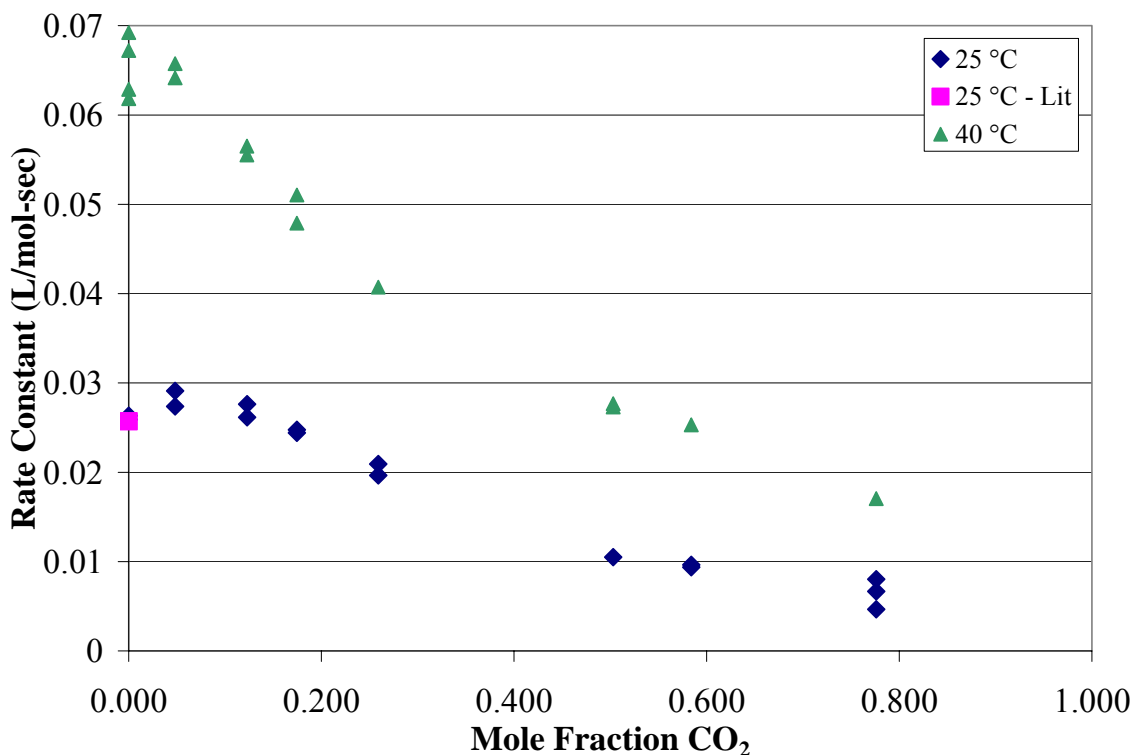


Figure 4-7: Second order rate constants for Menshutkin reaction in CO₂-expanded acetonitrile as a function of composition.

the measurements, thus the observed maximum may not be “real”, but rather an artifact of scatter in an “S-shaped” curve. The fact that it exists at 25 °C but disappears at 40 °C lends some credibility to this argument. However, it is important to consider that the peak may in fact be real and speculate as to what physical phenomenon is driving it.

To help determine the validity of the peak, *pseudo*-first-order rate constants are presented in Figure 4-8. The rationale was that if they did not show a peak in the same place then it could be ruled out as uncertainty in the concentration. If it did show a peak then it lends more credibility to the validity of the peak. As can be seen in Figure 4-6, the peak exists in the *pseudo*-first-order rate constants as well.

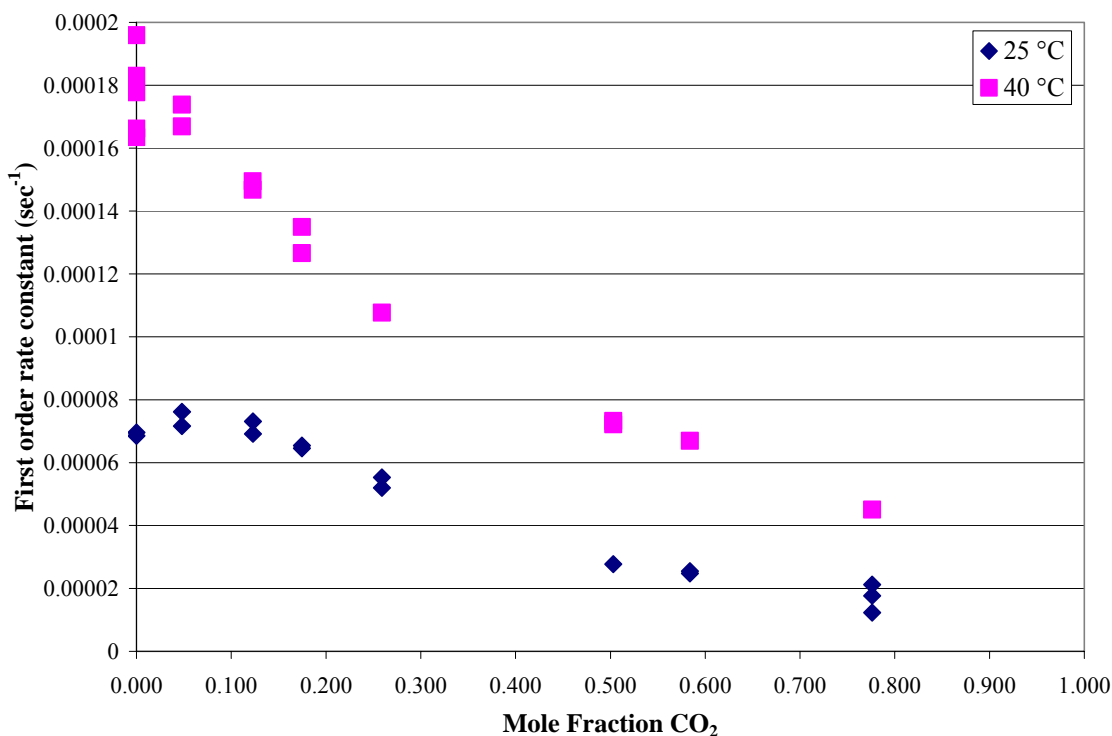


Figure 4-8: First order rate constants for Menshutkin reaction in CO₂-expanded acetonitrile as a function of composition.

If the peak is real, we speculate that the density changes as a function of composition of CO₂ / acetonitrile is the reason. The density of the liquid increases significantly as CO₂ is added to the system until it is approximately 0.6-0.7 CO₂, depending on temperature, at which point it reaches a maximum and decreases as more CO₂ is added to the system (Figure 4-9). While the cybotactic region of the reaction cannot have more acetonitrile in it than when it is in pure acetonitrile, the increase in

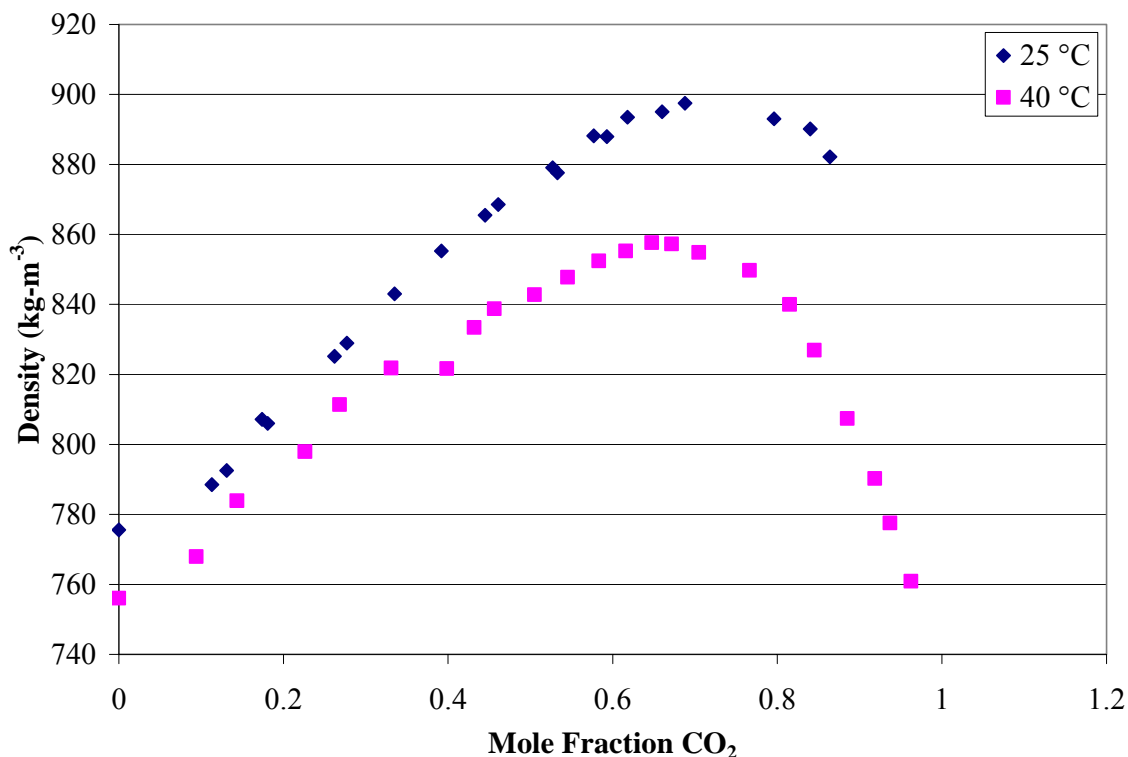


Figure 4-9: Density of Acetonitrile + CO₂.

density with a small amount of CO₂ could ensure that the reaction could “see” as much acetonitrile at low CO₂ compositions as it does when there is no CO₂ present. The partial molal volume of the transition state²¹ of typical Menshutkin reactions in normal liquids is on the order of 190-240 cm³mol⁻¹ (Table 4-1). Such a large transition state would be able to “see” at least as many molecules in its cybotactic region as the substrate does. The fact that the peak occurs at 25 °C and not at 40 °C could be explained by the fact that the density change as a function of CO₂ pressure is not as strong at 40 °C.

It is also important to consider that the large activation volume – additional volume required for the activated state²⁰ – of the reaction could have an effect. Typical activation volumes^{21, 22} of Menshutkin reactions is on the order of -25 to -65 cm³mol⁻¹ (Table 4-2). It is important to note that the behavior in normal liquids may be significantly different than that in gas-expanded liquids, but that it serves as a valid

preliminary starting point. Such high activation volumes can have a strong density effect with regard to hydrostatic pressure. However, the maximum pressure change in these reactions is on the order of approximately 30 bar, whereas most organic liquids require a pressure on the order of a kilobar before the density is significantly changed, so an effect due to hydrostatic pressure is unlikely.

Table 4-1: Partial molal volumes of the transition states of typical Menshutkin reactions.

| Solvent | Partial Molal Volume (cm³/mole) |
|----------------------|---|
| Acetone | 233.4 |
| Butyl Chloride | 212.7 |
| Carbon Tetrachloride | 190.1 |
| Cyclohexanone | 225.6 |
| Dichloromethane | 226.2 |
| Nitrobenzene | 225.1 |
| Nitromethane | 230.2 |
| Propionitrile | 231.5 |
| THF | 208.5 |

Table 4-2: Activation volumes of typical Menshutkin reactions.

| Reaction / Solvent | Activation Volume (cm³/mol) |
|---|---|
| <u>Reaction: Tri-n-propylamine with methyl iodide</u> | |
| Acetone | -28.6 |
| Cyclohexanone | -30.3 |
| Dichloromethane | -31.5 |
| Nitrobenzene | -26.4 |
| Nitromethane | -30.8 |
| Propionitrile | -26.6 |
| Butyl Chloride | -43.3 |
| THF | -47.5 |
| Carbon Tetrachloride | -64.7 |
| <u>Reaction: Methyl Iodide with Pyridine</u> | |
| Carbon Tetrachloride | -37.5 |
| Benzene | -35.1 |
| Acetone | -33.2 |
| Chlorobenzene | -30.7 |
| Methanol | -26.6 |
| Nitrobenzene | -21.3 |

Another seemingly unexpected aspect of the behavior is the fact that the curve is S-shaped. Other probes of the cybotactic region of GXLs, such as solvatochromic properties (α , β and π^*), exhibit very different behavior than this probe. Solvatochromic parameters of GXLs appear to stay near the same value as that of the pure liquid as CO₂ is added until the composition is approximately 0.8 CO₂, at which time the property more abruptly decreases.¹⁵ These are explored more thoroughly in the following section.

It is also important to point out that while the Menshutkin reaction rates behave in a way which is inconsistent with solvatochromic properties, they are consistent with several other similar measurements. Rates of the *cis-trans* isomerization of azo-benzene in CO₂-expanded dioxane show nearly linear behavior with respect to CO₂ pressure (Figure 4-10).²³ Furthermore, dielectric constants at 40 °C measured for CO₂-expanded

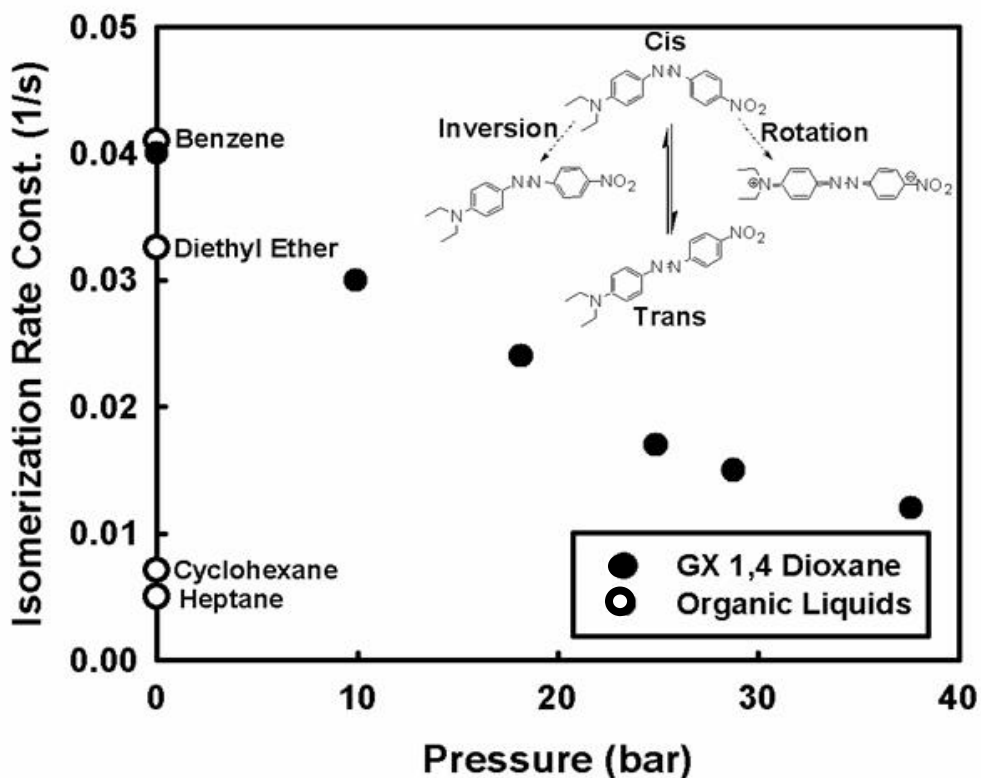


Figure 4-10: *Cis-trans* isomerization of azo-benzenes in CO₂-expanded dioxane as a function of CO₂ pressure.

methanol decrease almost linearly as a function of CO₂ pressure (Figure 4-11).²⁴ The rate of reaction measured in the latter study increases almost linearly as a function of CO₂ pressure which is consistent, albeit opposite, with the rate behavior in this and the azobenzene studies.

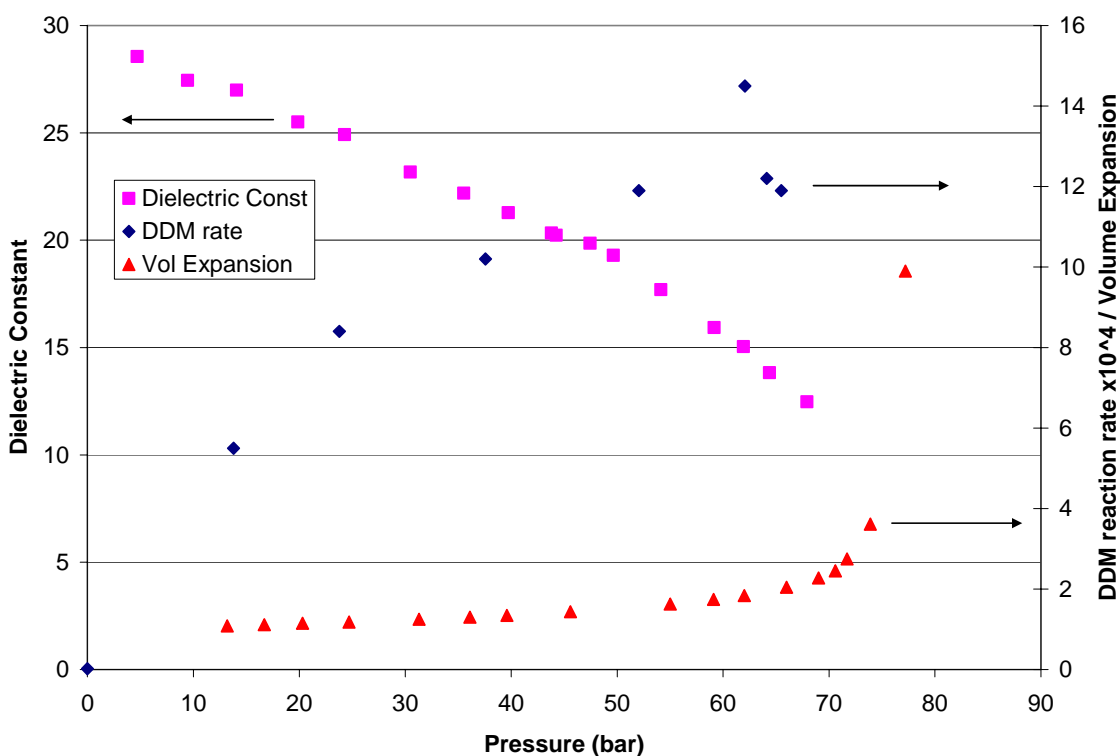


Figure 4-11: Dielectric constants of CO₂-expanded methanol as a function of CO₂ pressure.

Pi Shifts*

The π^* shifts in CO₂-expanded acetone at 40 °C are shown in Figure 4-12. The π^* data indicate that even though CO₂ is being added to the system, the cybotactic region around the probe is still mostly organic solvent. Based on the shape of the curve – the slow drop off at low CO₂-composition followed by a steep decrease – it appears that there is a local-polarity augmentation and the data suggest the presence of an acetonitrile-rich

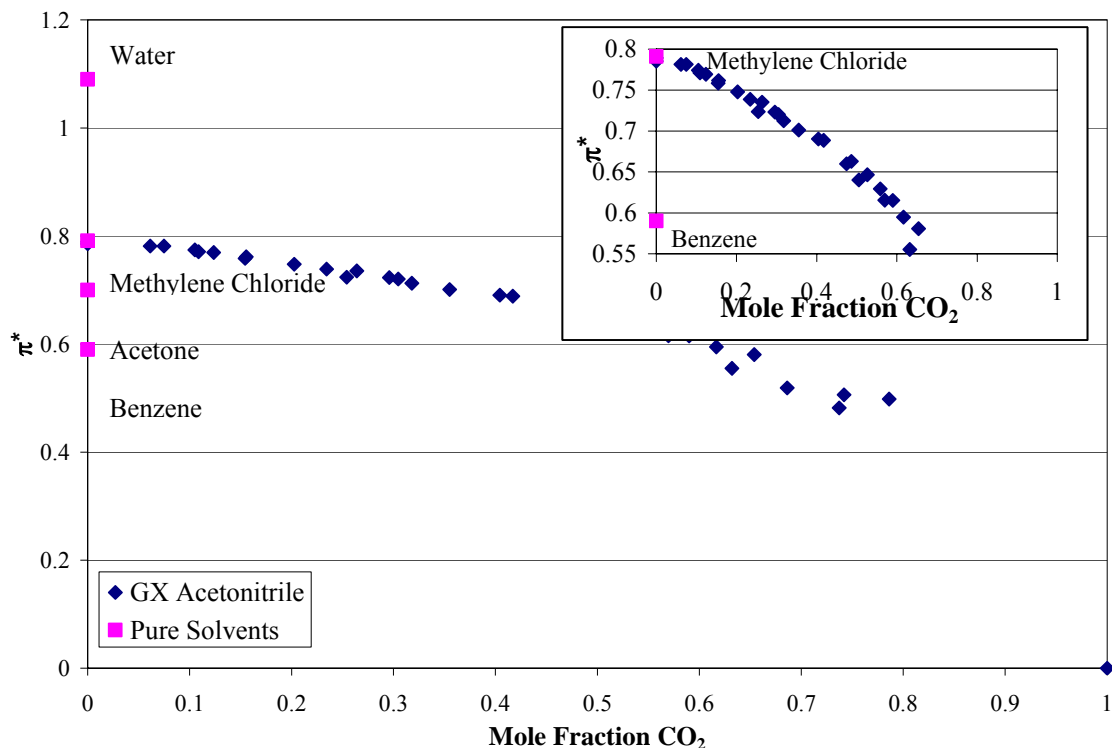


Figure 4-12: π^* of CO₂-expanded acetonitrile, 40 °C, compared with other solvents. Zoomed inset to emphasize difference in polarity between methylene chloride and benzene.

solvation shell in the cybotactic region of the probe. Furthermore, the data indicate that the polarity of acetonitrile / CO₂ mixtures can be tuned from a π^* of acetonitrile to less than that of benzene. This is very powerful when trying to use CO₂ as an anti-solvent in crystallization processes or to force a phase split of two organics which respond differently to the presence of CO₂. This behavior is consistent with π^* measurements for methanol and acetone.¹⁵

As mentioned above, this behavior is different than that of the second-order rate constants discussed in the previous section. The π^* measurements indicate a local polarity augmentation. If such an augmentation did actually exist, it would be expected that the kinetic data would behave similarly. The S-shaped curve is consistent with what could be expected in bulk properties such as the dielectric constant.

We speculate two reasons for this observation. The probe, the nucleophile and the solvent all contain nitrogen, which associates strongly with CO₂. The presence of the nitrogen may be bringing CO₂ into the cybotactic region. The second speculation is that the transition state is not present long enough for the solvent to rearrange, thus it responds to bulk polarity instead of local polarity.

One important consideration is that π^* versus reaction rate might not be the appropriate comparison. Typically, π^* shifts are compared with the natural logarithm of the reaction rates when looking for a correlation in mixed solvents.¹³ A correlation between the natural logarithm of the second order rate constant and π^* is shown in Figure 4-13. While the comparison is not linear, it shows only slight curvature. This suggests that even though the rate data are more consistent with bulk properties and

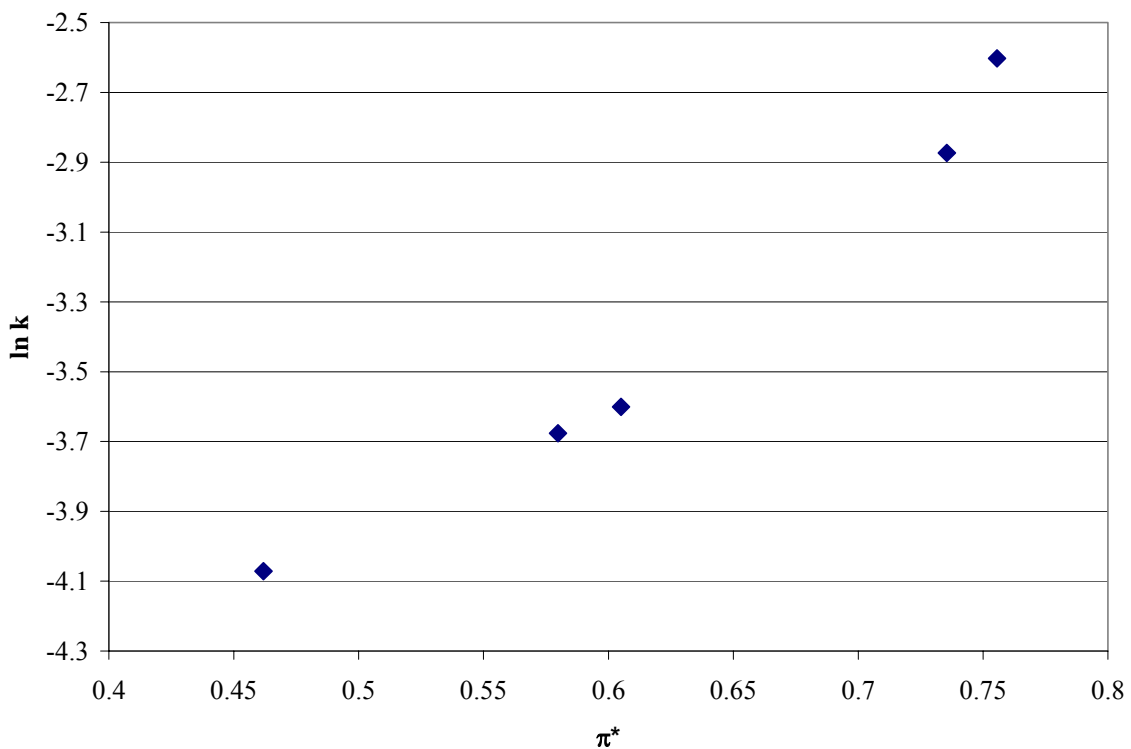


Figure 4-13: Correlation of π^* with second-order rate constants.

that π^* is indicative of what is happening in the cybotactic region, their behaviors can be correlated and that at least the trends are consistent with one another. Both are valid measures of solvent polarity. In an effort to see if the relationship is universal, Figure 4-14 shows data for methylene chloride and water.⁸ The relationship is not applicable to all classes of solvents.

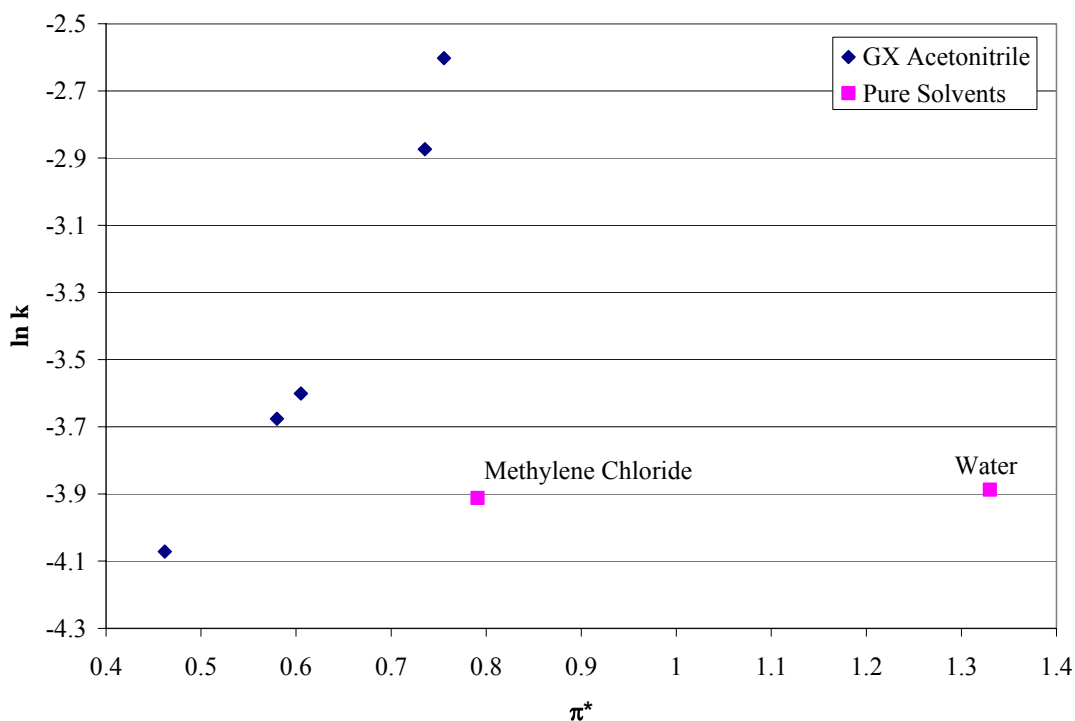


Figure 4-14: Correlation of π^* with second-order rate constants for GXL and pure solvents.

Z-Values

Z-values were measured in order to help elucidate this discrepancy and also to give another measure of the polarity of CO₂-expanded acetonitrile. As Figure 4-15 shows, the Z value decreases linearly and slowly as a function of CO₂ composition. Literature values of the Z-values of several solvents are plotted on the same graph in order to put into perspective the polarity.¹⁷ As Figure 4-15 shows, the addition of CO₂

tunes the polarity of acetonitrile to something DMF- or methylene chloride-like based on the Z-value scale. This is somewhat unexpected because one might expect that the polarity would decrease more than it appears to do. However, the results are consistent with the presence of an acetonitrile-rich solvation shell within the cybotactic region of the probe molecule. This is inconsistent with the kinetic results but consistent with the π^* values.

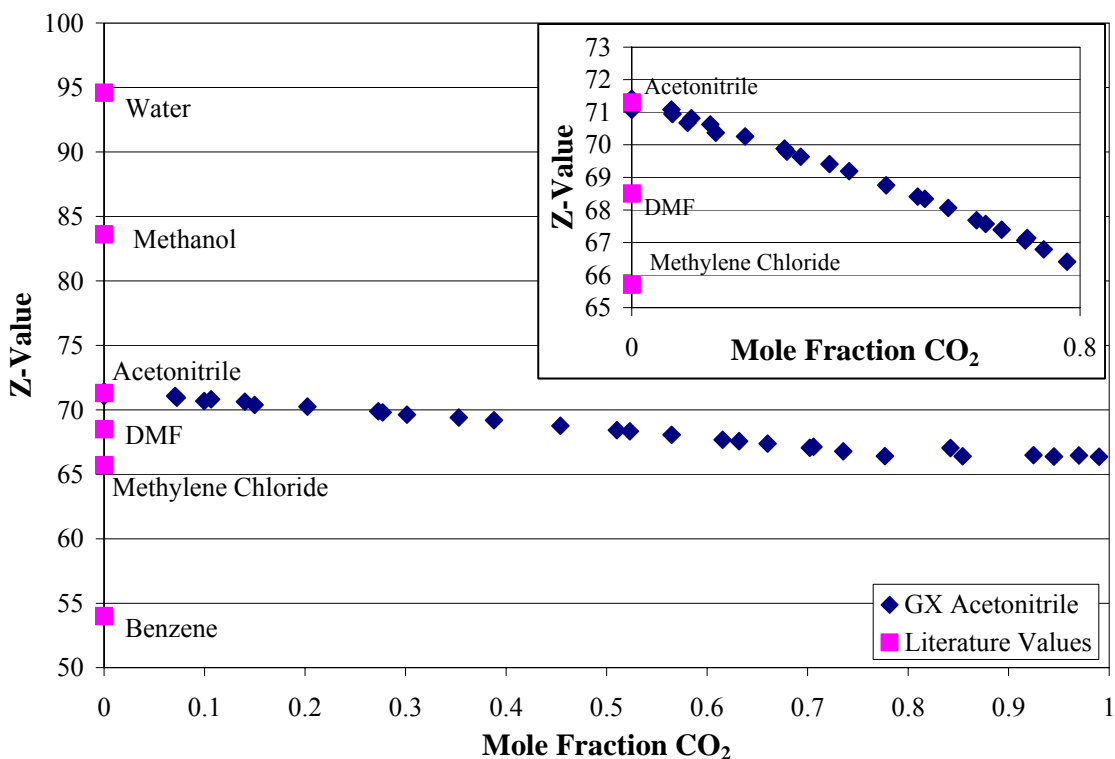


Figure 4-15: Z-values of CO₂-expanded acetonitrile as a function of CO₂ composition, T=40 °C, and Z-values of conventional solvents.

The natural logarithms of the second-order rate constants were plotted against the Z-values as a comparison to the π^* correlation in Figures 4-13 and 4-14 above (Figures 4-16 and 4-17). Two literature values^{8, 17} were plotted for the sake of comparison and to see if the correlation is universal. The natural logarithms of the rate constants correlate well with the Z-values, with a correlation constant of 0.9955. In this

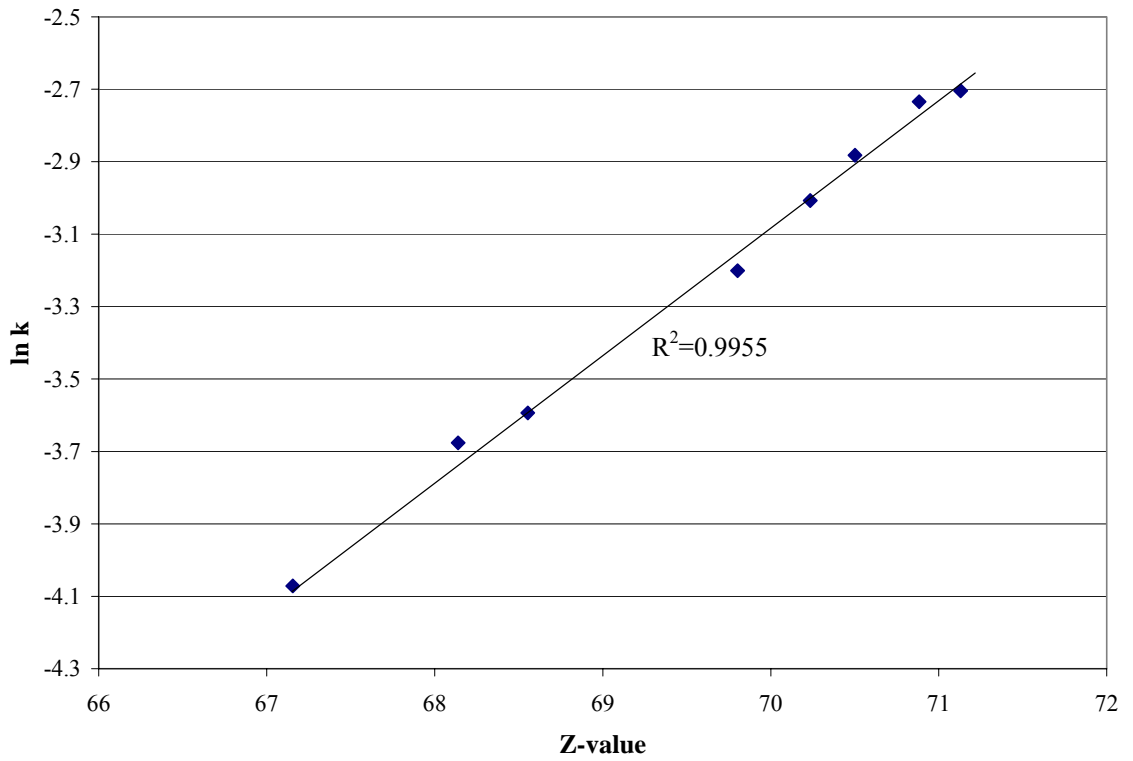


Figure 4-16: Correlation of Z-value with second order rate constants.

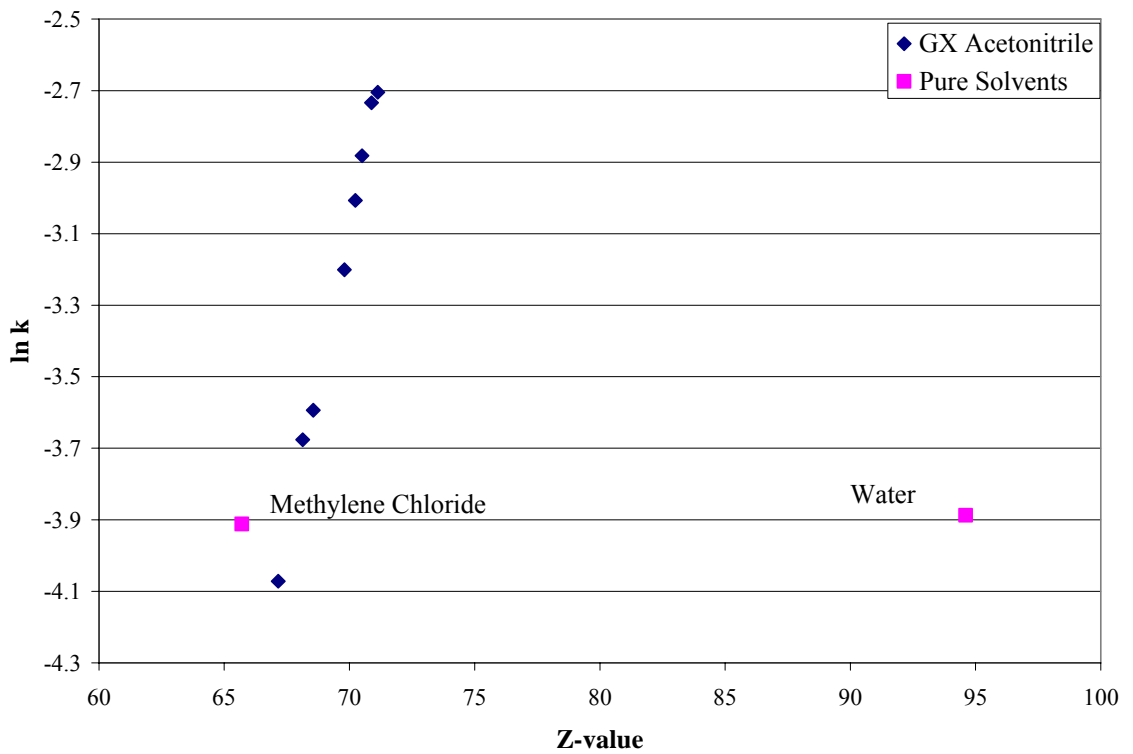


Figure 4-16: Correlation of Z-value with second order rate constants for CO₂-expanded acetonitrile and pure solvents.

instance, methylene chloride falls almost on the line while water is a strong outlier. The correlation is not universal, but may be valid for aprotic solvents. Further studies must be performed before such a conclusion can be drawn.

For the purpose of comparison, Z-values were plotted against π^* in order to determine whether there exists a correlation in CO₂-expanded acetonitrile (Figure 4-18). Observation of the data indicates a relationship between Z-values and π^* shifts, though the correlation is not linear. Literature values for several solvents are plotted in Figure 4-19 to see whether there is a universal relationship between Z-values and π^* shifts. Because π^* shifts are influenced more strongly by solute-specific interactions and are more sensitive to changes in the cybotactic region the relationship is not universal. In fact, it seems that there is no general relationship between Z-values and π^* despite the

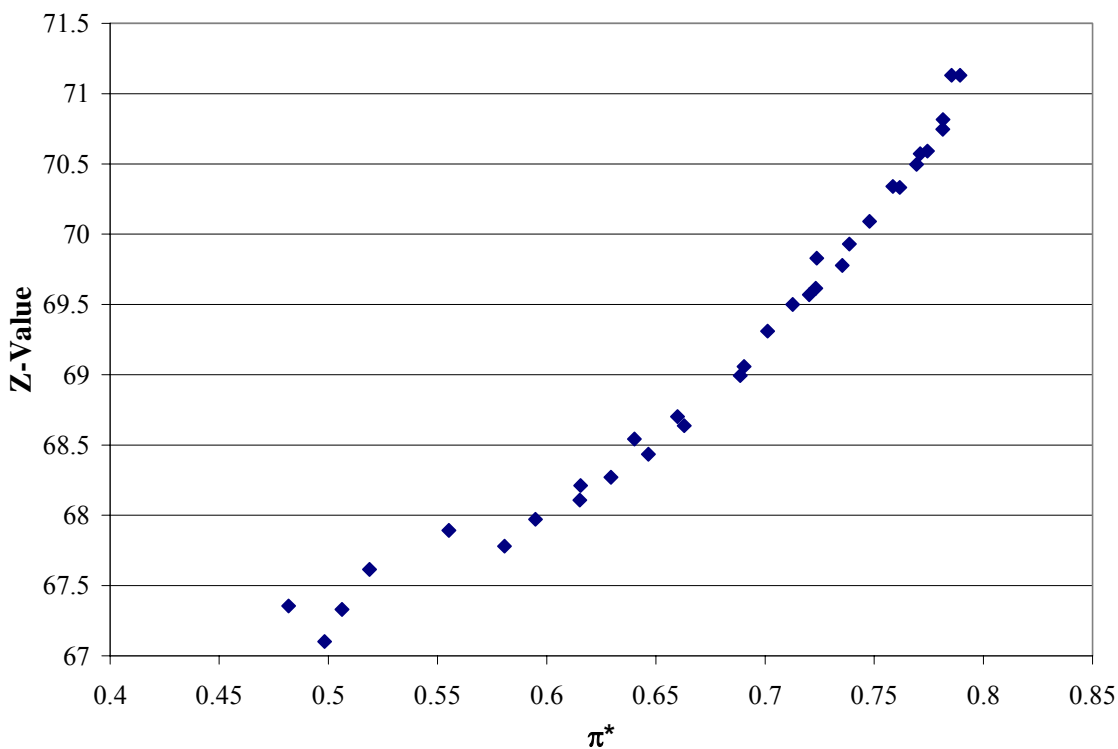


Figure 4-18: Correlation of Z-values with π^* of CO₂-expanded acetonitrile.

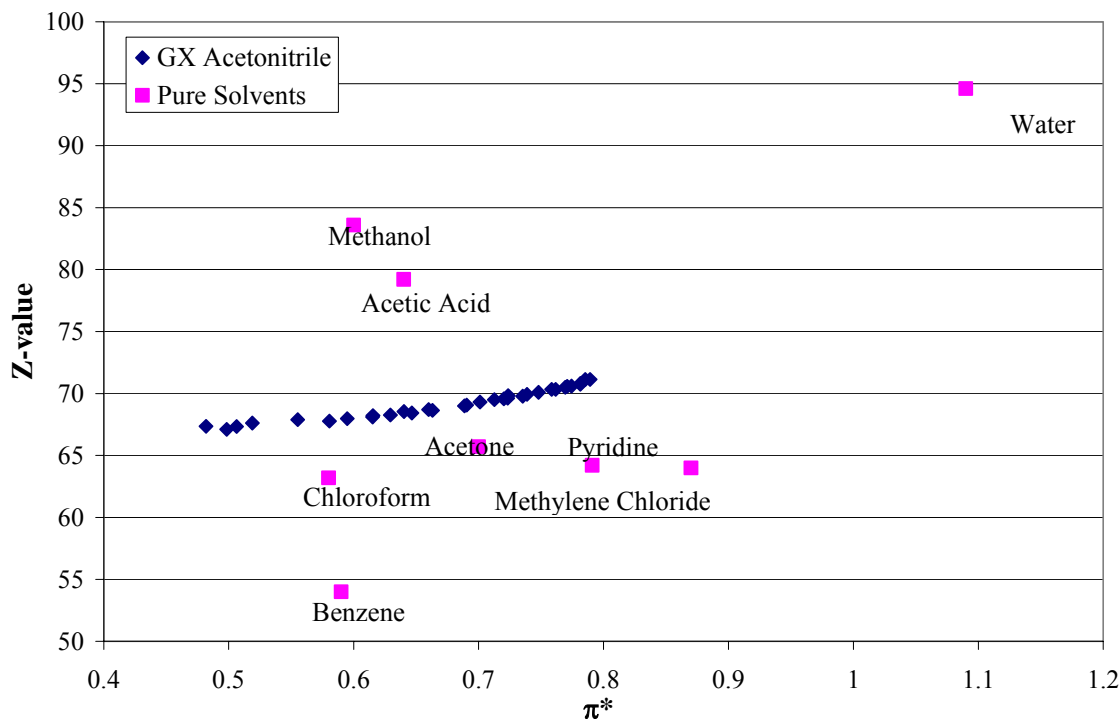


Figure 4-19: Correlation of Z-values with π^* of CO₂-expanded acetonitrile and conventional solvents.

fact that both are measures of solvent polarity. This is an excellent example of why it is difficult to define or choose a scale by which to determine solvent polarity.

Dipole Moment of the Transition State

In order to gain insight into the electrostatic properties of the transition state, a Kirkwood²⁵ plot (Figure 4-20) was generated. This is a plot of the rate constant versus the dielectric parameter (Equation 4-7) where ϵ is the dielectric constant of the solvent. The slope of the Kirkwood plot gives information on the dipole moments of the reacting species and the transition state.²⁶ The dielectric constant of acetonitrile was obtained from DIPPR and the dielectric constant of CO₂ was estimated by parameterizing functions of density from equations of state.²⁷ The dielectric constant of the mixed solvent is the volume fraction average of the two values.

$$\frac{\epsilon - 1}{2\epsilon + 1}$$

Eq. 4-7

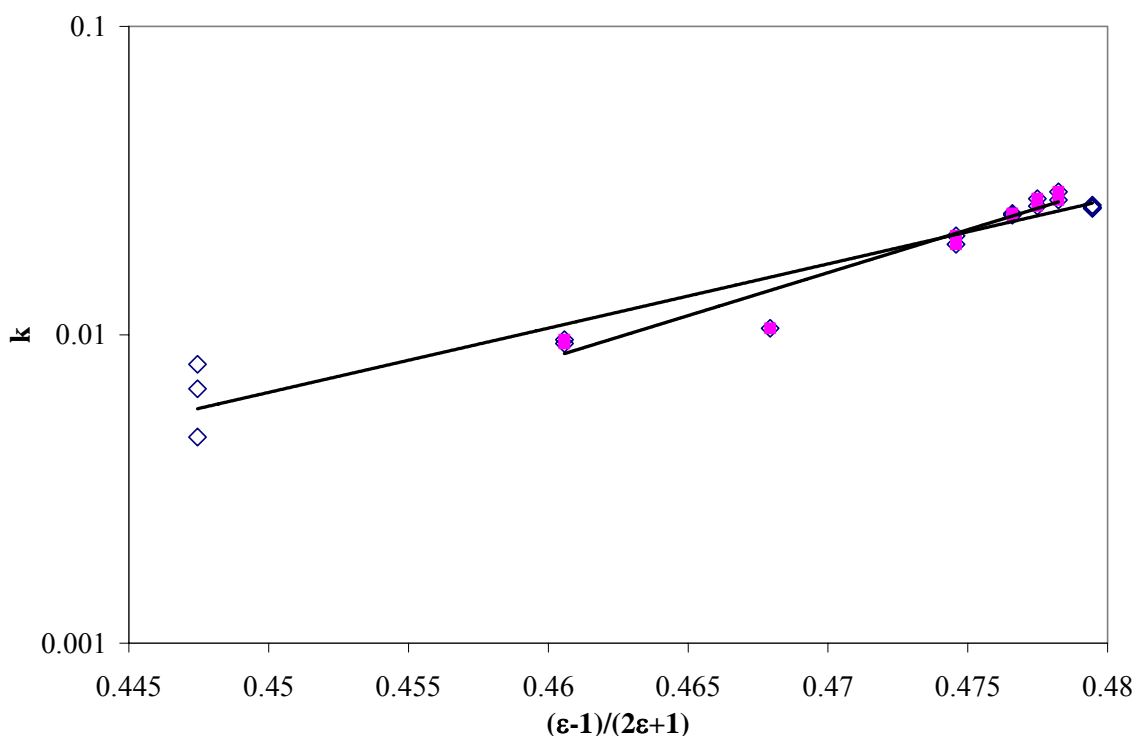


Figure 4-20: Kirkwood plot of data – Fit with and without the end points.

In order to use the slope to determine the dipole moment of the transition state it is necessary to know the dipole moments of the reacting species and the diameters of the reacting species and transition state.²⁶ The dipole moment of the amine was obtained from DIPPR and found to be 0.78 Debye while that of the substrate was estimated using the Spartan software package and found to be in the range 3.2-4.5 Debye. The diameter of each species was found by using the molar density and assuming spherical geometry. While it is a large assumption, it is standard.²⁸ Applying these estimates results in a transition state dipole moment of 5.4-7.4 Debye, which is substantially lower than typical Menshutkin reactions.^{21, 26, 28, 29} This can be attributed to the fact that this transition state

behaves differently than the transition states in the aforementioned Menschutkin reactions or to limitations in Kirkwood's theory.

Care must be taken when using the Kirkwood relationship because it assumes linearity. Inspection of Figure 4-20 tells us that the behavior is non-linear. The derivative is greatest at the right, where the system is more acetonitrile-rich, and decreases as one moves left towards the CO₂-rich region. A steeper derivative indicates a larger dipole moment, so it makes sense that the slope would be greater in the region that is rich in the more polar solvent. However, it makes it difficult to conclude anything about the polarity of the transition state.

In an effort to compare the three measures of polarity described above with the estimated dielectric constants, all data were normalized to their respective values in pure acetonitrile and put on the same plot along with the normalized dielectric constant calculated for the mixture (Figure 4-21). Each probe behaves very differently in response to the polarity of the surrounding medium, thus implying different conclusions. The rate constant variation with composition mimics that of the bulk phase, which is consistent with the examples expressed above. The dielectric constant is a bulk property; that it behaves as such is expected. The Z-values should respond to the cybotactic region because they do involve a solvent-sensitive electronic transition. At nearly 0.98 CO₂ the Z-value indicates a polarity of approximately that of acetone when one would expect that it would behave more like cyclohexane. One might speculate that the Z-value would drop significantly if measured in pure CO₂, but it cannot be measured due to the negligible solubility of the probe. The behavior of π^* as a function of composition is

consistent with other measurements in similar media and indicates the presence of acetonitrile-rich solvation shells about the probe.

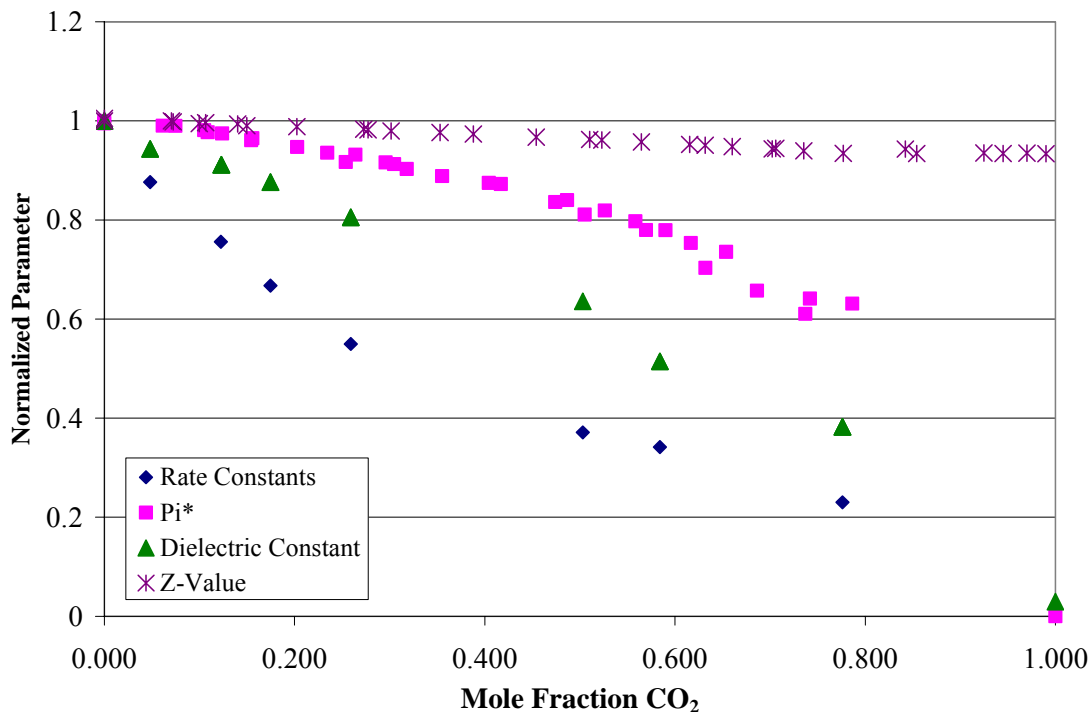


Figure 4-21: Polarity probe data and dielectric constants of CO₂ / acetonitrile mixtures, normalized to pure acetonitrile, 40 °C.

Inspection of all plots together can help provide insight into how best to measure polarity for the design of a particular process. For example, an appropriate composition for a particular reaction rate can be selected using the Menshutkin reaction or some other reaction probe. For the purpose of forcing a separation, whether for liquid-liquid systems or for crystallization, the Z-value or π^* might be more pertinent. The vast difference in the behavior of the probes from one another emphasizes the need to consider all of them when trying to learn about the polarity.

Temperature Dependence: Determination of the Activation Energy

In an effort to gain an understanding of the temperature-sensitivity of the Menshutkin reaction in question, the activation energy was calculated (Figure 4-22).

Having measured the reaction at four temperatures, we calculated an activation energy of 10.8 kcal/mole. This value is on the low end of activation energies typically reported for Menshutkin reactions^{28, 30} (10-20 kcal/mol, Table 4-3), but it is not unlike the activation energy of tri-n-propylamine with methyl iodide (8.4 kcal/mol).²⁸ The low activation energy is consistent with systems with increased solvation of the transition state.^{21, 28} The increased solvation is due to the similar polarity between the transition state and the solvent. If either the transition state or the solvent were non-polar the reaction would not run as readily.

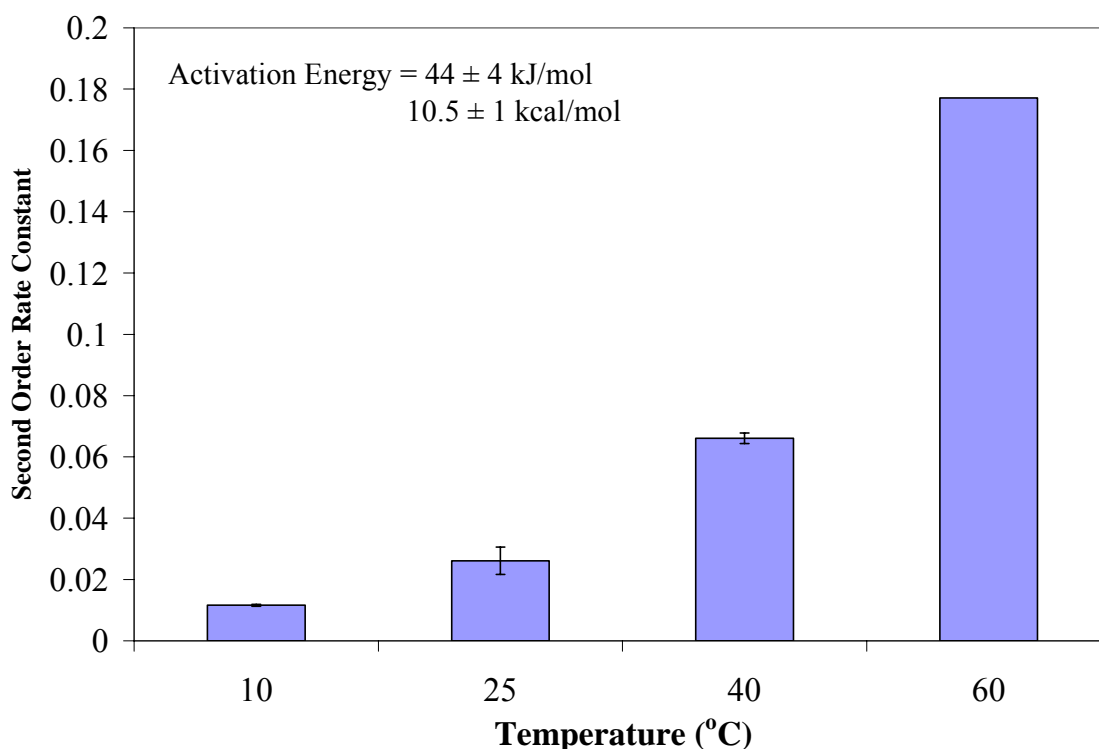


Figure 4-22: Determination of the activation energy of the Menshutkin reaction.

Summary

Rate constants of the Menshutkin reaction between tri-butylamine and methyl *p*-nitrobenzenesulfonate were measured in mixtures of acetonitrile and carbon dioxide at 25

and 40 °C and in pure acetonitrile at 10 and 60 °C. Plots of both the *pseudo*-first-order and second-order rate constants versus CO₂ composition show an approximate S-shaped decrease with the addition of CO₂ and the indication of a slight increase in rate with small amounts of CO₂ at 25 °C, which may be a result of local density augmentations or baseline noise of the measurement. The shape of the curve is consistent with bulk properties as opposed to local properties, which tells us that the polarity in this system behaves the same in the bulk and local phases relative to the probe reaction, that the rearrangement of the cybotactic region in response to the presence of the transition state is slower than the lifetime of the transition state, or that the presence of nitrogen in all reaction species are attracting enough CO₂ to the reaction site as to mimic the bulk phase. The behavior is consistent with other reaction probes of polarity of GXLs.

To complement the above findings, measurements of π^* and Z-values were made on CO₂-expanded acetonitrile at 40 °C. The π^* measurements in this system are consistent with π^* measurements of other expanded solvents. While Z-values have not been measured in GXLs as far as we have found, the results indicate that at 98% CO₂ the polarity of the mixture is equivalent to that of DMF when one would expect it to be more like cyclohexane. Thus it appears that there is a strong preferential solvation of the probe in acetonitrile which is indicative of the presence of solvation shells or heterogeneity in the cybotactic region.

The activation energy of this reaction is consistent with the low end of the range of other reactions of this type, indicating increased solvation of the transition state by the solvent.

REFERENCES

1. de la Fuente Badilla, J. C.; Peters, C. J.; de Swann Arons, J., Volume expansion in relation to the gas-antisolvent process. *J. Supercrit. Fluids* **2000**, 19, 13-23.
2. Kordikowski, A.; Schenk, A. P.; Van Nielen, R. M.; Peters, C. J., Volume expansions and vapor-liquid equilibria of binary mixtures of a variety of polar solvents and certain near-critical solvents. *J. Supercrit. Fluids* **1995**, 8, 205-216.
3. Musie, G.; Wei, M.; Subramaniam, B.; Busch, D. H., Catalytic oxidations in carbon dioxide-based reaction media, including novel carbon dioxide-expanded phases. *Coord. Chem. Rev.* **2001**, 219-2211, 789-820.
4. Wei, M.; Ghezai, T. M.; Busch, D. H.; Subramaniam, B., Carbon dioxide-expanded solvents: Unique and versatile media for performing homogeneous catalytic oxidations. *J. Am. Chem. Soc.* **2002**, 124, (11), 2513-2517.
5. Lowry, T. H.; Richardson, K. S., *Mechanism and Theory in Organic Chemistry*. 3 ed.; Harper Collins: New York, 1987.
6. Abboud, J. L. M.; Notario, R.; Bertran, J.; Sola, M., One Century of Physical Organic Chemistry: The Menschutkin Reaction. In *Progress in Physical Organic Chemistry*, Taft, R. W., Ed. John Wiley and Sons: New York, 1993; Vol. 19.
7. Skrzypczak, A.; Neta, P., Rate constants for reaction of 1,2-dimethylimidazole with benzyl bromide in ionic liquids and organic solvents. *International Journal of Chemical Kinetics* **2004**, 36, (4), 253-258.
8. Crowhurst, L.; Lancaster, N. L.; Perez Arlandis, J. M.; Welton, T., Manipulating solute nucleophilicity with room temperature ionic liquids. *J. Am. Chem. Soc.* **2004**, 126, (37), 11549-11555.
9. Sola, M.; Lledos, A.; Duran, M.; Bertran, J.; Abboud, J. L. M., Analysis of solvent effects on the Menschutkin reaction. *J. Am. Chem. Soc.* **1991**, 113, (8), 2873-2891.
10. Lu, J.; Liotta, C. L.; Eckert, C. A., Spectroscopically probing microscopic solvent properties of room-temperature ionic liquids with the addition of carbon dioxide. *J. Phys. Chem. A* **2003**, 107, 3995-4000.

11. Sigman, M. E.; Lindley, S.; Leffler, J. E., Supercritical carbon dioxide - Behavior and solvatochromic indicators in media of different densities. *J. Am. Chem. Soc.* **1985**, 49, (107), 1471-1472.
12. Yonker, C. R.; Smith, R. D., Solvatochromic behavior of binary supercritical fluids: the carbon dioxide/2-propanol system. *J. Phys. Chem.* **1988**, 92, 2374-2378.
13. Mancini, P. M.; Fortunato, G.; Adam, C.; Vottero, L. R.; Terenzani, A. J., Specific and non-specific solvent effects on aromatic nucleophilic substitution. Kinetics of the reaction of 1-fluoro-2,6-dinitrobenzene and homopiperidine in binary solvent mixtures. *J. Phys. Org. Chem.* **2002**, 15, 258-269.
14. Migron, Y.; Marcus, Y., Polarity and hydrogen-bonding ability of some binary aqueous-organic mixtures. *J. Chem. Soc. Faraday Trans.* **1991**, 87, (9), 1339-1343.
15. Wyatt, V. T.; Bush, D.; Lu, J.; Hallett, J. P.; Liotta, C. L.; Eckert, C. A., Determination of solvatochromic solvent parameters for the characterization of gas-expanded liquids. *J. Supercrit. Fluids* **2005**, 36, 16-22.
16. Kosower, E. M., The effect of solvent on spectra. I. A new empirical measure of solvent polarity: Z-values. *J. Am. Chem. Soc.* **1957**, 80, 3253-3260.
17. Kosower, E. M., *An Introduction to Physical Organic Chemistry*. John Wiley & Sons, Inc.: New York, 1968.
18. Reichardt, C., *Solvents and Solvent Effects in Organic Chemistry*. Second ed.; John Wiley and Sons: New York, 1988.
19. Lancaster, N. L.; Welton, T.; Young, G. B., A study of halide nucleophilicity in ionic liquids. *J. Chem. Soc. Perkin Trans. 2* **2001**, 2267-2270.
20. Hirschfelder, J. O.; Curtiss, C. F.; Bird, R. B., *Molecular Theory of Gases and Liquids*. John Wiley & Sons, Inc.: New York, 1954.
21. Hsieh, C.-K. Molecular thermodynamics and high pressure kinetics of polar reactions in solutions. University of Illinois at Urbana-Champaign, Urbana, Illinois, 1973.
22. McCabe, J. R.; Grieger, R. A.; Eckert, C. A., Solvent effects on the volume of a transition state. *I&EC Fundamentals* **1970**, 9, (1), 156-160.
23. Hallett, J. P.; Kitchens, C. L.; Hernandez, R.; Liotta, C. L.; Eckert, C. A., Exploiting the anomalous nanoscale chemistry of gas-expanded liquids (GXLs). **Submitted Dec. 2005**.

24. Weikel, R. R.; Hallett, J. P.; Liotta, C. L.; Eckert, C. A., Self-neutralizing in situ acid catalysts from carbon dioxide. *Topics in Catalysis* **Submitted 2005**.
25. Kirkwood, J. G., Theory of solutions of molecules containing widely separated charges with special application to zwitterions. *J. Chem. Phys.* **1934**, 2, (7), 351-361.
26. Eckert, C. A., Molecular thermodynamics of reactions in solutions. In *Solutions and Solubilities*, Dack, M. R. J., Ed. John Wiley and Sons: New York, 1975; Vol. I.
27. Lewis, J. E.; Biswas, R.; Robinson, A. G.; Maroncelli, M., Local density augmentation in supercritical solvent: Electronic shift of anthracene derivatives. *J. Phys. Chem. B* **2001**, 105, (16), 3306-3318.
28. Sawin, S. P. Pressure and solvent effects on a Menschutkin reaction. University of Illinois at Urbana-Champaign, Urbana, Illinois, 1971.
29. Eckert, C. A.; Ziger, D. H.; Johnston, K. P.; Ellison, T. K., The use of partial molal volume data to evaluate equations of state for supercritical fluid mixtures. *Fluid Phase Equilibria* **1983**, 14, 167-175.
30. Reinheimer, J. D.; Harley, J. D.; Meyers, W. W., Solvent effects in the Menschutkin reaction. *J. Org. Chem.* **1963**, 28, 1575-1579.

CHAPTER V

DIFFUSION COEFFICIENTS IN CO₂-EXPANDED METHANOL BY THE TAYLOR-ARIS DISPERSION TECHNIQUE

Introduction

Knowledge of diffusion coefficients in gas-expanded liquids is of clear importance for their practical application. The launch of an industrial scale processing GXL will require comprehensive understanding of the transport properties of the system so that processes may be designed and modeled. This knowledge becomes even more crucial when using a GXL as an extractive solvent. Furthermore, if such mixtures are to be used as mobile phases in chromatography, information on molecular diffusion coefficients of solutes is useful for the optimization of said chromatographic systems.¹

A common method for measuring diffusion coefficients of systems under pressure is to use that of Taylor² and Aris^{3,4} to measure dispersion; a property which results from diffusion in a flowing system.⁵ In this technique, a sharp pulse of solute is injected into a long, thin tube filled with solvent, a GXL in our case, flowing under laminar conditions. The solute pulse disperses as it is carried through the tube by the mobile phase. The resulting concentration profile is used to determine the diffusion coefficient of the solute in the solvent (Figure 5-1). Fast diffusion produces very little dispersion and vice versa (Figure 5-2).⁵ This is because the initial solute pulse is deformed by axial flow as

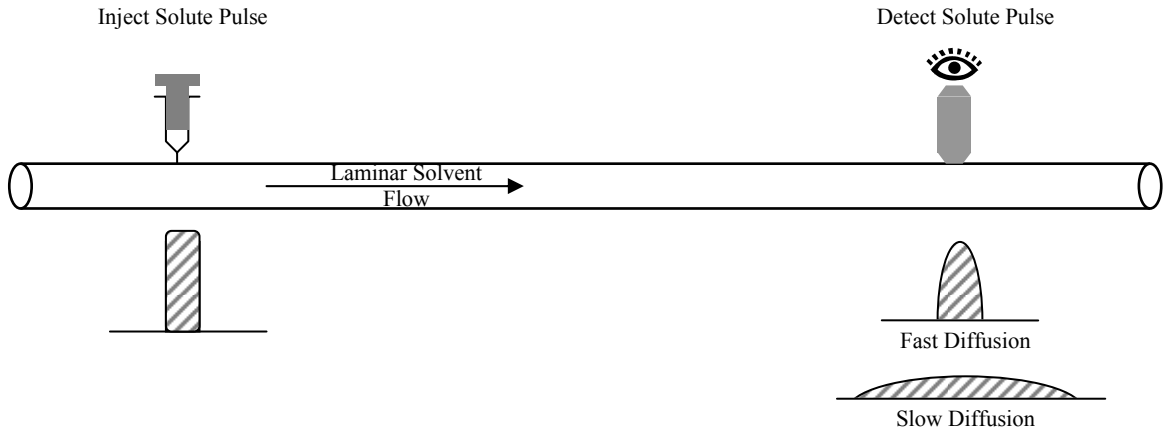


Figure 5-1: Taylor-Aris dispersion.

well as radial diffusion. Since the flow profile is laminar, the velocity is fastest at the center of the tube and slowest at the walls; therefore dispersion is most pronounced at the center of the tube. When diffusion is slow, the velocity effect dominates and the concentration profile broadens (Figure 5-2b). When diffusion is fast, the solute diffuses radially, thus narrowing the concentration profile (Figure 5-2c).

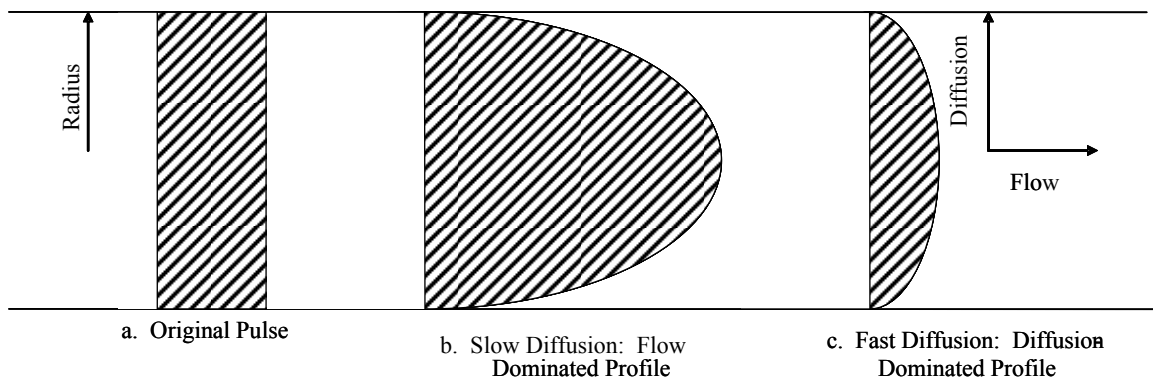


Figure 5-2: Flow profiles for the original pulse: slow diffusion and fast diffusion.

Since this project is part of a larger effort to elucidate the cybotactic region of GXLs, solutes that might have specific interactions with the fluid were chosen. Since many data were available for diffusion coefficients of substitute benzenes in ambient organic alcohols^{6, 7} and the binary diffusion coefficient of benzene in CO₂-expanded

methanol had been measured for the whole composition range⁸, we decided to choose a series of nitrogen-containing ring compounds which all have different dipole moments. The diffusion coefficients of benzene, pyridine, pyrimidine, pyrazine and 1,3,5-triazine (Figure 5-3) were measured in CO₂-expanded methanol by the Taylor-Aris dispersion technique. These diffusion coefficients will be used to estimate the viscosity of the methanol / CO₂ mixtures by applying a variation of the Stokes-Einstein Equation that is valid for supercritical fluids.⁹ The diffusion coefficients of these solutes in CO₂-expanded methanol will also be calculated using models developed by a collaborating researcher. Those results are beyond the scope of this particular study.

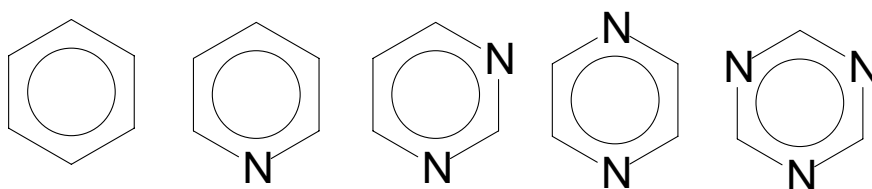


Figure 5-3: Solutes studied.

Experimental

Materials

Methanol (HPLC) and all solutes (benzene, toluene, phenol, 2-naphthol, pyridine, pyrimidine, pyrazine and 1,3,5-triazine, analytical grade) were purchased from Sigma-Aldrich. Carbon dioxide was purchased from Airgas. All were used as received.

Apparatus

All data were measured in a supercritical fluid chromatograph (SFC) (Berger Instruments) fitted with an autosampler (Berger Instruments, Model 718) and UV detector (Hewlett Packard 1050 Series). Data were acquired via software (Berger

Instruments SFC Chemstation Version 3.03). The column was replaced with 100 feet of coiled 1/16 inch tubing. The pumps were bypassed and replaced with syringe pumps (ISCO) to ensure a constant and controllable pulse-free flow. Pressure was maintained with a back pressure regulator (TESCOM 26-1764-24). A schematic is shown in Figure 5-4.

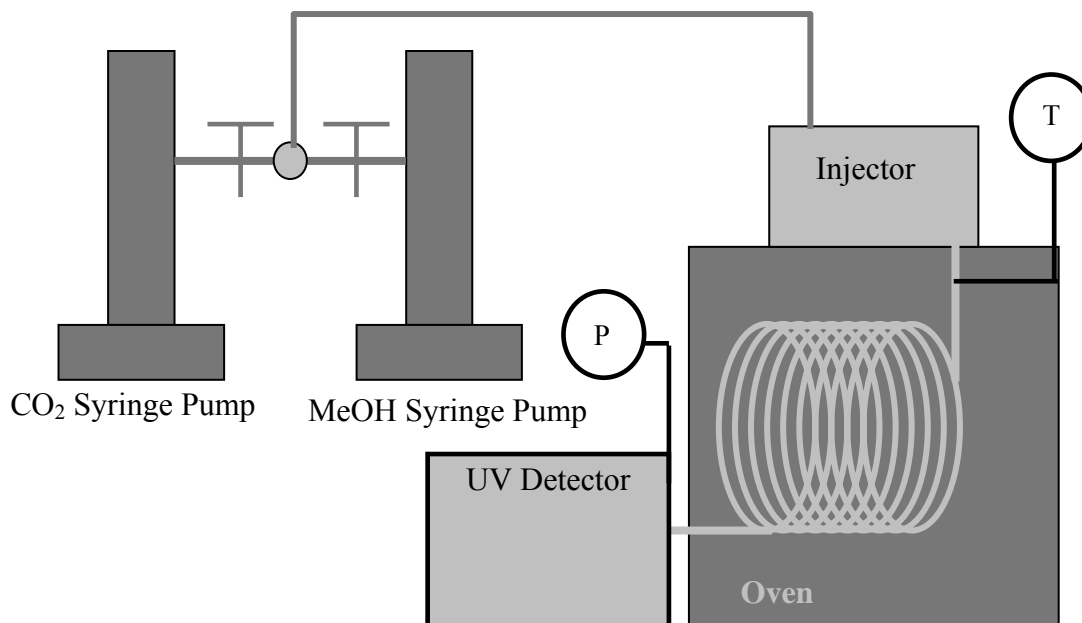


Figure 5-4: Supercritical fluid chromatograph.

Procedure

The procedure outlined below was validated via several diagnostics, the details of which can be found in Appendix B. Laminar flow is developed throughout the system by setting the total liquid flow rate to $0.2 \text{ ml}\cdot\text{min}^{-1}$ and allowing the system pressure to reach the desired pressure of 150 bar. Because the tube is coiled, it is important to note that laminar flow is not only determined by the Reynolds number, but also by the Dean and Schmidt numbers. Care had to be taken to choose a flow rate low enough such that

$(De)(Sc)^{0.5} < 10$.¹⁰ A known volume of solute in methanol solution is injected via a sample loop, with care taken to allow the mobile phase to flow through the loop for a short time; thus avoiding dispersion effects and tailing.⁸ The pulse flows through the 100 feet of column before entering the detector. The result is a Gaussian peak representing the concentration distribution of the initial pulse of solute that passes through the detector which has broadened based on the dispersion in the mobile phase.

The temporal variance of the Gaussian curve may be interpreted using Equation 5-1, where σ is the variance of the curve in length, D_{12} is the infinite dilution diffusion

$$\sigma^2 = \frac{2D_{12}L}{\bar{u}_0} + \frac{r_0^2 \bar{u}_0^2}{24D_{12}} \quad \text{Eq. 5-1}$$

coefficient of the solute (1) in the solvent (2), L is the length of the tube, \bar{u}_0 is the average velocity of the mobile phase, which is equal to the length divided by the retention time, and r_0 is the inner radius of the tube.¹⁰ The software package does not give a dispersion term, but rather gives the width of the peak at half its height, or $W_{1/2}$, which is 2.354σ . Furthermore, applying the “height of the theoretical plate” or “relative peak broadening” concept from Equation 5-2 to Equation 5-1 results in Equation 5-3.¹⁰

$$H = \sigma^2 / L = 1 / 2.354^2 W_{1/2}^2 L \quad \text{Eq. 5-2}$$

$$D_{12} = \left(\frac{\bar{u}_0}{4} \right) \left\{ H - \left[H^2 - \left(\frac{r_0}{3} \right)^2 \right]^{1/2} \right\} \quad \text{Eq. 5-3}$$

Once diffusion coefficients are measured, the viscosity, η , of the mobile phase can be estimated using a version of the Stokes-Einstein equation that is valid for

supercritical fluids (Equation 5-4) where D_i is the diffusion coefficient of the chosen solute in the mobile phase, κ is Boltzmann's constant, T is absolute temperature and σ

$$D_i \eta = \frac{5}{9} \frac{\kappa T}{\pi \sigma_i} \frac{\sigma}{\sigma_i} \quad \text{Eq. 5-4}$$

and σ_i are the average and individual collision diameters of the molecules, respectively.⁹

It is important to note that while diffusion depends on the solute and solvent, viscosity is only measured with regard to the solvent. Since these measurements have a solute present, it is important to account for interactions between that solute and itself or the solvent. This occurs in the collision diameter terms.

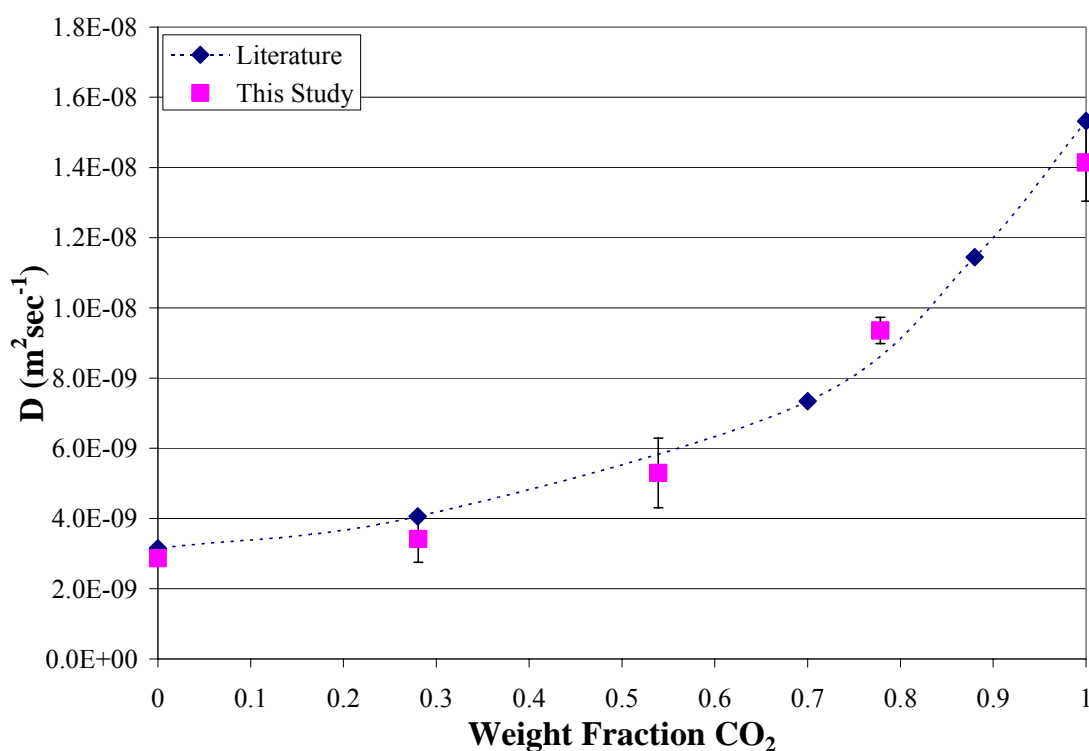
Results and Discussion

Before any measurements in CO₂-expanded methanol were made, a variety of measurements such as variation of diffusion coefficients in pure methanol with regard to solute concentration, ISCO temperature, flow rate and pressure were performed to ensure the validity of the experimental method. Details of these validation procedures are presented in Appendix B. Furthermore, the diffusion coefficients of several solutes were measured in methanol and showed relatively good agreement with literature values (Table 5-1).

Once we could be sure of our measurements on pure solvents, we attempted to reproduce the data of Sassiati, et. al.⁸ for diffusion coefficients of benzene in CO₂-expanded methanol as shown in Figure 5-5. Diffusion coefficients of benzene in the GXL are shown as a function of mass fraction of carbon dioxide. It is important to note that the dashed line in the figure is a curved line connecting the points that was put in to

Table 5-1: Our data compared with literature data for several solutes in methanol.

| Solute | <u>Lu, et. al.</u> | <u>Our Work</u> | <u>Our Work, Converted</u> |
|------------|---|---|---|
| | 298.2K, 1 bar ($D/10^{-5}$, cm^2/s) | 313.2K, 100 bar ($D/10^{-5}$, cm^2/s) | 298.2K and 1bar ($D/10^{-5}$, cm^2/s) |
| Benzene | 2.61±0.02 | 2.9-3.1 | 2.44-2.61 |
| Toluene | 2.42±0.02 | 2.76-2.83 | 2.33-2.38 |
| Phenol | 1.69±0.02 | 1.9-2.0 | 1.60-1.68 |
| 2-Naphthol | 1.45±0.01 | 1.67-1.73 | 1.41-1.46 |

**Figure 5-5: Diffusion coefficients of benzene in CO₂-expanded methanol as a function of weight fraction of CO₂, 313 K, 150 bar.**

guide the eye and is not a mathematical fit. The cited authors made their measurements at 210 nm while we made ours at 254 nm. We determined that this was the most suitable detection wavelength for benzene for our system, but according to the data it does not seem to matter. Our data match that of the literature satisfactorily.

Data were measured for all solutes in the full range of methanol / CO₂ mixtures. Data are presented in two ways – separated by solute in Figure 5-6 and overlaid in Figure 5-7 – in order to make it easier to understand the data. Several conclusions can be drawn from analysis of the data presented. All of the solutes studied behave in an expected manner; all diffuse faster as the amount of carbon dioxide is increased. What these graphs also tell us is that the differences in polarity of the solute molecules does not have an impact on the diffusion coefficients in CO₂-expanded methanol. Thus any inhomogeneities that may exist in the cybotactic region as a result of these different polarities are not manifested in the dispersion of a solute through these fluids. Therefore it seems that diffusivity has no discernable effects in the cybotactic region.

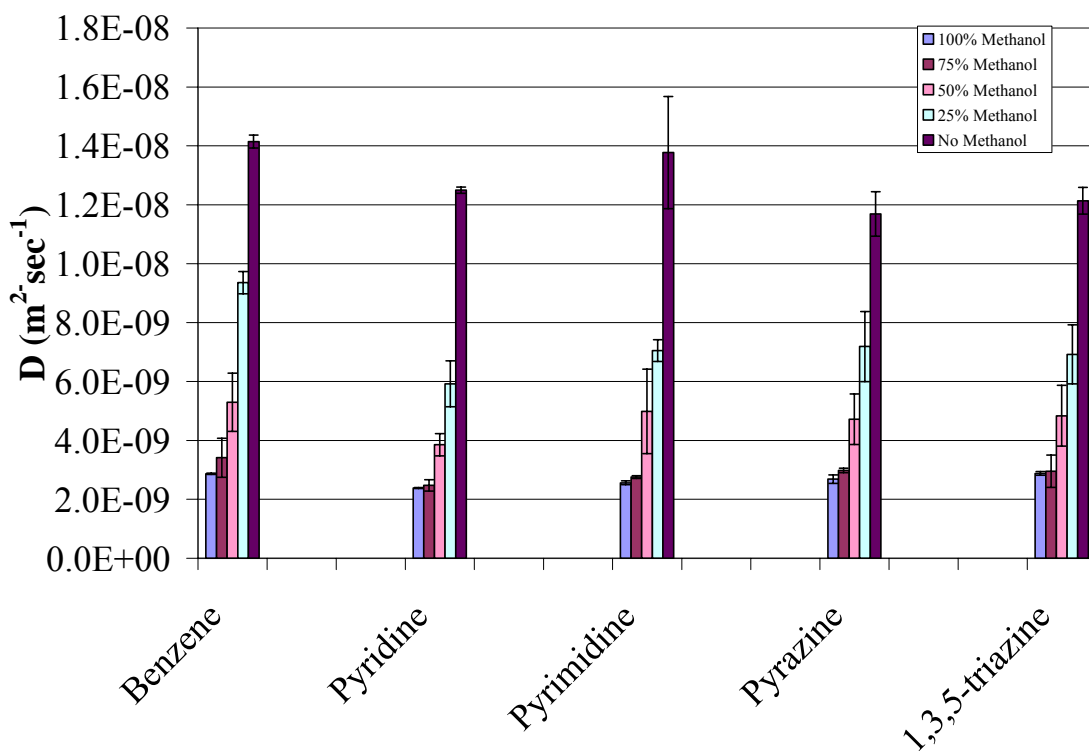


Figure 5-6: Diffusion coefficients of benzene, pyridine, pyrimidine, pyrazine and 1,3,5-triazine in CO₂-expanded methanol as a function of volume fraction of methanol, 313 K, 150 bar.

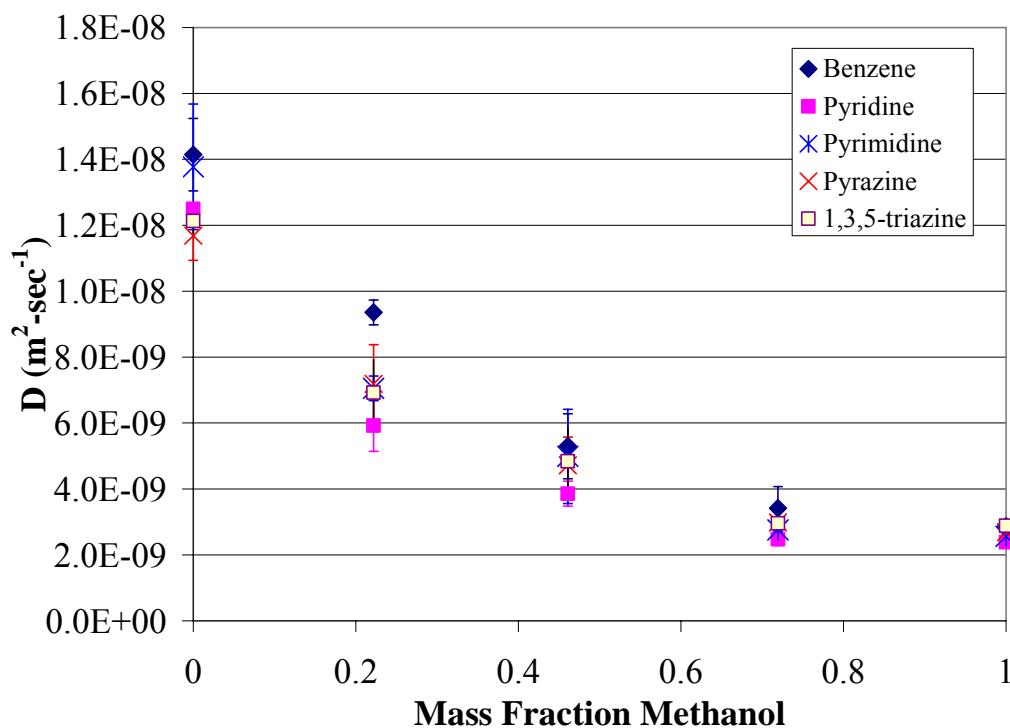


Figure 5-7: Diffusion coefficients of benzene, pyridine, pyrimidine, pyrazine and 1,3,5-triazine in CO₂-expanded methanol as a function of mass fraction of methanol, 313 K, 150 bar.

In order to strengthen the above conclusion, data of a variety of pseudoplanar compounds in an ambient ethanol were examined (Figure 5-8)¹¹. While we show that polarity of the molecule has little impact on the diffusion of that molecule through a solvent, the authors of the cited study show that size and shape has an effect. Larger, bulkier molecules diffuse through solvents much more slowly than smaller molecules of similar shapes. Thus diffusion is governed more strongly by physical constraints – i.e., steric effects – than chemical interactions.

The modified Stokes-Einstein Equation mentioned above⁹ was applied using the measured diffusion coefficients of benzene in the assorted mixtures of methanol and carbon dioxide in order to estimate the viscosity of each mixture (Figure 5-9). Collision diameter values for benzene, methanol and carbon dioxide were taken from the

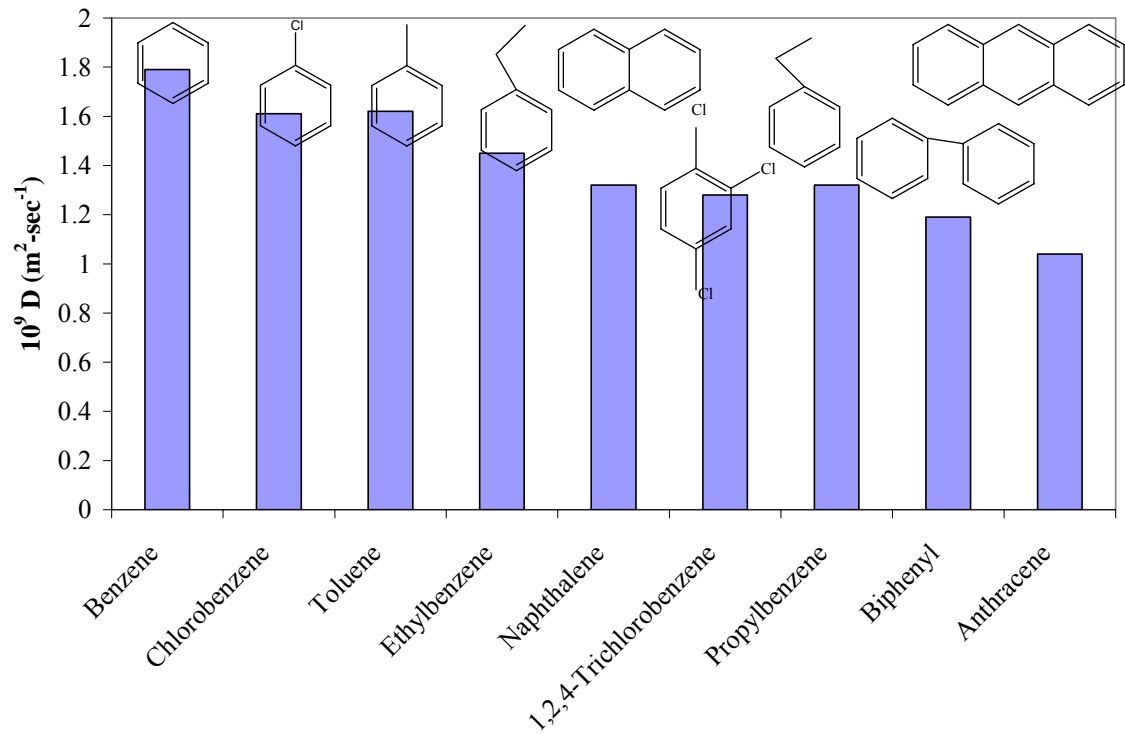


Figure 5-8: Diffusion coefficients of various pseudoplanar molecules in ethanol, 298.2 K, ambient pressure.

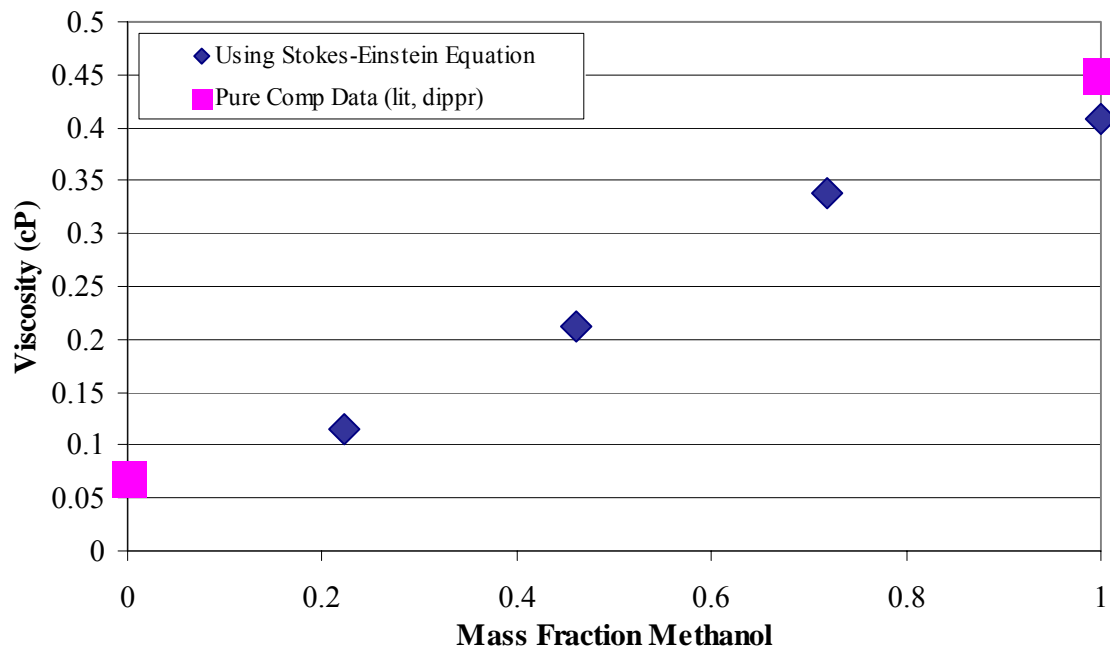


Figure 5-9: Viscosity of CO₂-expanded methanol as a function of mass fraction of methanol calculated from diffusion coefficients of benzene measured at 313 K, 150 bar via the Stokes-Einstein equation.

literature^{12, 13} and the true average of the three numbers was used as the average collision diameter. The viscosity of methanol was taken from the DIPPR chemical data base and the viscosity of carbon dioxide was interpolated from experimental data.¹⁴ The calculation and the data are satisfactorily close at the end points, indicating that the equation works well enough to make a rough estimation of the mixture of CO₂-expanded methanol given the composition of the liquid phase and the diffusion coefficient at that composition.

Summary

The Taylor-Aris dispersion technique measures diffusion coefficients in CO₂-expanded methanol successfully. Addition of CO₂ expectedly increases the diffusion coefficient of the mixture. Unexpectedly, diffusion coefficients are impacted more strongly by size and shape of solute molecule and less strongly by polarity or chemical make-up; thus diffusion is truly a bulk property with no discernable effects in the cybotactic region. Using the appropriate estimation techniques, diffusion coefficients can be used successfully to determine viscosity of GXLs.

REFERENCES

1. Souvignet, I.; Olesik, S. V., Molecular diffusion coefficients in ethanol / water / carbon dioxide mixtures. *Anal. Chem.* **1998**, 70, (14), 2783-2788.
2. Taylor, G., Dispersion of soluble matter in solvent flowing slowly through a tube. *Proceedings of the Royal Society of London. Series A, Mathematical and Physical Sciences* **1953**, 219, (1137), 186-203.
3. Aris, R., The dispersion of matter in turbulent flow through a pipe. *Proceedings of the Royal Society of London. Series A, Mathematical and Physical Sciences* **1954**, 223, (1155), 446-468.
4. Aris, R., On the dispersion of a solute in a fluid flowing through a tube. *Proceedings of the Royal Society of London. Series A, Mathematical and Physical Sciences* **1956**, 235, (1200), 67-77.
5. Cussler, E. L., *Diffusion: Mass Transfer in Fluid Systems*. Second ed.; Cambridge University Press: Cambridge, 1997.
6. Lu, J. G.; Kong, R.; Chan, T. C., Effects of molecular association on mutual diffusion: A study of hydrogen bonding in dilute solutions. *J. Chem. Phys.* **1998**, 110, (6), 3003-3008.
7. Gonzalez, L. M.; Bueno, J. L.; Medina, I., Determination of binary diffusion coefficients of anisole, 2,4-dimethyl phenol and nitrobenzene in supercritical carbon dioxide. *Ind. Eng. Chem. Res.* **2001**, 40, 3711-3716.
8. Sassiati, P. R.; Mourier, P.; Caude, M. H.; Rosset, R. H., Measurement of diffusion coefficients in supercritical carbon dioxide and correlation with the equation of Wilke and Chang. *Anal. Chem.* **1987**, 59, 1164-1170.
9. Woerlee, G. F., Expression for the viscosity and diffusivity product applicable for supercritical fluids. *Ind. Eng. Chem. Res.* **2001**, 40, (1), 465-469.
10. Bueno, J. L.; Saurez, J. J.; Dizy, J.; Medina, I., Infinite dilution diffusion coefficients: benzene derivatives as solutes in supercritical carbon dioxide. *J. Chem. Eng. Data* **1993**, 38, 344-349.

11. Chan, T. C.; Chan, M. L., Diffusion of pseudo-planar molecules: An experimental evaluation of the molecular effects on diffusion. *J. Chem. Soc. Faraday Trans.* **1992**, 88, (16), 2371-2374.
12. Hirschfelder, J. O.; Curtiss, C. F.; Bird, R. B., *Molecular Theory of Gases and Liquids*. John Wiley & Sons, Inc.: New York, 1954.
13. Bird, R. B.; Stewart, W. E.; Lightfoot, E. N., *Transport Phenomena*. John Wiley and Sons: New York, 1960.
14. Fenghour, A.; Wakeham, W. A.; Vesovic, V., The viscosity of carbon dioxide. *J. Phys. Chem. Ref. Data* **1998**, 27, (1), 31-44.

CHAPTER VI

CONCLUSIONS AND RECOMMENDATIONS

Gas-expanded liquids, specifically CO₂-expanded organic solvents, offer a variety of opportunities for reactions and separations. With recent attention to environmental and public health issues in society and politics, sustainable process technology development is a prevalent target of both industrial and academic chemical research. Benign solvents such as gas-expanded liquids are among the leading potential solutions to this large-scale problem. One of the goals of this study was to perform fundamental research on CO₂-expanded liquids so that reaction processes that utilize them could be designed.

Most of the work presented in the foregoing chapters and in the complementary appendices focuses on elucidating the cybotactic region of GXLs. In order to design a processing GXL successfully and optimally, it is imperative to understand both the bulk- and microscale properties of the solvent and how those properties impact one another.

Probing the cybotactic region experimentally proved to be a very challenging endeavor. By definition, the cybotactic region of a solvent depends on the probe molecule – thus the cybotactic region of a GXL measured in one instance may be completely different than in another instance, even for the same solvent. In some cases it was difficult to deconvolute bulk properties from those in the cybotactic region. In others

it was difficult to overcome the fast timescales of solvent rearrangement. While this study is important in and of itself, it needs to be viewed with its complementary parts to have maximum impact. The GXL project is a quintessential example of where the synergy of experimentation and simulation can produce results where the whole is greater than the sum of its parts.

This section is organized by project. All conclusions and recommendations for each project will be discussed under each subheading. At the end the general conclusions will be summarized.

Solid Solubility in Pure and Mixed Solvents

Conclusions

In Chapter III, heats of fusion and solubilities in pure and mixed solvents were reported for four previously unstudied compounds. The MOSCED model was applied to these compounds in an effort to predict their solubility in mixed solvents. We learned a great deal about these systems and MOSCED's abilities and limitations. Great care must be taken in solubility and heat of fusion measurements to ensure reproducibility. MOSCED requires more data for multi-functional compounds than it does for simpler compounds. Still it does not work as well as we would like, but it works better than Hansen and where UNIFAC cannot.

In terms of predicting solubility in mixed solvents, the likelihood of MOSCED working well depends on several more variables. It has to be able to predict the solubility of the compound in both pure liquids and the g^E model has to show the right behavior. In cases of high solid solubility the models must be extrapolated. This implies that predicting solid-liquid equilibrium might more model dependent than vapor-liquid

equilibrium. Right now the models can predict the solubility within 30-40% of the actual value. Overall, use of the models serves as a good qualitative tool but not a very good quantitative tool. While good for indicating trends, they are not yet at the point where they can predict the behavior well.

Recommendations

One of the conclusions presented above was that MOSCED predicts the mixed-solvent behavior well in cases where it predicts the endpoints well. Thus something that can be done is to force MOSCED to work for the specific pure solvents and see if it then predicts the behavior properly.

All of the measurements in this study were performed under ambient pressures. In order to incorporate this study with the rest of the GXL project, solid solubility measurements should be made in CO₂-expanded pure and mixed solvents. MOSCED's ability to predict solubility in expanded solvents should be tested. Since MOSCED parameters for CO₂ can be regressed from vapor-liquid equilibrium data, solvent mixture predictions are already possible and more accurate than UNIFAC. This can lead to myriad opportunities in understanding the cybotactic region via a synergistic approach. Molecular dynamics calculations can be incorporated into these efforts to understand crystallization kinetics and the role of the cybotactic region in particle formation.

In this study four solids were studied in four mixed-solvent systems. In order to improve MOSCED it is necessary to measure more solids in more solvent systems. One potential class of solids that this can be extended to is cellulose polymers. These are hydrogen bonding polymers that exhibit lower critical solution temperatures (LCST) when in solution with water. These biocompatible polymers are used in cosmetic

formulations¹ and drug delivery systems.² Adding CO₂ to these systems decreases the ability of the solvent to form hydrogen bonds and therefore lowers the LCST in water. These are ideal solutes because they would be impossible for UNIQUAC or COSMO to handle.

Another potential solid is hexamethylenetetraamine (HMTA, Figure 6-1). Its high melting point (280 °C) makes its solubility low and therefore an ideal candidate for MOSCED predictions while its high density of 1.331 g/ml makes solubility measurements easier. Its high melting point does have a drawback, however, in that it might be difficult to analyze via GC.

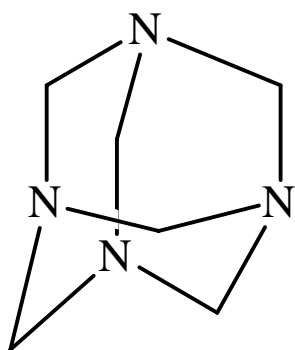


Figure 6-1: Structure of hexamethyltetraamine.

As far as adding new solvent systems, these choices are more difficult to make. The solvent selection for the work performed was based on taking advantage of different solvent interactions with regard to the different functional groups in the solids. For HMTA one would choose two different nitrogen-containing solvents where the nitrogens are part of different functional groups in order to optimize the solvents ability to dissolve the very symmetric nitrogens in the molecule.

Local Polarity of Gas-Expanded Liquids

Conclusions

In Chapter IV the Menshutkin reaction of tri-butylamine with methyl *p*-nitrobenzenesulfonate, π^* and *Z*-values were used as probes of local polarity in CO₂-expanded acetonitrile. In the case of the Menshutkin reaction, polarity is not measured directly, but is inferred from the second-order rate constant of the reaction; the faster the reaction, the more polar the surrounding medium. The rate constant decreases in an “S-shaped” fashion with regard to CO₂-mole fraction. This behavior is more consistent with bulk properties than with properties in the cybotactic region.

Solvatochromic property π^* and *Z*-values of CO₂-expanded acetonitrile were also measured and are consistent with π^* of other expanded solvents and *Z*-values of non-expanded solvents, indicating that solvation shells can exist in the cybotactic region of CO₂-expanded acetonitrile. Thus it is this particular reaction that measures properties consistent with bulk properties and not that acetonitrile has a negligible cybotactic region.

This discrepancy between the reaction kinetics and local properties can be explained by several theories. First of all, there are several nitrogen atoms – specifically an amine group – present in the reacting species. Amines associate strongly with CO₂, thus its presence may be bringing in more CO₂ atoms than the cybotactic region would normally contain. The presence of the albeit less polar due to charge stabilization amine group in the π^* probe, however, indicates that it is not likely the only factor. Another possible explanation could be the response time of the probe. While we are not set up for time-resolved analysis, it could be that solvent rearrangement is occurring more quickly than the reaction can occur. Thus the cybotactic region of the transition state is after solvent rearrangement. Or it could be that π^* and *Z*-values are exceptions and there is little difference between bulk and local properties for acetonitrile. It is not unlikely that

the local solvation around every probe is vastly different considering the cybotactic region, by definition, is the solvent's response to the solute's intermolecular forces, which are governed by the different moieties of the solutes and solvent.

The natural logarithms of the rate constants trend reasonably well with the π^* shifts and very well with the Z-values. Thus even though the rate constants may follow a slightly different trend, a meaningful relationship can still be extracted. Furthermore, while the Menshutkin reaction kinetics are inconsistent with π^* and Z-value measurements, they are consistent with other kinetic polarity probes and with dielectric constants in other solvent systems as well as dielectric constant calculations for this system.

From these kinetic data it is possible to infer transition state dipole moments by Kirkwood's theory. Kirkwood's theory tells us that the transition state is significantly more polar than the ground-state substrate molecule, thus justifying that it is a good probe of solvent polarity.

Recommendations

While great strides have been made in the four months I worked on this project, I have only scratched the surface. Thus I will make several recommendations for my successor so that this study can be fully realized.

The most important experiment to perform is to determine whether or not the peak is real. This can be done by running the experiment at 10 °C. If the peak exists at 10 °C and is more pronounced than it is at 25 °C then it can be concluded that it is real. If that is the case then efforts must be made to determine the reasons behind why that peak exists. While the density behavior theory presented in Chapter IV is founded in

truth, a great deal more may be occurring. Further speculations shouldn't be made until the data at 10 °C are measured.

The study discussed in Chapter IV includes work done on only one solvent system: CO₂-expanded acetonitrile. If this project is continued it needs to be run in several other solvent systems. Solvent selection is quite challenging due to the nature of the experiment. Solvents chosen must be clear in UV-vis wavelengths, must be polar enough such that the reaction will run at a reasonable rate and must not hydrogen bond since hydrogen bonding effects overwhelm polarity effects. A list of potential solvents is included in Table 6-1.

Table 6-1: Potential Menshutkin reaction solvents.

| Solvent | Density (g/cm³) | Dielectric Constant | Clear in UV |
|----------------------|---------------------------------------|--------------------------------|------------------------|
| Hexane | 0.66 | 1.89 | Yes |
| Carbon Tetrachloride | 1.58 | 2.3 | Yes |
| Chloroform | 1.48 | 4.89 | Yes |
| Methylene Chloride | 1.32 | 9.02 | Yes |
| Diethyl Ether | 0.71 | 4.42 | Yes |
| THF | 0.88 | 7.47 | Yes |
| Dioxane | 1.03 | 2.27 | Yes |
| Acetonitrile | 0.78 | 36 | Yes |
| CO ₂ | - | 1 | Yes |

Several measurements of the Menshutkin reaction were made in CO₂-expanded THF. The kinetic data did not behave in the same manner as they did in acetonitrile, so analysis of each point was very difficult. While pure THF and pure amine do not absorb in the UV, the solution of THF with the amine has a fairly large absorbance, which clouds the measurements. Because the data in THF behaved differently than they did in acetonitrile – specifically the reactant disappeared but the product peak never appeared – it can be concluded that the reaction went by a different mechanism. This could be a

result of the fact that THF was used without further purification but is very hygroscopic. The water present in the system may have interacted with the CO₂ to form carbonic acid which would slow down the reaction and change the mechanism. Furthermore, hydrogen bonding moieties could interact with the amine and change the mechanism. Before any conclusions can be made on the kinetics in THF the experiments must be repeated using pure, dry THF.

Inspection of Table 6-1 tells us that choosing a solvent in which to run this reaction could prove to be very challenging. Solvents that are spectrophotometrically clear tend to have low dielectric constants, thus they will likely result in very slow reaction rates. Solvents that are more polar, such as acetone, tend to have UV signatures and are therefore unsuitable for *in situ* analysis or form hydrogen bonds, such as methanol, and will cause the reaction to go by a different mechanism which makes this *in situ* analysis impossible. I recommend the development of a new analytical method which would allow these reactions to be run in a non-clear solvent such as acetone. They could possibly be run in a Parr reactor fitted with a sample loop. Once UV is taken out of the equation, a different probe reaction might prove to be more effective.

Since much of the overall GXL project is centered around CO₂-expanded methanol, it would be beneficial to understand the local polarity of it. However, before this reaction can be studied in CO₂-expanded methanol, a new analytical method must be developed. The reaction behaves differently when performed in hydrogen-bonding solvents and thus the resulting product peaks are at a different wavelength. If the new reaction details could be understood then this reaction can be used to study CO₂-expanded methanol.

One of the problems that we faced in analyzing the polarity behavior was that the reaction kinetics did not behave in a manner consistent with the presence of solvation shells in the cybotactic region. One of the theories used to explain this was that the presence of the amines was drawing more CO₂ into the cybotactic region of acetonitrile than would normally be present. There are several ways around this. The substrate could be replaced with an iodobenzenesulfonate and the nucleophile could be replaced with an iodide. This would eliminate the presence of the amines. Preliminary experiments would have to be performed to determine if this reaction runs and if it can be monitored by *in situ* UV spectroscopy. Another alternative is to eliminate the CO₂ from the process and run the reaction in ethane-expanded acetonitrile. Ethane does not complex with amines; thus if it was the CO₂ / amine association causing the rate to follow a trend consistent with bulk properties that trend would not occur if ethane was used. Ethane-expanded acetonitrile could also be analyzed with π^* and Z-value measurements in order to see if local effects vary with gas selection.

Finally, this reaction was performed using only the tertiary amine. It should also be run with the primary and secondary amines in order to gain complete understanding of the polarity of the cybotactic region of the medium. It should be noted, however, that a dialkylation product might result when using the secondary amine,³ thus the analysis becomes more complicated.

Diffusion Coefficients in Gas-Expanded Liquids

Conclusions

In Chapter V it was shown that diffusion is a bulk property with no discernable effects in the cybotactic region. The fluid dynamics of the system dominate and any

effects that occur in the cybotactic region seem to average out. Diffusion is not a function of polarity or atomic make up and seems to be much more strongly impacted by steric effects such as molecular size and shape.

While these measurements did not give as much insight into the cybotactic region as we had hoped, we were able to use a version of the Stokes-Einstein equation to estimate the bulk viscosity of the methanol / CO₂ mixtures. The calculation matched literature values where available so we feel that it is a reasonable estimation. Molecular dynamics simulations are needed to derive more information into the structure of the cybotactic region.

Recommendations

This project is complete as far as making bulk-phase measurements on the system considered. However, a better understanding of the cybotactic region could possibly be gained by performing some calculations. The molecular dynamics simulations of the methanol / CO₂ system are currently a work in progress by another group member. Upon completion of the simulations, meaningful information about the cybotactic region will hopefully be extracted.

In order to round out this project, more solvents and solutes should be measured. Since several other measurements have been made on CO₂-expanded acetonitrile and 1,4-dioxane, diffusion coefficient measurements can also be made on these systems. Considering the current set-up, care must be taken in choosing solvents because the harshness of the chemical environment can damage the o-ring in the back pressure regulator. Even o-rings that were said to be compatible with methanol and CO₂ separately were not able to withstand the mixture of the two.

Since the data measured did not show any differences based on chemical make-up, a new solute list should be chosen which has a similar base (such as a benzene ring) but different substituents; such as those in Figure 5-8. The data presented in Figure 5-8 are measured in ethanol under ambient conditions. They can be measured in CO₂-expanded methanol, acetonitrile and 1,4-dioxane to see if they show similar behaviors.

Microviscosity of Gas-Expanded liquids

Conclusions

Microviscosity measurements are discussed in Appendix C. While the results were not conclusive enough to warrant a full chapter in the thesis, enough work has been done that meaningful conclusions and several important recommendations can be made.

These are very difficult measurements to make in such inviscid media. The intensity of the fluorescence is proportional to the viscosity of the surrounding medium; thus when the viscosity is low the intensity is low. This introduces the problem of being within the uncertainty of the instrument. Fluorescence is very sensitive and very susceptible to baseline noise. The intensity must be significantly larger than the noise for the data to mean anything. Since the intensity is also proportional to the probe concentration the problem can be combated by adding more probe. However, when there is too much probe the system is subject to excimer formation and therefore signal quenching. It is a difficult balance to strike considering the concentration of the system is always changing. We never found that balance in our experiments.

Recommendations

The next step in deriving meaningful results out of this sort of experiment is to find the appropriate probe concentration range in which to operate. Part of the challenge

is the ever-changing concentration with the addition of CO₂. Another part of the challenge is that the concentration behavior of the fluorescent intensity is not quite linear. Before one can deconvolute potential internal interactions and excimer formation from effects of the microviscosity of the system it is imperative to gain an understanding of the interaction parameters involved under the operating conditions. Molecular dynamics simulations need to be tapped into in order to deconvolute the effects.

This project can also go into a different direction by using a more sensitive probe. Part of the challenge is that most conventional probes require the use of time-resolved fluorescence which our group is not set up for. One can envision synthesizing a more sensitive probe by replacing the cyano groups on the DCVJ molecule with something larger and still rigid, such as benzene rings. Such a probe should still fluoresce, so it could likely be analyzed by the same method. Another direction that this could go in is to use a time-resolved fluorescence probe. We are currently not set up for such experiments, so the first step would be to design or purchase the necessary equipment. There may be a group in the Chemistry Department that has the appropriate equipment. This should be investigated. If there does exist the capability for time-resolved fluorescence in another research group then another option would be to collaborate with said group.

The use of fluorescence also leads to a great amount of uncertainty. Fluorescence is very sensitive to environmental stimuli: two spectra taken of the same sample an hour apart may not be the same. A probe that can be analyzed via a different method that is more reproducible might be more suitable for these measurements since it takes several days to complete one experiment.

Work on microdiffusivity reactions using cage reactions as a probe^{4, 5} should be completed as complementary work. Several preliminary experiments involving a breaking, rearrangement and recombination of a peroxide molecule were performed. The basic idea is that this reaction is catalyzed via LASER flash photolysis. Upon excitation the molecule splits and the parts can either rearrange and recombine or they can diffuse out of the solvation shell where they will react with a chemical getter. Analysis of the product distribution – how much starting material is left, how much rearranged and how much escaped – gives information about the diffusion coefficient out of the solvation shell and therefore in the cybotactic region of the solution.^{4, 5} Combining the microdiffusivity with the microviscosity can lead to insight about the validity of the Stokes-Einstein equation on the molecular level and can help paint a picture of the cybotactic region.

Final Summary

The main theme of the work presented has been understanding the role of intermolecular forces on the structure of a solution on the molecular level and developing technology around said knowledge. When there is no CO₂ present in the system, such as in the case of the solid solubility project, great success was achieved and the groundwork for a new paradigm for solvent selection and design was developed. Once CO₂ enters the picture everything becomes somewhat more complex. A synergistic approach combining experimentation and theory is the key to understanding the cybotactic region of GXLs. Such an understanding will afford us the ability to develop sustainable technology to solve problems in myriad areas of chemical engineering taking advantage of the unique properties of the cybotactic region of GXLs.

REFERENCES

1. Ramachandran, P.; Reich, C.; Hartnett, D.; Robbins, C.; Sackariassen, K.; Patel, A. Hair rinse compositions which facilitate repair of split ends consisting of emulsions of water-insoluble adhesive polymers. US 95-421691 19950420. 1996.
2. Krögel, I.; Bodmeier, R., Floating or pulsatile drug delivery systems based on coated effervescent cores. *International Journal of Pharmaceutics* **1999**, 187, (2), 175-184.
3. Crowhurst, L.; Lancaster, N. L.; Perez Arlandis, J. M.; Welton, T., Manipulating solute nucleophilicity with room temperature ionic liquids. *J. Am. Chem. Soc.* **2004**, 126, (37), 11549-11555.
4. Otto, B.; Schroeder, J.; Troe, J., Photolytic cage effect and atom recombination of iodine in compressed gases and liquids: Experiments and simple models. *J. Chem. Phys.* **1984**, 81, (1), 202-213.
5. Adam, W.; Bronstein, I.; Trofimov, A. V.; Vasil'ev, R. F., Solvent-cage effect (viscosity dependence) as a diagnostic probe for the mechanism of the intramolecular chemically initiated electron-exchange luminescence (CIEEL) triggered from a spiroadamantyl-substituted dioxetane. *J. Am. Chem. Soc.* **1999**, 121, (5), 958-961.

APPENDIX A

SUMMARIZED DATA FROM CHAPTER III

Table A-1: Solubility of 3-nitrophthalimide in pure solvents – Experimental values and predictions.

| Solvent | Temperature (K) | Experimental | Wilson Prediction | UNIQUAC Prediction |
|-----------------|-----------------|------------------------|-------------------|--------------------|
| 2-Butanone | 283 | 5.73E-03 | 2.60E-03 | 5.10E-03 |
| | 298 | 1.29E-02 | 5.40E-03 | 9.60E-03 |
| | 313 | 2.31E-02 | 1.04E-02 | 1.71E-02 |
| Acetonitrile | 283 | 4.97E-03 | 4.50E-03 | 4.40E-03 |
| | 298 | 5.80E-03 | 9.00E-03 | 9.00E-03 |
| | 313 | 1.04E-02 | 1.69E-02 | 1.69E-02 |
| Benzyl Alcohol | 298 | 1.02E-02 | 2.80E-03 | 9.30E-03 |
| | 313 | 1.18E-02 | 5.70E-03 | 1.77E-02 |
| Chloroform | 283 | 1.16E-05 | 1.31E-04 | 6.60E-03 |
| | 298 | 2.36E-05 | 3.80E-04 | 1.24E-02 |
| | 313 | 9.84E-04 | 9.85E-04 | 2.19E-02 |
| Cyclohexane | 283 | Below Detection Limits | | |
| | 298 | 1.51E-03 | 2.24E-06 | 8.50E-03 |
| | 313 | 3.02E-03 | 9.56E-06 | 1.61E-02 |
| Dichloromethane | 283 | 8.88E-04 | 2.80E-04 | 6.70E-03 |
| | 298 | 2.26E-03 | 7.58E-04 | 1.26E-02 |
| | 313 | 2.37E-03 | 1.90E-03 | 2.23E-02 |
| Dioxane | 283 | 7.28E-03 | 2.70E-03 | 8.10E-03 |
| | 298 | 1.07E-02 | 5.60E-03 | 1.52E-02 |
| | 313 | 2.14E-02 | 1.07E-02 | 2.67E-02 |
| DMF | 283 | 8.82E-02 | 6.70E-02 | 7.36E-02 |
| | 298 | 1.34E-01 | 8.53E-02 | 9.27E-02 |
| | 313 | 2.03E-01 | 1.07E-01 | 1.15E-01 |
| Ethanol | 283 | 1.47E-03 | 7.68E-04 | 4.50E-03 |
| | 298 | 1.65E-03 | 1.80E-03 | 6.40E-03 |
| | 313 | 3.76E-03 | 3.80E-03 | 1.22E-02 |

Table A-1 (Continued).

| Solvent | Temperature (K) | Experimental | Wilson Prediction | UNIQUAC Prediction |
|----------------|------------------------|------------------------|--------------------------|---------------------------|
| Ethyl Acetate | 283 | 8.25E-03 | 4.70E-03 | 4.70E-03 |
| | 298 | 9.01E-03 | 8.80E-03 | 8.90E-03 |
| | 313 | 1.25E-02 | 1.58E-02 | 1.59E-02 |
| Isopropanol | 283 | 1.21E-03 | 5.98E-04 | 4.30E-03 |
| | 298 | 1.05E-03 | 1.40E-03 | 6.10E-03 |
| | 313 | 1.71E-03 | 3.10E-03 | 1.17E-02 |
| Methanol | 283 | 2.07E-03 | 8.52E-04 | 5.40E-03 |
| | 298 | 2.17E-03 | 1.90E-03 | 7.60E-03 |
| | 313 | 7.40E-03 | 4.00E-03 | 1.46E-02 |
| Nitromethane | 283 | 3.86E-03 | 1.20E-03 | 5.50E-03 |
| | 298 | 4.91E-03 | 2.70E-03 | 1.05E-02 |
| | 313 | 8.78E-03 | 5.60E-03 | 1.87E-02 |
| Toluene | 283 | Below Detection Limits | | |
| | 298 | 1.51E-03 | 1.60E-04 | 9.60E-03 |

Table A-2: Solubility of 3-nitrophthalimide in mixtures of ethanol and ethyl acetate – Experimental values and predictions.

| Fraction Ethanol | Temperature (K) | Experimental | Wilson Prediction | UNIQUAC Prediction |
|-------------------------|------------------------|---------------------|--------------------------|---------------------------|
| 0 | 283 | 8.25E-03 | 4.69E-03 | 4.71E-03 |
| | 298 | 9.01E-03 | 8.84E-03 | 8.90E-03 |
| | 313 | 1.25E-02 | 1.58E-02 | 1.59E-02 |
| 0.25 | 283 | 3.86E-03 | 8.77E-03 | 2.21E-02 |
| | 298 | 4.38E-03 | 1.54E-02 | 3.42E-02 |
| | 313 | 1.78E-02 | 2.55E-02 | 5.05E-02 |
| 0.5 | 283 | 3.16E-03 | 8.57E-03 | 3.26E-02 |
| | 298 | 3.93E-03 | 1.56E-02 | 4.94E-02 |
| | 313 | 1.11E-02 | 2.66E-02 | 7.03E-02 |
| 0.75 | 283 | 1.79E-03 | 5.59E-03 | 2.26E-02 |
| | 298 | 2.25E-03 | 1.08E-02 | 3.79E-02 |
| | 313 | 6.83E-03 | 1.94E-02 | 5.78E-02 |
| 1 | 283 | 1.47E-03 | 7.68E-04 | 7.69E-04 |
| | 298 | 1.65E-03 | 1.77E-03 | 1.77E-03 |
| | 313 | 3.76E-03 | 3.77E-03 | 3.77E-03 |

Table A-3: Solubility of 3-nitrophthalimide in mixtures of isopropanol and nitromethane – Experimental values and predictions.

| Fraction Isopropanol | Temperature (K) | Experimental | Wilson Prediction | UNIQUAC Prediction |
|-----------------------------|------------------------|---------------------|--------------------------|---------------------------|
| 0 | 283 | 3.86E-03 | 1.16E-03 | 1.16E-03 |
| | 298 | 4.91E-03 | 2.65E-03 | 2.66E-03 |
| | 313 | 8.78E-03 | 5.61E-03 | 5.63E-03 |
| 0.25 | 283 | 4.82E-03 | 2.31E-03 | 3.52E-03 |
| | 298 | 7.09E-03 | 5.00E-03 | 7.21E-03 |
| | 313 | 1.83E-02 | 1.00E-02 | 1.37E-02 |
| 0.5 | 283 | 3.68E-03 | 2.36E-03 | 4.34E-03 |
| | 298 | 6.41E-03 | 5.22E-03 | 8.84E-03 |
| | 313 | 1.46E-02 | 1.06E-02 | 1.66E-02 |
| 0.75 | 283 | 1.41E-03 | 1.70E-03 | 2.52E-03 |
| | 298 | 3.10E-03 | 3.81E-03 | 5.46E-03 |
| | 313 | 7.77E-03 | 7.87E-03 | 1.09E-02 |
| 1 | 283 | 1.21E-03 | 5.98E-04 | 6.00E-04 |
| | 298 | 1.05E-03 | 1.42E-03 | 1.43E-03 |
| | 313 | 1.71E-03 | 3.11E-03 | 3.12E-03 |

Table A-4: Solubility of 3-nitrophthalimide in mixtures of dioxane and 2-butanone – Experimental values and predictions.

| Fraction Dioxane | Temperature (K) | Experimental | Wilson Prediction | UNIQUAC Prediction |
|-------------------------|------------------------|---------------------|--------------------------|---------------------------|
| 0 | 283 | 5.73E-03 | 2.60E-03 | 6.08E-03 |
| | 298 | 1.29E-02 | 5.39E-03 | 1.05E-02 |
| | 313 | 2.31E-02 | 1.04E-02 | 1.71E-02 |
| 0.25 | 283 | 1.51E-02 | 2.77E-03 | 1.47E-02 |
| | 298 | 2.62E-02 | 5.71E-03 | 2.36E-02 |
| | 313 | 3.19E-02 | 1.10E-02 | 3.59E-02 |
| 0.5 | 283 | 1.24E-02 | 2.85E-03 | 2.44E-02 |
| | 298 | 1.88E-02 | 5.86E-03 | 3.63E-02 |
| | 313 | 2.92E-02 | 1.13E-02 | 5.17E-02 |
| 0.75 | 283 | 1.02E-02 | 2.82E-03 | 2.26E-02 |
| | 298 | 9.59E-03 | 5.82E-03 | 3.31E-02 |
| | 313 | 2.57E-02 | 1.12E-02 | 4.68E-02 |
| 1 | 283 | 7.28E-03 | 2.68E-03 | 1.56E-03 |
| | 298 | 1.07E-02 | 5.56E-03 | 3.15E-03 |
| | 313 | 2.14E-02 | 1.07E-02 | 6.00E-03 |

Table A-5: Solubility of 3-nitrophthalimide in mixtures of DMF and chloroform – Experimental values and predictions.

| Fraction DMF | Temperature (K) | Experimental | Wilson Prediction | UNIQUAC Prediction |
|--------------|-----------------|--------------|-------------------|--------------------|
| 0 | 283 | 1.16E-05 | 1.31E-04 | 1.34E-04 |
| | 298 | 2.36E-05 | 3.80E-04 | 3.86E-04 |
| | 313 | 9.84E-04 | 9.85E-04 | 9.95E-04 |
| 0.25 | 283 | 6.36E-03 | 3.24E-03 | 3.29E-03 |
| | 298 | 8.12E-03 | 6.35E-03 | 6.04E-03 |
| | 313 | 1.62E-02 | 1.16E-02 | 1.08E-02 |
| 0.5 | 283 | 3.73E-02 | 1.56E-02 | 1.87E-02 |
| | 298 | 4.29E-02 | 2.47E-02 | 2.74E-02 |
| | 313 | 5.87E-02 | 3.70E-02 | 3.94E-02 |
| 0.75 | 283 | 4.43E-02 | 3.90E-02 | 4.47E-02 |
| | 298 | 6.09E-02 | 5.34E-02 | 5.91E-02 |
| | 313 | 1.13E-01 | 7.11E-02 | 7.68E-02 |
| 1 | 283 | 8.82E-02 | 6.70E-02 | 7.36E-02 |
| | 298 | 1.34E-01 | 8.53E-02 | 9.27E-02 |
| | 313 | 2.03E-01 | 1.07E-01 | 1.15E-01 |

Table A-6: Solubility of 5-fluoroisatin in pure solvents – Experimental values and predictions.

| Solvent | Temperature (K) | Experimental | Wilson Prediction | UNIQUAC Prediction |
|-----------------|-----------------|--------------|-------------------|--------------------|
| 2-butanone | 283 | 6.50E-03 | 1.12E-02 | 5.40E-03 |
| | 298 | 6.78E-03 | 1.88E-02 | 9.00E-03 |
| | 313 | 1.54E-02 | 2.99E-02 | 7.40E-03 |
| Acetonitrile | 283 | 5.35E-03 | 2.90E-03 | 3.90E-03 |
| | 298 | 6.00E-03 | 5.70E-03 | 7.60E-03 |
| | 313 | 8.54E-03 | 1.07E-02 | 1.40E-02 |
| Benzyl Alcohol | 298 | 8.64E-03 | 6.90E-03 | 1.52E-02 |
| Chloroform | 283 | 1.60E-03 | 2.70E-03 | 3.90E-03 |
| | 298 | 1.66E-03 | 5.30E-03 | 6.60E-03 |
| | 313 | 8.24E-03 | 1.01E-02 | 1.81E-02 |
| Dichloromethane | 283 | 3.63E-03 | 2.70E-03 | 4.30E-03 |
| | 298 | 1.71E-02 | 5.50E-03 | 5.50E-03 |
| | 313 | 2.77E-03 | 1.06E-02 | 1.06E-02 |
| Dioxane | 283 | 1.88E-02 | 1.69E-02 | 1.63E-02 |
| | 298 | 2.74E-02 | 2.73E-02 | 2.56E-02 |
| | 313 | 4.26E-02 | 4.22E-02 | 3.84E-02 |
| DMF | 283 | 4.34E-02 | 2.86E-02 | 3.03E-02 |

Table A-6 (Continued).

| Solvent | Temperature (K) | Experimental | Wilson Prediction | UNIQUAC Prediction |
|----------------|------------------------|---------------------|--------------------------|---------------------------|
| DMF | 298 | 7.18E-02 | 4.28E-02 | 4.52E-02 |
| | 313 | 1.08E-01 | 6.11E-02 | 6.41E-02 |
| Ethanol | 283 | 3.78E-03 | 1.20E-03 | 3.30E-03 |
| | 298 | 4.24E-03 | 2.40E-03 | 5.80E-03 |
| | 313 | 5.62E-03 | 4.60E-03 | 1.06E-02 |
| Ethyl Acetate | 283 | 8.51E-03 | 5.20E-03 | 5.10E-03 |
| | 298 | 1.02E-02 | 9.50E-03 | 9.30E-03 |
| | 313 | 1.33E-02 | 1.63E-02 | 7.00E-03 |
| Isopropanol | 283 | 2.73E-03 | 1.10E-03 | 3.00E-03 |
| | 298 | 2.99E-03 | 2.30E-03 | 6.00E-03 |
| | 313 | 4.46E-03 | 4.50E-03 | 1.00E-02 |
| Methanol | 283 | 5.83E-03 | 1.10E-03 | 3.90E-03 |
| | 298 | 6.45E-03 | 2.20E-03 | 9.00E-03 |
| | 313 | 7.67E-03 | 4.20E-03 | 1.45E-02 |
| Nitromethane | 283 | 7.25E-03 | 1.40E-03 | 5.30E-03 |
| | 298 | 5.00E-03 | 3.00E-03 | 6.10E-03 |
| | 313 | 8.56E-03 | 6.00E-03 | 1.54E-02 |
| toluene | 313 | 9.35E-04 | 3.90E-03 | 1.38E-02 |

Table A-7: Solubility of 5-fluoroisatin in mixtures of ethanol and ethyl acetate – Experimental values and predictions.

| Fraction Ethanol | Temperature (K) | Experimental | Wilson Prediction | UNIQUAC Prediction |
|-------------------------|------------------------|---------------------|--------------------------|---------------------------|
| 0 | 283 | 8.51E-03 | 5.20E-03 | 5.09E-03 |
| | 298 | 1.02E-02 | 9.45E-03 | 9.31E-03 |
| | 313 | 1.33E-02 | 1.63E-02 | 1.59E-02 |
| 0.25 | 283 | 8.51E-03 | 6.88E-03 | 1.33E-02 |
| | 298 | 9.06E-03 | 1.21E-02 | 2.26E-02 |
| | 313 | 1.09E-02 | 2.02E-02 | 2.12E-02 |
| 0.5 | 283 | 8.47E-03 | 5.89E-03 | 1.61E-02 |
| | 298 | 1.00E-02 | 1.07E-02 | 2.82E-02 |
| | 313 | 1.18E-02 | 1.82E-02 | 1.77E-02 |
| 0.75 | 283 | 6.78E-03 | 3.77E-03 | 9.84E-03 |
| | 298 | 7.39E-03 | 7.07E-03 | 1.89E-02 |
| | 313 | 9.51E-03 | 1.25E-02 | 9.78E-03 |
| 1 | 283 | 3.78E-03 | 1.20E-03 | 8.59E-04 |
| | 298 | 4.24E-03 | 2.43E-03 | 1.77E-03 |
| | 313 | 5.62E-03 | 4.64E-03 | 3.44E-03 |

Table A-8: Solubility of 5-fluoroisatin in mixtures of isopropanol and nitromethane – Experimental values and predictions.

| Fraction Isopropanol | Temperature (K) | Experimental | Wilson Prediction | UNIQUAC Prediction |
|-----------------------------|------------------------|---------------------|--------------------------|---------------------------|
| 0 | 283 | 7.25E-03 | 1.43E-03 | 2.16E-03 |
| | 298 | 5.00E-03 | 3.03E-03 | 4.43E-03 |
| | 313 | 8.56E-03 | 5.98E-03 | 8.49E-03 |
| 0.25 | 283 | 6.74E-03 | 2.30E-03 | 4.22E-03 |
| | 298 | 1.08E-02 | 4.68E-03 | 8.13E-03 |
| | 313 | 1.62E-02 | 8.91E-03 | 1.47E-02 |
| 0.5 | 283 | 1.39E-02 | 2.42E-03 | 4.33E-03 |
| | 298 | 1.61E-02 | 4.95E-03 | 8.40E-03 |
| | 313 | 1.75E-02 | 9.44E-03 | 1.52E-02 |
| 0.75 | 283 | 6.14E-03 | 2.06E-03 | 2.53E-03 |
| | 298 | 9.49E-03 | 4.18E-03 | 5.10E-03 |
| | 313 | 1.17E-02 | 7.95E-03 | 9.63E-03 |
| 1 | 283 | 2.73E-03 | 1.12E-03 | 7.56E-04 |
| | 298 | 2.99E-03 | 2.31E-03 | 1.60E-03 |
| | 313 | 4.46E-03 | 4.47E-03 | 3.18E-03 |

Table A-9: Solubility of 5-fluoroisatin in mixtures of dioxane and 2-butanone – Experimental values and predictions.

| Fraction Dioxane | Temperature (K) | Experimental | Wilson Prediction | UNIQUAC Prediction |
|-------------------------|------------------------|---------------------|--------------------------|---------------------------|
| 0 | 283 | 6.50E-03 | 1.12E-02 | 2.40E-03 |
| | 298 | 6.78E-03 | 1.88E-02 | 4.54E-03 |
| | 313 | 1.54E-02 | 2.99E-02 | 8.08E-03 |
| 0.25 | 283 | 1.24E-02 | 1.27E-02 | 2.79E-03 |
| | 298 | 1.65E-02 | 2.09E-02 | 5.26E-03 |
| | 313 | 2.08E-02 | 3.31E-02 | 1.79E-02 |
| 0.5 | 283 | 1.54E-02 | 1.41E-02 | 3.17E-03 |
| | 298 | 2.12E-02 | 2.30E-02 | 5.97E-03 |
| | 313 | 2.56E-02 | 3.61E-02 | 2.72E-02 |
| 0.75 | 283 | 2.06E-02 | 1.55E-02 | 3.51E-03 |
| | 298 | 2.41E-02 | 2.52E-02 | 6.62E-03 |
| | 313 | 2.96E-02 | 3.92E-02 | 3.43E-02 |
| 1 | 283 | 1.88E-02 | 1.69E-02 | 3.79E-03 |
| | 298 | 2.74E-02 | 2.73E-02 | 7.15E-03 |
| | 313 | 4.26E-02 | 4.22E-02 | 3.84E-02 |

Table A-10: Solubility of 5-fluoroisatin in mixtures of DMF and chloroform – Experimental values and predictions.

| Fraction DMF | Temperature (K) | Experimental | Wilson Prediction | UNIQUAC Prediction |
|--------------|-----------------|--------------|-------------------|--------------------|
| 0 | 283 | 1.60E-03 | 2.65E-03 | 2.29E-03 |
| | 298 | 1.66E-03 | 5.34E-03 | 4.66E-03 |
| | 313 | 8.24E-01 | 1.01E-02 | 8.90E-03 |
| 0.25 | 283 | 8.18E-03 | 4.27E-03 | 5.31E-03 |
| | 298 | 1.14E-02 | 8.15E-03 | 9.41E-03 |
| | 313 | 1.58E-02 | 1.46E-02 | 1.61E-02 |
| 0.5 | 283 | 2.27E-02 | 8.63E-03 | 1.12E-02 |
| | 298 | 3.95E-02 | 1.51E-02 | 1.82E-02 |
| | 313 | 3.71E-02 | 2.50E-02 | 2.86E-02 |
| 0.75 | 283 | 3.79E-02 | 1.66E-02 | 1.98E-02 |
| | 298 | 5.34E-02 | 2.67E-02 | 3.05E-02 |
| | 313 | 7.61E-02 | 4.08E-02 | 4.51E-02 |
| 1 | 283 | 4.34E-02 | 2.86E-02 | 3.03E-02 |
| | 298 | 7.18E-02 | 4.28E-02 | 4.52E-02 |
| | 313 | 1.07E-01 | 6.11E-02 | 6.41E-02 |

Table A-11: Solubility of benzimidazole in pure solvents – Experimental values and predictions.

| Solvent | Temperature (K) | Experimental | Wilson Prediction | UNIQUAC Prediction |
|-----------------|-----------------|--------------|-------------------|--------------------|
| 2-Butanone | 283 | 2.17E-02 | 1.48E-02 | 2.15E-02 |
| | 298 | 2.42E-02 | 2.64E-02 | 3.62E-02 |
| | 313 | 3.52E-02 | 4.48E-02 | 5.92E-02 |
| Acetonitrile | 283 | 5.54E-03 | 8.60E-03 | 8.60E-03 |
| | 298 | 6.14E-03 | 1.60E-02 | 3.89E-02 |
| | 313 | 3.04E-02 | 2.82E-02 | 2.79E-02 |
| Chloroform | 283 | 2.94E-03 | 2.30E-03 | 1.80E-03 |
| | 298 | 4.43E-03 | 5.30E-03 | 4.20E-03 |
| | 313 | 7.69E-03 | 1.15E-02 | 9.10E-03 |
| Cyclohexane | 283 | 4.88E-05 | 4.90E-05 | 5.84E-05 |
| | 298 | 1.53E-04 | 1.78E-04 | 2.05E-04 |
| | 313 | 1.73E-04 | 5.51E-04 | 6.15E-02 |
| Dichloromethane | 283 | 4.04E-03 | 2.10E-03 | 1.90E-03 |
| | 298 | 1.09E-02 | 4.90E-03 | 4.40E-03 |
| | 313 | 1.19E-02 | 1.08E-02 | 9.50E-03 |
| Dioxane | 283 | 1.99E-02 | 2.01E-02 | 3.26E-02 |
| | 298 | 2.33E-02 | 3.46E-02 | 5.22E-02 |

Table A-11 (Continued).

| Solvent | Temperature | | Wilson | UNIQUAC |
|----------------|--------------------|---------------------|-------------------|-------------------|
| | (K) | Experimental | Prediction | Prediction |
| Dioxane | 313 | 5.16E-02 | 5.65E-02 | 7.91E-02 |
| DMF | 283 | 1.50E-01 | 8.69E-02 | 1.10E-01 |
| | 298 | 1.86E-01 | 1.19E-01 | 1.44E-01 |
| | 313 | 2.06E-01 | 1.57E-01 | 1.83E-01 |
| Ethanol | 283 | 7.13E-02 | 2.56E-02 | 2.51E-02 |
| | 298 | 8.59E-02 | 4.26E-02 | 4.24E-02 |
| | 313 | 9.30E-02 | 6.75E-02 | 6.83E-02 |
| Ethyl Acetate | 283 | 1.24E-02 | 5.50E-03 | 7.60E-03 |
| | 298 | 1.40E-02 | 1.12E-02 | 1.46E-02 |
| | 313 | 2.66E-02 | 2.14E-02 | 2.68E-02 |
| Heptane | 283 | 1.33E-04 | 4.86E-05 | 5.41E-05 |
| | 298 | 2.08E-04 | 1.77E-04 | 1.91E-04 |
| | 313 | 6.78E-04 | 5.46E-04 | 5.69E-04 |
| Isopropanol | 283 | 5.81E-02 | 2.24E-02 | 2.21E-02 |
| | 298 | 7.54E-02 | 3.75E-02 | 3.74E-02 |
| | 313 | 8.32E-02 | 6.00E-02 | 6.04E-02 |
| Methanol | 283 | 1.10E-02 | 2.52E-02 | 2.37E-02 |
| | 298 | 1.37E-01 | 4.22E-02 | 4.06E-02 |
| | 313 | 2.45E-01 | 6.75E-02 | 6.68E-02 |
| Nitromethane | 283 | 5.83E-03 | 2.80E-03 | 2.40E-03 |
| | 298 | 7.37E-03 | 5.80E-03 | 5.00E-03 |
| | 313 | 1.00E-02 | 1.14E-02 | 9.80E-03 |
| Toluene | 283 | 3.65E-04 | 4.41E-04 | 5.43E-04 |
| | 298 | 6.56E-04 | 1.20E-03 | 4.64E-02 |
| | 313 | 1.09E-03 | 3.10E-03 | 6.93E-02 |

Table A-12: Solubility of benzimidazole in mixtures of ethanol and ethyl acetate – Experimental values and predictions.

| Fraction Ethanol | Temperature (K) | Experimental | Wilson Prediction | UNIQUAC Prediction |
|-------------------------|------------------------|---------------------|--------------------------|---------------------------|
| 0 | 283 | 1.24E-02 | 5.52E-03 | 7.76E-03 |
| | 298 | 1.40E-02 | 1.12E-02 | 1.50E-02 |
| | 313 | 2.66E-02 | 2.14E-02 | 2.74E-02 |
| 0.25 | 283 | 5.29E-02 | 1.66E-02 | 2.69E-02 |
| | 298 | 5.43E-02 | 2.81E-02 | 4.41E-02 |
| | 313 | 8.10E-02 | 4.61E-02 | 6.90E-02 |
| 0.5 | 283 | 7.26E-02 | 2.41E-02 | 3.61E-02 |
| | 298 | 1.10E-01 | 3.98E-02 | 5.80E-02 |
| | 313 | 1.13E-01 | 6.32E-02 | 8.82E-02 |
| 0.75 | 283 | 9.85E-02 | 2.69E-02 | 3.36E-02 |
| | 298 | 1.37E-01 | 4.44E-02 | 5.53E-02 |
| | 313 | 1.69E-01 | 7.01E-02 | 8.59E-02 |
| 1 | 283 | 7.13E-02 | 2.56E-02 | 2.50E-02 |
| | 298 | 8.59E-02 | 4.26E-02 | 4.22E-02 |
| | 313 | 9.30E-02 | 6.75E-02 | 6.81E-02 |

Table A-13: Solubility of benzimidazole in mixtures of isopropanol and nitromethane – Experimental values and predictions.

| Fraction Isopropanol | Temperature (K) | Experimental | Wilson Prediction | UNIQUAC Prediction |
|-----------------------------|------------------------|---------------------|--------------------------|---------------------------|
| 0 | 283 | 5.83E-03 | 2.76E-03 | 2.54E-03 |
| | 298 | 7.37E-03 | 5.78E-03 | 5.30E-03 |
| | 313 | 1.00E-02 | 1.14E-02 | 1.03E-02 |
| 0.25 | 283 | 3.64E-02 | 1.05E-02 | 1.16E-02 |
| | 298 | 5.43E-02 | 1.86E-02 | 2.07E-02 |
| | 313 | 6.30E-02 | 3.17E-02 | 3.53E-02 |
| 0.5 | 283 | 7.24E-02 | 1.84E-02 | 2.29E-02 |
| | 298 | 1.02E-01 | 3.14E-02 | 3.84E-02 |
| | 313 | 1.07E-01 | 5.14E-02 | 6.14E-02 |
| 0.75 | 283 | 6.52E-02 | 2.38E-02 | 2.78E-02 |
| | 298 | 9.16E-02 | 3.98E-02 | 4.57E-02 |
| | 313 | 9.82E-02 | 6.36E-02 | 7.18E-02 |
| 1 | 283 | 5.81E-02 | 2.24E-02 | 2.20E-02 |
| | 298 | 7.54E-02 | 3.75E-02 | 3.72E-02 |
| | 313 | 8.32E-02 | 6.00E-02 | 6.02E-02 |

Table A-14: Solubility of benzimidazole in mixtures of dioxane and 2-butanone – Experimental values and predictions.

| Fraction Dioxane | Temperature (K) | Experimental | Wilson Prediction | UNIQUAC Prediction |
|------------------|-----------------|--------------|-------------------|--------------------|
| 0 | 283 | 2.17E-02 | 1.48E-02 | 2.19E-02 |
| | 298 | 2.42E-02 | 2.64E-02 | 3.68E-02 |
| | 313 | 3.52E-02 | 4.48E-02 | 5.92E-02 |
| 0.25 | 283 | 2.56E-02 | 1.68E-02 | 2.50E-02 |
| | 298 | 4.51E-02 | 2.96E-02 | 4.17E-02 |
| | 313 | 4.57E-02 | 4.94E-02 | 6.66E-02 |
| 0.5 | 283 | 2.61E-02 | 1.85E-02 | 2.80E-02 |
| | 298 | 4.88E-02 | 3.21E-02 | 4.62E-02 |
| | 313 | 5.36E-02 | 5.31E-02 | 7.28E-02 |
| 0.75 | 283 | 2.15E-02 | 1.96E-02 | 3.06E-02 |
| | 298 | 3.81E-02 | 3.39E-02 | 4.98E-02 |
| | 313 | 5.59E-02 | 5.55E-02 | 7.73E-02 |
| 1 | 283 | 1.99E-02 | 2.01E-02 | 3.28E-02 |
| | 298 | 2.33E-02 | 3.46E-02 | 5.22E-02 |
| | 313 | 5.16E-02 | 5.65E-02 | 7.96E-02 |

Table A-15: Solubility of benzimidazole in mixtures of DMF and chloroform – Experimental values and predictions.

| Fraction DMF | Temperature (K) | Experimental | Wilson Prediction | UNIQUAC Prediction |
|--------------|-----------------|--------------|-------------------|--------------------|
| 0 | 283 | 2.94E-03 | 2.76E-03 | 2.54E-03 |
| | 298 | 4.43E-03 | 5.78E-03 | 5.30E-03 |
| | 313 | 7.69E-03 | 1.14E-02 | 1.03E-02 |
| 0.25 | 283 | 3.70E-02 | 1.05E-02 | 1.16E-02 |
| | 298 | 5.14E-02 | 1.86E-02 | 2.07E-02 |
| | 313 | 6.20E-02 | 3.17E-02 | 3.53E-02 |
| 0.5 | 283 | 6.96E-02 | 1.84E-02 | 2.29E-02 |
| | 298 | 8.33E-02 | 3.14E-02 | 3.84E-02 |
| | 313 | 1.02E-01 | 5.14E-02 | 6.14E-02 |
| 0.75 | 283 | 1.09E-01 | 2.38E-02 | 2.78E-02 |
| | 298 | 1.36E-01 | 3.98E-02 | 4.57E-02 |
| | 313 | 1.51E-01 | 6.36E-02 | 7.18E-02 |
| 1 | 283 | 1.50E-01 | 2.24E-02 | 2.20E-02 |
| | 298 | 1.86E-01 | 3.75E-02 | 3.72E-02 |
| | 313 | 2.06E-01 | 6.00E-02 | 6.02E-02 |

Table A-16 : Solubility of 2-amino-5-nitrobenzophenone in pure solvents – Experimental values and predictions.

| Solvent | Temperature | Experimental | Wilson | UNIQUAC |
|-----------------|-------------|--------------|------------|------------|
| | (K) | | Prediction | Prediction |
| 2-Butanone | 283 | 1.69E-02 | 7.41E-02 | 7.49E-02 |
| | 298 | 2.20E-02 | 5.08E-02 | 5.15E-02 |
| 2-Propanol | 283 | 5.60E-04 | 5.56E-04 | 5.56E-04 |
| | 298 | 1.16E-03 | 1.40E-03 | 1.40E-03 |
| | 313 | 4.24E-03 | 3.30E-03 | 3.30E-03 |
| Benzonitrile | 298 | 5.29E-02 | 3.07E-02 | 3.07E-02 |
| Benzyl Alcohol | 298 | 1.70E-02 | 2.00E-03 | 1.90E-03 |
| Chlorobenzene | 298 | 5.94E-03 | 3.70E-03 | 3.70E-03 |
| Chloroform | 283 | 7.18E-03 | 1.60E-03 | 1.60E-03 |
| | 298 | 7.65E-03 | 3.80E-03 | 3.80E-03 |
| | 313 | 1.19E-02 | 8.60E-03 | 8.60E-03 |
| Dichloromethane | 283 | 2.42E-02 | 2.50E-03 | 3.29E-02 |
| | 298 | 3.80E-02 | 6.00E-03 | 6.00E-03 |
| | 313 | 4.26E-02 | 1.31E-02 | 1.30E-02 |
| Dioxane | 283 | 2.79E-02 | 2.80E-02 | 2.81E-02 |
| | 298 | 4.22E-02 | 4.29E-02 | 4.31E-02 |
| | 313 | 5.66E-02 | 6.37E-02 | 6.38E-02 |
| DMF | 283 | 6.18E-02 | 4.82E-02 | 5.17E-02 |
| | 298 | 9.34E-02 | 7.24E-02 | 7.76E-02 |
| | 313 | 1.09E-01 | 1.03E-01 | 1.10E-01 |
| Ethanol | 283 | 6.30E-04 | 4.87E-04 | 4.86E-04 |
| | 298 | 1.33E-03 | 1.20E-03 | 1.20E-03 |
| | 313 | 3.24E-03 | 2.80E-03 | 2.80E-03 |
| Ethyl Acetate | 283 | 2.23E-02 | 1.82E-02 | 1.82E-02 |
| | 298 | 3.07E-02 | 3.11E-02 | 3.11E-02 |
| | 313 | 4.74E-02 | 5.02E-02 | 5.03E-02 |
| Methanol | 283 | 5.97E-04 | 3.83E-04 | 3.81E-04 |
| | 298 | 1.66E-03 | 9.27E-04 | 9.22E-04 |
| | 313 | 1.47E-03 | 2.10E-03 | 2.10E-03 |
| Nitromethane | 283 | 1.01E-02 | 3.60E-03 | 3.60E-03 |
| | 298 | 1.90E-02 | 8.40E-03 | 8.30E-03 |
| | 313 | 2.23E-02 | 1.80E-02 | 1.76E-02 |
| Toluene | 283 | 2.08E-03 | 9.77E-04 | 9.74E-04 |
| | 298 | 2.15E-03 | 2.40E-03 | 2.40E-03 |
| | 313 | 3.80E-03 | 5.50E-03 | 5.40E-03 |

Table A-17: Solubility of 2-amino-5-nitrobenzophenone in mixtures of ethanol and ethyl acetate – Experimental values and predictions.

| Fraction Ethanol | Temperature (K) | Experimental | Wilson Prediction | UNIQUAC Prediction |
|------------------|-----------------|--------------|-------------------|--------------------|
| 0 | 283 | 2.23E-02 | 1.84E-02 | 1.82E-02 |
| | 298 | 3.07E-02 | 3.13E-02 | 3.11E-02 |
| | 313 | 4.74E-02 | 5.05E-02 | 5.03E-02 |
| 0.25 | 283 | 5.57E-03 | 1.26E-02 | 1.14E-02 |
| | 298 | 9.52E-03 | 2.32E-02 | 2.15E-02 |
| | 313 | 1.23E-02 | 4.00E-02 | 3.78E-02 |
| 0.5 | 283 | 4.40E-03 | 5.93E-03 | 4.74E-03 |
| | 298 | 8.21E-03 | 1.23E-02 | 1.03E-02 |
| | 313 | 9.45E-03 | 2.36E-02 | 2.06E-02 |
| 0.75 | 283 | 3.08E-03 | 2.06E-03 | 1.58E-03 |
| | 298 | 3.91E-03 | 4.72E-03 | 3.77E-03 |
| | 313 | 5.87E-03 | 1.01E-02 | 8.33E-03 |
| 1 | 283 | 6.30E-04 | 4.92E-04 | 4.88E-04 |
| | 298 | 1.33E-03 | 1.21E-03 | 1.20E-03 |
| | 313 | 3.24E-03 | 2.81E-03 | 2.78E-03 |

Table A-18: Solubility of 2-amino-5-nitrobenzophenone in mixtures of isopropanol and nitromethane – Experimental values and predictions.

| Fraction Isopropanol | Temperature (K) | Experimental | Wilson Prediction | UNIQUAC Prediction |
|----------------------|-----------------|--------------|-------------------|--------------------|
| 0 | 283 | 1.01E-02 | 3.65E-03 | 3.61E-03 |
| | 298 | 1.90E-02 | 8.44E-03 | 8.32E-03 |
| | 313 | 2.23E-02 | 1.80E-02 | 1.76E-02 |
| 0.25 | 283 | 3.54E-03 | 4.61E-03 | 4.40E-03 |
| | 298 | 5.29E-03 | 1.07E-02 | 9.86E-03 |
| | 313 | 1.01E-02 | 2.25E-02 | 2.03E-02 |
| 0.5 | 283 | 3.40E-03 | 3.79E-03 | 3.39E-03 |
| | 298 | 4.96E-03 | 9.08E-03 | 7.81E-03 |
| | 313 | 9.35E-03 | 1.98E-02 | 1.66E-02 |
| 0.75 | 283 | 2.01E-03 | 2.29E-03 | 1.75E-03 |
| | 298 | 4.33E-03 | 5.66E-03 | 4.21E-03 |
| | 313 | 5.30E-03 | 1.28E-02 | 9.37E-03 |
| 1 | 283 | 5.60E-04 | 5.63E-04 | 5.60E-04 |
| | 298 | 1.16E-03 | 1.43E-03 | 1.42E-03 |
| | 313 | 4.24E-03 | 3.36E-03 | 3.33E-03 |

Table A-19: Solubility of 2-amino-5-nitrobenzophenone in mixtures of dioxane and 2-butanone – Experimental values and predictions.

| Fraction Dioxane | Temperature (K) | Experimental | Wilson Prediction | UNIQUAC Prediction |
|------------------|-----------------|--------------|-------------------|--------------------|
| 0 | 283 | 1.69E-02 | 3.37E-02 | 3.41E-02 |
| | 298 | 2.20E-02 | 5.08E-02 | 5.15E-02 |
| | 313 | 3.53E-02 | 7.41E-02 | 7.49E-02 |
| 0.25 | 283 | 1.21E-02 | 3.48E-02 | 3.44E-02 |
| | 298 | 2.35E-02 | 5.18E-02 | 5.15E-02 |
| | 313 | 3.29E-02 | 7.47E-02 | 7.46E-02 |
| 0.5 | 283 | 1.60E-02 | 3.43E-02 | 3.34E-02 |
| | 298 | 2.42E-02 | 5.09E-02 | 5.01E-02 |
| | 313 | 3.59E-02 | 7.34E-02 | 7.27E-02 |
| 0.75 | 283 | 1.53E-02 | 3.21E-02 | 3.13E-02 |
| | 298 | 2.92E-02 | 4.80E-02 | 4.73E-02 |
| | 313 | 3.74E-02 | 6.98E-02 | 6.91E-02 |
| 1 | 283 | 2.79E-02 | 2.82E-02 | 2.80E-02 |
| | 298 | 4.22E-02 | 4.32E-02 | 4.30E-02 |
| | 313 | 5.66E-02 | 6.40E-02 | 6.37E-02 |

Table A-20: Solubility of 2-amino-5-nitrobenzophenone in mixtures of DMF and chloroform – Experimental values and predictions.

| Fraction DMF | Temperature (K) | Experimental | Wilson Prediction | UNIQUAC Prediction |
|--------------|-----------------|--------------|-------------------|--------------------|
| 0 | 283 | 7.18E-03 | 1.58E-03 | 1.59E-03 |
| | 298 | 7.65E-03 | 3.85E-03 | 3.87E-03 |
| | 313 | 1.19E-02 | 8.66E-03 | 8.69E-03 |
| 0.25 | 283 | 9.94E-03 | 5.29E-03 | 4.72E-03 |
| | 298 | 1.52E-02 | 1.11E-02 | 9.93E-03 |
| | 313 | 1.96E-02 | 2.16E-02 | 1.96E-02 |
| 0.5 | 283 | 1.83E-02 | 1.36E-02 | 1.33E-02 |
| | 298 | 2.37E-02 | 2.51E-02 | 2.45E-02 |
| | 313 | 3.38E-02 | 4.31E-02 | 4.21E-02 |
| 0.75 | 283 | 4.12E-02 | 2.82E-02 | 2.92E-02 |
| | 298 | 4.75E-02 | 4.65E-02 | 4.80E-02 |
| | 313 | 5.69E-02 | 7.16E-02 | 7.37E-02 |
| 1 | 283 | 6.18E-02 | 4.85E-02 | 5.14E-02 |
| | 298 | 9.34E-02 | 7.28E-02 | 7.74E-02 |
| | 313 | 1.09E-01 | 1.04E-01 | 1.09E-01 |

APPENDIX B

VALIDATION OF TAYLOR-ARIS DISPERSION MEASUREMENTS

Introduction

The validation work included in this appendix was performed by me and Dr. Xiuyang Lu, a visiting professor from Zhejiang University in Hangzhou, China. The experimental and analytical methods used are outlined in Chapter V of this thesis.

Diagnostics

Influence of Detection Wavelength

The influence of wavelength on the diffusion coefficient of benzene in methanol at 313 K and 100 bar is shown in Figure B-1. From the results we can see that different wavelengths give different results. Since the detector has the ability to measure up to five wavelengths simultaneously, it was very easy to compare the results of several wavelengths and ensure that they were ascertained under identical conditions. This is important to point out because while we determined that the best place to detect benzene is at 254 nm, the literature tells us that benzene should be detected at either 210 nm¹ or 239 nm.² From our studies, however, we determined that 210 nm is unsuitable for these purposes and that 239 nm works, but 254 nm

produces a stronger signal.

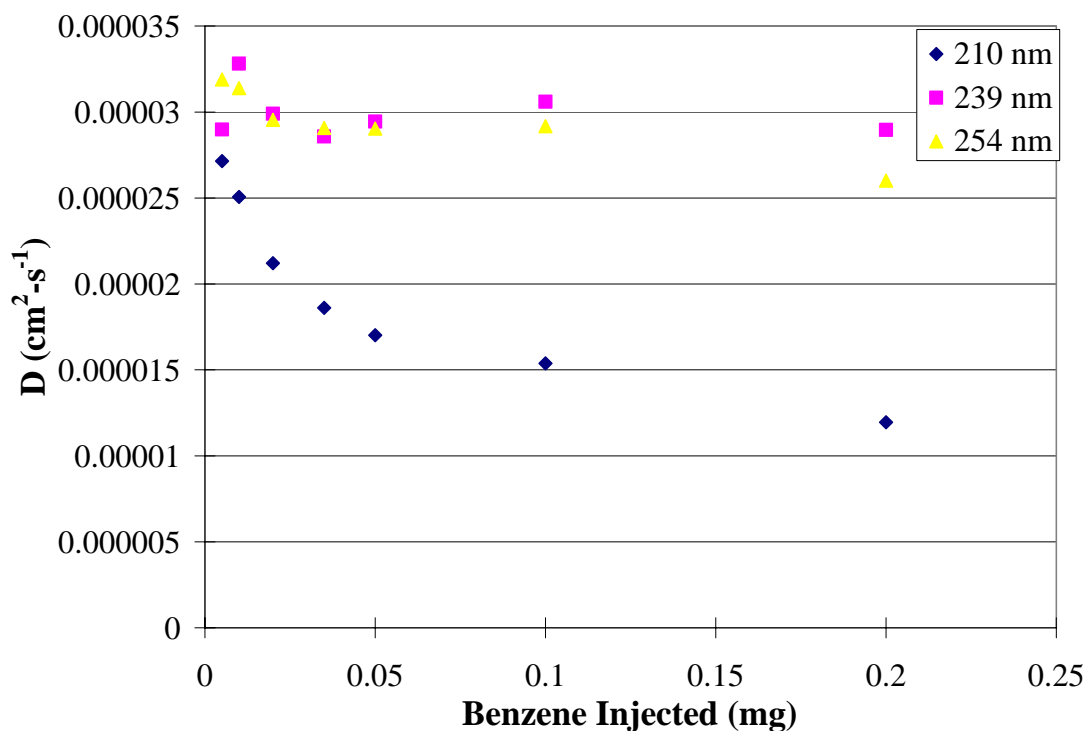


Figure B-1: Influence of detector wavelength and injected amount of solute on the diffusion coefficient of benzene in methanol, 313 K, 100 bar, $v_{\text{Methanol}}=0.2$ ml/min.

Influence of Amount of Solute Injected

Diffusion coefficient data must be measured at infinite dilution in order to eliminate effects from self-diffusion of the solute.³ In practice, infinite dilution is very difficult to achieve because it is typically below the detection limits of any instrument. Thus it was important to determine the appropriate operating range to be as close to infinite dilution as possible while still working in the range where the intensity is linear with the concentration. The limits of the detector were tested by measuring the diffusion coefficients of four compounds – benzene, toluene, 2-naphthol and phenol – as a function of injected quantity. Data for benzene are already presented above in Figure B-1, data for the remaining compounds are shown

in Figures B-2 through B-4.

Comparison of these four figures indicates that benzene is the most sensitive of the four compounds to the amount of solute injected. At higher injected quantity, the diffusion coefficient of benzene (Figure B-1) decreases due to the interactions between solute molecules; the system is not sufficiently dilute and self-diffusion is occurring. At lower injected quantities the diffusion coefficient increases sharply. We have not determined a definitive explanation but speculate that the peak areas are so low as to be below the limits of the detector or that there is mixing within the detector that becomes problematic when the solute is very dilute. Knowledge of such behavior is important in the design of future experiments with the equipment.

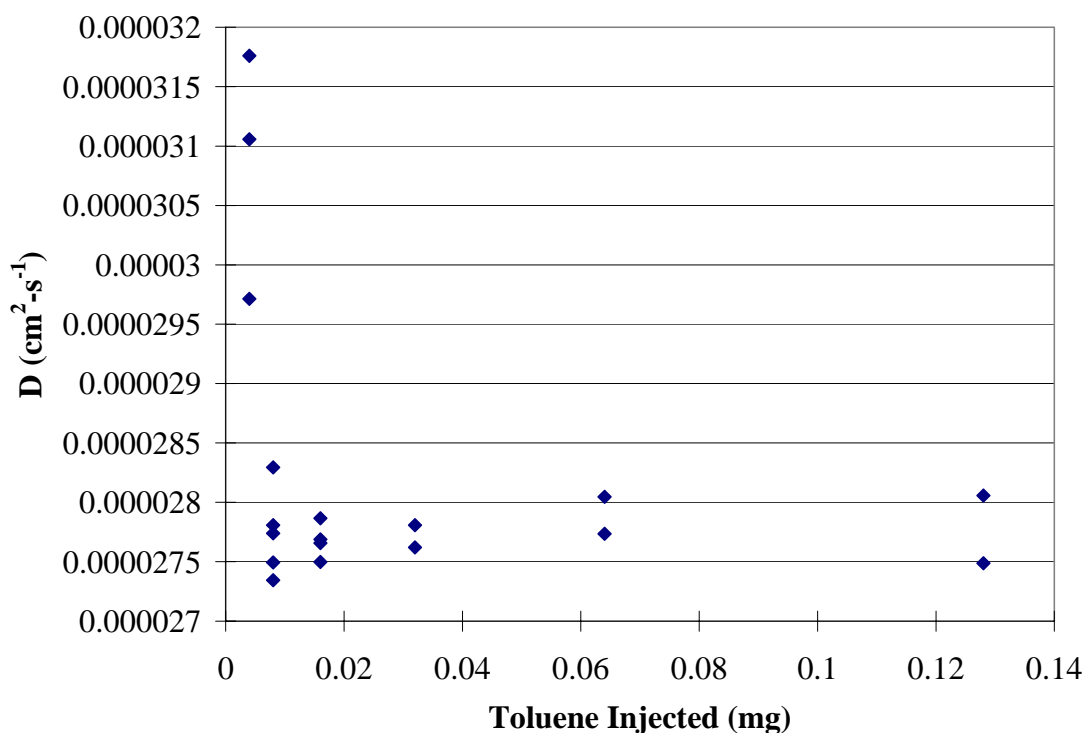


Figure B-2: Influence injected amount of solute on the diffusion coefficient of toluene in methanol, 313 K, 100 bar, $v_{\text{Methanol}}=0.2$ ml/min, 260 nm.

Toluene (Figure B-2) and 2-naphthol (Figure B-3) show similar behaviors at low concentrations, but do not show the same decrease at higher solute amounts. Their threshold for self-diffusion seems to be beyond the limits tested in this study. Phenol does not show either behavior (Figure B-4), indicating that the entire injection range would be suitable for measurement.

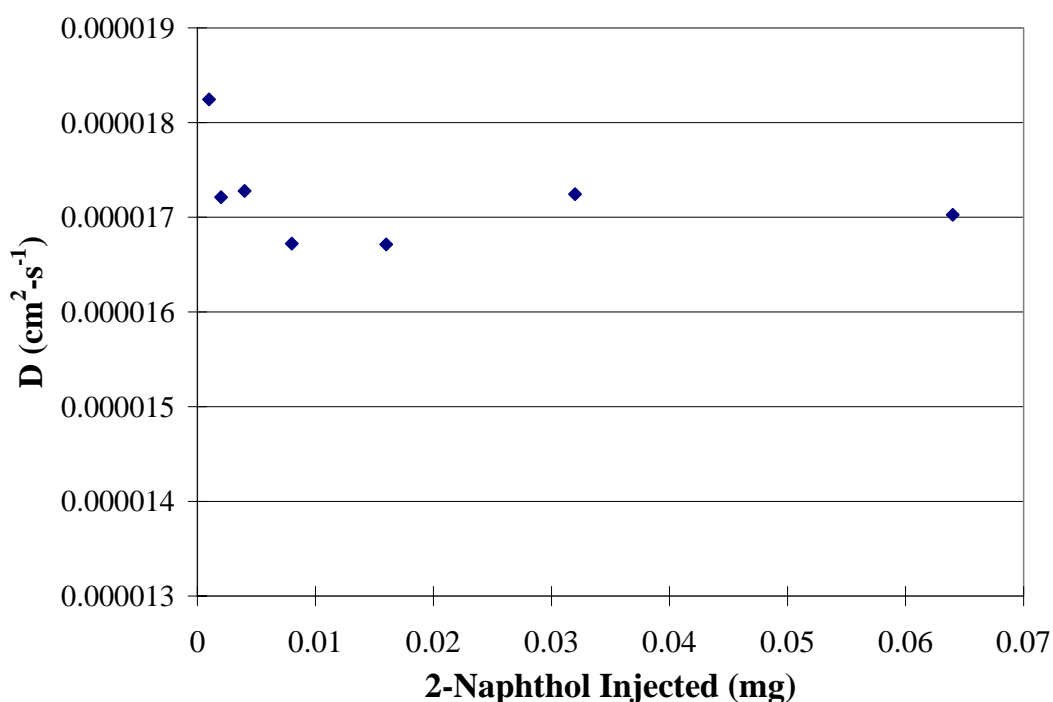


Figure B-3: Influence injected amount of solute on the diffusion coefficient of 2-naphthol in methanol, 313 K, 100 bar, $v_{\text{Methanol}}=0.2$ ml/min, 274 nm.

We also looked at the linearity of the detector with regard to peak area versus injected quantity. Data for the peak area of phenol as a function of injected quantity are in Figure B-5. We wanted to make sure that we were running our experiments in the area where the detector is linear. Based on this and the measurements above, it seems that the appropriate operating range for the peak area should be between 10,000-100,000 mAu-sec. Anything lower and the concentration might become too low and fall into that ‘upturn’ area. Anything higher and self-diffusion might occur.

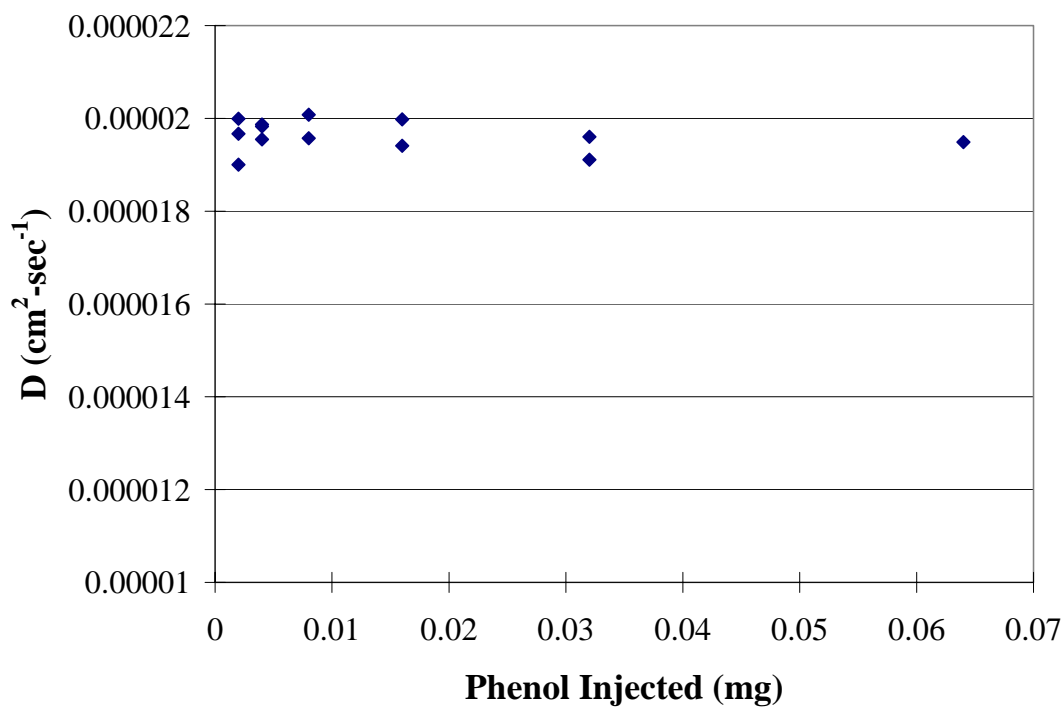


Figure B-4: Influence injected amount of solute on the diffusion coefficient of phenol in methanol, 313K, 100 bar, $v_{\text{Methanol}}=0.2$ ml/min, 272

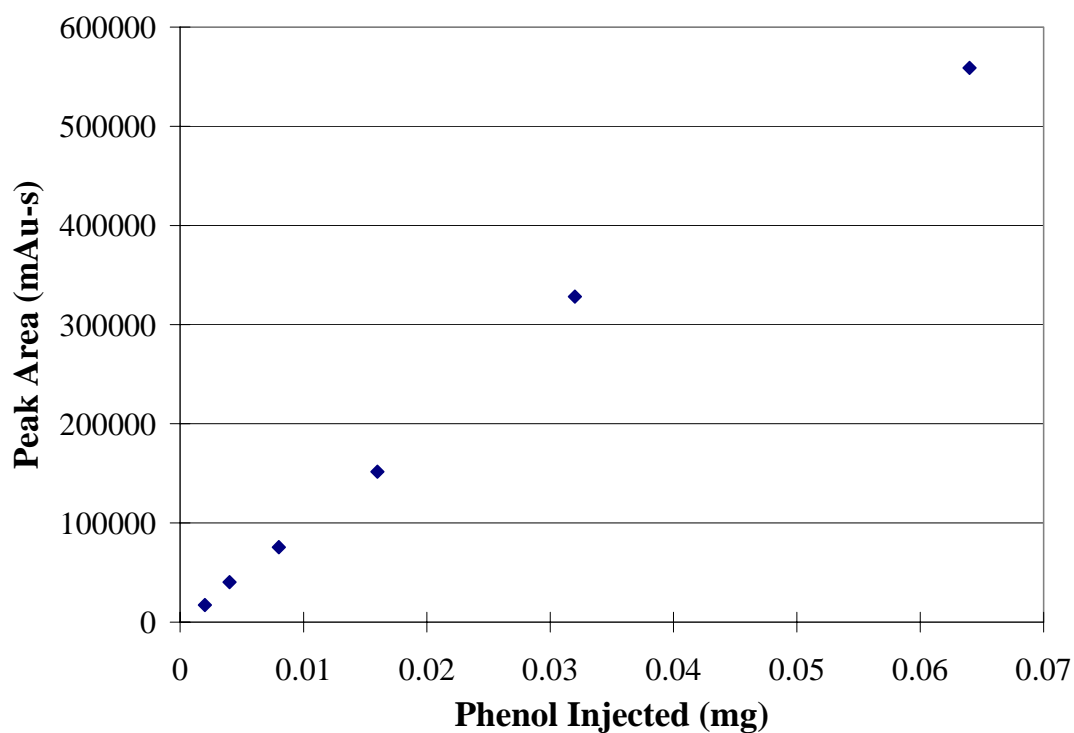


Figure B-5: Influence injected amount of phenol on the peak area 313 K, 100 bar, $v_{\text{Methanol}}=0.2$ ml/min, 272 nm.

Influence of Flow Rate

It is important to choose the flow rate of the mobile phase carefully because the flow profile must be laminar for the Taylor-Aris dispersion technique to be valid. Since the flow is through a coiled tube and not a straight tube, having a Reynolds number of less than 2100 was not the only determining factor in choosing a flow rate. It was also important that the square root of the product of the Dean and Schmidt numbers be less than approximately 10. This means that the flow rate must be less than approximately 2.5 ml/min for methanol. However, the calculations were based on assumptions for a coiled tube that may not have been valid for 100 feet of length and imperfect circles. The influence of flow rate on the diffusion coefficient for benzene in methanol was measured at 313 K and 100 bar and appears in Figure B-6. The data confirm the calculation and indicate that 0.25 ml/min is the maximum flow rate for methanol under the operating conditions. Beyond that limit the flow

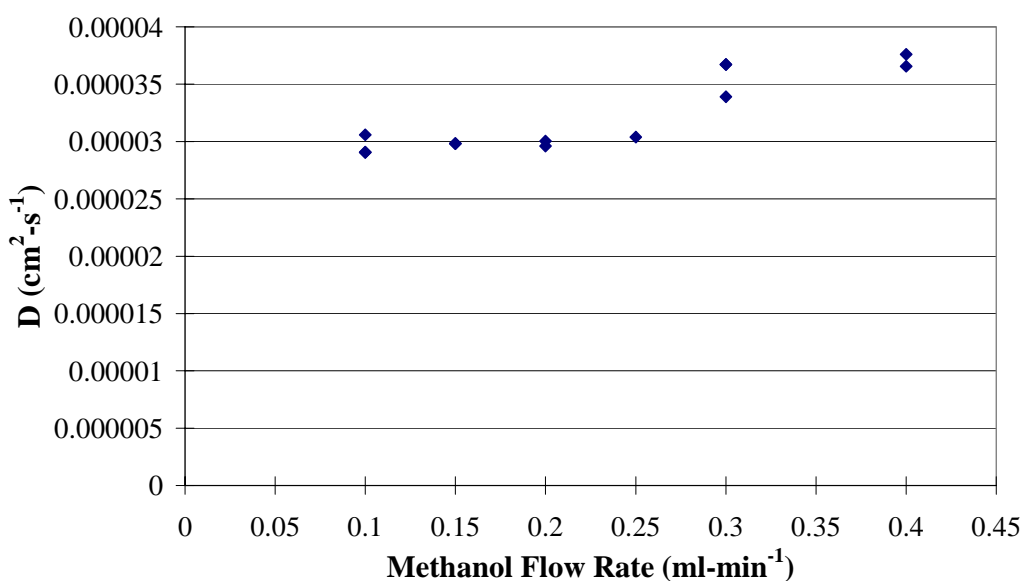


Figure B-6: Influence of methanol flow rate on the diffusion coefficient of benzene, 313 K, 100 bar, 0.01 mg injection.

may no longer be laminar and dispersion due to turbulent flow makes it difficult to decipher diffusion coefficients from the resulting data.

Influence of Pressure

The influence of hydrostatic pressure in the mobile phase on the diffusion coefficients of benzene in methanol at 295 K are shown in Figure B-7. As pressure is increased, the diffusion coefficient decreases. This is expected from a fundamental standpoint. More importantly, the behavior is linear within the range of the experiments.

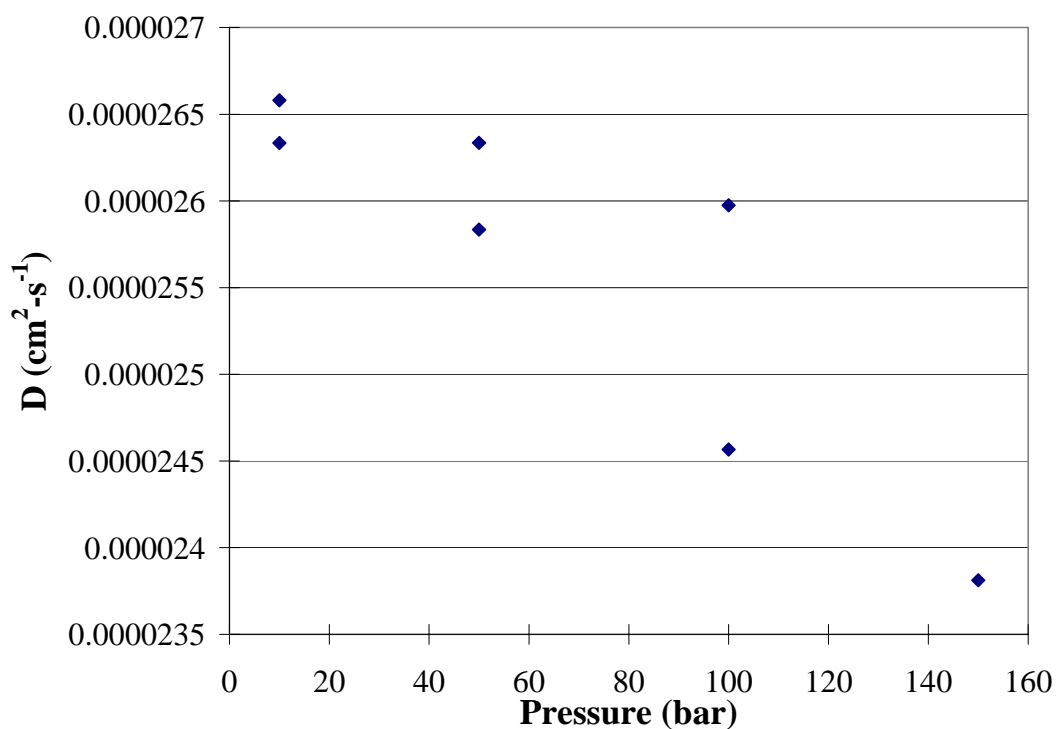


Figure B-7: Influence of hydrostatic pressure of methanol on the diffusion coefficient of benzene, 313 K, 0.01 mg injection, $v_{\text{Methanol}}=0.2$ ml/min.

Influence of System Temperature

The influence of system temperature on the diffusion coefficients of benzene and toluene in methanol are shown in Figures B-8 and B-9, respectively. In both

cases, the diffusion coefficient increases linearly with temperature for the range of temperatures studied.

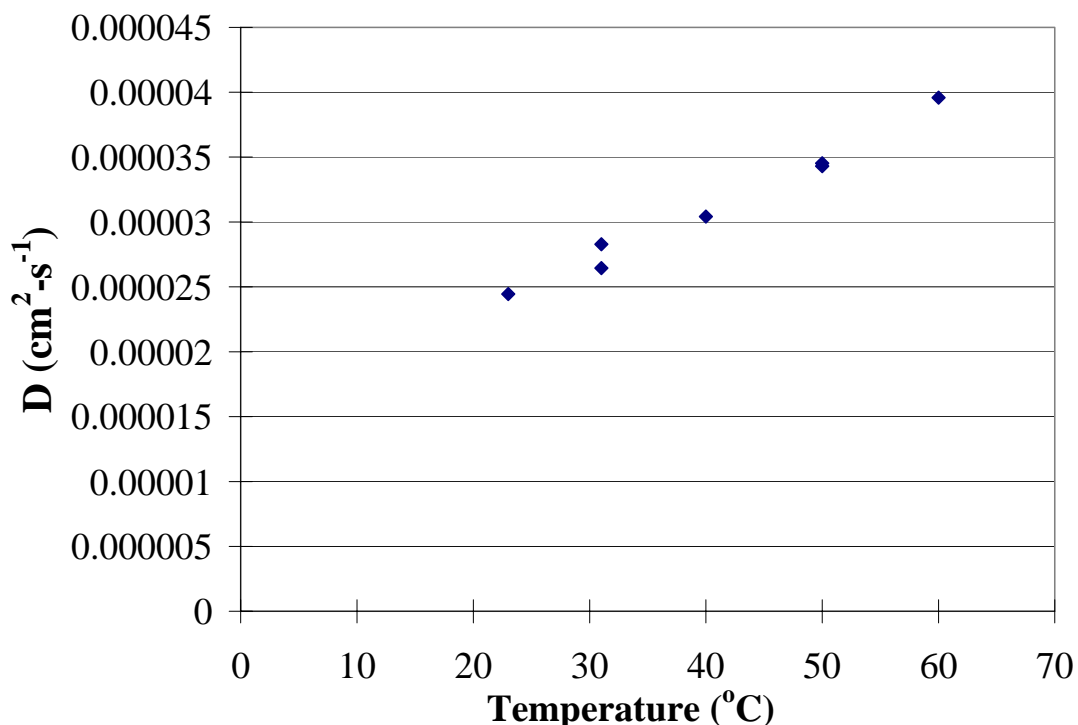


Figure B-8: Influence of temperature of methanol on the diffusion coefficient of benzene, 100 bar, 0.01 mg injection, $v_{\text{Methanol}}=0.2$ ml/min.

Influence of Chiller Temperature

Since the syringe pumps for the methanol and CO₂ were to be chilled so that their density could be known and to ensure that liquid CO₂ was being dispensed into the system, it was necessary to understand the impact of the chiller temperature on the resulting diffusion coefficient. If the chiller had any impact it would need to be corrected for. Data for the diffusion coefficient of toluene as a function of chiller temperature are shown in Figure B-10. It is obvious that the influence of chiller temperature on the diffusion coefficients of toluene in methanol at 323 K and 100 bar

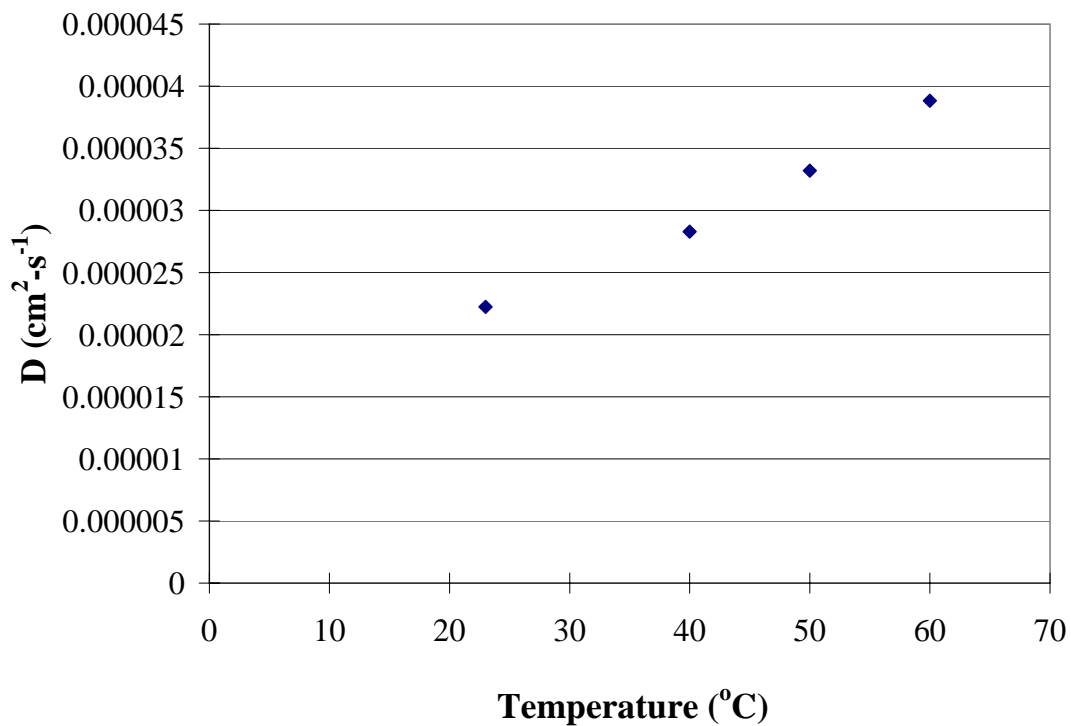


Figure B-9: Influence of temperature of methanol on the diffusion coefficient of toluene, 14 bar, 0.01 mg injection, $v_{\text{Methanol}}=0.2$ ml/min.

is

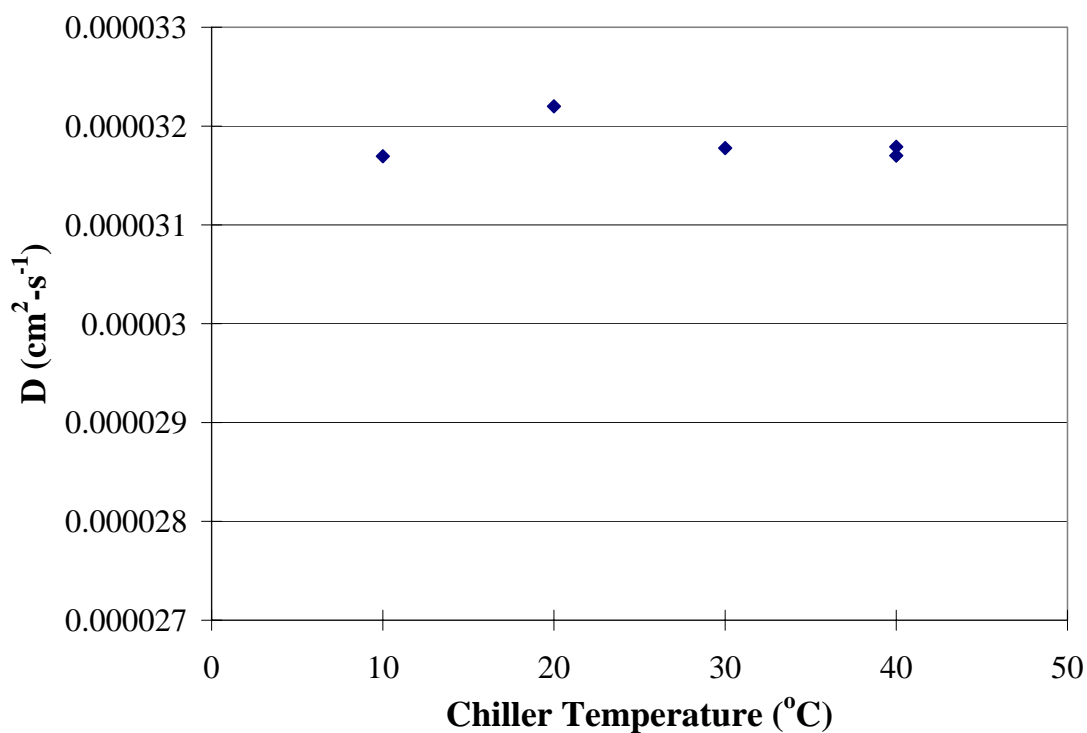


Figure B-10: Influence of chiller temperature on the diffusion coefficient of toluene, 313 K, 100 bar, 0.01 mg injection, $v_{\text{Methanol}}=0.2$ ml/min.

is negligible, which indicates that the pre-heater is sufficient for heating the mobile phase to the requisite temperature.

Upon validation of the above parameters, data of the solids were compared with that of the literature and data for the diffusion of benzene in mixtures of methanol and carbon dioxide were measured and confirmed. These are discussed in detail in Chapter V.

Summary of system requirements

- Results are very sensitive to the detection wavelengths, especially for solutes with sharp peaks in their spectrum such as benzene. Careful selection of the wavelength should be made and the UV detector linearity at selected wavelength should be checked.
- Although we still cannot give a satisfactory explanation as to why the diffusion coefficients go up sharply at lower injected quantities, being aware that the problem exists makes it easier to avoid. The injection quantity should be checked for all solids in methanol before taking data in mixtures.
- The peak area should be considered in the selection of the injected quantity. Based on studies for the above compounds, the peak area should be in the range of 10,000-100,000 mAU-sec as well as satisfying the above criterion.
- A Gaussian curve is assumed for the calculation of the diffusion coefficient from the response curve. Thus it is important to ensure that the response curve is Gaussian.

Determination of system requirements

Since our work involved compounds that had not yet been studied via the Taylor-Aris dispersion method, it was important to determine the appropriate wavelength and injection quantity for each solid. For each of the remaining four solutes, their UV signatures in methanol were obtained from the literature⁴ where available and all were measured via a separate (not on the SFC) UV spectrophotometer. A series of stock concentrations ranging from 1-32 mg solute/ml methanol were prepared and run through the system at the desired operating conditions (40 °C, 150 bar, 0.2 ml/min mobile phase). Since the data acquisition software has the ability to analyze up to five wavelengths simultaneously, each solute was measured at five different wavelengths and the one which gave the best results based on shape and area of resulting peak was chosen. Parameters determined for all solutes studied are summarized in Table B-1.

Table B-1: Detector wavelength and concentration requirements for all solutes studied.

| Solid | Wavelength (nm) | Concentration (mg/ml) |
|----------------|-----------------|-----------------------|
| Benzene | 251 | 32 |
| Pyridine | 252 | 1 |
| Pyrimidine | 241 | 1 |
| Pyrazine | 260 | 2 |
| 1,3,5-Triazine | 270 | 4 |

REFERENCES

1. Sassi, P. R.; Mourier, P.; Caude, M. H.; Rosset, R. H., Measurement of diffusion coefficients in supercritical carbon dioxide and correlation with the equation of Wilke and Chang. *Anal. Chem.* **1987**, *59*, 1164-1170.
2. Funazukuri, T.; Kong, C. Y.; Kagei, S., Infinite-dilution binary diffusion coefficients of 2-propanone, 2-butanone, 2-pentanone, and 3-pentanone in carbon dioxide by the Taylor dispersion technique from 308.15 K in the pressure range from 8-35 MPa. *Int. J. Thermophys.* **2000**, *21*, (6), 1279-1290.
3. Cussler, E. L., *Diffusion: Mass Transfer in Fluid Systems*. 2 ed.; Cambridge University Press: Cambridge, 1997.
4. Silverman, R. M.; Bassler, G. C.; Morrill, T. C., *Spectroscopic Identification of Organic Compounds*. Fourth Edition ed.; John Wiley & Sons: New York, 1963.

APPENDIX C

MICROVISCOSITY: FLUORESCENT EXCITATION OF A MOLECULAR ROTOR AS A PROBE OF THE CYBOTACTIC REGION OF GAS-EXPANDED LIQUIDS

Introduction

As mentioned in Chapter V, elucidation of the transport properties of gas-expanded liquids is of clear importance in the design of industrial scale processes. Since an important feature of GXLs is the possibility of non-uniform molecular distribution,^{1,2} it is imperative to study local as well as bulk transport properties. Local composition and viscosity data are needed in the design of chemical reactions; for example appropriate solvent selection and amount of CO₂, in order to optimize kinetics and selectivity whereas bulk properties are necessary for the engineering aspects of process design. In this chapter, measurements on the microviscosity of CO₂-expanded methanol and acetone are presented and discussed. These data are meant to serve as a complement to Chapter V.

Microviscosity is a measurement of the rigidity of a fluid on the molecular level; in other words, it is the resistance to movement within the cybotactic region. It is typically measured by a molecular rotor - a probe molecule which undergoes a torsional rotation and subsequent relaxation upon excitation. Some examples of molecular rotors include fluorescent dyes such as *p*-(dialkylamino)benzylidenemalonitriles³⁻⁶ and

substituted stilbenes.⁷ An example of the former, 9-(dicyanovinyl) julolidine (DCVJ, Figure C-1), is used in this study.

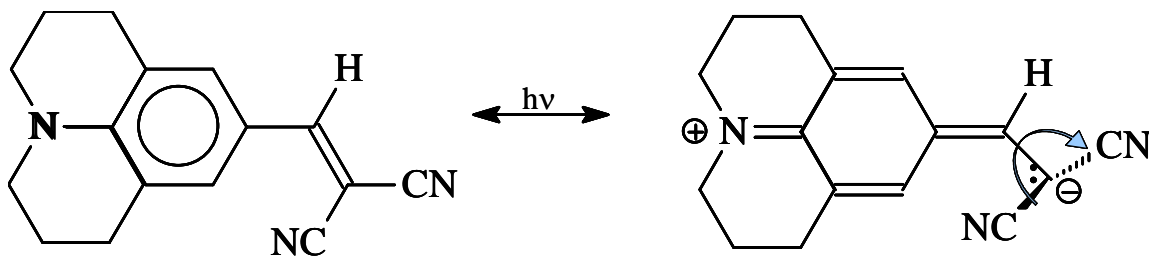


Figure C-1: Structure of DCVJ in both the ground state and excited state.

The photophysical properties of DCVJ as a solvent-dependent molecular rotor are well-described^{5, 6, 8-10} and its use as a fluorescence spectroscopic probe has been demonstrated as an effective technique for measuring the microviscosity of a variety of materials including polymers,⁵ proteins,⁸ room temperature ionic liquids¹⁰ and cell membranes.⁴ In the current work this technique is used to measure the microviscosity of CO₂-expanded methanol and CO₂-expanded acetone as a function of CO₂ pressure to obtain further insight into the local composition and structure.

A simplified illustration of the fluorescence emission mechanism for DCVJ is shown in Figure C-2, where S₀ is the ground state, S₁ is the first excited state, A is the absorbance (excitation process), F is the fluorescence (emission process) and k_r and k_{nr} are the radiative and non-radiative deactivation rates, respectively.¹⁰ The fluorescence quantum yield, Φ_f, is defined by Equation C-1 as the number of quanta emitted per quantum absorbed.¹⁰

$$\Phi_f = k_r / (k_r + k_{nr}) \quad \text{Eq. C-1}$$

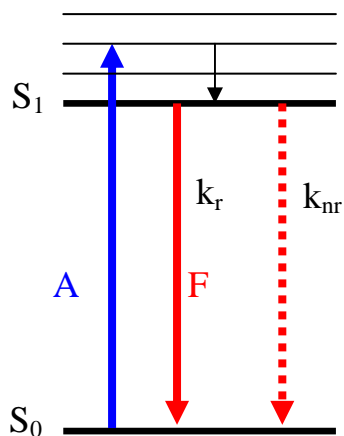


Figure C-2: Simplified fluorescence emission mechanism.

Upon excitation, a rotation occurs about the donor-acceptor bond in DCVJ, indicated by the curved arrow in Figure C-1. Subsequent deactivation is governed by two competing pathways: radiative and non-radiative. The singlet excited state can be non-radiatively deactivated via internal, torsional relaxation about the donor-acceptor double bond, provided the solvent shell is not too rigid. However, an increase in the viscosity of the surrounding medium can hinder intramolecular rotation, consequently making radiative decay the dominant force and thereby increasing the fluorescent quantum yield. This enhancement of the fluorescent quantum yield in a more highly constrained microenvironment leads to the ability to correlate the resultant peak intensity with a measure of microenvironment rigidity, or microviscosity.¹⁰ In other words, an increase in microviscosity results in an increase in intensity. This behavior is illustrated in the fluorescence emission potential diagram in Figure C-3.

Experimental

Materials

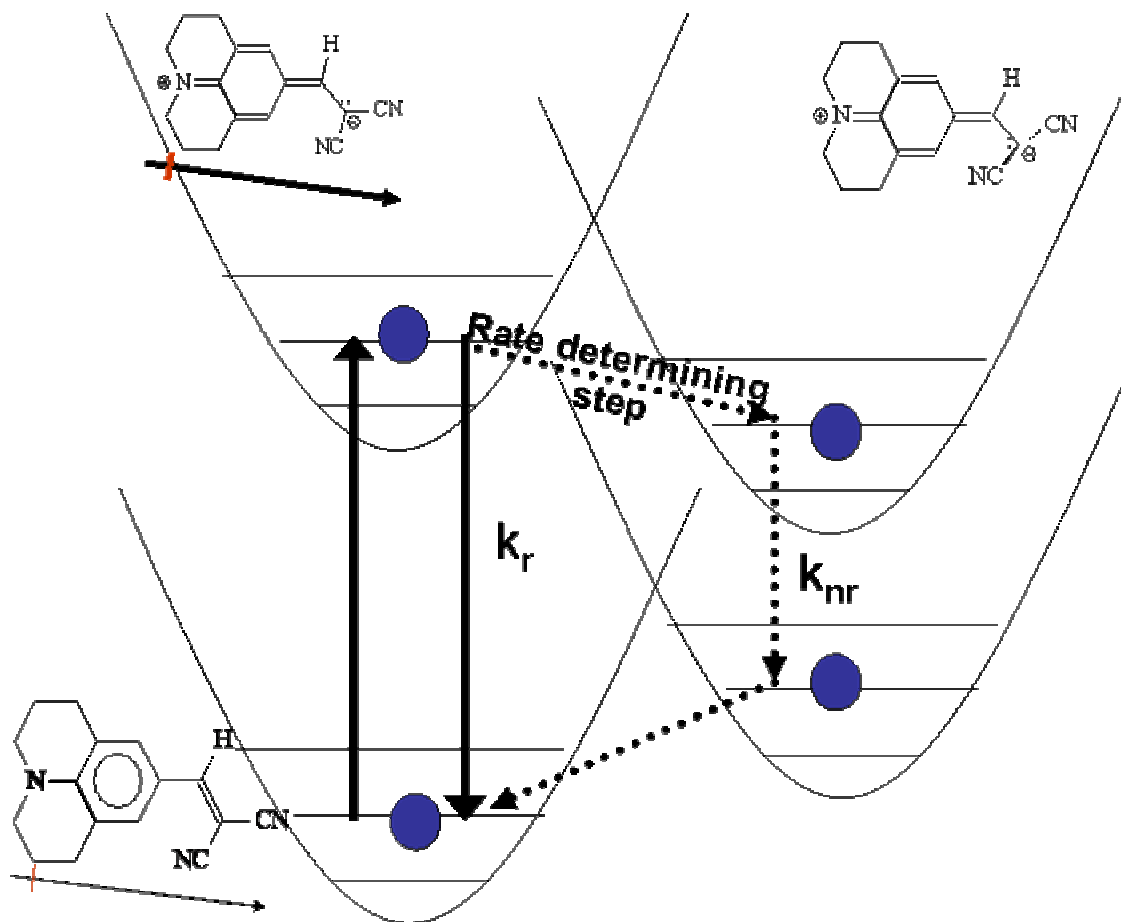


Figure C-3: Fluorescence emission potential diagram for DCVJ excitation.

DCVJ was purchased from Molecular Probes. Carbon dioxide and ethane were purchased from Airgas. Alcohols (dried over molecular sieves), acetone (HPLC, dried over molecular sieves) and alkanes (anhydrous) were purchased from Sigma-Aldrich. All but the alcohols and acetone were used as received.

Apparatus

A stainless steel vessel with three sapphire windows (6.4 mm thick) was constructed for fluorescence spectroscopy. The windows were sealed with Teflon gaskets capable of withstanding pressures exceeding 250 bar. The path length of the cell is 2.2 cm and the internal volume is 9.8 cm³. The temperature control unit for the cell, furnished by Omega, consists of heating cartridges inserted into the body, a

microprocessor thermometer, and a temperature controller. An external thermocouple was used to ensure the performance of the temperature control unit. The temperature variation was maintained within ± 0.1 °C of the setpoint. Pressure was monitored by a Druck pressure transducer and readout with an uncertainty of 0.01% in the range of 0-207 bar. A Teflon-coated magnetic spin bar constantly agitated the contents in the cell throughout measurements to facilitate equilibrium. A Shimadzu RF-5301PC spectrofluorophotometer was used for all fluorescent measurements and had a wavelength accuracy of ± 1.5 nm.

Procedure

A known stock solution of DCVJ (4.5×10^{-3} M) and the solvent of interest was prepared and a known amount of the solution was sealed into the cell. The sealed cell was carefully evacuated to approximately 3 psi to remove the majority of air with minimal solvent loss. The cell was heated and allowed to reach equilibrium temperature for approximately one hour. Initial measurements were conducted in the absence of CO₂ and then CO₂ was added to the cell via an ISCO syringe pump. Care was taken to ensure that the phase boundary occurred within the cell (not liquid-full) and was above the line of the window, thus the phase visible through the window was the gas-expanded liquid phase. Phase equilibrium was ensured by observation that the spectrum and pressure no longer changed with time. CO₂ was added and measurements were taken at regular intervals until the cell was liquid full. In order to perform measurements on the whole range of mole fractions, multiple loadings of various volumes were necessary. Reproducibility was tested by releasing CO₂ from the cell and conducting measurements when equilibrium was achieved.

Analysis

Since fluorescence is not a directly quantitative technique for the acquisition of microviscosity, the system had to be calibrated in order to decipher viscosity from fluorescent intensity. This calibration was done by correlating the fluorescent intensity with the viscosity of known pure solvents. Since one of the solvent systems of interest was CO₂-expanded methanol, an homologous series of alcohols was used for the purpose of the calibration: ethanol, 1-octanol, ethylene glycol and glycerol. Examples of the calibration spectra and the curve are found in Figures C-4 and C-5, respectively.¹⁰ A line was fit to the data and the resulting equation was used to convert the measured fluorescent intensity to the microviscosity of the immediate environment of the probe in the gas-expanded liquid.

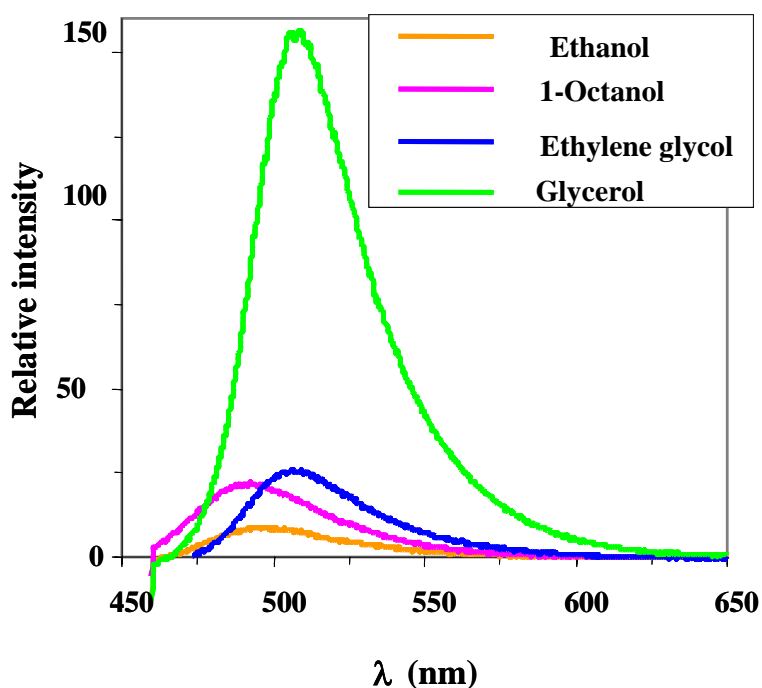


Figure C-4: Fluorescence emission spectra of DCVJ in conventional liquid solvents at 25 °C ($C_{\text{DCVJ}} = 4.5 \times 10^{-6}$ mol/L).

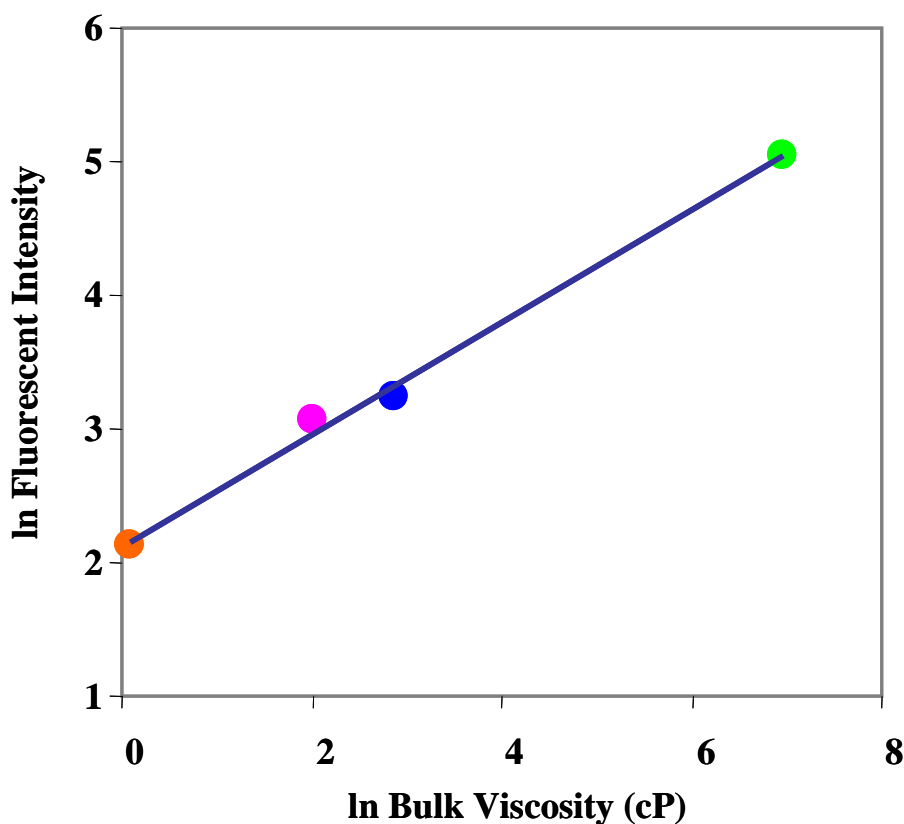


Figure C-5: Viscosity dependence of fluorescence intensity of DCVJ for the liquid solvents in Figure C-4.

One of the major assumptions made in the use of the above calibration technique is that there is negligible heterogeneity on the molecular scale of the above solvents, thus the microviscosity is equivalent to the bulk viscosity. While this assumption may not be perfect, it is the conventionally used technique.¹⁰ It was confirmed by using the calibration curve to calculate the microviscosity values of mixtures of 2-propanol and ethylene glycol at 25 °C and comparing them with bulk viscosities calculated via Eyring's relationship between viscosity and composition for liquid mixtures (Equation C-2),¹¹ where the subscripts 1 and 2 apply to liquids 1 and 2. The microviscosity and bulk

$$\log \eta_{\text{mixture}} = x_1 \log \eta_1 + x_2 \log \eta_2 \quad \text{Eq. C-2}$$

viscosity of these mixtures correlate relatively well (Figure C-6). While it appears that there may be some indication of curvature in the microviscosity behavior relative to that of the bulk viscosity, it is more likely a result of experimental uncertainty than any physical phenomenon.

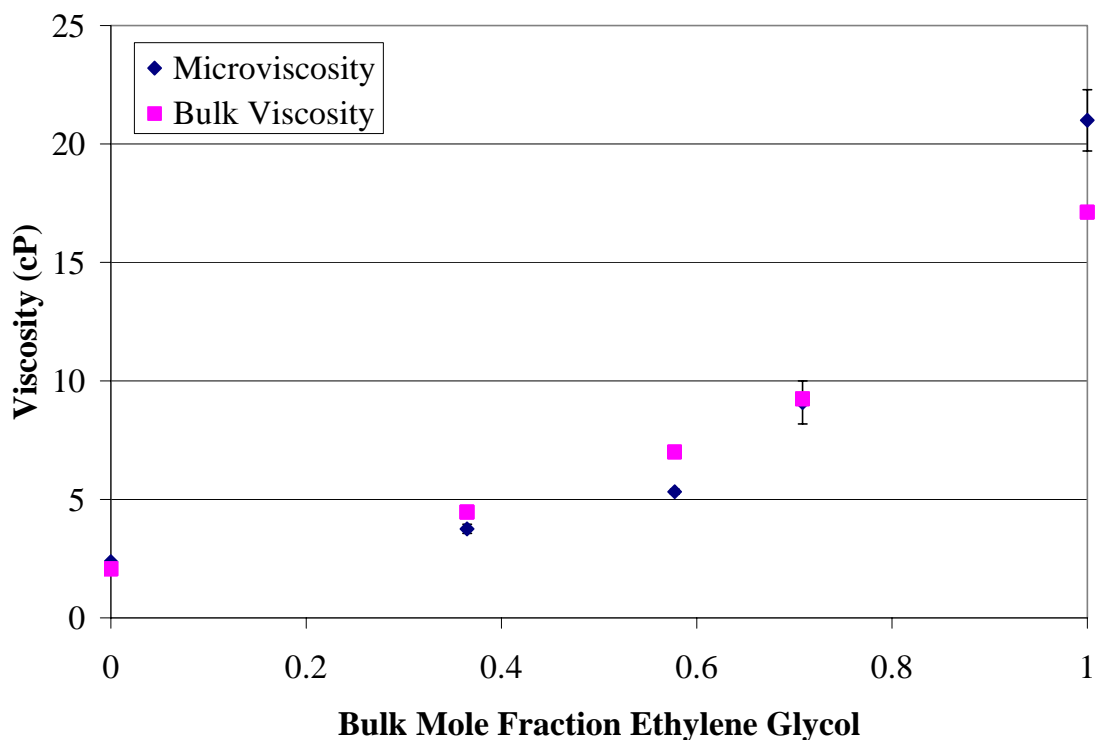


Figure C-6: Confirmation of calibration technique by comparison with mixtures of 2-propanol and ethylene glycol at 25 °C.

In an effort to ensure the precision of our measurements, the above data were compared to that of Kung and Reed⁶ (Figure C-7). Our data is in satisfactory agreement with that of the literature. While we do show some scatter, it appears to be within the limits of the experimental precision of the instrument.

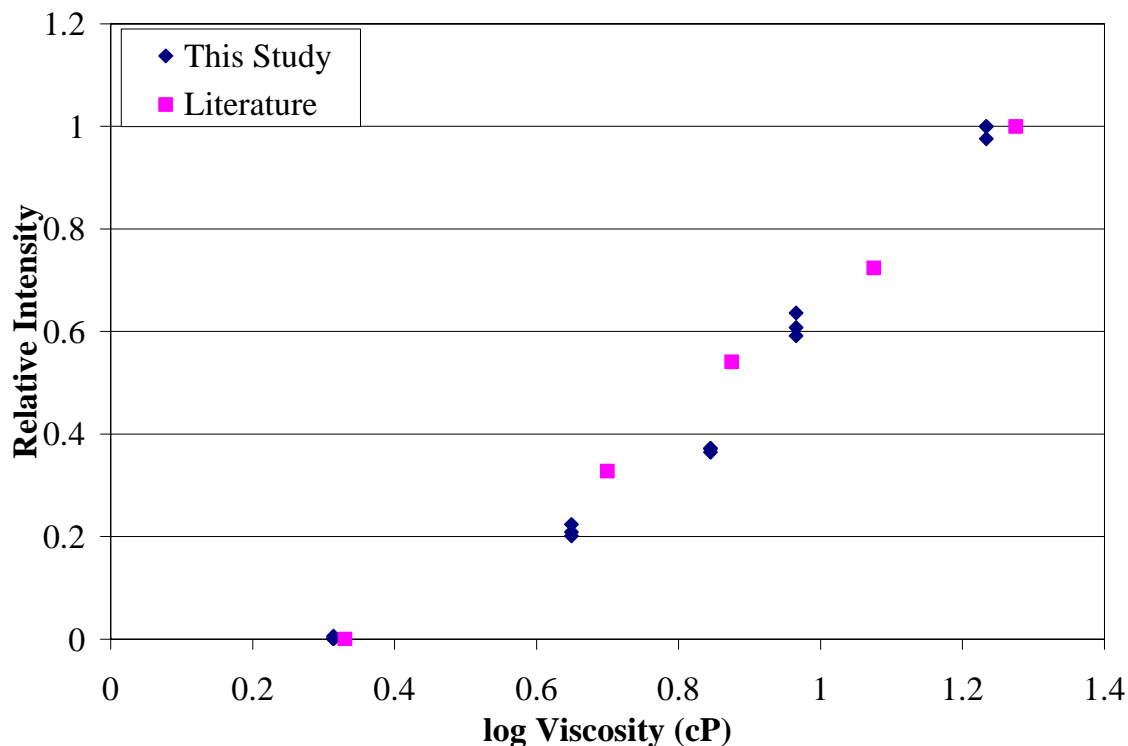


Figure C-7: Confirmation of measurement technique by comparison with literature data for 2-propanol and ethylene glycol mixtures at 25 °C.

As CO₂ was added to the organic solvent, the overall concentration of DCVJ decreased due to the increased volume of liquid. The density of CO₂ was calculated by an equation of state.¹² The density, along with a material balance, was used to determine the total liquid volume and the intensity values were multiplied by the volume expansion factor under corresponding conditions. This ensured that all of the intensities were evaluated for the same concentration of probe. It was also assumed that the fluorescent intensity is a linear function of probe concentration, which is a standard assumption for this type of measurement. The data presented in the following sections are relative to mole fraction of CO₂ in the system. This mole fraction was calculated from the system pressure the initial amount of solvent and measured VLE data for that system.^{13, 14}

Results and Discussion

Before results on expanded solvents can be analyzed, it is important to perform a series of preliminary tests. The work performed in this appendix was not performed in the ideal order. Measurements were made on expanded solvents first and then other data were measured in order to help elucidate unexpected behavior. As a result, the analyses presented are not all conclusive. They will nonetheless be presented and analyzed in the best manner possible, keeping in mind that the work is not complete and therefore many future recommendations will be made.

Figure C-8 shows the behavior of the fluorescence intensity of DCVJ as a function of concentration of DCVJ in methanol at room temperature. Solutions were prepared by serial dilutions of a stock solution and measurements were not made in any particular order (for example low concentration to high concentration, etc.). The measurements were made in the same high pressure cell used to make the high pressure measurements (instead of a cuvette) so that the data could be compared. As the data seem to indicate, there is a clear increase in intensity with increase in concentration between 10^{-6} and 10^{-5} molar, as expected, but then there is a sharp decrease in intensity as concentration increases beyond that point. One theory as to why this would happen is that the DCVJ is forming excimers upon reaching a critical concentration, a phenomenon which is observed in aqueous solutions in the presence of γ -cyclodextrin.¹⁵ Further studies to confirm the formation of such excimers in our systems were not performed.

This result makes the analysis of the rest of the data difficult and inconclusive because they were measured at 10^{-5} - 10^{-4} molar concentrations. The reason such high concentrations were used initially was to keep the fluorescence intensities adequately

higher than the baseline noise of the instrument. A lack of sensitivity of the probe is part of the problem as well as the excimer formation. It must be kept in mind that all data presented must be used with caution as the concentration of DCVJ used was above the

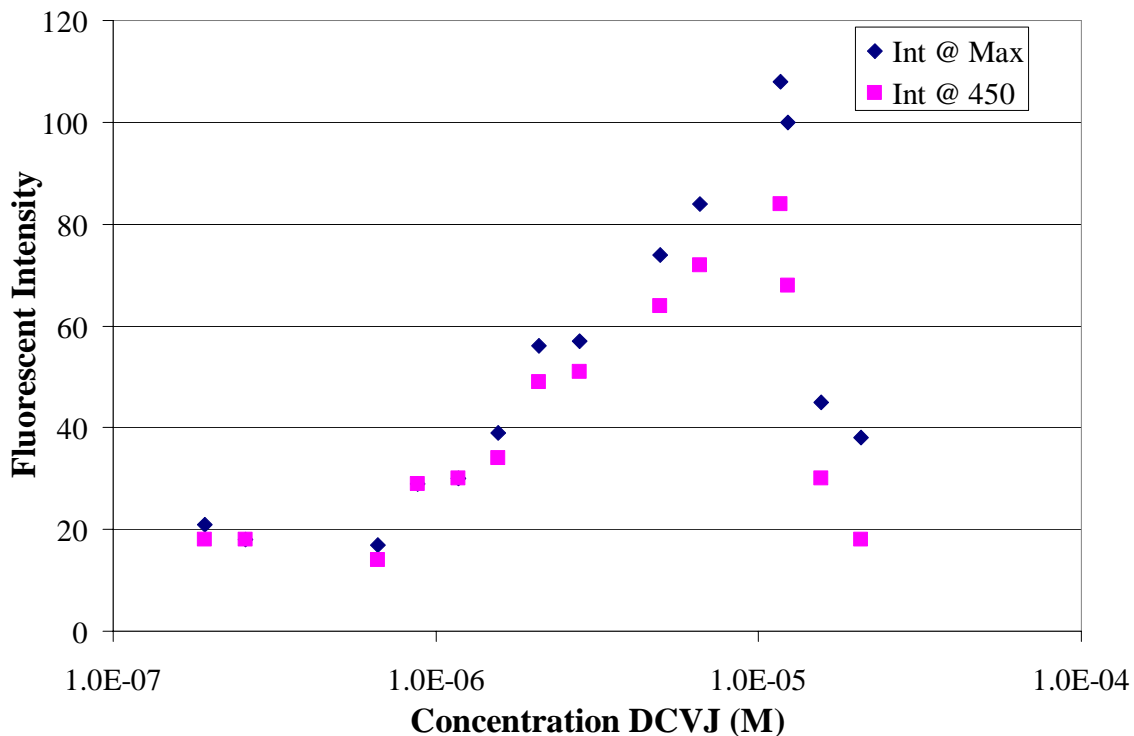


Figure C-8: Concentration behavior of fluorescent intensity of DCVJ measured at the intensity maximum and at 450 nm.

range where the fluorescence intensity can be linearly correlated with DCVJ concentration. All will be presented and analyzed as thoroughly as possible.

The microviscosity of methanol / cyclohexane mixtures were measured at 50 °C and compared to the bulk viscosity values as determined by Eyring's equations for estimating the viscosity of liquid mixtures¹¹ (Figure C-9). From these data it appears there are no local augmentations of the viscosity in these systems. The microviscosity simply increases with an increase in cyclohexane concentration and therefore bulk viscosity is measured within experimental uncertainty. However, due to the fact that

there is little difference between the bulk viscosities of methanol and cyclohexane, it is difficult to definitively conclude. If any augmentations exist, they might be so small as to be within the precision of the measurement.

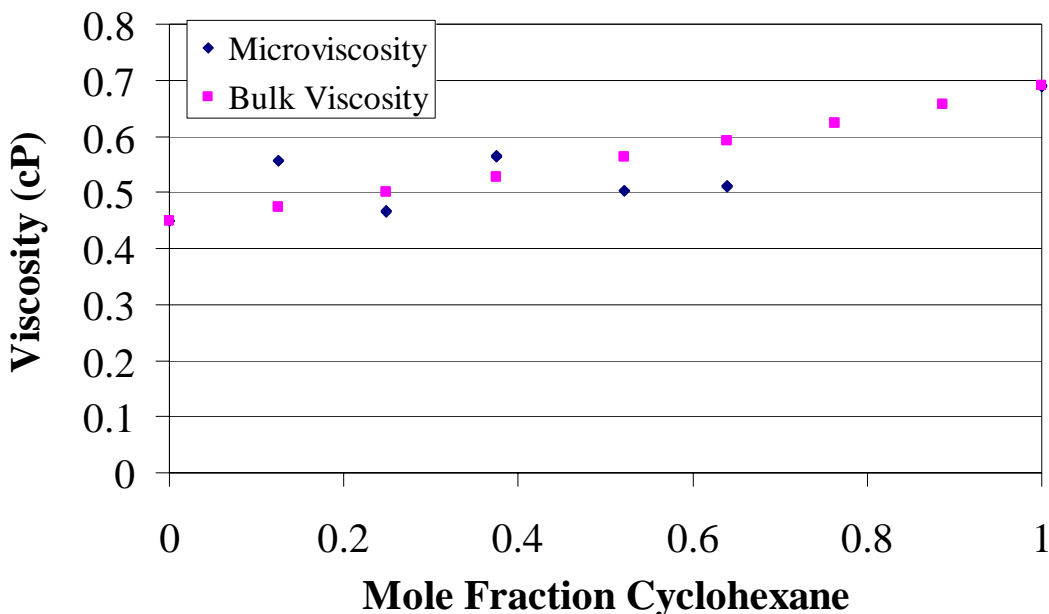


Figure C-9: Comparison between bulk and microviscosity of mixtures of methanol and cyclohexane at 50 °C.

We expected that mixtures of methanol with carbon dioxide would behave similarly to mixtures of methanol and cyclohexane due to the similarity in polarity between carbon dioxide and cyclohexane, keeping in mind that liquid CO₂ is less viscous than cyclohexane. However, that does not seem to be the case. Data for CO₂-expanded methanol at 40 °C are shown in Figure C-10. Bulk viscosity data for the pure components¹⁶ and several mixtures¹⁷ of methanol and CO₂ are shown on the graph for the sake of comparison. Because the critical composition of CO₂ / methanol at 40 °C is approximately 80% CO₂ by mole, values are only reported for compositions up to 80% CO₂. Beyond 80% CO₂ there exists only a single liquid phase. The data indicate that the microviscosity of the mixture increases slowly as the amount of CO₂ increases to about

40% by mole before it levels off and slowly seems to drop within experimental error. The maximum microviscosity is roughly twice that of pure methanol under the same conditions.

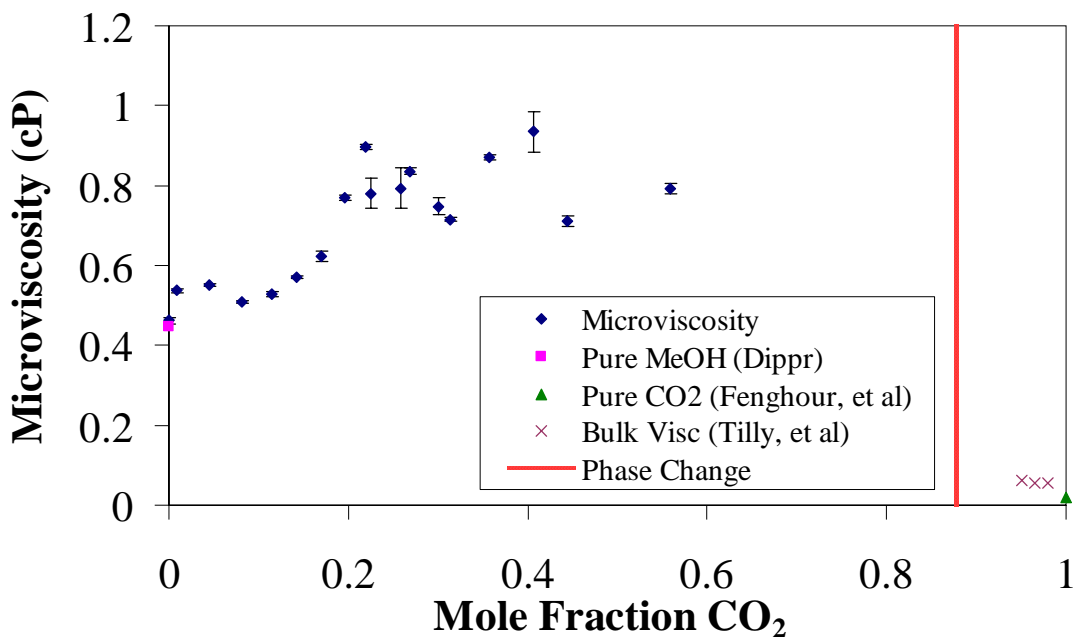


Figure C-10: Microviscosity of mixtures of methanol and carbon dioxide compared with bulk viscosity values at 40 °C.

The bulk phase viscosity of CO₂ is much less than that of methanol, thus it is expected that expansion of methanol with CO₂ would cause a decrease in viscosity of the fluid.¹⁷ That the opposite behavior occurs in the cybotactic region indicates that there are non-additive solvent effects creating non-uniformity in the microstructure of the system. Because of the high dipole moment of the excited state of DCVJ, it will be preferentially solvated by the methanol as opposed to the CO₂; thus local density augmentations in the system would be expected. However, DCVJ should not “see” any more methanol upon CO₂ addition than it “sees” when in solution with just methanol. Thus the viscosity increase is unexpected. Since methanol self-associates due to hydrogen bonding, we

speculate that each DCVJ molecule is trapped in a cluster of methanol molecules that are hydrogen bonded to one another. Upon addition of the CO₂, the non-polarity of the CO₂ may cause electrostrictive forces among the clusters, thus forcing the clusters to compress. We speculate that these electrostrictive effects combined with the hydrogen bonding properties of methanol create clusters of methanol molecules around the DCVJ molecules which tighten upon the addition of CO₂, thus resulting in an apparent increase of microviscosity in the area directly surrounding the DCVJ. Once a particular threshold of CO₂ is added, the hydrogen-bonded clusters can no longer support themselves. They subsequently break down and the microviscosity decreases once again.

Due to the nature of the experiment, it is impossible to separate the effect of pressure from the effect of composition because the pressure increases as CO₂ is added. In an effort to decouple pressure and composition, two additional experiments were performed: one which tested the effect of the hydrostatic pressure of methanol on the microviscosity of methanol and how that compares to the effect of hydrostatic pressure on the bulk viscosity, the other testing the same effect in a mixture of methanol and carbon dioxide. The first experiment was performed using a syringe pump filled with methanol. A known amount of the DCVJ stock solution in methanol was added to the cell. The methanol from the syringe pump was added to the cell under pressure. The microviscosity of the liquid was measured as a function of pressure and compared to bulk viscosity under the same conditions.¹⁸ Data are presented in Figure C-11. The effect of hydrostatic pressure on the microviscosity behaves very similarly to that of the bulk viscosity, thus it seems that such an experiment would be a valid assessment of a mixed solvent system.

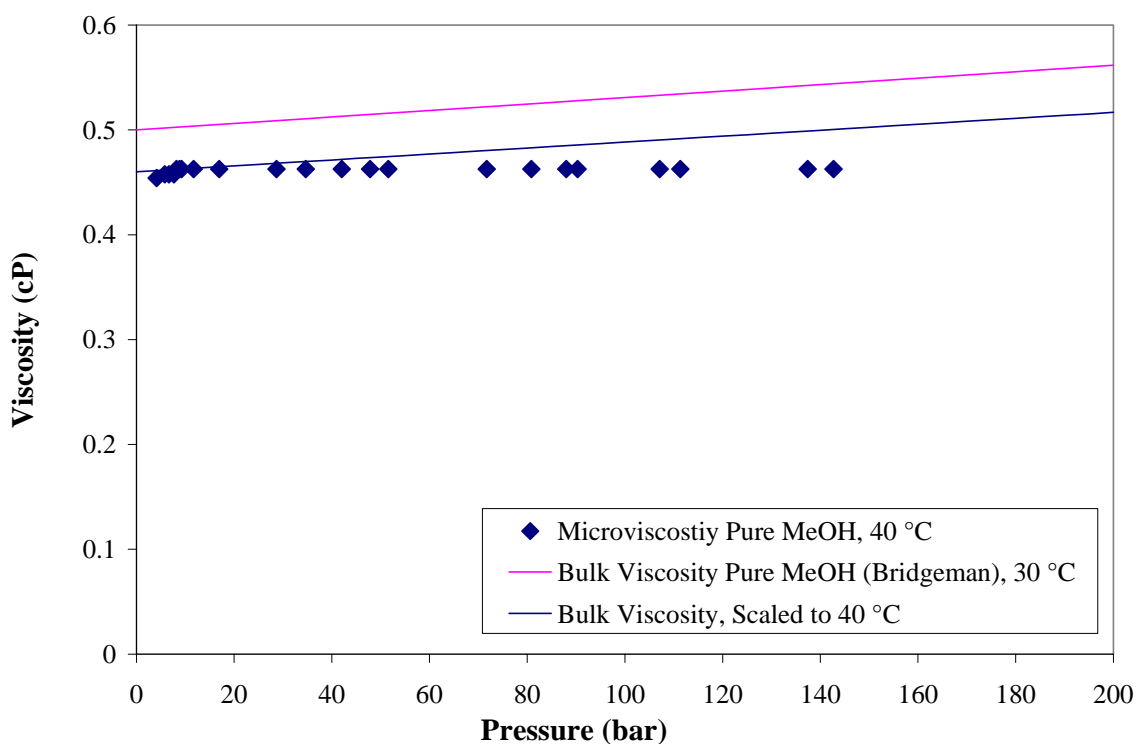


Figure C-11: Effect of hydrostatic pressure on the microviscosity of methanol as compared to the bulk viscosity at 40 °C.

The second experiment was performed using a syringe pump filled with a known monophasic mixture of methanol and CO₂ such that when the mixture was added to the system the pressure increased without changing the composition. The conditions of the pump were chosen to ensure that the liquid in the pump was uniformly mixed. A known amount of DCVJ stock solution was added to the cell and left open to the air. The methanol evaporated, leaving a known amount of DCVJ in the cell. The mixture was added to the cell until it was at a high enough pressure to ensure no phase boundary was present. The results are presented in Figure C-12.

According to the data, the microviscosity of the mixture is always lower than that of the bulk viscosity of methanol at similar pressures. As the pressure increases the microviscosity also increases, which is consistent with the trend of pure methanol. While

this data makes sense on its own, it conflicts with the data on CO₂-expanded methanol in Figure C-10. In the expanded system, the microviscosity of a mixture that is 55% methanol has a microviscosity of nearly double that of pure methanol. That is at a lower operating pressure than the liquid-full experiment. Thus the data are inconclusive and the non-linear concentration/intensity relationship may be the reason for the inconsistency.

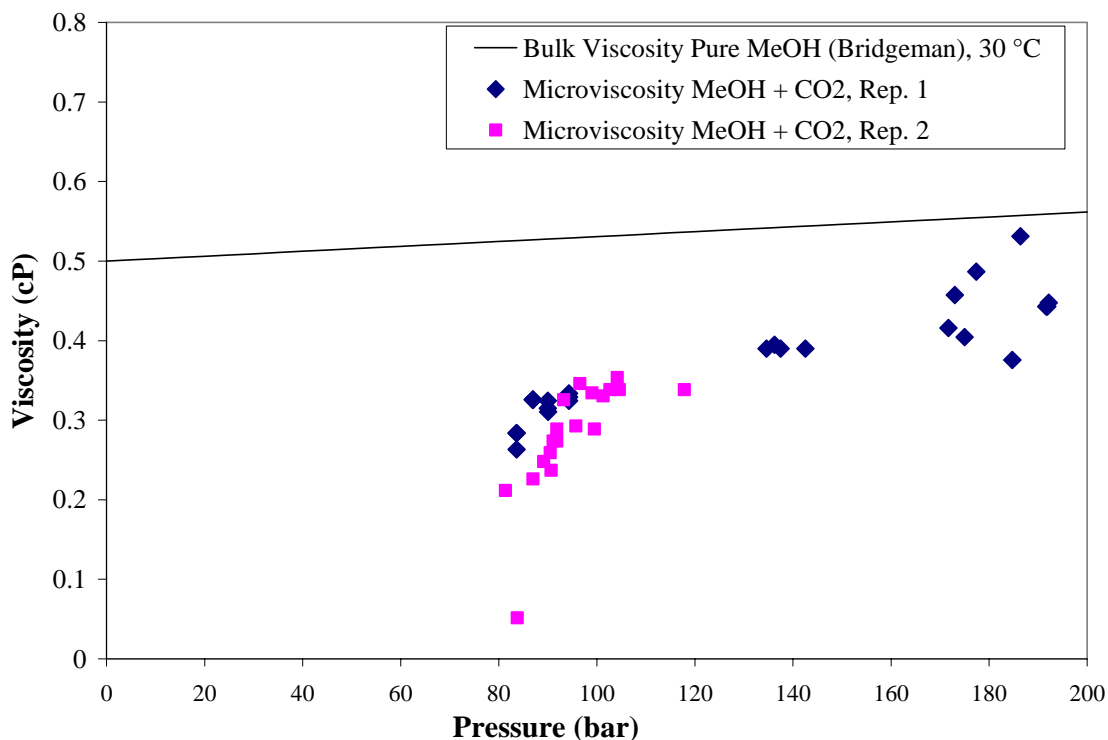


Figure C-12: Effect of hydrostatic pressure on the microviscosity of a mixture of 0.55 methanol and 0.45 CO₂ as compared to the bulk viscosity of methanol at 40 °C.

Due to its similarity to carbon dioxide, ethane was also used as an expansion gas for methanol to see if it behaved differently in the cybotactic region. Data are presented in Figure C-13. Data were measured until about 40% ethane because beyond that composition the system becomes one phase. It appears that the behavior is similar to that of CO₂-expanded methanol in that the microviscosity increases until it nearly doubles that of pure methanol at approximately 40% ethane.

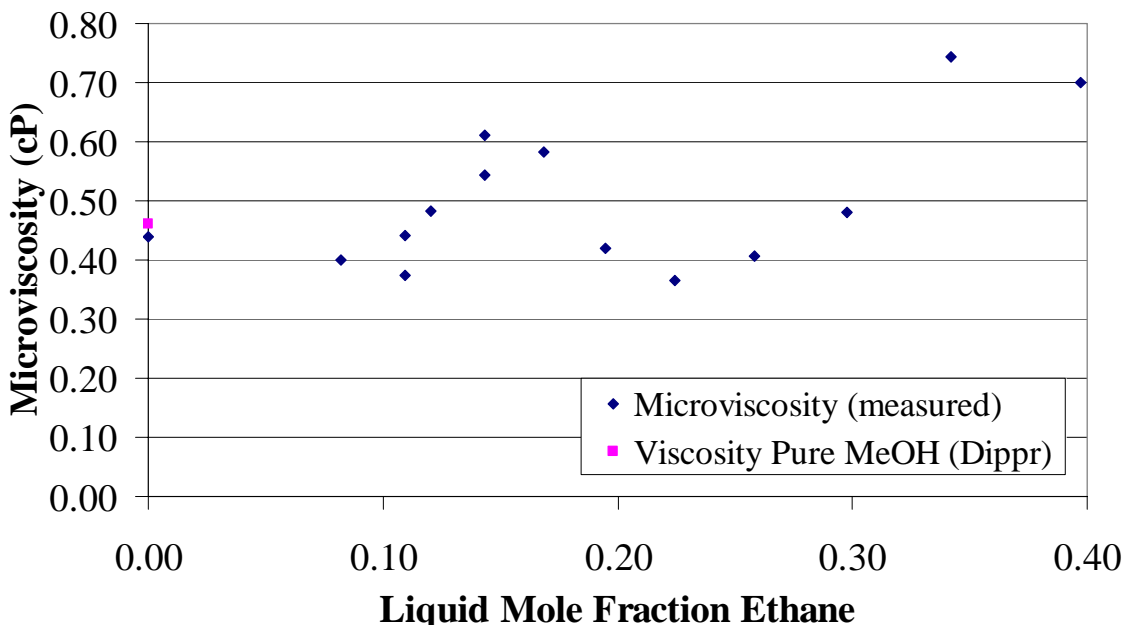


Figure C-13: Microviscosity of ethane-expanded methanol at 40 °C.

Measurements were also made on CO₂-expanded acetone. Since methanol is polar and protic, we wanted to measure the microviscosity of a solvent that was polar but aprotic in order to understand the role that hydrogen bonding plays in the cybotactic region. Data are presented in Figure C-14. The microviscosity of CO₂-expanded acetone also increases as a function of CO₂ composition and pressure, effectively refuting the hydrogen bonding argument made previously. Electrostrictive forces may still play a role, but the behavior is more likely caused by the aforementioned excimer formation of DCVJ and is therefore difficult to interpret.

Even though the calibration curve was not extrapolated in any of the above measurements because the microviscosity was always higher than that of pure methanol, the linearity of the calibration curve at low viscosity was tested by using the known value of the viscosity of carbon dioxide under a variety of operating conditions¹⁶ (Figure C-15). In this experiment, DCVJ solution was put into the cell and the solvent evaporated, as in

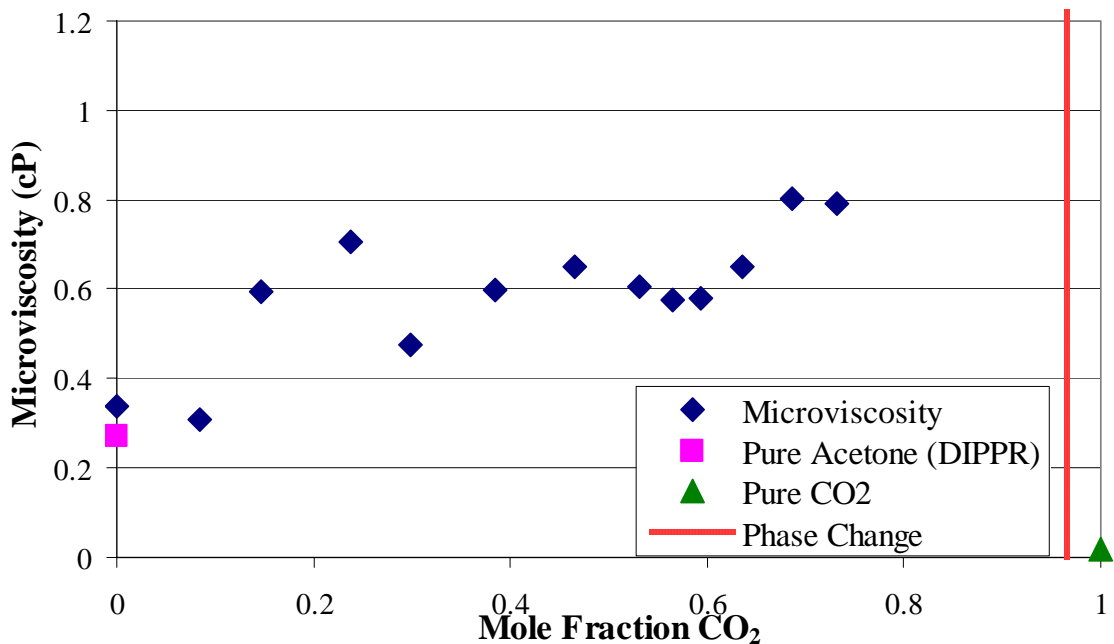


Figure C-14: Microviscosity of mixtures of acetone and CO₂ compared with bulk viscosity values at 40 °C.

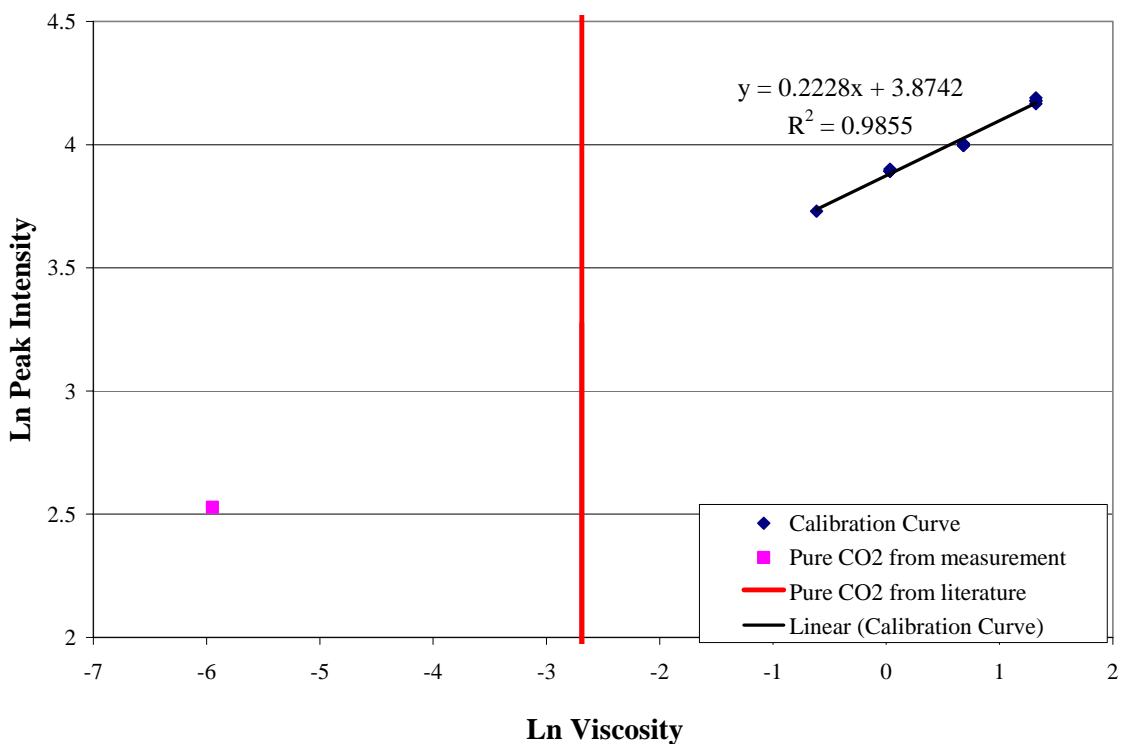


Figure C-15: Extrapolation of calibration curve to the viscosity of CO₂.

the hydrostatic pressure experiment discussed above. In this case, carbon dioxide was added until the cell was liquid full. The presence of the liquid was determined visually. It appears that the calibration is not valid when extrapolated beyond the limits of the calibration curve. The calculated viscosity of carbon dioxide is higher than the actual viscosity by a factor of 30.

Summary

Microviscosity data are very difficult to measure when the system is inviscid due to the insensitivity of the probe and the uncertainty in the measurement. Since the instrument is a limiting factor, a more sensitive probe must either be found or designed and synthesized. Furthermore, the concentration behavior of any new probe must be tested for linearity and any indication of excimer formation. The data presented above could be re-run at lower probe concentrations to avoid the excimer formation and the data may prove to be more conclusive, but the non-linearity of the concentration behavior makes it difficult to analyze conclusively and absorption values may be too low. It is difficult to say if the apparent enhancement of the microviscosity as a function of CO₂ pressure and composition of both methanol and acetone are real due to the complications in measurement.

REFERENCES

1. Tucker, S. C., Solvent density inhomogeneities in supercritical fluids. *Chem. Rev.* **1999**, 99, 391-418.
2. Zagrobelny, J.; Bright, F. V., Influence of solute-fluid clustering on the photophysics of pyrene emission in supercritical ethane and trifluoromethane. *J. Am. Chem. Soc.* **1992**, 114, (20), 7821-7826.
3. Loutfy, F. O.; Arnold, B. A., Effect of viscosity and temperature on torsional relaxation of molecular rotors. *J. Phys. Chem.* **1982**, 86, 4205-4211.
4. Haidekker, M. A.; Ling, T.; Anglo, M.; Stevens, H. Y.; Frangos, J. A.; Theodorakis, E. A., New fluorescent probes for the measurement of cell membrane viscosity. *Chemistry and Biology* **2001**, 8, (2), 123-131.
5. Loutfy, R. O., Fluorescence probes for polymer free-volume. *Pure & Appl. Chem.* **1986**, 58, (9), 1239-1248.
6. Kung, C. E.; Reed, J. K., Microviscosity measurements of phospholipid bilayers using fluorescent dyes that undergo torsional relaxation. *Biochemistry* **1986**, 25, 6114-6121.
7. Sharafy, S.; Muszkat, K. A., Viscosity dependence of fluorescence quantum yields. *J. Am. Chem. Soc.* **1971**, 93, (17), 4119-4125.
8. Kung, C. E.; Reed, J. K., Fluorescent molecular rotors: A new class of probes for tubulin structure and assembly. *Biochemistry* **1989**, 28, 6678-6686.
9. Loutfy, R. O.; Lee, K. L., Electrochemistry and Spectroscopy of Intramolecular Charge-Transfer Complexes. *p-N,N*-Dialkylaminobenzylidenemalononitriles. *J. Phys. Chem.* **1980**, 84, 2803-2808.
10. Lu, J.; Liotta, C. L.; Eckert, C. A., Spectroscopically probing microscopic solvent properties of room-temperature ionic liquid with the addition of carbon dioxide. *J. Phys. Chem. A* **2003**, 107, 3995-4000.
11. Hirschfelder, J. O.; Curtiss, C. F.; Bird, R. B., *Molecular Theory of Gases and Liquids*. John Wiley & Sons, Inc.: New York, 1954.

12. Ely, J. F.; Haynes, W. M.; Bain, B. C., Isochoric measurements on carbon dioxide on (0.982 carbon dioxide + 0.018 nitrogen) from 250 to 320 K at pressures to 35MPa. *J. Chem. Thermodyn.* **1989**, 21, 879-894.
13. Chang, C. J.; Chiu, K.-L.; Day, C.-Y., A new apparatus for the determination of P-x-y diagrams and Henry's constants in high pressure alcohols with critical carbon dioxide. *J. Supercrit. Fluids* **1998**, 12, 223-237.
14. Adrian, T.; Maurer, G., Solubility of carbon dioxide in acetone and propionic acid at temperatures between 298 K and 333 K. *J. Chem. Eng. Data* **1997**, 42, (4), 668-672.
15. Bhattacharyya, A.; Bhattacharyya, K.; Bhattacharyya, B.; Roy, S., A study of aggregation of 9-(dicyano-vinyl)julolidine. *Indian Journal of Biochemistry and Biophysics* **1995**, 32, 442-446.
16. Fenghour, A.; Wakeham, W. A.; Vesovic, V., The viscosity of carbon dioxide. *J. Phys. Chem. Ref. Data* **1998**, 27, (1), 31-44.
17. Tilly, K. D.; Foster, N. R.; Macnaughton, S. J.; Tomasko, D. L., Viscosity correlations for binary supercritical fluids. *Ind. Eng. Chem. Res.* **1994**, 33, (3), 681-688.
18. Weale, K. E., *Chemical reactions at high pressures*. E. & F. N. Spon Ltd.: London, 1967.

VITA

Malina Elizabeth Janakat was born in East Rutherford, NJ on November 22, 1978 and lived there until she went off to college. She is the first-generation American daughter of Sozar and Jean Janakat. Malina graduated as the salutatorian of her class at Henry P. Becton Regional High School in East Rutherford, NJ in 1996. While in high school she was an active member of the debate team, a variety of academic clubs, editor of the art and literary magazine and a member of the varsity bowling team. Malina graduated with honors from the Stevens Institute of Technology in Hoboken, NJ in 2001 with a Bachelor of Engineering in Chemical Engineering and a minor in Literature. While at Stevens she was very active in the dramatic society, was a founding member of the equestrian club and participated in several academic / professional organizations such as Tau Beta Pi and AIChE. In the fall of 2001 Malina enrolled in the Georgia Institute of Technology. Her graduate studies were directed by Professor Charles A. Eckert and Professor Charles L. Liotta and focus on green chemistry. In addition to her research, she took on leadership roles in the Association of Chemical Engineering Graduate Students and was an active participant in the Relay for Life. She also had the opportunity to perform a research project at Universität Stuttgart in Germany. She will complete her Ph.D. in Chemical and Biomolecular Engineering in the spring of 2006 and will begin her career as a Research and Development Engineer at Frito Lay in Plano, TX soon after. Selected presentations follow.

Presentations

Zaman, Abbas (speaker) A.; Janakat, Malina E.; Moudgil, Brian M. "Role of Electrostatic Repulsion and Particle Size on Viscosity and the Onset of Shear Thickening of Aqueous Colloidal Dispersions" *AICHE Annual Meeting*, Reno, Nevada, November 7, 2001.

Eckert, Charles A.; Liotta, Charles L.; Lazzaroni, Michael J. (speaker); Bush, David; Janakat, Malina E. "Solid Solubility in Gas Expanded Liquids" *AICHE Annual Meeting*, San Francisco, California, November 20, 2003.

Janakat, Malina E. (speaker); Liotta, Charles L.; Eckert, Charles A. "Microviscosity of Gas-Expanded Liquids" *International Symposium on Supercritical Fluids*, Orlando, Florida, May 4, 2005.

Janakat, Malina E.; Hallett, Jason P. (speaker); Liotta, Charles L.; Eckert, Charles A. "Transport Properties of Gas-Expanded Liquids" *International Green Chemistry & Engineering Conference*, Washington, D.C., June 21, 2005.

Posters

Bush, David; Lazzaroni, Michael J.; Janakat, Malina E.; Eckert, Charles A.; Frank, Timothy C.; Gupta, Sumnesh K.; Olson, James D. "Prediction and Correlation of Solid Solubility in Solvents and Solvent Mixtures" *Conference on Properties and Phase Equilibria for Product and Process Design*, Snowbird, Utah, May, 2004

Janakat, Malina E.; Liotta, Charles L.; Eckert, Charles A. "Microviscosity of CO₂-expanded Methanol" *DECHEMA Solvents for Green Synthesis Conference*, Bruchsal, Germany, October 4, 2004

Janakat, Malina E.; Liotta, Charles L.; Eckert, Charles A. "Microstructure and Transport Properties of Gas-Expanded Liquids" *AICHE National Meeting*, Austin, Texas, November 9, 2004 (M.E. Janakat, C.L. Liotta, C.A. Eckert)

Janakat, Malina E.; Kitchens, Christopher L.; Hallett, Jason P.; Lu, Xiuyang; Maxey, Natalie, B.; Donaldson, Megan; Liotta, Charles L.; Eckert, Charles A. "Transport Properties of Gas-Expanded Liquids" *AICHE Annual Meeting*, Cincinnati, Ohio, November 3, 2005